



Universitat Autònoma de Barcelona

ADVERTIMENT. L'accés als continguts d'aquesta tesi queda condicionat a l'acceptació de les condicions d'ús establertes per la següent llicència Creative Commons:  http://cat.creativecommons.org/?page_id=184

ADVERTENCIA. El acceso a los contenidos de esta tesis queda condicionado a la aceptación de las condiciones de uso establecidas por la siguiente licencia Creative Commons:  <http://es.creativecommons.org/blog/licencias/>

WARNING. The access to the contents of this doctoral thesis it is limited to the acceptance of the use conditions set by the following Creative Commons license:  <https://creativecommons.org/licenses/?lang=en>

Institut de Recerca Hospital de la Santa Creu i Sant Pau
Universitat Autònoma de Barcelona

Antineoplastic effect of CXCR4-targeted protein nanoparticles in head and neck squamous cell carcinoma mouse models

PhD Thesis

PhD in Biotechnology, Universitat Autònoma de Barcelona

Elisa Rioja Blanco

Dr. Ramon Mangués Bafalluy

Dra. Lorena Alba-Castellón

Barcelona, 2022

SUMMARY

Head and neck squamous cell carcinoma (HNSCC) represents the seventh most common cancer worldwide, with more than 850,000 new cases and 400,000 deaths in 2020. Current treatment, consisting of a combination of surgery, chemotherapy, and radiotherapy, achieves loco-regional control of the disease. However, these patients are still at risk of developing loco-regional recurrence and distant metastasis, dramatically affecting their prognosis and survival. Although the treatment for recurrent and/or metastatic patients has recently improved with the addition of targeted monoclonal antibodies and immunotherapy, up to 30%–40% of HNSCC patients still die because of the disease, highlighting the urge for novel therapeutic strategies.

In the last years, the chemokine receptor 4 (CXCR4) has emerged as a promising molecular target. CXCR4 is overexpressed in more than 20 cancer types, including HNSCC, and its overexpression has been related to enhanced proliferation, angiogenesis, invasion, and metastasis. Remarkably, CXCR4 overexpression in HNSCC primary tumors associates with loco-regional recurrence, distant metastasis, and worse patient prognosis. Consequently, different CXCR4-targeted anticancer therapies have been developed in the last decades, mainly CXCR4 inhibitors, being the antagonist AMD3100 (plerixafor) the only one in the market. In this context, our group has developed the T22-based protein nanoparticle platform, that incorporates the CXCR4 ligand T22 cationic peptide, for the selective delivery of cytotoxic domains to CXCR4-overexpressing cancer cells. The aim of the present thesis is to study the suitability of these T22-based nanoparticles for the treatment of HNSCC.

First, we demonstrate that the T22-nanocarrier selectively internalizes in CXCR4⁺ HNSCC cancer cells. Consequently, the nanocarrier displays a CXCR4-dependent tumor accumulation *in vivo*, with negligible biodistribution to non-tumor bearing organs. In addition, this nanoparticle platform presents a great versatility allowing the incorporation of cytotoxic peptidic domains to generate therapeutic nanoparticles. Following this strategy, we have previously developed T22-PE24-H6 and T22-DITOX-H6, that incorporate the toxin catalytic domain of *Pseudomonas aeruginosa* exotoxin A and the diphtheria toxin domain, respectively. In the present work, we demonstrate that both nanotoxins exhibit a CXCR4-dependent cytotoxic effect in HNSCC cancer cells. Remarkably, we describe for the first time that both nanotoxins trigger caspase-3/GSDME-dependent pyroptosis, a pro-inflammatory type of programmed cell death alternative to apoptosis. This cytotoxic effect translates into a potent antitumor effect *in vivo*, especially in the case of T22-DITOX-H6 that practically arrests tumor growth, in the

absence of toxicity in other healthy organs. Lastly, T22-DITOX-H6 treatment is capable of effectively blocking metastatic dissemination to the cervical lymph nodes, lungs, and liver in the absence of histopathological alterations in an orthotopic mouse model that replicates the metastatic pattern of HNSCC patients.

Overall, in the present thesis we demonstrate that the T22-based nanoparticles, that incorporate toxin domains, induce pyroptosis in CXCR4⁺ cancer cells, a cell death mechanism alternative to apoptosis with a great potential to improve the treatment of patients with metastatic HNSCC.

RESUMEN

El carcinoma escamoso de cabeza y cuello (CECC) representa el séptimo cáncer más común en el mundo, con más de 850.000 nuevos casos y 400.000 muertes en 2020. El tratamiento actual, que incluye una combinación de cirugía, quimioterapia y radioterapia, consigue un control loco-regional de la enfermedad. Sin embargo, los pacientes de CECC continúan en riesgo de desarrollar recidivas loco-regionales y metástasis a distancia, afectando de forma dramática a su pronóstico y supervivencia. A pesar de que el tratamiento para pacientes con recidivas y/o metástasis ha mejorado en los últimos años gracias a la incorporación de anticuerpos monoclonales e inmunoterapia, hasta un 30-40% de los pacientes de CECC mueren a consecuencia de la enfermedad, poniendo de manifiesto la necesidad de nuevas terapias.

En los últimos años, el receptor de quimiocinas 4 (CXCR4) ha sido propuesto como una prometedora diana terapéutica. CXCR4 se encuentra sobreexpresado en más de 20 tipos de cánceres, entre ellos el CECC, y esta sobreexpresión ha sido relacionada con una mayor proliferación, angiogénesis, invasión y diseminación metastática. De forma importante, la sobreexpresión de CXCR4 en tumores primarios de CECC está asociada con el desarrollo de recidivas loco-regionales, metástasis y un peor pronóstico de los pacientes. En consecuencia, distintas terapias dirigidas a CXCR4 han sido desarrolladas en las últimas décadas, principalmente inhibidores de CXCR4, siendo el antagonista de CXCR4 AMD3100 (plerixafor) el único fármaco en el mercado. En este contexto, nuestro grupo ha desarrollado nanopartículas proteicas basadas en el péptido T22, un ligando de CXCR4, para la entrega selectiva de dominios citotóxicos a las células tumorales con sobreexpresión de CXCR4. El objetivo de la presente tesis doctoral es estudiar el potencial de estas nanopartículas basadas en el péptido T22 para el tratamiento del CECC.

En primer lugar, en este trabajo se demuestra que el nanotransportador basado en T22 internaliza de forma selectiva en las células tumorales de CECC CXCR4⁺. Además, este nanotransportador también presenta una acumulación en tumor dependiente de CXCR4 *in vivo*, con una biodistribución despreciable en otros órganos. Por otro lado, estas nanopartículas basadas en el péptido T22 presentan una gran versatilidad, permitiendo incorporar dominios peptídicos citotóxicos para generar nanopartículas terapéuticas. Siguiendo esta estrategia, hemos desarrollado previamente las nanotoxinas T22-PE24-H6 y T22-DITOX-H6, que incorporan los dominios catalíticos de la exotoxina A de *Pseudomonas aeruginosa* y de la toxina diftérica respectivamente. En este trabajo, se demuestra que ambas nanotoxinas presentan un efecto citotóxico dependiente de

CXCR4 en células tumorales de CECC. Cabe destacar que se describe por primera vez la capacidad de ambas nanotoxinas de activar la piroptosis mediada por caspasa-3/GSDME, un tipo de muerte celular programada proinflamatoria, alternativa a la apoptosis. Este efecto citotóxico se traduce en un potente efecto antitumoral *in vivo*, especialmente en el caso de T22-DITOX-H6 que prácticamente frena el crecimiento tumoral, en ausencia de toxicidad en otros órganos. Por último, el tratamiento con T22-DITOX-H6 es capaz de bloquear la diseminación metastática a los ganglios linfáticos cervicales, pulmones e hígado sin provocar alteraciones histopatológicas en un modelo murino ortotópico que reproduce el patrón de metástasis de los pacientes de CECC.

En resumen, en la presente tesis doctoral demostramos que las nanotoxinas que incorporan el ligando T22, son capaces de inducir piroptosis en células tumorales CXCR4⁺, un mecanismo de muerte celular alternativo a la apoptosis con un gran potencial para mejorar el tratamiento de los pacientes con CECC metastásico.

RESUM

El carcinoma escatós de cap i coll (CECC) representa el setè càncer més comú en el món, amb més de 850.000 nous casos i 400.000 morts en 2020. El tractament actual, que inclou una combinació de cirurgia, quimioteràpia i radioteràpia, aconsegueix un control loco-regional de la malaltia. No obstant això, els pacients de CECC continuen en risc de desenvolupar recidives loco-regionals i metàstasis a distància, afectant de manera dramàtica al seu pronòstic i supervivència. A pesar que el tractament per a pacients amb recidives i/o metàstasis ha millorat en els últims anys gràcies a la incorporació d'anticossos monoclonals i immunoteràpia, fins a un 30-40% dels pacients de CECC moren a conseqüència de la malaltia, posant de manifest la necessitat de noves teràpies.

En els últims anys, el receptor de quimiocines 4 (CXCR4) ha estat proposat com una prometedora diana terapèutica. CXCR4 es troba sobreexpressat en més de 20 tipus de càncers, entre ells el CECC, i aquesta sobreexpressió ha estat relacionada amb una major proliferació, angiogènesi, invasió i disseminació metastàtica. De manera important, la sobreexpressió de CXCR4 en tumors primaris de CECC està associada amb el desenvolupament de recidives loco-regionals, metàstasis i un pitjor pronòstic dels pacients. En conseqüència, diferents teràpies dirigides a CXCR4 han estat desenvolupades en les últimes dècades, principalment inhibidors de CXCR4, sent l'antagonista de CXCR4 AMD3100 (plerixafor) l'únic fàrmac en el mercat. En aquest context, el nostre grup ha desenvolupat nanopartícules proteiques basades en el pèptid T22, un lligant de CXCR4, per al lliurament selectiu de dominis citotòxics a les cèl·lules tumorals amb sobreexpressió de CXCR4. L'objectiu de la present tesi doctoral és estudiar el potencial d'aquestes nanopartícules basades en el pèptid T22 per al tractament del CECC.

En primer lloc, en aquest treball es demostra que el nanotransportador basat en T22 internalitza de manera selectiva en les cèl·lules tumorals de CECC CXCR4⁺. A més, aquest nanotransportador també presenta una acumulació en tumor dependent de CXCR4 *in vivo*, amb una biodistribució menyspreable en altres òrgans. D'altra banda, aquestes nanopartícules basades en el pèptid T22 presenten una gran versatilitat, permetent incorporar dominis peptídics citotòxics per a generar nanopartícules terapèutiques. Seguint aquesta estratègia, hem desenvolupat prèviament les nanotoxines T22-PE24-H6 i T22-DITOX-H6, que incorporen els dominis catalítics de l'exotoxina A de *Pseudomonas aeruginosa* i de la toxina diftèrica respectivament. En aquest treball, es demostra que totes dues nanotoxines presenten un efecte citotòxic

dependent de CXCR4 en cèl·lules tumorals de CECC. Cal destacar que es descriu per primera vegada la capacitat de totes dues nanotoxinas d'activar la piroptosi mediada per caspasa-3/GSDME, un tipus de mort cel·lular programada proinflamatòria, alternatiu a l'apoptosi. Aquest efecte citotòxic es tradueix en un potent efecte antitumoral *in vivo*, especialment en el cas de T22-DITOX-H6 que pràcticament frena el creixement tumoral, en absència de toxicitat en altres òrgans. Finalment, el tractament amb T22-DITOX-H6 és capaç de bloquejar la disseminació metastàtica als ganglis limfàtics cervicals, pulmons i fetge sense provocar alteracions histopatològiques en un model murí ortotòpic que reproduïx el patró de metàstasi dels pacients de CECC.

En resum, en la present tesi doctoral vam demostrar que les nanotoxines que incorporen el lligand T22 són capaces d'induir piroptosi en cèl·lules tumorals CXCR4⁺, un mecanisme de mort cel·lular alternatiu a l'apoptosi amb un gran potencial per a millorar el tractament dels pacients amb CECC metastàtic.

TABLE OF CONTENTS

Abbreviations	1
Introduction	6
1. Head and neck cancer.....	6
1.1. Risk factors.....	7
1.1.1. Smoking and alcohol.....	7
1.1.2. Human papillomavirus (HPV).....	8
1.1.3. Other risk factors.....	9
1.2. Epidemiology.....	9
1.3. Treatment.....	10
1.3.1. Early-stage disease.....	10
1.3.2. Locally advanced disease.....	11
1.3.3. Recurrent or metastatic disease.....	12
1.3.4. New therapies.....	12
1.3.5. Mechanisms of action of anticancer drugs.....	15
2. Cancer metastasis and cancer stem cells (CSCs).....	19
2.1. Changes in the primary tumor: acquisition of migration and invasion capacities.....	20
2.2. Intravasation and bloodstream circulation.....	22
2.3. Extravasation and homing.....	23
2.4. Colonization and development of metastasis.....	23
2.5. Cancer stem cells (CSCs) and therapies.....	24
3. CXCR4/CXCL12 axis.....	26
3.1. Chemokines and chemokine receptors.....	26
3.2. CXCR4 and its ligand CXCL12.....	27
3.2.1. CXCR4 structure and expression.....	27
3.2.2. CXCR4 ligand: CXCL12.....	27
3.2.3. CXCR4 signaling.....	27
3.3. CXCR4/CXCL12 axis in cancer.....	29
3.3.1. Proliferation, apoptosis, and tumor growth.....	30
3.3.2. Recruiting cells into the tumor microenvironment.....	30
3.3.3. Angiogenesis.....	31
3.3.4. Epithelial-mesenchymal transition (EMT).....	32
3.3.5. Matrix metalloproteinases activation.....	32

3.3.6. Distant metastasis and metastatic cancer stem cells (CSCs).....	33
3.3.7. CXCR4/CXCL12 as a therapeutic target for drug development.....	34
4. Targeted drug delivery for cancer treatment.....	37
4.1. Antibody drug conjugates (ADCs).....	38
4.2. Immunotoxins.....	39
4.3. Nanoparticles and nanocarriers.....	39
4.3.1. Passive targeting.....	40
4.3.2. Active targeting.....	41
4.3.3. Inorganic nanoparticles.....	42
4.3.4. Organic nanoparticles.....	42
4.3.5. Protein-based nanoparticles.....	44
4.3.5.1. Strategies for the development of protein-based nanoparticles.....	45
4.4. T22-based protein nanoparticles.....	48
4.4.1. T22-GFP-H6 nanocarrier.....	48
4.4.2. T22-PE24-H6 and T22-DITOX-H6 nanotoxins....	49
Research objectives.....	52
Results.....	55
Chapter 1: Self-assembling protein nanocarrier for selective delivery of cytotoxic polypeptides to CXCR4+ head and neck squamous cell carcinoma tumors.....	55
Chapter 2: CXCR4-targeted nanotoxins induce GSDME-dependent pyroptosis in head and neck squamous cell carcinoma.....	70
Chapter 3: A Novel CXCR4-Targeted Diphtheria Toxin Nanoparticle Inhibits Invasion and Metastatic Dissemination in a Head and Neck Squamous Cell Carcinoma Mouse Model.....	88
Discussion.....	104
Conclusions.....	113
List of publications.....	115
Annex: Supplementary information.....	116
Chapter 1: Self-assembling protein nanocarrier for selective delivery of cytotoxic polypeptides to CXCR4+ head and neck squamous cell carcinoma tumors.....	116

Chapter 2: CXCR4-targeted nanotoxins induce GSDME-dependent pyroptosis in head and neck squamous cell carcinoma.....	124
Chapter 3: A Novel CXCR4-Targeted Diphtheria Toxin Nanoparticle Inhibits Invasion and Metastatic Dissemination in a Head and Neck Squamous Cell Carcinoma Mouse Model.....	135
References.....	140

ABBREVIATIONS

5-FdU	5-Fluoro-2'-deoxyuridine
5-FU	5-Fluorouracil
ADC	Antibody-drug conjugate
ADCC	Antibody-dependent cellular cytotoxicity
AKT	Protein kinase B
ALDH1	Aldehyde dehydrogenase 1
ALL	Acute lymphocytic leukemia
APC	Antigen-presenting cell
AUC	Area under the curve
bFGF	Basic fibroblast growth factor
BLI	Bioluminescent signal
CAF	Cancer-associated fibroblast
CBC	Cell blood count
c-MET	Tyrosine-protein kinase Met or hepatocyte growth factor receptor (HGFR)
CRC	Colorectal cancer
CRE	Creatinine
cryo-EM	Cryo-electron microscopy
CSC	Cancer stem cell
CTC	Circulating tumor cell
CTLA-4	Cytotoxic T-Lymphocyte Antigen 4
CXCL12	C-X-C Motif Chemokine Ligand 12
CXCR4	Chemokine receptor 4
DAPI	4',6-diamidino-2-phenylindole
DFNA5	Non-syndromic hearing impairment protein 5
DITOX	Diphtheria toxin catalytic domain
DLBCL	Diffuse large B-cell lymphoma
DMEM	Dulbecco's Modified Eagle's Medium
ECM	Extracellular matrix
EDTA	Ethylenediaminetetraacetic acid
EF-2	Ribosomal elongation factor 2

EGF	Epidermal growth factor
EGFR	Epidermal growth factor receptor
EMT	Epithelial-mesenchymal transition
EPC	Epithelial precursor cell
EpCAM	Epithelial cell adhesion molecule
EPR	Enhanced permeability and retention
ERK	Extracellular signal-regulated kinase
FBS	Fetal bovine serum
FDA	Food and Drug Administration
FGFR	Fibroblast growth factor receptor
FLI	Fluorescence intensity
GFP	Green fluorescent protein
GOT	Glutamic oxaloacetic transaminase
GPT	Glutamic pyruvic transaminase
GSDM	Gasdermin
H&E	Hematoxylin & eosin
H6	Polyhistidine tag
HCT	Hematocrit
HER2	Human epidermal growth factor receptor 2
HGB	Hemoglobin
HGF	Hepatocyte growth factor
HIF-1	Hypoxia inducible factor 1
HIV	Human immunodeficiency virus
HL	Hodgkin lymphoma
HNSCC	Head and neck squamous cell carcinoma
HPV	Human papillomavirus
IC50	Half maximal inhibitory concentration
IHC	Immunohistochemistry
IL	Interleukin
INF γ	Interferon gamma
JAK	Janus kinase
KO	Knock-out

LDH	Lactate dehydrogenase
LN	Lymph node
M	Molar (mol/L)
mAb	Monoclonal antibody
MAPK	Mitogen-activated protein kinase
MCH	Mean corpuscular hemoglobin
MCHC	Mean corpuscular hemoglobin concentration
MCV	Mean cell volume
MEK	Mitogen-activated extracellular signal-regulated kinase
MFI	Mean fluorescence intensity
MMAE	Monomethyl auristatin E
MMP	Matrix metalloproteinase
MPS	Mononuclear phagocyte system
MPV	Mean platelet volume
MRD	Minimal residual disease
mTOR	Mammalian target of rapamycin
NAB	Nanoparticle albumin-bound
NF- κ B	Nuclear factor kappa B
NK	Natural killer
NSG	NOD-scid IL2R γ ^{null}
OS	Overall survival
OSCC	Oral squamous cell carcinoma
PAMD	Polymeric plerixafor
PARP	Poly (ADP-ribose) polymerase
PBD	Pyrrrolobenzodiazepine
PBS	Phosphate buffered saline
PCT	Plateletcrit
PD-1	Programmed cell death protein 1
PDC	Programmed cell death
PD-L1	Programmed death-ligand 1
PDW	Platelet distribution width
PDXs	Patient-derived tumor xenografts

PE	<i>Pseudomonas aeruginosa</i> exotoxin A
PEG	Polyethylene glycol
p-EMT	Partial epithelial-mesenchymal transition
PFS	Proliferation-free survival
PGK1	Phosphoglycerate Kinase 1
PI	Propidium iodide
PI3K	Phosphoinositide 3-kinase
PJVK	Pejvakin
PLGA	Poly(lactic-co-glycolic acid)
PSMA	Prostate-specific membrane antigen
Raf	Rapidly accelerated fibrosarcoma (receptor tyrosine kinase effector)
Ras	Rat sarcoma virus (GTPase)
RB	Retinoblastoma
RBC	Red blood cell count
RDW	Red blood cell distribution width
ROI	Region of interest
sALCL	Systemic anaplastic large cell lymphoma
SD	Standard deviation
SDF-1	Stromal cell-derived factor 1
SDS-PAGE	Sodium dodecyl sulfate polyacrylamide gel electrophoresis
SEM	Standard error of the mean
SMANCS	Neocarzinostatin (NCS) conjugated to poly(styrene-co-maleic acid) (SMA)
SPF	Specific pathogen-free
STAT	Signal transducer and activator of transcription
STR	Short tandem repeat
TAM	Tumor-associated macrophage
TBS	Tris-buffered saline
TBS-T	Tris-buffered saline-Tween
TCGA	The Cancer Genome Atlas
TGF- β	Transforming growth factor-beta
TNF- α	Tumor necrosis factor-alpha
UA	Uric acid

VCAM-1	Vascular cell adhesion molecule 1
VEGF	Vascular endothelial growth factor
VLP	Virus-like particle
WB	Western blotting
WBC	White blood cell
zVAD	Carbobenzoxy-valyl-alanyl-aspartyl-[O-methyl]- fluoromethylketone

INTRODUCTION

1. Head and neck cancer

Head and neck cancer includes all types of neoplasia that arise in different locations along the oral cavity, pharynx, larynx, nasal cavity, and sinuses (Figure 1). The vast majority of head and neck cancers (90%) are squamous cell carcinomas (HNSCC) that derive from the squamous cell epithelium that constitutes the mucosal lining of the upper aerodigestive tract (Marur et al., 2010; Argiris et al., 2018; Cramer et al., 2019).

HNSCC is a heterogeneous disease as primary tumors arise in widely diverse anatomical structures. Moreover, HNSCC tumors can also present different etiologies and molecular signatures with tumor cells ranging from differentiated keratinizing cells to undifferentiated cells (Marur et al., 2010; Leemans et al., 2018).

HNSCC can be classified according to the location of the primary tumor into (i) tumors of the oral cavity (including lips, tongue, gums, cheeks, mouth floor, and hard-palate), (ii) pharynx (further divided into nasopharynx, oropharynx, and hypopharynx), (iii) larynx, and (iv) paranasal sinuses and nasal cavity (Marur and Forastiere, 2008). The most common location is the oral cavity, particularly tumors emerging in the tongue, followed by the pharynx (Bray et al., 2018; Siegel et al., 2019; Sung et al., 2021) (Figure 1).

The most important clinical prognostic factor is the presence of lymph node metastases in the neck, which can affect up to 60-70% of patients depending on the location and extension of the primary tumor. The incidence of distant metastasis in HNSCC is small compared to other types of cancer, however, distant metastasis importantly determines patient survival and outcome. Besides, lymph node spread influences the rate of distant metastasis development, patients with advanced nodal disease have a higher incidence of distant metastasis. Primary tumor location also affects the frequency of distant metastasis, being higher for tumors located in the pharynx. The most common distant metastatic sites are the lungs, with an incidence of 70-85%, followed by bone (15-39%), and liver (10-30%). Other less frequent distant metastatic sites are the skin (1-2%) and the brain (0.4%) (Ferlito et al., 2001; Takes et al., 2012) (Figure 1).

Due to this heterogeneity, HNSCC patient clinical evolution and prognosis dramatically vary depending on many factors including the location of the primary tumor, tumor staging, and lymph node affectation (Argiris et al., 2018).

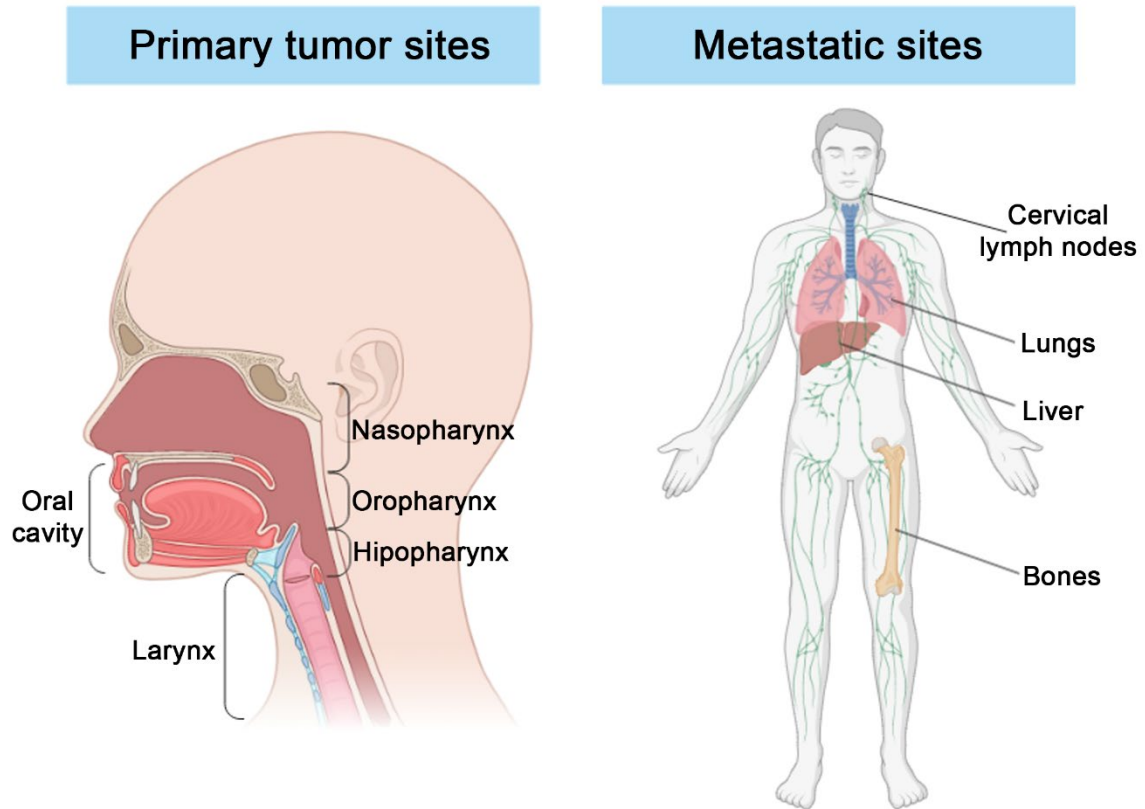


Figure 1. Frequent primary and metastatic tumor sites in HNSCC. Primary HNSCC tumors can arise at the oral cavity, larynx, and pharynx. Common metastatic sites include the cervical lymph nodes, lungs, and liver, although HNSCC can also spread to the bones, brain, and skin. Adapted from J. Cramer *et al.*, 2019 and L. Angus *et al.*, 2019 (Angus et al., 2019; Cramer et al., 2019). Created with BioRender.com.

1.1. Risk factors

1.1.1. Smoking and alcohol

Tobacco and alcohol are considered the classical risk factors for HNSCC. Smoking and alcohol consumption are related to 75% of all head and neck cancers with primary tumors mainly located in the oral cavity, oropharynx, hypopharynx, and larynx (Argiris et al., 2018; Cramer et al., 2019). Moreover, both factors display a synergistic effect with a 30-fold increased risk of developing HNSCC for individuals who both smoke and drink (Siegel et al., 2021). Smokeless tobacco and chewing betel quid, traditional in Southeast Asia, are also well-known risk factors for cancers of the oral cavity (Argiris et al., 2018; Siegel et al., 2021).

Head and neck cancers associated with alcohol and/or tobacco are characterized by many mutations and chromosomal aberrations, being losses of chromosomes 3p, 9p and mutations of TP53 the most common alterations. Chromosome arm 9p includes the tumor suppressor gene CDKN2A, which encodes the p16 protein that mediates cell cycle arrest. Loss of CDKN2A drives cells through the G1–S checkpoint of the cell cycle contributing to uncontrolled DNA replication. TP53 inactivation is also frequent in HNSCC, with somatic mutations in the TP53 gene found in 84% of human papilloma virus negative (HPV⁻) tumors. P53 protein is a crucial tumor suppressor participating in cell cycle arrest and apoptosis induction upon DNA damage. Another common mutation is the amplification of CCND1, present in 30-50% of head and neck cancers. This oncogene encodes cyclin D1 which is involved in cell-cycle progression. Besides proteins involved in the cell cycle, genes encoding several growth factor receptors are mutated in HNSCC. In this regard, epidermal growth factor receptor (EGFR) expression is highly expressed in more than 90% of HNSCCs (Marur et al., 2010; Leemans et al., 2018).

1.1.2. Human papillomavirus (HPV)

In the last decades, there has been an increase in the incidence of oropharyngeal cancer, especially among young white men in Western countries. These higher rates have been related to human papilloma virus (HPV) infection, which is displayed in 72% of oropharyngeal tumors in certain geographical areas (Argiris et al., 2018; Cramer et al., 2019). HPV⁺ tumors are mainly located in the base of the tongue and tonsils. More than 90% of HPV⁺ tumors are caused by HPV-16, which is also associated with other virus-related cancers (Marur et al., 2010; Leemans et al., 2018).

HPV-related HNSCC incidence is rapidly increasing, representing 40-80% of all oropharyngeal cancers in the USA and being the primary cause of tonsillar cancer in North America and Europe (Marur et al., 2010; Leemans et al., 2018). Currently, oropharyngeal cancer is the most common HPV-associated cancer, surpassing cervical cancer incidence in the USA (Senkomago et al., 2019).

HPV is transmitted through unprotected sexual contact, thus HPV⁺ head and neck cancers have been related to oral sex practices. Prevention includes HPV vaccination, which is suggested to reduce oral HPV infection by 88–93% (Cramer et al., 2019). However, immunization rates are still low with only 51% of 13 to 17-year-old teenagers vaccinated in the USA in 2018 (American Cancer Society. Cancer Facts & Figures 2020.).

HPV⁺ head and neck tumors clearly differ from the ones related to alcohol and tobacco consumption. This type of tumors is poorly differentiated (non-keratinizing) with basaloid

histology (Argiris et al., 2018). Moreover, their genetic profile is characterized by p53 downregulation, retinoblastoma RB pathway inactivation, and p16 upregulation; opposite characteristics compared to the tumors associated with alcohol and tobacco. Importantly, these patients present better prognosis than HPV⁻ patients, as HPV⁺ tumors have a higher response rate to chemotherapy and radiotherapy (3-year overall survival (OS) 82.4% versus 57.1%) (Marur et al., 2010; Vokes et al., 2015; Leemans et al., 2018; Cramer et al., 2019).

Altogether, it is clear that HPV status should be taken into consideration at the time of diagnosis. In this context, p16 immunostaining has been recently included in the HNSCC staging system, differentiating between HPV⁺ and HPV⁻ oropharyngeal cancers (Marur et al., 2010; Vokes et al., 2015; Leemans et al., 2018).

1.1.3. Other risk factors

Although alcohol, tobacco, and HPV are the three major risk factors for the development of HNSCC, there are other agents that, despite being less frequent, deserve to be considered.

HNSCC is mainly related to external and environmental factors. Oral health has been described as a risk factor, relating poor oral hygiene with a higher risk of developing oral cancers. Moreover, HNSCC has also been related to radiation and occupational exposure (wood, asbestos, formaldehyde, etc.) (Argiris et al., 2018). Importantly, Epstein-Barr virus (EBV) has been strongly associated with nasopharyngeal and salivary gland cancers, being endemic in certain areas of Southern China (Tsao et al., 2017). Lastly, immunosuppressed patients due to poor nutrition, advanced age, immunosuppressive treatment or AIDS, also have an increased risk of developing oropharyngeal cancer (Shaw and Beasley, 2016).

Besides environmental agents, several genetic factors have been also related to HNSCC. In this context, familiar inheritance has been associated with a small subset of HNSCC patients that exhibit p16 mutated, a somatic mutation related to other types of cancer as well. Moreover, genetic polymorphisms in enzymes involved in tobacco and alcohol metabolism have also been proposed to be related to a higher risk of developing HNSCC (Suárez et al., 2006; Argiris et al., 2018). Last but not least, some cancer susceptibility syndromes exhibit an increased risk of developing HNSCC including hereditary non-polyposis colorectal cancer, Fanconi anemia, ataxia telangiectasia, Bloom's syndrome, and Li-Fraumeni syndrome (Shaw and Beasley, 2016).

1.2. Epidemiology

HNSCC is currently the 7th most common cancer worldwide, accounting for approximately 5% of all new cancer cases in the world. In 2020, more than 850,000 new cases and

400,000 deaths were registered worldwide, comprising around 5% of all cancer deaths (Sung et al., 2021).

The most common head and neck cancers are located in the oral cavity (39%) and pharynx (34%), and the incidence is higher among men compared to women (2-fold). Despite the reduction of alcohol and tobacco consumption especially in developed countries, HNSCC incidence is increasing worldwide due to an increment in HPV⁺ cancers mainly related to unprotected oral sex practices. Demographics of HPV⁺ HNSCC are also different, presenting a higher incidence in younger men compared to patients with alcohol and smoking-related head and neck tumors (Cramer et al., 2019). Importantly, HNSCC is very common in Southeast Asia being the leading cause of cancer mortality among men in India, Pakistan, Sri Lanka, and Bangladesh, which correlates with betel quid frequent consumption in these countries (Bray et al., 2018; Sung et al., 2021).

Despite the therapeutic advances, HNSCC 5-year relative survival rate has only slightly improved for patients in the last decades, being 66% in 2021 (Siegel et al., 2021). The main problem with head and neck cancers is the fact that approximately 70% of patients are diagnosed at loco-regional or advance stages. Furthermore, depending on the location and extent of the tumor, up to 60% of patients with HNSCC will develop loco-regional recurrence and/or distant metastasis, with a median overall survival (OS) being less than one year for these patients (Sacco and Cohen, 2015).

1.3. Treatment

Current treatment choice for HNSCC depends on different factors, including the location of the primary tumor and the stage of the disease. Importantly, the main goal is to achieve a high cure rate while still preserving vital structures and their functions, focusing on the importance of organ preservation. As has been already discussed, HPV⁺ head and neck patients present excellent survival outcomes and treatment responses. Thus, we are going to focus on HPV⁻ HNSCC, which represents the vast majority of head and neck cancers and display lower survival rates.

1.3.1. Early-stage disease

One-third of all HNSCC patients are diagnosed at stage I or II, presenting localized primary tumors that do not invade adjacent structures with small (<6 cm) and/or few lymph node metastasis (Deschler et al., 2014; Leemans et al., 2018; Lydiatt et al., 2018). Treatment for these patients consists of a single therapeutic approach, either surgery or radiation. Treatment election mainly varies depending on the location of the primary tumor. For tumors located in the oral cavity, surgery and radiotherapy can be used, but surgery is generally

preferred as it allows staging (biopsy can be collected) and avoids the toxic effects of radiotherapy. In contrast, laryngeal and pharyngeal tumors are usually treated with radiotherapy, as tumor resection is complex. However, in the last decades advances in surgical techniques allow for minimally invasive surgical treatment options and endoscopic surgery which are associated with lower patient morbidity (Robert I. and Shin, 2008; Argiris et al., 2018; Cramer et al., 2019).

Treatment for early-stage patients is very effective, resulting in 90% of stage I and 70% of stage II patients cured. However, these patients are still at high risk for recurrence and development of second primary tumors (Robert I. and Shin, 2008).

1.3.2. Locally advanced disease

Most HNSCC patients (around 70%) exhibit locally advanced disease at diagnosis, importantly affecting their prognosis, treatment, and survival. At this stage, the primary tumor invades adjacent structures and the lymph node affection aggravates (Deschler et al., 2014; Leemans et al., 2018; Lydiatt et al., 2018). Surgery, radiotherapy, and chemotherapy are usually the treatments of choice.

Surgery aims to remove the primary tumor and lymph node metastasis. Over the last few years, the trend in surgery has been to achieve complete tumor excision using more conservative approaches and to use reconstructive techniques in order to preserve organ function (Cramer et al., 2019).

The implementation of concurrent chemoradiotherapy in the last decade was a major advance for patient treatment. It consists of the simultaneous administration of both chemotherapy and radiotherapy, either without previous initial surgical resection or after surgery. Concomitant treatment has improved loco-regional control but has not shown any effect on distant recurrence rate and induces important toxic effects. Currently, it is the standard treatment for patients with unresectable primary tumors or after resection when the patient presents risk of developing loco-regional recurrence (Robert I. and Shin, 2008; Argiris et al., 2018).

Another therapy that has shown promising results is induction (neoadjuvant) chemotherapy, consisting of a combination of docetaxel, cisplatin, and fluorouracil (5-FU). This therapy has improved loco-regional control (20-40% response rates) and has slightly lowered the rate of distant metastasis; thus, it has been approved as first-line treatment for patients with operable or inoperable primary tumors. However, induction chemotherapy does not affect overall survival and has dramatically increased the rate of morbidity (Robert I. and Shin, 2008; Argiris et al., 2018; Cramer et al., 2019).

Moreover, despite the advances in the treatment, 5-year overall survival is still 49-25% and at least 50% of these patients will develop loco-regional recurrence and/or distant metastasis (Cramer et al., 2019).

1.3.3. Recurrent or metastatic disease

HNSCC is generally considered a loco-regional disease, with only 5% of patients with distant metastasis at presentation (de Bree et al., 2018). However, up to 60% of patients develop loco-regional recurrence and up to 30% distant metastasis after treatment. Importantly, the median overall survival for recurrent or metastatic patients remains less than one year (Sacco and Cohen, 2015). In most cases, HNSCC patients who develop recurrent and/or distant disease are no longer candidates for curative therapy and the main goals are palliation and prolongation of patient survival (Argiris et al., 2018; de Bree et al., 2018). Palliative treatment is mainly based on platinum-derived drugs (cisplatin, carboplatin, etc.), including platinum doublets (combination of a platinum drug with taxanes (paclitaxel and docetaxel), gemcitabine, vinorelbine, or irinotecan). However, the use of platinum doublets has not improved patient survival and has increased treatment toxicity. After cetuximab's approval (EGFR inhibitor) in 2006, the EXTREME regimen became the best therapeutic solution for these patients. This regimen consists of the combination of a platinum-based drug, 5-FU, and cetuximab, showing a 30% response rate, a median patient free survival of 3-4 months, and an overall survival of 6-8 months (Sacco and Cohen, 2015). However, the approval of anti-PD-1 immune checkpoints pembrolizumab and nivolumab in 2016 changed the paradigm for the treatment of recurrent and/or metastatic patients. After the phase III KEYNOTE-048 trial, pembrolizumab alone or with chemotherapy was established as the first-line treatment for recurrent and/or metastatic HNSCC patients. However, only 15-20% of patients benefit from the anti-PD-1 treatment, highlighting the urge for markers predictive of response to immune checkpoints inhibitors and for novel therapeutic solutions (Mehra et al., 2018; Bauml et al., 2019; Pei et al., 2021; Shibata et al., 2021).

1.3.4. New therapies

Current research is mainly focusing on the development of novel therapies for recurrent and metastatic HNSCC, which are responsible for the high mortality of this disease. Classic HNSCC treatment comprises chemotherapy that does not achieve curation for most patients and is associated with systemic toxicity. Cetuximab's approval in 2006 opened the door for the use of molecularly targeted therapies in HNSCC. These therapies take advantage of the preclinical and clinical observations that tumor cells, despite exhibiting a plethora of genetic alterations, are mainly dependent on a single oncogenic pathway. This

concept, known as “oncogene addiction” (Weinstein, 2002), was exploited to inhibit different oncogenes that are critical for the proliferation and survival of cancer cells (Sharma and Settleman, 2007; Luo et al., 2009; Pagliarini et al., 2015).

Epithelial growth factor receptor (EGFR) was the first explored target as it is highly overexpressed in many epithelial cancer cells. In HNSCC, up to 90% of tumors present EGFR overexpression and high levels of this protein correlate with decreased survival. In consequence, the first molecularly targeted drug to be approved for HNSCC treatment was cetuximab, a chimeric IgG1 monoclonal antibody (mAb) that competitively inhibits ligand binding to EGFR, leading to EGFR internalization and altering EGFR dependent signaling. Moreover, cetuximab also displays immunostimulatory capacity (ADCC). Nevertheless, mucositis (inflammation of the gastrointestinal tract), stomatitis (inflammation of the mouth and lips), and dermatitis have been observed in patients undergoing this treatment. These secondary effects are similar to or even greater than those observed in patients treated with chemoradiotherapy, showing no benefits in the substitution of chemotherapy with cetuximab in terms of toxicity (Sakashita et al., 2015). Cetuximab is also used for recurrent and/or metastatic patients as monotherapy, achieving a 13% response rate. Moreover, when combined with chemotherapy, it improves response rates, progression-free survival (PFS), and overall survival (OS) (EXTREME regimen). However, low response rates and the development of resistance to cetuximab, highlight the need to develop novel drugs (Braig et al., 2017; Muraro et al., 2021).

In this framework, other EGFR-targeted therapies have been evaluated, such as mAbs panitumumab, zalutumumab, and imgatuzumab, which induce a modest tumor response but do not show a notable clinical activity in patients with HNSCC. Small molecules and antisense oligonucleotides are also being developed to bind to the intracellular EGFR domain to inhibit the downstream components of the receptor signaling cascades. Moreover, other molecular targets are being explored in this context including mTOR (activated in >70% of HNSCC patients) and STAT (activation of these transcription factors is associated with a negative prognosis). Importantly, current clinical studies using mTOR inhibitors as monotherapy have induced modest clinical effects and no significant benefit for patients (<https://clinicaltrials.gov>; Santuray et al., 2018).

Importantly, molecularly targeted therapies present variable response rates, as not all patients respond to these therapies to the same extent. Moreover, although exhibiting a robust initial response to the treatment, chronic exposure to the targeted molecule usually generates therapy resistance leading to recurrence. Data indicate that cancer cells develop

mutations in different pathway components or are capable of bypassing the signaling pathway, thus becoming resistant to the treatment (Pagliarini et al., 2015).

Last but not least, in recent years immunotherapy has received attention as a novel strategy for cancer treatment. This therapy is based on the fact that tumor cells are able to evade the immune system through alterations in immune surveillance either in cancer cells and/or tumor microenvironment. In fact, the immune system is recognized as a key player in the development, establishment and spread of HNSCC. There are two main immunotherapeutic strategies: (i) inhibition of immunosuppressive signaling and (ii) promotion of immunostimulatory signaling. The approval of pembrolizumab and nivolumab in 2016 for the treatment of HNSCC patients who developed platinum-refractory recurrent and/or metastatic disease, unleashed a new era for immunotherapy in HNSCC. Both mAbs target PD-1, a receptor expressed on the membrane of T cells which upon activation leads to proliferation arrest and apoptosis of T lymphocytes. Pembrolizumab and nivolumab achieve an improved response and overall survival (OS) with a better toxicity profile compared to chemotherapy. Importantly, in both treatments, a substantial minority of patients show durable survival benefits. Moreover, durvalumab, an antibody against programmed cell death 1 ligand 1 (PD-L1), has shown promising response rates in a phase I/II trial for advanced-stage disease (<https://clinicaltrials.gov>; Santuray et al., 2018; Cramer et al., 2019; Piechutta and Berghoff, 2019). Similarly, mAbs targeting CTLA-4 (checkpoint receptor protein that inhibits T cell activation) such as ipilimumab are in clinical trials. Following the second strategy, several mAbs are currently being investigated by targeting CD40 costimulatory receptor expressed on antigen-presenting cells (APCs) like selicrelumab or SEA-CD40 among others (<https://clinicaltrials.gov>; Santuray et al., 2018; Piechutta and Berghoff, 2019). Despite the improvements in OS with pembrolizumab and nivolumab in HNSCC, the response rates for both treatments remain low (<20%) as most patients do not respond to a single agent anti-PD-1 therapy and those who respond do not benefit to the same extent (Prat et al., 2017; Santuray et al., 2018). Thus, several clinical trials are evaluating combination therapies. Combinations of anti-CTLA-4 and anti-PD-1 agents have shown a synergistic effect in melanoma patients and are undergoing phase II clinical trials for HNSCC patients. Moreover, current immunotherapy treatment also induces important side effects. In contrast to standard chemotherapy agents, immunotherapy side effects are related to autoimmunity, being autoimmune endocrinopathies the most common secondary effects for anti-PD-1 agents. Remarkably, the anti-CTLA-4 agent ipilimumab shows even more important side effects than anti-PD-1 treatment, including pneumonitis and colitis (Moskovitz and Ferris, 2018).

Cancer vaccines have also shown remarkable potential as this approach reduces cancer immune escape by enhancing the functions of APCs. Multiple therapeutic vaccines are under investigation in phase I/II trials for HNSCC patients with promising results both alone and in combination with chemoradiotherapy (Tan et al., 2018; Cramer et al., 2019).

Altogether, these therapeutic advances have not yet reached patients cure and still present important toxic side effects (Fojo and Parkinson, 2010; Dy and Adjei, 2013). Nevertheless, these novel therapies highlight the potential of targeted therapies in HNSCC treatment, as for the first time in decades, novel treatments are slightly improving patient's outcome. Thus, there is still an important therapeutic opportunity to develop more effective strategies for the treatment of recurrent and metastatic HNSCC patients.

1.3.5. Mechanisms of action of anticancer drugs

Classical chemotherapy is a broad term that includes different drugs that induce cytotoxicity in dividing cells, interfering with their normal cell division, and ultimately leading to cell death. Chemotherapy is based on the fact that cancer cells display a high proliferation rate and exploit their enhanced sensitivity to DNA damage, but it does not specifically target malignant cells, thus inducing severe side effects in healthy tissues (Luo et al., 2009). Chemotherapeutic drugs can be divided into different categories, including alkylating agents, such as cisplatin (Shaloam and Tchounwou, 2014); antimetabolites, such as 5-FU and gemcitabine (Avendaño et al., 2008); and microtubule inhibitors, including taxanes and vinorelbine (Nabors et al., 2016), all of them currently used for the treatment of HNSCC among other cancer types (Sacco and Cohen, 2015; Cramer et al., 2019).

On the other hand, the recently developed molecularly targeted therapies mainly comprise two types of molecules: monoclonal antibodies (mAbs) and small molecule inhibitors. In contrast to conventional chemotherapy, molecularly targeted drugs do not contain any cytotoxic compound. Their mechanism of action is based on their interaction with different cellular pathways that are deregulated in cancer such as oncogenes, either by blocking or activating signals that alter cell growth, cell cycle regulation, and cell death among others (Luo et al., 2009; Baudino, 2015; Lee et al., 2018). Interestingly, in the 2000-2015 period most of the FDA approved drugs for oncology use were targeted agents, highlighting the relevance of this strategy (Pérez-Herrero and Fernández-Medarde, 2015). However, as previously mentioned, molecularly targeted drugs have achieved small benefits in terms of therapeutic effect, while still displaying toxic side effects and triggering the development of therapeutic resistance by target cancer cells (Fojo and Parkinson, 2010; Dy and Adjei, 2013).

Up to date, conventional drug development has focused on the activation of the apoptotic pathway to eliminate cancer cells. However, in recent years other types of programmed cell death (PCD) apart from apoptosis, have been found to be involved in cancer (Gong et al., 2019; Nagarajan et al., 2019; Fang et al., 2020). One of the hallmarks of cancer cells is their ability to evade apoptosis, partially explaining the incapacity of most cytotoxic and molecularly targeted therapies to completely eliminate tumor cells (Holohan et al., 2013; Okushi et al., 2015). In HNSCC, one of the mechanisms leading to both chemotherapy and radiotherapy resistance is the ability of cancer cells to escape apoptosis (Picon and Guddati, 2020; Kanno et al., 2021). Thus, apoptosis resistance has emerged as a major problem leading to therapeutic failure during cancer treatment. In this context, triggering other types of PCD to bypass the apoptotic pathway has become a promising approach to develop more efficient cancer treatments (Gong et al., 2019; Nagarajan et al., 2019; Fang et al., 2020).

Cell death can be classified into necrosis and PCD. Necrosis is a passive, accidental form of cell death generally caused by an environmental perturbation, in which the cell membrane integrity is lost, leading to increased permeability, cell swelling, and ultimately to the uncontrolled release of the cellular content, causing inflammation (Nagarajan et al., 2019; Xia et al., 2019). On the other hand, PCD is considered to be a regulated and controlled process that occurs during specific events, such as upon pathological stimuli.

Apoptosis is by far the most studied and well-known type of PCD. The apoptotic pathway is characterized by cell shrinkage, with nuclear and cytoplasmic condensation, preserving the integrity of the plasma membrane and leading to the formation of apoptotic bodies. Unlike necrosis, apoptosis generally does not induce inflammation as no cellular leakage is produced. Many stress and damage signals can trigger apoptosis, including nutrient deprivation, oxidative stress, and chemotherapy (Singh et al., 2019; Carneiro and El-Deiry, 2020). These signals lead to the activation of proteins of the caspase family that can act as initiators (caspases 8, 9, and 10) or effectors (caspases 3, 6, and 7) of the apoptotic pathway. Initiator caspases activate effector caspases, leading to the proteolytic cleavage of thousands of proteins and the formation of the apoptosome, and at last to the breakdown of the nuclear membrane and the genomic DNA (Singh et al., 2019; Carneiro and El-Deiry, 2020) (Figure 2).

However, more recently other types of PCD have raised attention as they have been related to different pathological conditions including nervous system diseases, infectious diseases, autoimmune diseases, cardiovascular diseases, and remarkably cancer. In this context, in

the last years cancer research has focused on other types of PCD, more specifically pyroptosis (Yu et al., 2021).

Pyroptosis is a pro-inflammatory type of PCD mediated by gasdermins. The gasdermin superfamily includes gasdermin A (GSDMA), gasdermin B (GSDMB), gasdermin C (GSDMC), gasdermin D (GSDMD), gasdermin E (GSDME) also known as DFNA5, and DFNB59 (Pejvakin, PJVK). All these proteins, except for PJVK, present two conserved domains in their structures, the N-terminal pore-forming domain and the C-terminal repressor domain. In normal conditions, gasdermins are inactive by the interaction of the N-terminal and the C-terminal domains, which results in the inhibition of the pore-forming domain. Upon extra or intracellular stimuli, different caspases or granzymes can cleave these gasdermins, releasing the N-terminal from the C-terminal domain. Once the N-terminal domain is dissociated, it oligomerizes with other N-terminal domains leading to the formation of pores in the cell membrane, inducing pyroptosis (Yu et al., 2021). Pyroptosis is characterized by cell swelling, plasma membrane lysis, chromatin fragmentation and release of the intracellular content which causes inflammation. Despite sharing some aspects, pyroptosis strongly differs from its apoptotic counterpart. Pyroptotic cells exhibit swelling and a lot of bubble-like protrusions on the surface of the cellular membrane before its rupture. Moreover, the formation of pores in the plasma membrane (1–2 μm in diameter) allows the release of mature IL-1 β and IL-18, leading to inflammation. At the same time, water enters through these pores causing cell swelling and osmotic lysis, resulting in cell rupture and cell content release, further promoting inflammatory responses (Figure 2). As a consequence, pyroptotic cells are permeable to low molecular weight dyes, such as propidium iodide (PI), while also maintaining Annexin V staining, which binds to the phosphatidylserine present in the cell membrane. In addition, during both apoptosis and pyroptosis cells undergo chromatin condensation and DNA fragmentation, but in the pyroptotic pathway the nuclear membrane remains intact and the intensity of DNA damage is lower compared to apoptotic cells, displaying random DNA fragmentation (Nagarajan et al., 2019; Fang et al., 2020; Yu et al., 2021).

Different stimuli can activate pyroptosis, including bacteria, viruses, toxins, and chemotherapeutic drugs, that induce caspase activation leading to gasdermin pore formation. Importantly, although pyroptosis was considered to be mediated exclusively via caspase-1, recent studies have discovered that a plethora of caspases, including caspase-3/4/5/6/8/9/11, are also capable of activating pyroptosis via gasdermin cleavage (Yu et al., 2021). Among the gasdermin superfamily, GSDMD and GSDME are the most studied members.

GSDMD was the first gasdermin to be associated with pyroptosis in 2015 (Shi et al., 2015). GSDMD is capable of exerting pyroptosis via two mechanisms: (i) the canonical pathway, and (ii) the non-canonical pathway. The canonical pathway is mediated by the formation of a protein complex known as the inflammasome, which leads to the activation of caspase-1. On the other hand, in the non-canonical pathway the inflammasome directly activates caspase-4/5. In both pathways, these caspases activate GSDMD and the pro-inflammatory interleukins IL-1 β and IL-18, inducing pyroptosis (Nagarajan et al., 2019; Fang et al., 2020; Raudenská et al., 2021; Yu et al., 2021).

Another way to activate pyroptosis is the caspase-3/Gasdermin E (GSDME) pathway. The ability of GSDME to initiate pyroptosis in response to chemotherapy was first described in 2017 (Wang et al., 2017). In this pathway, the activation of caspase-3, either by mitochondrial intrinsic pathway or via death receptor, catalyzes the cleavage of GSDME into the N-terminal domains that form pores in the cell membrane, thus inducing pyroptosis (Raudenská et al., 2021; Yu et al., 2021). Interestingly, many currently used chemotherapeutic drugs and targeted therapies are capable of activating caspase-3/GSDME pyroptosis, including cisplatin and paclitaxel among others (Lu et al., 2018; Kong et al., 2019; Zhang et al., 2019, 2020a, 2020b). Importantly, some studies have reported that GSDME expression is silenced in tumor cells, while some normal tissues express GSDME. Given its tumor suppressive role, it has been hypothesized that cancer cells silence GSDME to avoid cell death. Thus, the activation of this pathway in normal tissues might be responsible for the severe off-target toxicities observed in current chemotherapeutic treatments (Wang et al., 2017).

Recently, pyroptosis has been related to various human diseases, especially cancer, including HNSCC (Huang et al., 2017; Chen et al., 2018). Pyroptotic activation has been observed in different types of cancer *in vivo*, which suggests its implication in the tumorigenic process. Moreover, several studies have shown that some components of the pyroptotic pathway can inhibit cancer progression (Wang et al., 2019; Xia et al., 2019). Thus, pyroptosis has been proposed as an alternative strategy to apoptosis to overcome therapy resistance. In addition, being an pro-inflammatory PCD, pyroptosis activation might attract immune cells to the tumor site, including tumor-infiltrating natural killers (NK), CD8⁺ T-lymphocytes, and tumor-associated macrophages (TAMs), further contributing to the antitumor effect (Zhang et al., 2020c; Raudenská et al., 2021; Yu et al., 2021). For instance, a recent study has proved that GSDME acts as a tumor suppressor by activating pyroptosis, enhancing the phagocytosis of tumor cells by tumor-associated macrophages (Zhang et al.,

2020c). Thus, the development of novel therapies capable of activating pyroptosis in cancer cells represents an enticing avenue of research to overcome therapy resistance.

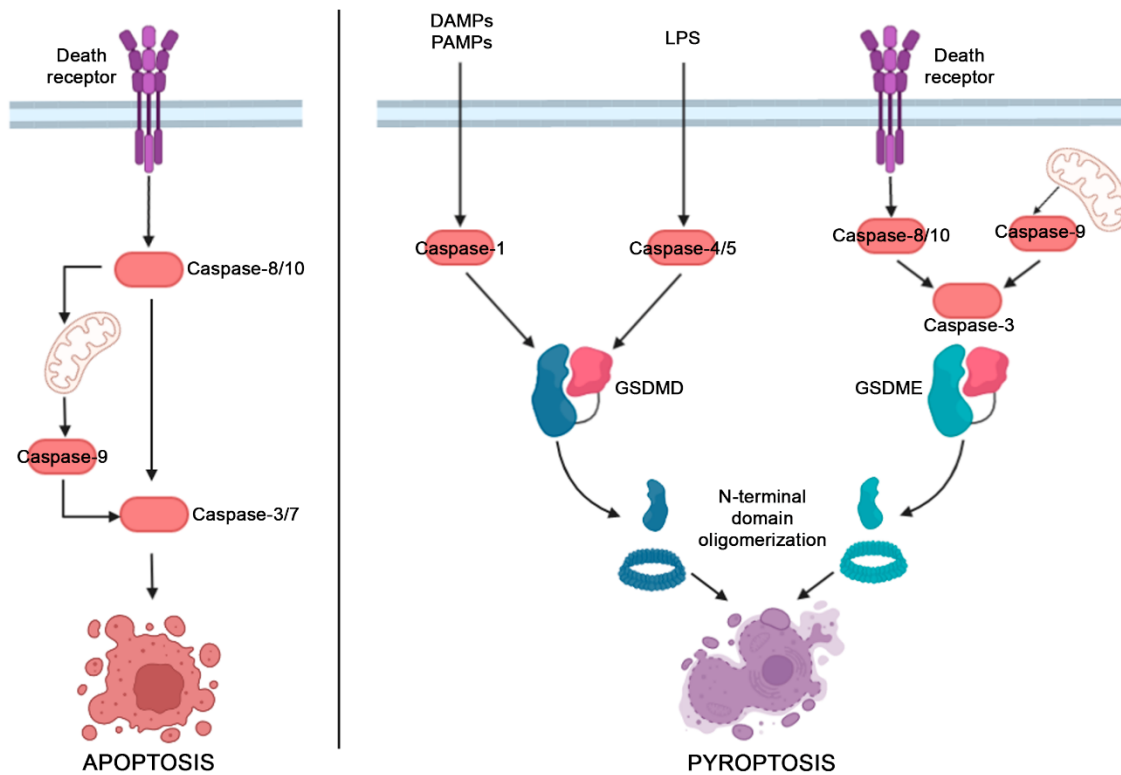


Figure 2. Comparison between the apoptotic and the pyroptotic signaling pathways. Recently, other PCD pathways apart from apoptosis have been related to cancer, including pyroptosis. These mechanisms of cell death represent a promising target for the development of novel cancer treatments. Adapted from Raudenská et al. 2021 (Raudenská et al., 2021). Created with BioRender.com.

2. Cancer metastasis and cancer stem cells (CSCs)

The development of secondary tumors in organs distant from the primary site is known as metastasis. The metastatic process is a highly complex chain of events that involves changes in tumor cells as well as in the tumor microenvironment, which finally lead to the development of metastasis located far away from the primary tumor site. The different processes that conduct tumor cells towards metastasis have been widely studied in the last decades, as metastasis has a huge clinical relevance being responsible for 90% of patient deaths from solid tumors (Gupta and Massagué, 2006; Chaffer and Weinberg, 2011).

In order to develop distant metastasis, cancer cells must acquire new properties to overcome different barriers: (i) invasion of surrounding tissues, (ii) entry into the vasculature of lymph and blood systems (intravasation), (iii) survival and circulation in the bloodstream, (iv) exit the bloodstream (extravasation), (v) survival in the microenvironment of the distant

organ (homing), (vi) adaptation to the new tissue allowing cell proliferation and formation of a secondary tumor (colonization). Importantly, these barriers act as a selective pressure that selects for clones with fitness to colonize distant organs (Gupta and Massagué, 2006; Chaffer and Weinberg, 2011) (Figure 3).

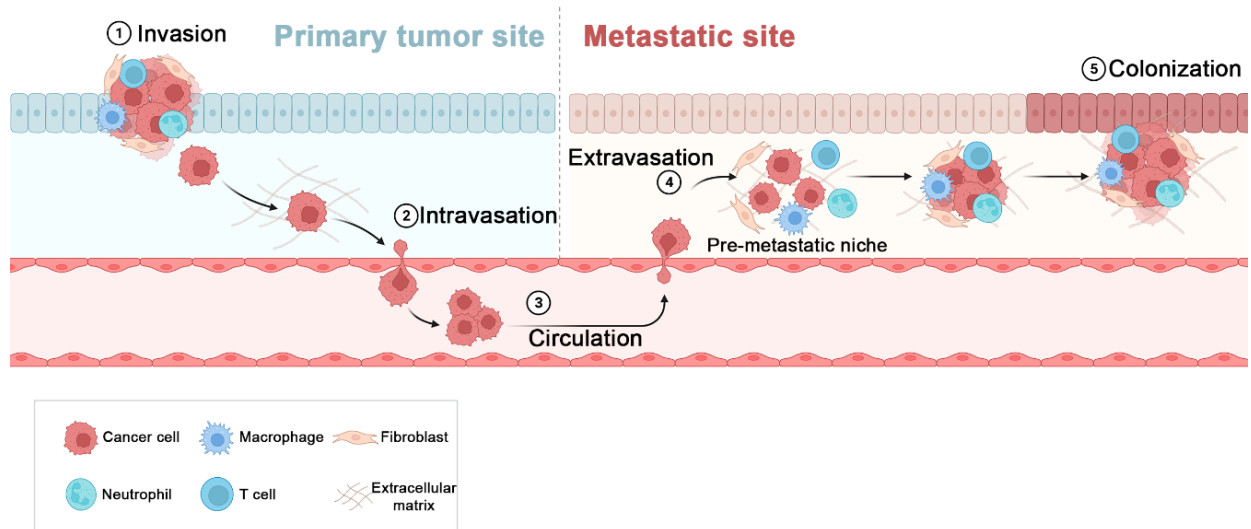


Figure 3. Schematic representation of the different steps involved in the development of distant metastasis. Tumor cells within the primary tumor acquire a cancer stem cell phenotype that enables their translocation to distant organs where they can establish distant metastasis. Created with BioRender.com.

2.1. Changes in the primary tumor: acquisition of migration and invasion capacities

Cancer arises from the accumulation of mutations that ultimately lead to the development of a malignant phenotype. These mutant clones evolve and are subjected to further genetic and epigenetic alterations and microenvironmental pressure, promoting the selection of clones that have acquired the different “hallmarks of cancer”, such as unlimited proliferation potential, resistance to antiproliferative and apoptotic cues, or metastatic potential. Many of these phenotypic traits are caused by the activation of different oncogenes and/or the silencing of tumor suppressors, that regulate different programs related to proliferation, migration, apoptosis, or differentiation, among others. Interestingly, cancer cells reactivate these programs that are normally used during embryogenesis and development to acquire different phenotypic traits (Luo et al., 2009; Prasetyanti and Medema, 2017).

Despite the increasing mechanistic understanding of cancer initiation and progression, whether the acquisition of malignant traits is required only by a specific cell population remains a subject of debate. The cancer stem cell (CSC) hypothesis states that only certain cells have the ability to initiate and propagate tumors (Reya et al., 2001; Batlle and Clevers,

2017). This hypothesis is based on the observation that most solid neoplastic tissues are not homogeneous, presenting intratumor heterogeneity, with multiple genetically and epigenetically distinct tumor cell subpopulations within the same tumor (Celià-Terrassa and Kang, 2018). This subset of cancer cells, called cancer stem cells (CSCs) is characterized by enhanced tumor-initiating potential compared to other cells within the tumor, self-renewal capacity, and the ability to differentiate and generate non-CSC cancer cells. Despite representing a small proportion of malignant cells, CSCs would be responsible for tumor initiation. Moreover, they acquire several properties, such as motility, invasiveness, and apoptosis resistance which support their involvement in metastatic development (Dalerba and Clarke, 2007; Chaffer and Weinberg, 2011; Ayob and Ramasamy, 2018). However, compelling data suggest that in many cancer types, CSC hierarchies are not rigid, pointing towards CSC plasticity, where CSCs and non-CSCs might interconvert upon different stimuli (Batlle and Clevers, 2017).

Besides the transformed epithelial cancer cells themselves, tumor microenvironment also plays a key role in tumor progression and metastasis. In normal conditions, stromal tissue confers a tumor-suppressive environment (lack of nutrients, hypoxia, physical barriers, etc.). However, some tumor cells are able to proliferate in this tumor microenvironment, as it generates a selective pressure leading to the clonal selection of a tumor aggressive phenotype (e.g. intratumor hypoxia leads to the expression of HIF-1 that activates genes promoting angiogenesis, cell survival, and invasion) (Gupta and Massagué, 2006).

Crosstalk between the tumor microenvironment and cancer cells is also crucial for tumor progression and the acquisition of migration and invasion capacities. The activation of the epithelial-to-mesenchymal transition (EMT) involves the interaction of tumor cells with stromal cells. Carcinoma cells undergoing EMT exhibit a diminished intercellular adhesiveness (e.g., loss of E-cadherin expression) and greater motile properties, thus enhancing cell migration. EMT confers cancer cells with a CSC-like phenotype that leads to a greater metastatic potential. Importantly, recent studies have questioned the indispensability of EMT for metastatic development (Shamir et al., 2014; Fischer et al., 2015). However, data accumulate suggesting that EMT in cancer cells might be transient, with cancer cells adopting reversible intermediate mesenchymal states, known as partial-EMT (p-EMT), depending on environmental cues (Jolly et al., 2015; Nieto et al., 2016; Pal et al., 2021). These observations support once again the plasticity of the CSC phenotype, against the classic CSC hierarchy.

Moreover, cancer cells are able to recruit a variety of cell types into the surrounding stroma, such as fibroblasts, granulocytes, macrophages, mesenchymal stem cells, and

lymphocytes; creating an inflammatory microenvironment that results in the release of EMT-inducing signals. In addition, tumor stroma also mediates the activation of the expression of different proteases, such as metalloproteinases (MMPs) that are able to degrade the extracellular matrix (ECM) and disrupt the basement epithelial membrane, leading to an increased migration capacity for cancer cells. Carcinoma-associated fibroblasts (CAFs) can secrete factors that promote tumor cell growth and invasiveness and also angiogenesis through recruitment of endothelial precursor cells (EPCs) from circulation. Activated macrophages are also recruited to tumors and release many growth factors that also promote tumor growth. Lastly, tumor microenvironment also confers an immune-suppressive niche for cancer cells to proliferate. The tumor-suppressive role of lymphocytes (T, B, and NK cells) is suppressed by the release of immuno-suppressive cytokines (e.g., TGF β , IL-10, and IL-23). Furthermore, tumor cells do not provide the costimulatory signals necessary to activate an immune response. Altogether, these events ultimately lead to the mobilization of the cancer cells towards other organs and tissues in order to establish secondary tumors (Gupta and Massagué, 2006; Chaffer and Weinberg, 2011).

2.2. Intravasation and bloodstream circulation

In order to metastasize, cancer cells must invade the tumor-associated vasculature to spread to distant organs and tissues, in a process called intravasation. This event is facilitated by the ability of tumor cells to generate novel blood vessels in a process known as angiogenesis (Gupta and Massagué, 2006; Chaffer and Weinberg, 2011).

Once cancer cells have entered the bloodstream, these circulating tumor cells (CTCs) have the potential to travel to tissues located far away from the primary tumor site. However, to do so, they have to survive several stresses, including physical damage from hemodynamic shear forces, and immune-mediated killing. Cancer cells must evade the mechanism of cell death that is induced by the loss of adhesive supports, referred to as anoikis. In addition, CTCs may promote their survival in the bloodstream surrounding themselves with immune cells (lymphocytes, platelets, neutrophils) (Szczerba et al., 2019). Moreover, it has also been observed that CTCs can form clusters also known as tumor emboli, that present greater metastatic potential than single tumor cells (Aceto et al., 2014; Pantel and Speicher, 2016; Mohme et al., 2017). CTCs and CTC clusters have been reported in several types of cancer, including HNSCC and correlate with metastatic potential that associates with poor prognosis (McMullen et al., 2016; Wu et al., 2016; Economopoulou et al., 2017; Akolkar et al., 2019).

2.3. Extravasation and homing

To develop metastasis, circulating tumor cells must once again cross the endothelium of the blood vessels into a new tissue in a process known as extravasation. Extravasation is the least understood metastatic process and current knowledge is based on the normal process of leukocyte extravasation into inflammatory sites. However, it is clear that extravasation is a multi-step process. The first step involves the transient adhesion of cancer cells to the blood vessel wall mediated by selectins expressed by endothelial cells. This transient adhesion leads to the rolling of cancer cells on the surface of the endothelium. In the second step, the chemokines expressed by endothelial cells activate the expression of integrins in cancer cells, allowing their firm adhesion to the endothelial walls. Once lodged in the endothelial vasculature, metastatic cells must cross the endothelium to reach the metastatic site. The predominant mode of extravasation appears to be the paracellular migration, during which tumor cells migrate between two endothelial cells. Tumor cells are able to induce changes in the vascular permeability of blood vessels to enter the organs. An example is the activation of the Src family of kinases in the endothelial cells by the expression of VEGF by tumor cells, which disrupts the endothelial cell junctions, thus facilitating extravasation (Gupta and Massagué, 2006; Gout et al., 2008; Miles et al., 2008; Chaffer and Weinberg, 2011; Strilic and Offermanns, 2017).

Once the CTCs have extravasated, they home the organ in which they will form a secondary tumor. However, the formation of metastasis is clearly favored in some target organs and it varies depending on the cancer type, displaying a characteristic metastatic pattern of dissemination for each cancer. This fact was first described by Paget in 1889, who developed the “seed and soil” hypothesis, exposing that cancer cells would only home and colonize organ microenvironments that were compatible with their growth (Paget, 1989). The layout of the circulation, trapping cancer cells in the microvasculature of distant organs, only partially explains this metastatic tropism. Besides, the interaction of cancer cells with the homing tissue also plays an important role in this process. The expression of different proteins by tumor cells and target organs, such as integrins and chemokines mediates the homing and colonization of the metastatic cells (Gupta and Massagué, 2006; Chaffer and Weinberg, 2011).

2.4. Colonization and development of metastasis

In general, the colonization of a new organ is an extremely inefficient process in which the majority of tumor cells that have undergone extravasation will not be able to colonize the new site and will die (approximately only 0.01% of the cancer cells will survive) (Gout et al., 2008). To perform a successful colonization, a pre-metastatic niche must exist in the

secondary site to support cell survival and proliferation. In this regard, the intrinsic expression of growth factors and cytokines in the new organ together with the factors secreted by the primary tumor itself, can recruit stromal cells and mobilize bone marrow hematopoietic progenitors, creating a pre-metastatic niche in the new organ for tumor cells to home and expand. Moreover, this pre-metastatic niche can also release signals and factors that attract CTCs to the metastatic site (Gupta and Massagué, 2006; Chaffer and Weinberg, 2011).

Once homed into the new site, cancer cells can enter a state of cell-cycle arrest, remaining quiescent (dormancy). To escape dormancy, cancer cells must adapt to the new microenvironment and be able to interact with it, which provides growth and survival signals. These proliferating cells can then generate micrometastasis (small lesions) and at last macrometastasis (actively growing large lesions) in the colonized organ (Gupta and Massagué, 2006; Chaffer and Weinberg, 2011).

However, cancer cells can remain dormant in the metastatic microenvironment, just after arrival or as part of the minimal residual disease (MRD) that remains in cancer patients after therapy. These dormant cells can remain quiescent in the homing organ for years until they start proliferating to develop metastatic lesions. MRD has been reported in several types of cancer, including HNSCC (Sproll et al., 2018). Conventional chemotherapeutic drugs only affect actively dividing cells, explaining why quiescent cells present in such metastatic sites are resistant to conventional treatments and are responsible for patient recurrence. Moreover, the tumor microenvironment can also provide a protective niche for tumor cells from therapy, establishing a signaling dialogue between cancer and stromal cells (Sabath, 2018). In addition, CSCs within the primary tumor can also enter states of quiescence explaining their heightened resistance to chemotherapeutic drugs (Gupta and Massagué, 2006; Chaffer and Weinberg, 2011; Ayob and Ramasamy, 2018).

2.5. Cancer stem cells (CSCs) and therapies

In the last decades, the concept of cancer stem cells (CSCs) has gained relevance in order to explain the complex processes leading to tumor formation and at last to the development of metastasis. In the last decades, numerous studies have emerged supporting the existence of CSCs in many cancer types, including HNSCC (Costea et al., 2006; Faber et al., 2013b). However, the understanding of CSC hierarchies within tumors and their plasticity is still under extensive study (Batlle and Clevers, 2017).

These facts highlight the importance of finding treatments that can effectively eliminate CSCs with the aim of avoid recurrence and the development of metastasis. As CSCs display

distinctive markers, many studies have focused on the development of therapies that selectively target this type of cells (Chen et al., 2013; Dragu et al., 2015). In this context, research has focused on the development of inhibitors, such as monoclonal antibodies, to target CSCs surface markers, also in HNSCC. CD44 is a large cell surface glycoprotein that is involved in cell adhesion and migration and is one of the most well-known markers for CSCs. In HNSCC, CD44 expression has been related to tumor initiation and chemotherapy resistance both in cell lines and primary tumor tissues (Major et al., 2013; Mohajertehran et al., 2018). Importantly, a phase I clinical study evaluating the therapeutic effect of the anti-CD44 immunoconjugate bivatuzumab mertansine for patients with advanced HNSCC was initiated in 2014, but no results have been published yet (Peitzsch et al., 2019). Another CSC marker widely studied in HNSCC is c-Met, a tyrosine kinase receptor for hepatocyte growth factor (HGF) which has been associated with metastasis, invasion, and decreased survival (Major et al., 2013). Several c-Met inhibitors have already been evaluated in clinical trials for the treatment of HNSCC. A phase II clinical study has evaluated the efficiency of the combination of the c-Met inhibitor tivantinib and cetuximab for recurrent and/or metastatic HNSCC, showing slightly better responses for the combination compared to cetuximab alone. The c-Met inhibitor captamatinib (INC280) and the humanized monoclonal antibody against HGF ficlatuzumab have also undergone clinical trials, but further clinical validation is needed (Peitzsch et al., 2019). Another promising CSC-specific target in HNSCC is ALDH1, a member of the aldehyde dehydrogenase family, which is highly expressed in many stem and progenitor cells. HNSCC ALDH1⁺ cell lines and primary tissue samples have shown tumor formation and invasion capacities, self-renewal, and resistance to chemotherapeutic drugs. Moreover, ALDH1 overexpression correlates with poor patient outcome (Major et al., 2013; Mohajertehran et al., 2018). Targeting with the small molecule inhibitor Aldi-6 led to the selective elimination of ALDH⁺ cells, decreased tumor burden, and sensitized HNSCC cells for cisplatin treatment in a HNSCC preclinical model (Peitzsch et al., 2019). Other interesting HNSCC CSC markers are; CD133, a pentaspan transmembrane glycoprotein that has also been identified as a putative CSC marker in other solid tumors, and CD117, a receptor tyrosine kinase type III, and thus could also be exploited as molecular targets (Major et al., 2013; Mohajertehran et al., 2018). More recently, a study has described that blockade of the fatty acid receptor CD36 dramatically inhibited the expansion of oral squamous carcinoma CSCs in organs distant to the primary tumor (Pascual et al., 2017).

Nevertheless, the role of CSCs has not been fully elucidated and little clinical data regarding CSC-targeted therapies in HNSCC is available. Thus, it is crucial to identify and study other CSC markers that can be used for therapeutic targeting (Peitzsch et al., 2019). Moreover,

the apparent plasticity of CSCs also complicates therapy design, highlighting the necessity of better understanding stem cells and CSCs plasticity to design novel therapies (Batlle and Clevers, 2017).

In this context, overactivation of the CXCR4/CXCL12 axis has been related to cancer stemness and metastatic potential in different types of cancer, including HNSCC, thus presenting a huge potential as a target for drug development (Kucia et al., 2005; Costea et al., 2006; Hermann et al., 2007; Gelmini et al., 2008; Faber et al., 2013b).

3. CXCR4/CXCL12 axis

3.1. Chemokines and chemokine receptors

Chemokines are a family of small proteins (8-10 kDa) that belong to the cytokine superfamily. Chemokines display chemoattractant properties that regulate cell migration and participate in several homeostatic processes, including inflammation, trafficking, and homing of several immune cell types, formation of tissues during morphogenesis, neovascularization, angiogenesis, and adaptive immune responses. However, dysregulation of chemokines and chemokine receptors is related to several pathological conditions, such as autoimmune and chronic diseases, viral infections, and remarkably cancer (Albert et al., 2013; Pozzobon et al., 2016).

Currently, almost 50 chemokines and 25 receptors have been described. Importantly, some chemokines can bind to more than one receptor, and in the same way, some receptors can be activated by more than one chemokine.

Chemokines are classified into 3 subfamilies based on the arrangement of the two N-terminal cysteine residues: (i) C- and CC- chemokines that present one or two adjacent cysteines, (ii) CXC- chemokines with two cysteines separated by another residue, and (iii) CX3C- chemokines that contain 3 residues between the two cysteines. The CXC- subfamily can be further classified by the presence or absence of the ELR motif (glutamic acid-leucine-arginine) at the N-terminus. Moreover, according to their roles, chemokines can be classified into homeostatic (constitutively expressed in different tissues) and inflammatory (expressed in response to inflammation).

On the other hand, chemokine receptors are G-protein coupled receptors that belong to the 7-transmembrane receptor family, except for one small group of receptors (ACKR) that are not associated with G-proteins and may act as scavengers for chemokines. Chemokine receptors are classified depending on the chemokine that they bind into CR, CCR, CXCR, and CX3CR receptors. After binding of the ligand, chemokine receptors undergo different structural changes on their cytoplasmic loops and tail leading to G-protein activation which

further activates several downstream signaling pathways, resulting in different cellular responses (Pozzobon et al., 2016).

3.2. CXCR4 and its ligand CXCL12

3.2.1. CXCR4 structure and expression

Like most chemokine receptors, CXCR4 is a 7-transmembrane G-protein coupled receptor highly expressed in a wide range of cell types, such as leukocytes, endothelial, epithelial and hematopoietic stem cells, stromal fibroblasts, and cancer cells. CXCR4 plays important roles in several physiological processes, including hematopoiesis, immune response, neurogenesis, germ cell development, cardiogenesis, and vascular formation.

CXCR4 expression is mainly regulated by the transcriptional factors NRF1, which promotes receptor transcription, and YY1 which, on the contrary, acts as a negative regulator. CXCR4 expression is upregulated by different signaling molecules including second messengers (Ca²⁺, cAMP), cytokines (IL-2, IL-10, TGF- β), and growth factors (bFGF, VEGF). On the other hand, its expression is down-regulated by other cytokines such as TNF- α , IFN- γ , and IL-1 β .

3.2.2. CXCR4 ligand: CXCL12

CXCL12, also known as stromal cell-derived factor 1 (SDF-1), is a secreted homeostatic chemokine associated with several physiological processes. It is CXCR4 main specific ligand, and its presence is ubiquitous in embryonic and adult tissues. During embryogenesis, CXCL12 plays a crucial role in proliferation and differentiation of immature progenitors. In adults, it is involved in the maintenance of tissue homeostasis and immune cell trafficking (Teicher and Fricker, 2010). There are 6 different CXCL12 isoforms as a result of different alternative splicing events, being the α and β isoforms the most relevant ones. CXCL12 binding to CXCR4 induces the phosphorylation of the receptor C-terminal domain which leads to its internalization and activation of different signaling pathways. Once inside the cell, CXCR4 can be recycled back to the cell surface or degraded by the lysosomes.

3.2.3. CXCR4 signaling

CXCL12 binding to CXCR4 induces the activation of the G-protein that is coupled to the receptor. G-protein activation occurs by the dissociation of G α subunit from the G β /G γ dimer which leads to the activation of several signaling pathways. Two different CXCR4 signaling pathways have been described: (i) G-protein dependent signaling and (ii) G-protein independent signaling (Busillo and Benovic, 2007; Pozzobon et al., 2016) (Figure 4).

To date, most of the downstream signaling pathways are activated via G-protein dependent signaling. In this type of signaling, G α subunit stimulates the activity of Src family of tyrosine kinases that activate Ras/Raf/MEK/ERK pathway modulating cell cycle progression, cell proliferation, cell migration and cell survival. Simultaneously, G β /G γ and G α subunits can activate PI3Ks which phosphorylate AKT, further regulating gene transcription, cell migration, and cell adhesion (Busillo and Benovic, 2007; Pozzobon et al., 2016) (Figure 4).

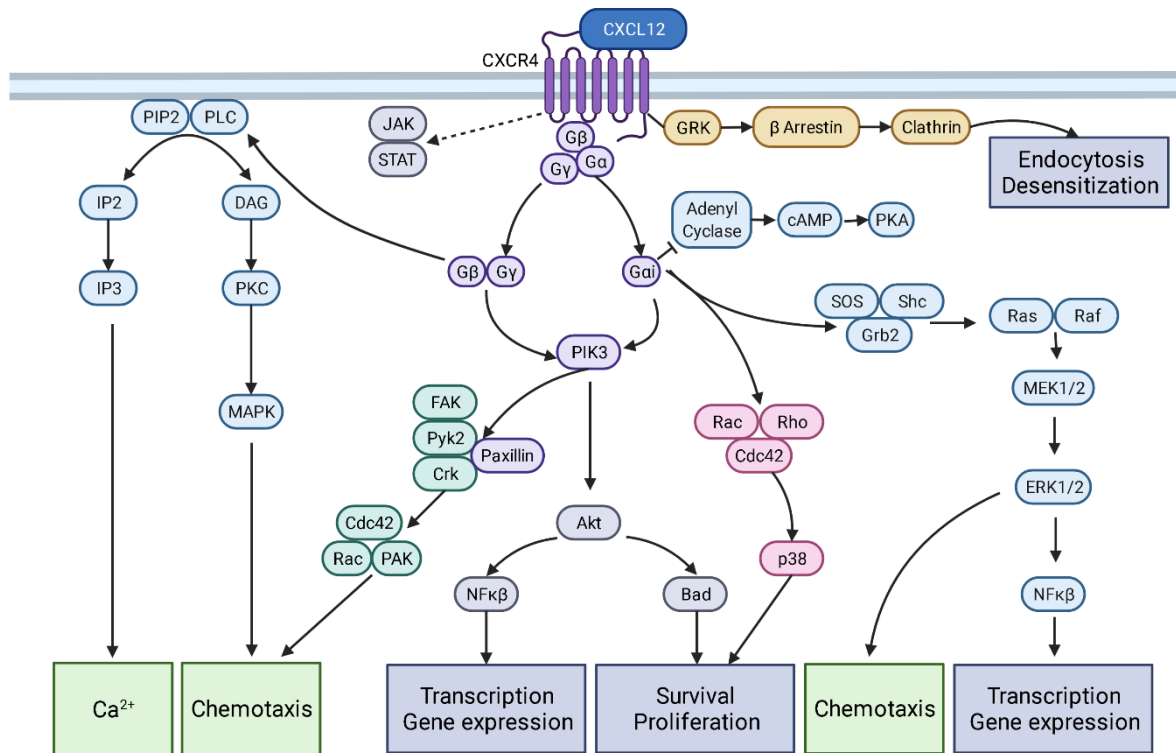


Figure 4. CXCR4/CXCL12 axis signaling pathway. The binding of CXCL12 to its receptor CXCR4 triggers a signaling cascade that regulates transcription, gene expression, cell survival, proliferation, and migration. Adapted from Teicher and Fricker, 2010 (Teicher and Fricker, 2010). Created with BioRender.com.

As it has been already mentioned, CXCR4 can also trigger a G-protein independent signaling pathway. After receptor binding, CXCR4 promotes the recruitment of G-protein coupled receptor kinases (GRKs) that phosphorylate the CXCR4 C-terminus resulting in the association with β -arrestins. Arrestin recruitment leads to receptor internalization and in some cases can promote cell migration by enhancing ERK and p38 activation. Moreover, CXCR4 phosphorylation can lead to JAK/STAT signaling pathway activation, which regulates several cellular processes including Ca²⁺ mobilization and transcription of different target genes involved in cell cycle progression and apoptosis (cell proliferation and survival) (Busillo and Benovic, 2007; Pozzobon et al., 2016) (Figure 4).

The CXCR4/CXCL12 axis is regulated by receptor desensitization, internalization, and degradation, processes in which the previously mentioned arrestins play an important role (Figure 4). Moreover, CXCR4 oligomerization into dimers or even heterodimers with other GPCRs, modulates CXCR4 dependent signaling increasing the complexity of chemokine-mediated responses (Busillo and Benovic, 2007; Pozzobon et al., 2016).

3.3. CXCR4/CXCL12 axis in cancer

CXCR4/CXCL12 axis dysregulation has been related to different pathological conditions, such as autoimmune diseases, viral infections (CXCR4 is a co-receptor for HIV internalization in T lymphocytes), and importantly cancer where it has been associated with several processes such as tumor growth, invasion, angiogenesis, and metastasis.

CXCR4/CXCL12 levels are increased in many cancer types compared to normal tissues including breast cancer, gastric cancer, pancreatic cancer, and oral squamous cell carcinoma. In HNSCC, CXCR4/CXCL12 has been found to be overexpressed in several patient cohorts. Interestingly, in these studies, CXCR4 was only expressed by tumor cells and not by the normal epithelium. In contrast, CXCL12 has been found more frequently in stromal cells adjacent to cancer cells (Albert et al., 2013; Guo et al., 2016).

CXCR4/CXCL12 expression correlates with metastasis and worse prognosis in different cancers. High expression of CXCR4 and CXCL12 significantly correlates with development of metastasis, and low overall and disease-free survival. Similarly, in HNSCC some studies have related CXCR4 overexpression in the primary tumor with higher incidence of lymph node metastasis (Ishikawa et al., 2006; Uchida et al., 2011; León et al., 2016). Interestingly, CXCR4 expression has been observed along the invasive edge in HNSCC tumors (Ishikawa et al., 2006). Moreover, several reports have described a higher level of CXCR4 expression in primary tumor cells in patients with infiltrated lymph nodes and distant metastasis compared to their counterparts without. Thus, this axis may serve as an independent predictor factor for poor survival in HNSCC cancer patients as well as other types of cancer (Albert et al., 2013; Guo et al., 2016).

Despite being a membrane receptor, CXCR4 has been found in the membrane, cytoplasm, and cell nucleus of cancer cells. Several studies have related CXCR4 location to prognosis. Cytoplasmatic and membrane expression has been associated with metastasis and poor prognosis, whereas nucleic expression has been related to enhanced survival. In HNSCC studies, CXCR4 location was mainly in the membrane and the cytoplasm, but nuclear localization has also been reported (Albert et al., 2013; Guo et al., 2016).

CXCR4/CXCL12 axis can be involved in cancer via two different mechanisms: (i) autocrine effect, when the same cell expresses both the ligand and the receptor; and (ii) indirect effect, which enables the recruitment of different cells into the tumor site or the spread of the cancer cells to other locations. Thus, CXCR4/CXCL12 can activate different signaling pathways enhancing proliferation and migration of the tumor cells, inducing angiogenesis, and promoting invasion and distant metastasis (Guo et al., 2016) (Figure 5).

3.3.1. Proliferation, apoptosis, and tumor growth

Several studies support the idea that CXCR4/CXCL12 promotes tumorigenesis (Figure 5). CXCL12 enhances cell growth, migration, and invasion, activating different signaling pathways, such as EGFR, MAPK, PI3K/Akt, Wnt pathway, and NF- κ B. Moreover, CXCL12 can also suppress apoptosis, presumably via NF- κ B and the up-regulation of the anti-apoptotic gene Bcl-2 that inhibits the pro-apoptotic protein BAD (Guo et al., 2016).

In HNSCC, several *in vitro* and *in vivo* preclinical models have associated the CXCR4/CXCL12 axis to proliferation and tumor growth. Some *in vitro* studies using HNSCC cell lines have found enhanced proliferation in the cell lines after CXCL12 stimulation via ERK 1/2 and Akt pathways. Moreover, CXCR4 overexpression in oral squamous cell carcinomas (OSCC) cell lines led to cell cycle arrest and apoptosis involving the NF- κ B pathway (Albert et al., 2013).

3.3.2. Recruiting cells into the tumor microenvironment

The tumor microenvironment is formed by different non-tumoral cells (stromal fibroblasts, endothelial cells and immune cells), connective tissue and extracellular matrix, that support tumor structure, angiogenesis and growth (Domanska et al., 2013). As it has been previously discussed, tumor-stromal interactions play a crucial role in tumor initiation and progression. CXCL12 expression in the tumor site can attract CXCR4⁺ immune cells and fibroblasts to support tumor development. CXCR4⁺ inflammatory, vascular, and stromal cells can assist tumor growth by secreting growth factors (EGF), cytokines, chemokines, and pro-angiogenic factors (VEGF) (Domanska et al., 2013; Guo et al., 2016). Moreover, CXCL12 is physiologically expressed in many organs and tissues, such as lungs, liver, and bone marrow. CXCL12 gradients can attract different stromal and immune cells to these organs where they create potential metastatic niches for CXCR4⁺ cancer cells to home and grow, even protecting them from chemotherapy (Guo et al., 2016) (Figure 5).

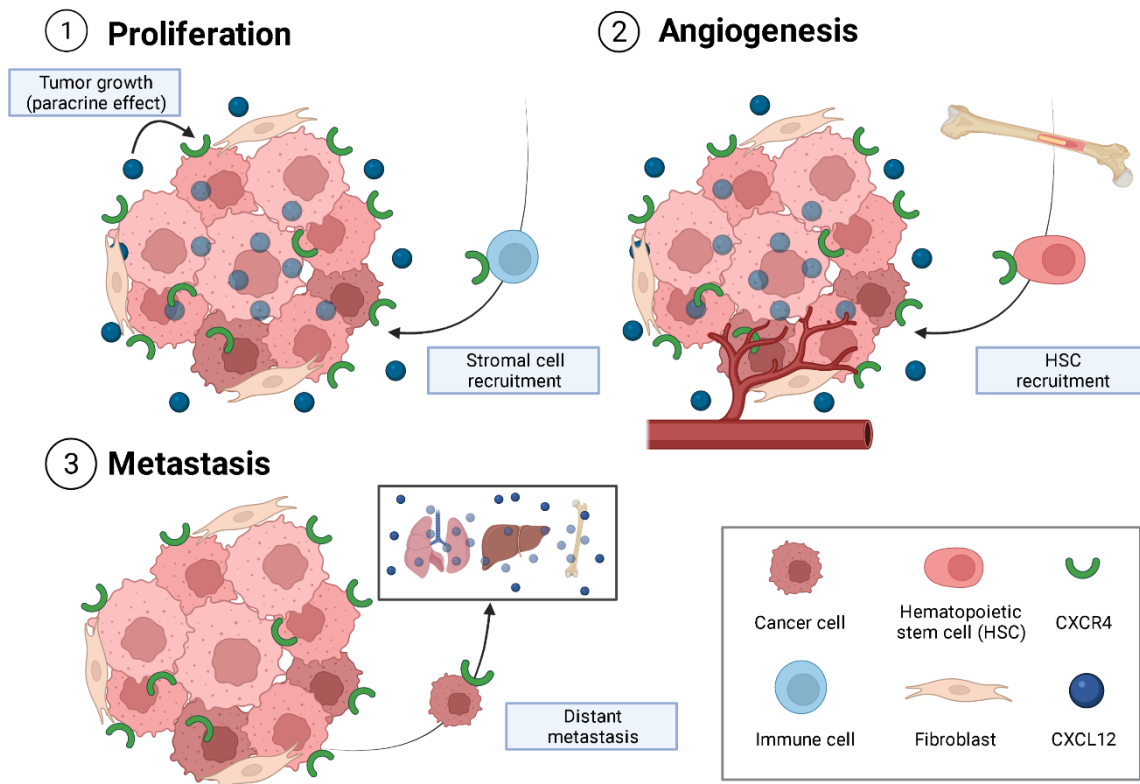


Figure 5. CXCR4/CXCL12 axis is involved in tumor proliferation, angiogenesis, and development of distant metastasis. Modified from M. Domanska et al., 2013 and F. Guo et al., 2016 (Domanska et al., 2013; Guo et al., 2016). Created with BioRender.com.

3.3.3. Angiogenesis

Several studies have shown a correlation between CXCR4 expression and increased tumor vascularization in different cancer types, including HNSCC. Four different mechanisms have been proposed linking tumor angiogenesis and CXCR4 expression.

Firstly, CXCL12 expression in the tumor tissue upregulates VEGF by activating the PI3K/Akt pathway in the cancer cells, leading to tumor vascularization. The other way around, VEGF induces CXCR4 expression facilitating cancer cell migration towards CXCL12. Moreover, intratumoral hypoxia as a result of uncontrolled tumoral growth, is known to promote tumor angiogenesis. The hypoxic environment leads to the overexpression of HIF-1 α which induces the expression of several target genes, including VEGF, CXCR4, and CXCL12. Altogether, these findings suggest a positive feedback loop between CXCL12/CXCR4 axis and VEGF that promotes tumor vascularization (Albert et al., 2013; Guo et al., 2016) (Figure 5).

The second mechanism relates again to CXCL12 and VEGF expression. In this case, CXCL12 reduces PGK1 expression, leading to an increased secretion of VEGF thus promoting angiogenesis. In the opposite way, CXCL12 can upregulate different

angiogenesis-associated genes, including IL-6 which induces angiogenesis by enhancing VEGF and FGF expression among others (Guo et al., 2016).

Lastly, CXCL12 can recruit endothelial progenitor cells from the bone marrow into the tumor niche. Hypoxia upregulates CXCL12 leading to a recruitment of CXCR4⁺ bone marrow progenitor cells to the tumor that stimulate the formation of new blood vessels by expressing VEGF (Domanska et al., 2013) (Figure 5).

In HNSCC, several *in vivo* preclinical models have shown enhanced angiogenesis in CXCR4-expressing tumor-bearing mice. Interestingly, treatment with a CXCR4 antagonist led to an antiangiogenic effect and suppression of tumor growth, suggesting that CXCR4 may be a good target for antiangiogenic drugs (Albert et al., 2013).

3.3.4. Epithelial-mesenchymal transition (EMT)

Carcinoma cells that undergo EMT acquire fibroblast-like properties that enable them to reduce cell-cell adhesion, increasing cell motility and invasion capacities (Albert et al., 2013). EMT has been described as an important, although not indispensable, step for invasion and metastasis of tumor cells (Fischer et al., 2015).

Several studies have shown that CXCR4/CXCL12 axis is involved in EMT through the activation of different pathways, such as MEK/ERK, PI3K/Akt, or Wnt/ β -catenin in different cancer types, including HNSCC (Guo et al., 2016). It has been demonstrated that CXCL12 is able to upregulate different mesenchymal markers in HNSCC cells expressing CXCR4 via the activation of the PI3K/Akt pathway. Moreover, CXCR4⁺ highly metastatic HNSCC cell lines present a downregulation of different epithelial markers, such as E-cadherin, cytokeratin, and β -catenin, whereas several mesenchymal markers including vimentin, and the transcription factors Snail, and Twist are upregulated. Importantly, the transcription factor Twist has been correlated with overexpression of CXCR4 and lymph node metastasis in HNSCC. Thus, CXCR4 seems to perform an important role in EMT and consequently in the acquisition of invasive and metastatic properties (Albert et al., 2013).

3.3.5. Matrix metalloproteinases activation

Matrix metalloproteinases (MMPs) are a large group of enzymes that degrade the extracellular matrix (ECM). Physiologically, MMPs participate in tissue-remodeling processes, but their dysregulation facilitates tumor cell migration, invasion, and spread to distant secondary areas, thus enhancing metastasis.

In several HNSCC cell lines, CXCL12 promoted the activation of different MMPs, including MMP-9 and MMP-13 via ERK pathway. Moreover, the activation of these two MMPs correlates with poor patient prognosis in different cancers, remarkably in HNSCC.

Altogether, these facts highlight the important role of CXCR4/CXCL12 axis in the acquisition of cell invasion and motility capacities, which represent a critical step in the metastatic process (Albert et al., 2013).

3.3.6. Distant metastasis and metastatic cancer stem cells (CSCs)

As it has been already mentioned, metastasis is one of the major problems that cancer patients must face, being the leading cause of cancer death (Guan, 2015; Dillekås et al., 2019). In HNSCC, approximately 60% of the patients develop lymph node metastasis and 30% distant metastasis, mainly in the lungs, liver and bones, importantly determining patient outcome (Albert et al., 2013).

Cancer metastasis is a highly complex process involving many different steps that ultimately lead to the development of tumor metastasis in organs far away from the primary tumor site. As previously mentioned, EMT, MMPs activation and other processes in which CXCR4/CXCL12 axis is involved, increase tumor cell migration and invasion further contributing to the development of metastasis. Moreover, several organs such as the liver, lungs, bone marrow, and lymph nodes physiologically exhibit peak expression levels of CXCL12. Interestingly, these organs represent common metastatic sites in many different types of cancer, including HNSCC, which correlates with their CXCL12 levels. Several studies both *in vitro* and *in vivo* in different cancer types suggest that activation of the CXCR4/CXCL12 axis can promote metastasis. CXCR4⁺ cancer cells can migrate from the primary tumor site towards this CXCL12 gradient and establish metastasis at these high-expressing CXCL12 organs (Domanska et al., 2013; Guo et al., 2016) (Figure 5).

In addition, CXCL12 is also expressed in the endothelial basal lamina of the blood vessels. High CXCL12 levels may attract CXCR4⁺ cancer cells to the blood vessels supporting hematogenous metastasis. Moreover, under the tumor hypoxic conditions, HIF-1 α can upregulate CXCL12 expression in these endothelial cells, thus recruiting more CXCR4⁺ to the vessels and enhancing metastasis (Guo et al., 2016).

PI3K/Akt, ERK, and NF- κ B signaling pathways are widely accepted to be involved in the metastatic process. In HNSCC, the CXCR4/CXCL12 axis promotes metastasis by the activation of ERK1/2, Akt/PKB, and NF- κ B pathways. ERK1/2 is able to upregulate the expression of MMP-9 increasing cancer metastasis (Albert et al., 2013).

As previously discussed, the CXCR4/CXCL12 axis has been related to CSCs and CXCR4 expression has been described as a stem cell marker in several solid tumors, including HNSCC (Costea et al., 2006; Faber et al., 2013a). One of the first studies regarding CSCs performed by Hermann et al. in 2007, described a subpopulation of CD133⁺ tumor cells that presented tumorigenic capacity (Hermann et al., 2007). Further separation of this group into CXCR4⁻ and CXCR4⁺ cells, showed that although both cell subsets displayed tumorigenic capacity, only the CXCR4⁺ group was able to form spontaneous metastasis in a pancreatic mouse model. This experiment clearly suggests that CXCR4 confers cancer cells the ability to metastasize (Dalerba and Clarke, 2007).

In order to develop metastasis, CSCs must detach from their original site and enter the peripheral blood or lymphatic vessels to reach distant sites. This migration occurs thanks to chemoattracting gradients, that direct these cells to the vessels and their metastatic niches. Once they reach the new site, the environmental niche protects CSCs from apoptosis allowing them to expand. The CXCR4/CXCL12 axis is well-known to be involved in this type of processes, as we have previously described (Kucia et al., 2005; Gelmini et al., 2008). Altogether, these facts clearly suggest that the upregulation of the CXCR4/CXCL12 axis is importantly involved in CSCs and the metastatic process to colonize distant organs in several types of cancer.

3.3.7. CXCR4/CXCL12 as a therapeutic target for drug development

As previously mentioned, current cancer therapy presents severe limitations usually leading to treatment failure. Commonly, patients undergo recurrence after conventional chemotherapy and radiotherapy. These treatments are not able to completely eliminate all cancer cells, leading to the selection of a drug-resistant cancer cell population. Chemotherapy-resistant cells are able to re-grow and disseminate after treatment, causing cancer recurrence. These cells are the aforementioned CSCs, quiescent tumor cells endowed with tumor-initiating capacity. CSCs exhibit chemotherapy resistance as this type of treatment only kills proliferating cells. Therefore, the elimination of CSCs would be crucial for the treatment of cancer disease. Theoretically, the depletion of the CSC population within a tumor would prevent its growth and metastatic spread (Hermann et al., 2008; Chen et al., 2013).

Multiple novel therapeutic systems have been designed to target CSC-specific surface markers and signaling pathways aiming to eliminate CSCs and altering their supporting tumor microenvironment. As described above, the CXCR4/CXCL12 axis participates in many different cancer events and its expression has been related to cancer cell stemness and metastatic potential. Therefore, the CXCR4/CXCL12 axis has been exploited as a

promising molecular target for cancer drug development (Hermann et al., 2008; Chen et al., 2013).

In the last decades, CXCR4 antagonist have been studied for cancer treatment. AMD3100 also known as plerixafor, was the first antagonist to be developed for HIV infection. During the phase I clinical trial, AMD3100 induced the mobilization of CD34⁺ human hematopoietic cells from the bone marrow to the peripheral blood (Domanska et al., 2013). These findings showed its potential for the treatment of leukemia as it is able to mobilize leukemic cancer cells from their protective niche in the bone marrow to the circulation where they are exposed to chemotherapeutic drugs (Tsou et al., 2018). Thus, AMD3100 has been evaluated in numerous clinical trials as a chemosensitizer in combination with chemotherapy for hematologic tumors. In a phase II study, 46 recurrent AML patients were treated with AMD3100 prior to mitoxantrone, etoposide and cytarabine chemotherapy. This study achieved an overall complete remission rate of 46%, resulting in 1-year overall free survival of 37% and disease-free survival of 42.9%. Moreover, up to date all clinical studies performed in hematologic neoplasias demonstrate that the combination therapy of AMD3100 with conventional chemotherapy is safe and does not affect hematological recovery. However, although these results are promising and represent an improvement compared to chemotherapy alone, they are still far from total patient curation and further clinical trials are necessary to validate the benefits of combination treatment (Domanska et al., 2013).

Although research has mainly focused on the treatment of hematologic tumors, plerixafor has also demonstrated promising results for the treatment of solid tumors. AMD3100 has proven to reduce tumor growth and metastatic spread in combination with chemotherapy in several preclinical animal models for different types of cancer, including HNSCC (Guo et al., 2016; Uchida et al., 2018). However, few clinical trials have been performed regarding the effect of AMD3100 in solid tumors. Interestingly, AMD3100 in combination with pembrolizumab is undergoing a phase II clinical study for metastatic HNSCC patients, but no results have been published so far (<https://clinicaltrials.gov>).

One of the main limitations of AMD3100 is its short availability in blood once injected in patients. It is estimated to have a distribution half-life of 0.3 h and a terminal half-life of 5.3 h, which results in patients receiving an AMD3100 daily injection, thus reducing patient's quality of life (Uchida et al., 2018). In order to overcome this limitation, other CXCR4 antagonists have been developed in the last years, including AMD3465, which has shown promising results in combination with chemotherapy for AML, CTCE-9908, FC131, or the small peptide T22 (Guo et al., 2016). CTCE-9908 is a small peptide that mimics the

sequence of the N-terminal part of CXCL12. This inhibitor was able to reduce the number of metastasis in breast cancer, osteosarcoma, and melanoma mouse models (Domanska et al., 2013). Interestingly, although a phase I/II clinical trial of CTCE-9908 in advanced metastatic patients was completed in 2008, there is no information on its further development (Tsou et al., 2018). Currently, three CXCR4 antagonists are undergoing clinical trials. Mavorixafor (AMD11070) is a small-molecule CXCR4 antagonist that targets a drug-binding pocket of CXCR4. Interestingly, it has been able to inhibit lung metastasis in a preclinical model of OSCC. Mavorixafor is being evaluated in a phase II and a phase III clinical trials for the treatment of WHIM syndrome. In addition, balixafortide (POL6326), a CXCR4 antagonist in the form of cyclic peptide, has proven to be effective in combination with eribulin (30% response) for the treatment of metastatic breast cancer and it is currently being evaluated in a phase III clinical trial (Miao et al., 2020). Lastly, another peptide CXCR4 antagonist motixafortide (BL-8040, TN14003) has been able to prevent primary tumor growth and lung metastasis in an orthotopic mouse model of HNSCC (Wong and Korz, 2008; Mishan et al., 2016). It has been evaluated in different clinical trials and it is currently undergoing a phase II clinical trial for the treatment of metastatic pancreatic cancer in combination with pembrolizumab. Nevertheless, despite the active research focusing on the development of novel CXCR4 antagonists, the only drug approved by the FDA is still AMD3100 (<https://clinicaltrials.gov>; Miao et al., 2020).

Besides the development of CXCR4 antagonists, targeting CXCL12 has also been exploited. In this context, several inhibitors have been developed, including olaptased pegol (NOX-A12) (Guo et al., 2016). This compound exploits an interesting strategy, NOX-A12 is a PEGylated mirror image L-RNA aptamer (spiegelmer) that binds and inhibits CXCL12 with high affinity. It has been tested in combination with other drugs in phase II studies for the treatment of chronic lymphocytic leukemia and multiple myeloma, and in solid tumors for the treatment of metastatic colorectal and pancreatic cancer. However, no results regarding these clinical trials have been published so far (<https://clinicaltrials.gov>; Tsou et al., 2018).

Moreover, targeting CXCR4/CXCL12 can enhance immunotherapy efficacy. As previously mentioned, CXCR4/CXCL12 axis contributes to tumor immune suppression by recruiting specific cell populations to the tumor site that protect cancer cells and enhance tumor growth by creating an immune suppressive environment. Blocking the CXCR4/CXCL12 pathway has shown to reduce the recruitment of endothelial, myeloid, and dendritic cells to the tumors reducing the tumor immune suppression and the metastatic spread in different mouse models. In this context, AMD3100 treatment has shown the ability to recruit effector T-cells to the tumor enhancing the elimination of cancer cells (Guo et al., 2016; Tsou et al.,

2018), thus it is undergoing a clinical trial in combination with the PD-1 inhibitor pembrolizumab for HNSCC, as introduced before. Similarly, motixafortide (BL8040) is able to enhance the immune infiltration of pancreatic tumors and, as previously mentioned, is also undergoing a clinical trial in combination with immune check-point inhibitor pembrolizumab (Miao et al., 2020).

Altogether, these results highlight the great potential of targeting the CXCR4/CXCL12 axis, especially in combination with chemotherapeutic agents. However, there is still room for the development of more efficient therapies targeting CXCR4. Firstly, blocking the CXCR4 pathway alone seems not to be enough to achieve complete remission. Monotherapies using only CXCR4 inhibitors have shown poor efficacy, thus current research is focused on the combination of blocking the CXCR4/CXCL12 pathways with other therapies, including chemotherapy, presenting promising results (Domanska et al., 2013). Nevertheless, these strategies still mainly rely on conventional chemotherapeutic drugs, which distribute equally to all tissues because of their passive diffusion, inducing important systemic toxicities and undesired side effects for patients. Thus, novel tumor-targeted approaches are urgently needed.

Besides, the most widely used anti-CXCR4 agent, AMD3100, is administered intravenously and presents a short half-life in blood that forces its daily administration to patients. In this regard, several other molecules are under research, as previously discussed. However, none of them has been approved by the FDA so far. Thus, the development of drugs with longer circulation time in the bloodstream is also important. In this context, the use of nanocarriers has been widely studied in the last decade holding the potential of enhancing drug circulation in blood by avoiding renal filtration, while reducing hepatic metabolism. The aforementioned olaptosed pegol (NOX-A12) already exploits this interesting approach, as the conjugation to polyethylene glycol (PEG) has proven to enhance their therapeutic effect (Petros and Desimone, 2010; Serna et al., 2018).

4. Targeted drug delivery for cancer treatment

Current cancer therapy is still mainly based on chemotherapeutic drugs, small molecular weight chemicals that mainly inhibit the proliferation of cancer cells. Among these molecules, we find fluoropyrimidines, platinum-based agents, microtubule inhibitors, and alkylating agents, which constitute the backbone of current anti-cancer treatment. However, in the absence of targeting, chemotherapeutic drugs also inhibit the growth of other fast-dividing cells including hair follicles, bone marrow, and gastrointestinal tract cells. Thus, conventional chemotherapy leads to severe side effects including anemia, thrombocytopenia, nausea and vomiting, cardiotoxicity, and immunosuppression that

enhances patient susceptibility to develop infectious diseases. Moreover, chemotherapeutic drugs also accumulate in the liver, which metabolizes them, and the kidneys that excrete the drug metabolites, often leading to hepatic and renal damage. Consequently, systemic toxicity forces the reduction of the administered dose, which fails to reach the optimal local concentration in the tumor to achieve its full effect. In addition, the small size of these chemotherapeutic drugs is below the renal filtration cut-off (between 5 and 7 nm), leading to their clearance by the kidney, thus diminishing drug concentration in blood and its circulation time. All these facts manifest the problematic of current chemotherapeutic treatment and the necessity of new strategies in drug development (Pérez-Herrero and Fernández-Medarde, 2015; Serna et al., 2018). In this regard, targeted drug delivery has emerged as a promising alternative to improve drug accumulation within tumor tissues, while reducing their biodistribution to normal tissues (Lammers et al., 2016; Wilhelm et al., 2016).

4.1. Antibody drug conjugates (ADCs)

Antibody drug conjugates (ADCs) are formed by a monoclonal antibody (mAb) chemically bound to a small cytotoxic drug. In this case, the antibody serves a double purpose both acting as a carrier and a targeting moiety. Since the approval of the first ADC gemtuzumab ozogamicin in 2000, several generations of ADCs have been developed with improved stability, efficacy, and less immunogenicity, including humanized mAbs. Currently, there are nine ADCs in the market, including Trastuzumab Emtamsine, targeted to HER2/neu receptor for breast cancer treatment, and Brentuximab Vedotin, targeted to the surface protein CD30, for Hodgkin lymphoma (HL) and systemic anaplastic large cell lymphoma (sALCL) treatment (Mangues et al., 2016; Serna et al., 2018; Drago et al., 2021). Regarding HNSCC, the first ADC tested for HNSCC was ABBV-221, an anti-EGFR mAb bound to the cytotoxic drug auristatin E. A phase I clinical study has been completed with promising results. Currently, other ADCs are undergoing phase I/II clinical studies for HNSCC and other cancers (<https://clinicaltrials.gov>; Santuray et al., 2018; Cramer et al., 2019). However, ADCs display several disadvantages including their poor payload capacity, limited tumor uptake, and high toxicity (Donaghy, 2016; Masters et al., 2018). These off-target side effects are mainly related to the early release of the payload in circulation, due to defective drug conjugation, which importantly compromises the clinical use of ADCs. In addition, it is estimated that <1% of the administered ADC dose can reach the tumor site, forcing the use of high doses which leads to important side effects and life-threatening toxicities. Due to these severe side effects and lack of improved efficacy compared to the free drug, 20 ADCs have been discontinued in the last decades. Moreover, ADCs can only be coupled with few

drug molecules to avoid interference with antigen binding. Nevertheless, there are still more than 70 ADCs in clinical trials, that have been improved for instance using site-specific conjugation (Junutula et al., 2008; Schumacher et al., 2016; Yamada and Ito, 2019) or bi-specific targeting (Maruani, 2018; Shim, 2020), for the treatment of several types of cancer, including HNSCC (Serna et al., 2018).

4.2. Immunotoxins

Immunotoxins are cancer therapeutics that contain a toxin fused to a targeting moiety. Different targeting agents can be used, such as ligands, antibodies, and peptides (Akbari et al., 2017; Li et al., 2017). In addition, toxin domains from bacteria, plants or human origin can be exploited for immunotoxin development. Interestingly, one immunotoxin reached the market, denileukin diftitox (Ontak), a drug based on interleukin 2 (IL-2) fused to *Corynebacterium diphtheriae* toxin approved by the FDA for the treatment of leukemia and lymphoma. However, it was withdrawn from the market due to toxicity concerns. Other bacterial toxins have also been studied for their therapeutic use, such as *Pseudomonas aeruginosa* exotoxin A (PE) which has also been fused to different targeting agents and is currently in clinical trials for the treatment of mesothelioma and leukemia (Serna et al., 2018). However, current immunotoxins present several side effects, remarkably their high immunogenicity, which limits their long-term use in patients. Different strategies are being studied to overcome these undesired side effects, including antibody humanization, PEGylation, and modification of human B- and T-cell epitopes, with promising results (Akbari et al., 2017; Li et al., 2017). Despite current shortcomings, this approach opens the possibility of delivering natural toxins that show even higher cytotoxicity than conventional chemotherapeutic drugs to cancer cells (Mangues et al., 2016; Vazquez et al., 2016; Serna et al., 2018).

4.3. Nanoparticles and nanocarriers

Nanotechnology can be defined as the development of small-scale materials that because of their inherent properties can be applied in several areas including optics, electronics, and medicine. Nanomedicine is the use of nanoscale or nanostructured materials (1-1,000 nm) in medicine that, according to their structure, have unique biomedical effects, such as the ability to cross biological barriers. There are several medical fields in which nanotechnology can be useful, including imaging and diagnostics, being drug delivery the most promising application of nanomedicine (Wagner et al., 2006).

Nanocarriers are nanoscale systems capable of transporting anticancer agents, such as small molecular weight drugs or macromolecules, like genes or proteins, into cancer tissues. Theoretically, nanocarriers allow antitumoral drugs to accumulate within the tumor,

avoiding normal tissues, thus increasing tumor drug concentration and reducing systemic toxicity. Moreover, nanocarriers also increase drug stability and circulation time, as they protect them from degradation and renal clearance (Petros and Desimone, 2010; Pérez-Herrero and Fernández-Medarde, 2015). Two different strategies have been developed to achieve tumor targeting: (i) passive and (ii) active targeting (Figure 6).

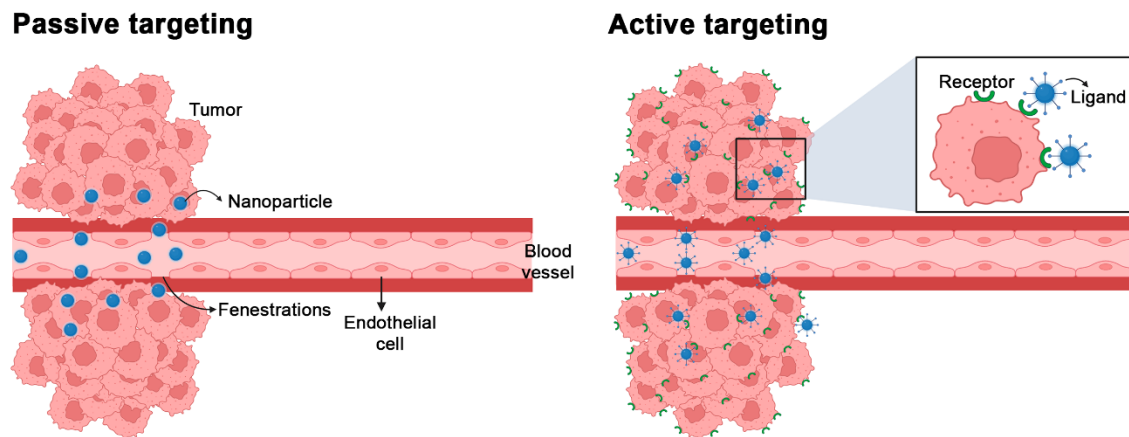


Figure 6. Comparison between passive and active targeting strategies in nanomedicine. Active targeting allows for targeted drug delivery which improves drug accumulation within tumor tissues. Created with BioRender.com.

4.3.1. Passive targeting

Passive targeting is based on the enhanced permeability and retention (EPR) effect. The EPR effect was first described in animal models by Matsumura and Maeda in 1986 finding that newly-formed tumor blood vessels displayed increased permeability as they were poorly developed, presenting fenestrations (Matsumura and Maeda, 1986). This enhanced permeability together with the poor lymphatic drainage of tumors allowed the passive accumulation of the nanocarriers in tumoral tissues (Figure 6). However, in reality, it is estimated that approximately only 0.7% of the administered nanoparticle dose is able to reach the tumor, strongly compromising their translation into the clinic (Lammers et al., 2016; Wilhelm et al., 2016). In fact, nanoparticle formulations available in the market have only improved patient's treatment by reducing the toxicity compared to chemotherapeutic agents, lacking an enhanced therapeutic effect (Danhier, 2016). Despite being well validated in cell-derived xenograft animal models, the EPR effect has been highly questioned lately as clinical data suggest that it might not be so frequent in human beings (Danhier, 2016; Shi et al., 2017; Zhou et al., 2020). Tumor xenografts usually grow much faster than human solid tumors (Danhier, 2016), which translates into a deficient vasculature development, with blood vessels being leakier and presenting fenestrations.

The different growth rates also alter the development of the tumor microenvironment, which can also influence nanocarrier accumulation. Altogether, the extravasation of nanoparticles is a highly inefficient process, as tumor vasculature in humans exhibits a highly heterogeneous permeability, strongly varying depending on the tumor type, location, and patient. In addition, the high interstitial fluid pressure of solid tumors avoids successful uptake and homogenous distribution of drugs in the tumor (Heldin et al., 2004). Thus, the EPR effect seems not to be translatable into the clinic, partially explaining the poor nanoparticle accumulation within tumors that has been observed in preclinical studies (Danhier, 2016; Zhou et al., 2020).

4.3.2. Active targeting

The aim of this strategy is to target internalization-prone cell surface receptors or molecules that are overexpressed in cancer cells or in the tumor microenvironment compared to healthy tissues to enhance drug delivery towards the tumor (Figure 6). Several surface receptors overexpressed in cancer cells have been exploited so far, such as transferrin receptor, folate receptor, glycoproteins (e.g. lectins), and EGFR. Another strategy is to target the tumor endothelial cells via VEGF, VCAM-1, integrins, or MMPs (Danhier et al., 2010). Different targeting agents can be used to develop active targeted therapies including aptamers, monoclonal antibodies (mAbs), antibody derivatives such as antibody fragments, and receptor-specific peptidic ligands. These targeting molecules can be functionalized to the surface of different nanocarriers enabling their use in targeted drug delivery (Serna et al., 2018). Active targeting enables the selective nanoparticle delivery to cancer cells, while reducing potential off-target effects in non-tumor bearing tissues. Importantly, different studies have reported an enhanced tumor uptake of targeted nanoparticles (Byrne et al., 2008; Danhier et al., 2010).

Recently, several studies have shown that another transport mechanism apart from passive diffusion via the EPR effect, is involved in nanoparticle extravasation to the tumor (Lu et al., 2012; de Lázaro and Mooney, 2020; Pandit et al., 2020; Sindhvani et al., 2020). Transcytosis is a type of active transport mechanism in which macromolecules are carried from one side of a cell to the other, being especially common for transportation of proteins and other macromolecules (Tuma and Hubbard, 2003). Interestingly, albumin-bound paclitaxel (Abraxane) extravasates the bloodstream by glycoprotein 60-mediated endothelial cell transcytosis (Gradishar, 2006; Desai and Desai, 2009). Remarkably, a recent study by Sindhvani, et al. (Sindhvani et al., 2020) carried out in both xenograft models and human tumor specimens has shown that the main mechanism involved in nanoparticle delivery to tumors appears to be transcytosis, rather than the EPR effect. This

finding represents a change of paradigm and opens the possibility to develop actively targeted nanoparticles that enter the tumors via active transport, thus improving nanoparticle tumor accumulation (Pandit et al., 2020; Sindhwani et al., 2020).

Besides, the design of nanoparticles is highly dependent on their composition, which further determines their size, shape, flexibility, and surface properties, importantly affecting their therapeutic outcome. A wide variety of materials have been used to synthesize nanoparticles that can be broadly classified into (i) inorganic and (ii) organic nanoparticles (Mitragotri and Stayton, 2014; Richards et al., 2016).

4.3.3. Inorganic nanoparticles

Metallic and organometallic compounds have been widely used to develop nanoparticles thanks to their interesting physicochemical properties. Iron oxide nanoparticles, gold nanoparticles, mesoporous silica nanoparticles, quantum dots, and carbon nanotubes are some examples of inorganic nanoparticles. However, despite their huge potential as imaging and diagnostic tools, their use as drug nanocarriers has been questioned. Iron oxide and gold nanoparticles, due to their physical structure, lack space to load the drugs which leads to small cargo capacities. Besides, due to their inorganic nature, most of these nanoparticles are poorly biodegradable and even toxic, leading in some cases to pulmonary damage and undesirable organ accumulation (Richards et al., 2016; Ventola, 2017). Thus, in general, inorganic nanoparticles lack an essential property for drug delivery: biocompatibility. In this regard, no inorganic nanocarrier has been approved by the FDA or is undergoing clinical trials as an anticancer treatment (Petros and Desimone, 2010; Pérez-Herrero and Fernández-Medarde, 2015).

4.3.4. Organic nanoparticles

On the other hand, many organic materials, such as lipids and polymers, present interesting properties for their application in therapeutic delivery.

Liposomes. Liposomes, which are spherical vesicles with a lipid bilayer membrane structure, were one of the first nanocarriers to be developed and approved for anticancer treatment. Liposomal nanoparticles are synthesized from natural lipids with polar and nonpolar components that self-assemble into colloidal particles. These structures allow the encapsulation of both hydrophilic and hydrophobic compounds, protecting them during circulation in the body. The first FDA-approved liposomal anticancer treatment was the liposome-encapsulated doxorubicin (Doxil) in 1995 for the treatment of HIV-related Kaposi's sarcoma, ovarian cancer and multiple myeloma. Currently, there are 5 liposomal-based anticancer drugs on the market, including DepoCyt and Daunoxome. Moreover, two

targeted liposomes, GAH-targeted doxorubicin-containing immunoliposomes (MCC-465) and transferrin-targeted oxaliplatin-containing liposomes (MBP-426), are currently in clinical trials (<https://clinicaltrials.gov>). The main advantages of liposomal nanoparticles include their biocompatibility and their ability to be functionalized and to encapsulate a wide range of small molecules. However, liposomes show several problems regarding their *in vivo* stability and industrial reproducibility, showing a highly specific cargo-dependency that questions their universal applicability as nanocarriers (Petros and Desimone, 2010; Pérez-Herrero and Fernández-Medarde, 2015).

Polymeric micelles. Polymeric micelles are formed by aggregated hydrophobic polymers surrounded by hydrophilic polymeric chains that form nanosized spheroidal micelles. Their hydrophilic surface provides them with advantageous properties including longer circulation times and the ability to encapsulate very hydrophobic drugs. Currently, only Paclical, a micellar formulation of encapsulated paclitaxel (XR-17), is in the market as it was granted orphan drug status in 2009 by the FDA for the treatment of ovarian cancer (Ventola, 2017). Moreover, other polymeric micelles loaded with other classical chemotherapeutic drugs, such as platinum-based compounds or irinotecan, are in clinical trials. Remarkably, one of the most promising formulations is Genexol-PM, a micelle-encapsulated paclitaxel which is being studied for the treatment of advanced HNSCC (Keam et al., 2019). However, current polymeric micelles present several problems, like insufficient stability in systemic circulation and premature drug leakage in systemic circulation (Pérez-Herrero and Fernández-Medarde, 2015).

Dendrimers. Dendrimers are branched polymer complexes generated through highly controlled successive polymerization steps that enable industrial reproducibility and control over nanoparticle properties. However, current research regarding their use for biomedical purposes is still mainly in preclinical studies due to their high toxicity and poor biocompatibility (Petros and Desimone, 2010)

Polymeric nanocarriers. Polymeric nanocarriers comprise a heterogeneous group of nanostructures that include both polymer-drug conjugates and polymeric nanoparticles. Polymer-drug conjugates are defined as polymeric structures conjugated to anticancer drugs via a cleavable linker. This system allows higher stability in circulation and theoretically, enables the drug release in the tumor, thus increasing drug tumor uptake while reducing systemic toxicity. On the other hand, polymeric nanoparticles can be further classified into nanospheres and nanocapsules. Nanospheres consist of a solid polymer matrix, which can encapsulate hydrophobic drugs, whereas nanocapsules contain an aqueous hydrophilic core that is more amenable to the loading of hydrophilic payloads such

as nucleic acids. Polymeric nanocarriers have shown high stability, homogeneous size distribution, controllable physicochemical properties, high drug payload, and controlled drug release. Another important advantage is their great versatility, as they can be synthesized from natural, synthetic, or pseudosynthetic polymers that have already been approved by the FDA. Conjugation to polyethylene glycol (PEG) was one of the first strategies to be exploited in polymer-drug development. PEGylation increases drug hydrophilicity, impairs uptake by reticuloendothelial cells, minimizes clearance by neutralizing antibodies, and reduces renal filtration, globally enhancing the therapeutic effect (Petros and Desimone, 2010; Serna et al., 2018). Besides, other compounds such as polyglutamate and poly-lactic-glycolic acid (PLGA) are also exploited to develop nanocarriers. Currently, there are two FDA approved polymer-drug conjugates for anticancer treatment: neocarzinostatin conjugated to styrene maleic anhydride (SMANCS or Zinostatin Stimalamer) and PEG-L-asparaginase (Pegaspargase or Oncaspar), the last one was the first polymer-drug conjugate to be approved by the FDA in 1994 for the treatment of acute lymphoblastic leukemia (ALL). Importantly, Opaxio, formerly known as Xyotax (paclitaxel-poliglumex), a nanometric polymer of polyglutamate conjugated to paclitaxel, is currently in development for the treatment of head and neck carcinomas among other cancers (Pérez-Herrero and Fernández-Medarde, 2015). In addition, there are also numerous clinical trials regarding polymers conjugated to classical chemotherapeutic drugs, including the galactosamine-targeted PHPMA doxorubicin (PK2), a polymer-drug conjugate (Petros and Desimone, 2010; Ventola, 2017). Nevertheless, despite their appealing properties, polymeric nanodrugs can be difficult to purify and store, limiting their large-scale production (Richards et al., 2016).

4.3.5. Protein-based nanoparticles

Recently, proteins have emerged as promising candidates as drug delivery platforms. Protein-based nanoparticles include drugs conjugated to protein nanocarriers as well as formulations where the protein itself is the active therapeutic drug. The first protein-based nanoparticles exploited the properties of proteins in blood serum, which enabled stable transportation of drugs during circulation. In this context, albumin, a protein carrier naturally present in blood, gained attention as a potential drug carrier and many albumin-based nanoparticles have been developed in the last decades. However, more recently other more advanced approaches have been developed, including engineered proteins that confer nanoparticles with interesting properties (Ventola, 2017).

Several of the aforementioned nanoparticles exhibit different shortcomings regarding their toxicity and *in vivo* limited performance. It has been reported that non-biodegradable

nanoparticles can accumulate in different organs such as the liver and spleen, leading to toxic side effects (Naahidi et al., 2013). Many currently studied nanocarriers, such as dendrimers, metals, carbon nanotubes, and different polymers are highly stable and thus poorly biocompatible, leading to important intrinsic toxicities and compromising their use in patients (Naahidi et al., 2013; Serna et al., 2018). In contrast, protein-based nanoparticles exhibit a great potential as biomaterials as they are biocompatible, biodegradable, and tunable.

Besides, recombinant proteins are produced in cell factories (bacteria, yeasts, insect, or mammalian cells) which enables fully scalable, environmentally friendly processes. Moreover, this technology reduces the cost and complexity compared to classical chemical production. Since its FDA approval in the 1980's, therapeutic proteins have been produced by recombinant technologies worldwide (Sanchez-Garcia et al., 2016; Vazquez et al., 2016). In addition, this system allows for the introduction of surface modifications including covalent attachment of drugs and targeting ligands (Lohcharoenkal et al., 2014).

Another advantage of protein-based nanoparticles is that no protein corona has been observed surrounding them, which represents an important advantage for their *in vivo* performance (Corchero et al., 2014; De Pinho Favaro et al., 2018). Once in the bloodstream, most nanoparticles, including inorganic ones and liposomes, are rapidly coated by many different proteins forming a "protein corona" (Ke et al., 2017; Miceli et al., 2017; Xiao and Gao, 2018). The majority of these proteins are opsonins, a group of proteins that are recognized by cells of the mononuclear phagocyte system (MPS) mainly by Kupffer cells in the liver sinusoids, leading to nanoparticle clearance via phagocytosis (Wilhelm et al., 2016). Moreover, the adsorption of these proteins to the nanoparticle surface alters its properties and may lead to aggregation and loss of their targeting capability (Salvati et al., 2013; Wilhelm et al., 2016).

4.3.5.1. Strategies for the development of protein-based nanoparticles

In the last decades, diverse protein-based nanoparticles have been developed following different strategies (Figure 7).

Synthetic protein nanoparticles. This type of nanoparticles represents the first strategy to be exploited to develop protein nanocarriers, inspired by the proteins present in blood. Synthetic protein nanoparticles are usually produced from natural proteins, such as albumin, which is a natural carrier in circulation in the body. During the synthesis of these nanoparticles, due to different conditions such as concentration and pH, proteins suffer several conformational changes that unfold them. Once unfolded, the now exposed

interactive groups (thiol groups, disulfide bonds) enable that interaction with other proteins leading to the formation of nanoparticles that entrap the drug molecule during their assembly (Ko and Gunasekaran, 2006). The best example of protein polymeric nanoparticles is Abraxane, human albumin nanoparticles containing the chemotherapeutic drug paclitaxel that was first approved by FDA in 2004 for the treatment of metastatic breast cancer (Miele et al., 2009; Ventola, 2017). After the success of Abraxane, other albumin-bound nanoparticles (NABs) have entered clinical trials, including NAB-docetaxel among others (Ventola, 2017).

Protein assemblies. Another approach for the development of protein nanocarriers are protein assemblies. Natural proteins display interesting properties and biological activities that can be useful in the development of materials. The supramolecular organization of such proteins into polymers, hydrogels, fibers, or even viral capsids enriches the options to create novel protein-based biomaterials and enables the development of nanoparticles based on protein assemblies (Corchero et al., 2014). In nature, a wide variety of proteins hold the ability to self-assemble into capsule-like architectures. An example is ferritin, an iron-storage protein, but many others can act as carriers and storage compartments. In this regard, the ability of these proteins to self-assemble into nano-cages has been exploited to develop nanocarriers, including the previously mentioned ferritin as well as small heat-shock proteins and vaults, among others (Schoonen and Van Hest, 2014; Lee et al., 2016). Another example of natural nano-cages with interesting properties are viral capsids. Viral capsids present a wide range of sizes and shapes, moreover, the different types of existing viruses show different tropisms which can also be exploited. In addition, it has been demonstrated that capsid proteins in the absence of viral genetic material are still able to self-assemble into virus-like particles (VLPs). These particles hold a great potential as nanocarriers and have been useful for the development of protein vaccines and in gene therapy (Schoonen and Van Hest, 2014; Ferrer-Miralles et al., 2015; Lee et al., 2016). However, there are still concerns about their biomedical use regarding the residual viral pathogenic potential that might lead to immunostimulation, in addition to the ineffective drug loading during production and low transfection rates (Seow and Wood, 2009; Ferrer-Miralles et al., 2015).

De novo rationally designed nanoparticles. The poor functional flexibility and tunability of natural nano-cages has boosted the development of de novo rationally designed protein-based nanoparticles (Céspedes et al., 2014). Self-assembly of soluble proteins into nanoparticles can be achieved by the fusion of different domains, such as oligomerization domains of natural oligomers. Collagen-mimetic peptides, β -sheets forming amyloid

structures, and α -helix coiled-coils are examples of natural domains that allow protein self-assembly. Moreover, these protein nanoparticles can also be functionalized with other domains, including endosomal escape domains or targeting ligands. All these facts enable the production of protein nanoparticles in a cost-effective manner in recombinant cell factories, that can be used for therapeutic drug delivery (Corchero et al., 2014; Vazquez et al., 2016).

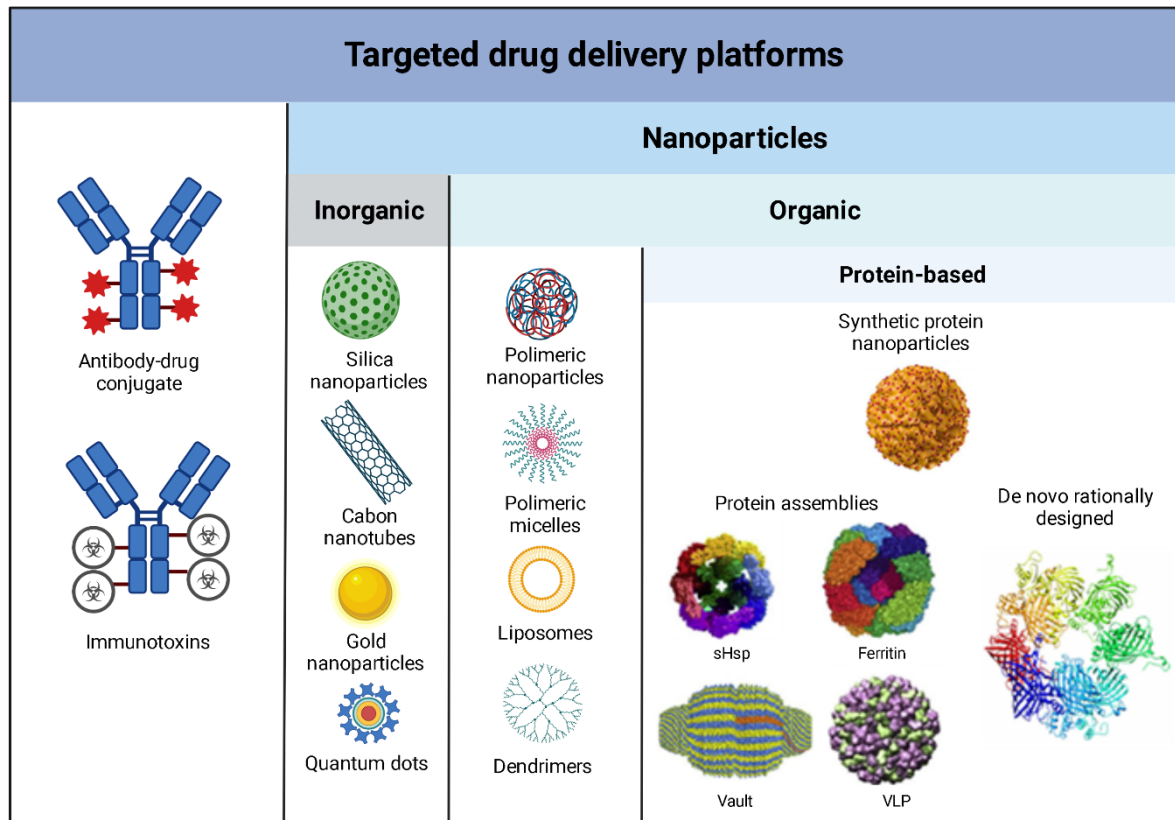


Figure 7. Classification of the most common inorganic and organic nanoparticles, focusing on protein-based nanoparticles. Modified from A. Richards et al., 2017; J. Lee et al., 2016; S. Zolot et al., 2013; and T. Butterfield et al., 2017 (Zolot et al., 2013; Lee et al., 2016; Richards et al., 2016; Butterfield et al., 2017). Created with BioRender.com.

Recently, the Nanobiotechnology group led by Prof. Villaverde, in collaboration with our group, has developed a novel engineering oligomerization approach based on the fusion of a cationic peptide at the N-terminal domain and a polyhistidine tag at the C-terminal domain of a core protein, enabling the oligomerization of neighbor proteins forming regular size nanoparticles. Interestingly, this self-assembly occurs spontaneously in *Escherichia coli*, and appears to be mediated by the interactions between divalent cations present in the media and the imidazole rings of the polyhistidine tags of different monomers (López-Laguna et al., 2019). Moreover, the N-terminal cationic peptide can be a therapeutic ligand, allowing the development of targeted protein nanoparticles that can deliver cytotoxic compounds. Importantly, these protein nanoparticles can be chemically bound to

conventional chemotherapeutic drugs or directly incorporate cytotoxic protein domains in their structure, avoiding additional conjugation steps (Céspedes et al., 2018; Sánchez-García et al., 2018). This novel approach for the development of protein nanoparticles presents great flexibility compared to previous strategies as potentially any core protein fused to a cationic ligand and a polyhistidine tag can promote self-assembly (Unzueta et al., 2012a; Céspedes et al., 2014).

4.4. T22-based protein nanoparticles

T22-based nanoparticles are designed following the previously discussed cationic peptide plus polyhistidine oligomerization approach, which has enabled the development of different protein nanoparticles that hold great therapeutic potential. These T22-nanoparticles, which are recombinantly produced in *E. coli*, present different protein domains in their structure:

- **T22**, an engineered version of the polyphemusin II peptide from the Atlantic horseshoe crab *Limulus polyphemus*, is a CXCR4 antagonist, firstly developed for the treatment of HIV-1 infection (Murakami et al., 2002). This T22 ligand allows nanoparticle targeting against CXCR4⁺ cancer cells. Moreover, being a cationic peptide, it also contributes to the self-assembly of the nanoparticles (Unzueta et al., 2012b).
- A **scaffold protein**, that acts as the protein core fused to the T22 ligand and the polyhistidine tag. Different proteins can be incorporated into the nanoparticles, conferring them with interesting properties.
- **Polyhistidine tag** (H6), that enables protein purification by affinity chromatography and also allows the formation of the nanoparticles through the interaction with divalent cations (Unzueta et al., 2012b). Moreover, it has also been reported that it can enhance the endosomal escape ability of the nanoparticles (Ferrer-Miralles et al., 2011).

Following this strategy, different T22-based nanoparticles have been generated with different properties.

4.4.1. T22-GFP-H6 nanocarrier

T22-GFP-H6 is a fusion protein that includes the green fluorescent protein (GFP) as the scaffold protein, fused to the T22 ligand and the polyhistidine tag. T22-GFP-H6 monomers (6 nm) self-assemble into organized clusters of 11 monomers forming cyclic-shaped nanoparticles of 14 nm (Figure 8). These nanoparticles display great stability both *in vitro* and *in vivo*. In this context, high salt concentrations disturb nanoparticle formation but do not interfere once nanoparticles are already assembled. Moreover, nanoparticle size

enables a long circulation time as it exceeds the renal filtration cut-off. Importantly, GFP maintains its fluorescence upon oligomerization, suggesting that no conformational changes happen during nanoparticle formation. GFP fluorescence enables T22-GFP-H6 follow up both *in vitro* (internalization within the cells) and *in vivo* (biodistribution to the different organs and tissues) (Unzueta et al., 2012a; Céspedes et al., 2014).

In addition, T22-GFP-H6 can be conjugated with different antitumor drugs to act as a therapeutic protein nanocarrier. In this regard, T22-GFP-H6 has been linked to 5-Fluoro-2'-deoxyuridine (5-FdU or FdU), the main antitumor active metabolite of the chemotherapeutic drug 5-FU, frequently used for the treatment of a wide range of solid tumors. This T22-GFP-H6-FdU nanoconjugate has already been successfully tested in a colorectal cancer murine model (Céspedes et al., 2018).

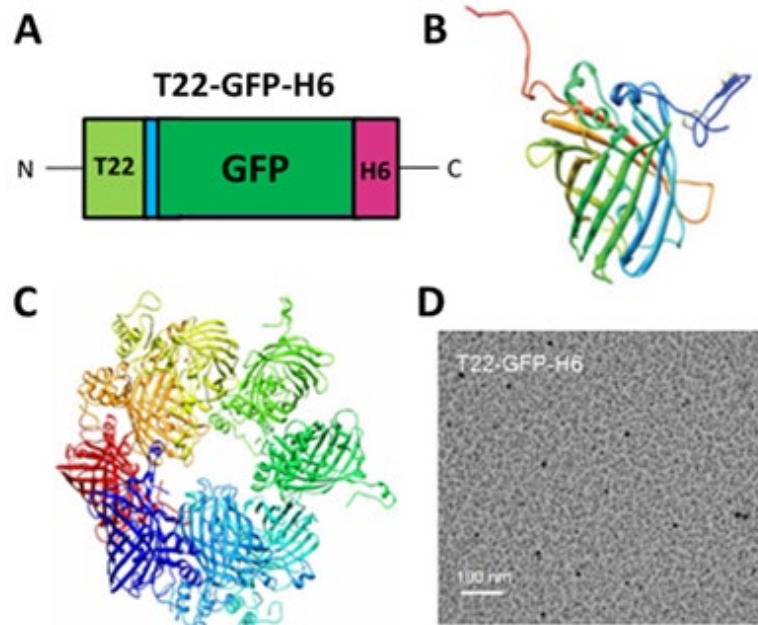


Figure 8. T22-GFP-H6 protein-only nanoparticles allow the follow up of the nanoparticle distribution *in vivo*. A) Schematic representation of the T22-GFP-H6 construct, presenting the T22 domain at the N-terminus, followed by the GFP domain, and the polyhistidine tag (H6) at the C-terminus. B) Predicted structure of the T22-GFP-H6 monomers, containing the ligand- (blue) and H6- (red) overhanging ends. C) Potential organization of T22-GFP-H6 monomers as octamers. D) TEM image of T22-GFP-H6 protein nanoparticles. Modified from MV. Céspedes et al., 2014 and U. Unzueta et al., 2012 (Unzueta et al., 2012a; Céspedes et al., 2014).

4.4.2. T22-PE24-H6 and T22-DITOX-H6 nanotoxins

Lately, the interest in the development of protein-only nanoparticles has focused its efforts on protein toxins as they are promising candidates as they represent an alternative to conventional chemotherapeutic drugs. In general, toxins present the ability to kill exposed cells even at low concentrations. Moreover, toxins are capable of eliminating not only

proliferative but also quiescent cells (Alewine et al., 2015). Importantly, therapeutic toxin-based platforms should be selectively targeted and stable to avoid toxic side effects in normal tissues. In this regard, the incorporation of bacterial toxin domains as scaffolds in the T22-based nanoparticle enables the formation of nanotoxins with intrinsic cytotoxic properties.

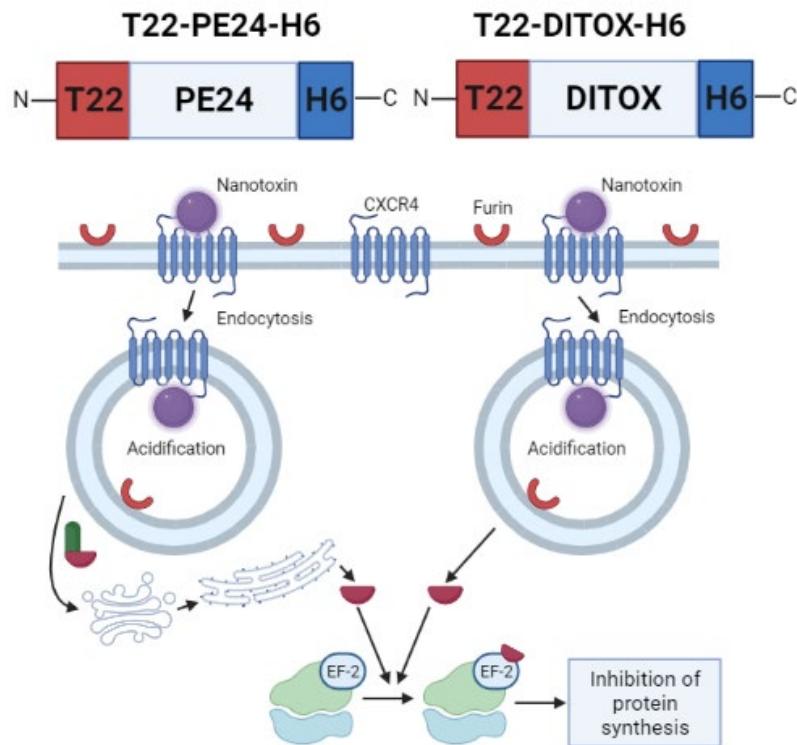


Figure 9. T22-PE24-H6 and T22-DITOX-H6 protein-only nanoparticles present cytotoxic domains derived from bacterial toxins. Schematic representation of the T22-PE24-H6 and T22-DITOX-H6 constructs, presenting the T22 domain at the N-terminus, followed by the toxin domain, and the polyhistidine tag (H6) at the C-terminus. Both toxin-based nanoparticles display a similar mechanism of cell death by inhibiting the ribosomal elongation factor 2 (EF-2), leading to the irreversible inhibition of protein synthesis. Modified from L. Sánchez-García et al., 2018 (Sánchez-García et al., 2018).

Following this strategy, we generated T22-PE24-H6, incorporating the de-immunized catalytic domain of *Pseudomonas aeruginosa* exotoxin A, and T22-DITOX-H6, which includes the translocation and catalytic domains of the diphtheria toxin from *Corynebacterium diphtheriae* (Figure 9). T22-PE24-H6 and T22-DITOX-H6 monomers self-assemble into toroid-shaped nanoparticles of approximately 60 nm and 38 and 90 nm nanoparticles, respectively. In both cases, size is in a range considered to be optimal for cell uptake and *in vivo* performance (bigger than 7 nm to avoid renal clearance but smaller than 100 nm to prevent aggregation and undesired macrophage clearance (Serna et al., 2018)). Both nanoparticles have proved to be highly stable in different physiological buffers including high salt concentrations. Importantly, these nanoparticles have been engineered

to incorporate furin-mediated cleavage sites that upon internalization within the cells are able to release the toxin catalytic domain in the acidic endosomal environment. This system enables the stable delivery of the toxin drug to the target CXCR4⁺ cells without drug leakage and its activation only once inside the cell, thus reducing undesired toxic side effects. Toxin active fragments of the *Pseudomonas aeruginosa* exotoxin A and the diphtheria toxin perform an ADP-ribosylation of the ribosomal elongation factor 2 (EF-2), leading to the irreversible inhibition of protein synthesis, thus triggering cell death (Sánchez-García et al., 2018) (Figure 9).

RESEARCH OBJECTIVES

Despite the improvement of HNSCC therapy, with the approval of targeted monoclonal antibodies (cetuximab) and immune check-point inhibitors (pembrolizumab), up to 30-40% of HNSCC patients still die as a consequence of the disease. Importantly, recurrence and development of metastasis represent the leading causes of patient mortality. In this regard, previous studies have associated CXCR4 overexpression in HNSCC primary tumors with a higher risk of developing loco-regional recurrence and distant metastasis as well as with worse patient prognosis. CXCR4 has also been related to invasion, migration, angiogenesis, stem cell phenotype, therapy resistance, and metastasis. In addition, CXCR4 is overexpressed in HNSCC tumors compared to normal tissue, making the receptor an ideal target for drug delivery. Thus, the present thesis aimed to study the therapeutic potential of novel CXCR4-targeted protein nanoparticles for the treatment of HNSCC. To achieve this goal, we have evaluated the (i) biodistribution, (ii) antitumor, and (iii) antimetastatic effect of these novel CXCR4-targeted protein nanoparticles, as recapitulated in the following chapters.

Chapter 1: Self-assembling protein nanocarrier for the selective delivery of cytotoxic polypeptides to CXCR4⁺ head and neck squamous cell carcinoma tumors

A major problem of conventional chemotherapeutic drugs currently used in the clinic is their lack of selectivity, thus affecting tumor cells but also healthy tissues, resulting in severe toxicities. In the last decades, different nanoparticles and nanocarriers have been developed seeking to enhance tumor drug delivery. However, it is estimated that less than 1% of the administered dose reaches the tumor site, leading to their accumulation in healthy organs such as liver and kidneys. In this context, targeted drug delivery aims to increase drug tumor uptake by targeting different receptors overexpressed in tumor tissues. Here, we aimed to study the CXCR4-dependent internalization and biodistribution of a novel protein nanocarrier, named T22-GFP-H6, for the selective delivery of cytotoxic polypeptides to CXCR4⁺ HNSCC cancer cells.

In detail, the specific objectives of this chapter were:

- Studying the T22-GFP-H6 internalization in human HNSCC cell lines and its dependence on the CXCR4 receptor.
- Assessing T22-GFP-H6 biodistribution and CXCR4-dependent tumor accumulation in a subcutaneous HNSCC mouse model.
- Evaluating the ability of the nanocarrier to selectively deliver cytotoxic polypeptides to CXCR4⁺ HNSCC tumor cells.

Chapter 2: CXCR4-targeted nanotoxins induce GSDME-dependent pyroptosis in head and neck squamous cell carcinoma

Bacterial toxin domains represent a promising alternative to conventional chemotherapeutic drugs, holding a great potential as anticancer agents. Toxins display a potent cytotoxic effect and are capable of eliminating both proliferating and quiescent cells. These toxin polypeptidic domains can be coupled to targeting moieties or incorporated into a fusion protein to obtain nanotoxins, being recombinantly expressed in a cost-effective and scalable way, avoiding additional chemical conjugation steps. In this chapter, we evaluated the suitability of T22-PE24-H6 and T22-DITOX-H6, two CXCR4-targeted nanotoxins that incorporate the de-immunized catalytic domain of *Pseudomonas aeruginosa* exotoxin A and the diphtheria toxin respectively, for the treatment of HNSCC.

Specifically, the main objectives of this chapter were:

- Assessing the CXCR4-dependent cytotoxic effect of T22-PE24-H6 and T22-DITOX-H6 nanotoxins in different HNSCC cell lines.
- Determining the cell death mechanism induced by T22-PE24-H6 and T22-DITOX-H6 in the HNSCC cell lines.
- Studying the antitumor effect of T22-PE24-H6 and T22-DITOX-H6 nanotoxins in a CXCR4-overexpressing HNSCC subcutaneous mouse model.
- Analyzing the potential toxic effects derived from the nanotoxins treatment in non-tumor bearing organs.
- Evaluating the potential clinical repercussions of a T22-PE24-H6 or T22-DITOX-H6 based therapy for HNSCC patients.

Chapter 3: A novel CXCR4-targeted diphtheria toxin nanoparticle inhibits invasion and metastatic dissemination in a head and neck squamous cell carcinoma mouse model

Loco-regional recurrence and distant metastasis represent the leading causes of HNSCC patient mortality. Up to 60% of HNSCC patients will develop loco-regional recurrences and up to 30% distant metastases after treatment. Remarkably, recurrent and/or metastatic patients present a very poor clinical outcome, with a median overall survival of less than a year. Current treatment options for these patients are mostly palliative, emphasizing the necessity of novel therapeutic approaches. In this context, CXCR4 emerges as a promising therapeutic target, since its overexpression has been related to loco-regional and distant recurrence, lymph node metastasis, and poor overall

survival in HNSCC patients. Consequently, we aimed to study the potential antimetastatic effect of the T22-DITOX-H6 nanotoxin in an HNSCC disseminated mouse model with endogenous CXCR4 expression.

To do that, we followed different specific objectives:

- Evaluating the effect of the T22-DITOX-H6 nanotoxin in tumor invasion in a HNSCC orthotopic mouse model.
- Assessing the antimetastatic effect of T22-DITOX-H6 in an HNSCC orthotopic mouse model that replicates the metastatic pattern found in HNSCC patients.

RESULTS

CHAPTER 1

Self-assembling protein nanocarrier for selective delivery of cytotoxic polypeptides to CXCR4⁺ head and neck squamous cell carcinoma tumors

Elisa Rioja-Blanco, Irene Arroyo-Solera, Patricia Álamo, Isolda Casanova, Alberto Gallardo, Ugutz Unzueta, Naroa Serna, Laura Sánchez-García, Miquel Quer, Antonio Villaverde, Esther Vázquez*, Ramon Mangués*, Lorena Alba-Castellón*, Xavier León

*co-corresponding authors

Acta Pharmaceutica Sinica B

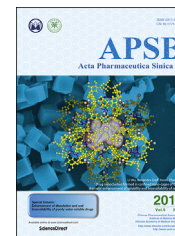
2021



Chinese Pharmaceutical Association
Institute of Materia Medica, Chinese Academy of Medical Sciences

Acta Pharmaceutica Sinica B

www.elsevier.com/locate/apsb
www.sciencedirect.com



ORIGINAL ARTICLE

Self-assembling protein nanocarrier for selective delivery of cytotoxic polypeptides to CXCR4⁺ head and neck squamous cell carcinoma tumors

Elisa Rioja-Blanco^{a,b}, Irene Arroyo-Solera^{a,b,c}, Patricia Álamo^{a,b,c},
Isolda Casanova^{a,b,c}, Alberto Gallardo^{a,d}, Ugutz Unzueta^{a,b,c},
Naroa Serna^{c,e,f}, Laura Sánchez-García^{c,e,f}, Miquel Quer^{c,g},
Antonio Villaverde^{c,e,f}, Esther Vázquez^{c,e,f,*}, Ramon Mangués^{a,b,c,*},
Lorena Alba-Castellón^{a,b,*}, Xavier León^{c,g}

^aInstitut d'Investigació Biomèdica Sant Pau (IIB-Sant Pau), Barcelona 08041, Spain

^bInstitut de Recerca contra la Leucèmia Josep Carreras, Barcelona 08025, Spain

^cCIBER de Bioingeniería, Biomateriales y Nanomedicina (CIBER-BBN), Madrid 28029, Spain

^dDepartment of Pathology, Hospital de la Santa Creu i Sant Pau, Barcelona 08041, Spain

^eInstitut de Biotecnologia i de Biomedicina, Universitat Autònoma de Barcelona, Bellaterra 08193, Spain

^fDepartament de Genètica i de Microbiologia, Universitat Autònoma de Barcelona, Bellaterra 08193, Spain

^gDepartment of Otorhinolaryngology, Hospital de la Santa Creu i Sant Pau, Barcelona 08041, Spain

Received 5 July 2021; received in revised form 3 September 2021; accepted 15 September 2021

KEY WORDS

Targeted drug delivery;
Protein nanoparticles;
CXCR4 receptor;
HNSCC;
Cell targeting;
Recombinant proteins;
Nanotoxins;
Cancer therapy

Abstract Loco-regional recurrences and distant metastases represent the main cause of head and neck squamous cell carcinoma (HNSCC) mortality. The overexpression of chemokine receptor 4 (CXCR4) in HNSCC primary tumors associates with higher risk of developing loco-regional recurrences and distant metastases, thus making CXCR4 an ideal entry pathway for targeted drug delivery. In this context, our group has generated the self-assembling protein nanocarrier T22-GFP-H6, displaying multiple T22 peptidic ligands that specifically target CXCR4. This study aimed to validate T22-GFP-H6 as a suitable nanocarrier to selectively deliver cytotoxic agents to CXCR4⁺ tumors in a HNSCC model. Here we demonstrate that T22-GFP-H6 selectively internalizes in CXCR4⁺ HNSCC cells, achieving a high accumulation in CXCR4⁺ tumors *in vivo*, while showing negligible nanocarrier distribution in non-tumor bearing organs. Moreover, this T22-empowered nanocarrier can incorporate bacterial toxin domains to generate therapeutic nanotoxins that induce cell death in CXCR4-overexpressing tumors in the absence

*Corresponding authors. Tel.: +34 935537919 (Ramon Mangués); +34 935537921 (Lorena Alba-Castellón).

E-mail addresses: esther.vazquez@uab.cat (Esther Vázquez), rmangués@santpau.cat (Ramon Mangués), lalba@santpau.cat (Lorena Alba-Castellón).
Peer review under responsibility of Chinese Pharmaceutical Association and Institute of Materia Medica, Chinese Academy of Medical Sciences

<https://doi.org/10.1016/j.apsb.2021.09.030>

2211-3835 © 2022 Chinese Pharmaceutical Association and Institute of Materia Medica, Chinese Academy of Medical Sciences. Production and hosting by Elsevier B.V. This is an open access article under the CC BY-NC-ND license (<http://creativecommons.org/licenses/by-nc-nd/4.0/>).

Please cite this article as: Rioja-Blanco Elisa et al., Self-assembling protein nanocarrier for selective delivery of cytotoxic polypeptides to CXCR4⁺ head and neck squamous cell carcinoma tumors, Acta Pharmaceutica Sinica B, <https://doi.org/10.1016/j.apsb.2021.09.030>

of histological alterations in normal organs. Altogether, these results show the potential use of this T22-empowered nanocarrier platform to incorporate polypeptidic domains of choice to selectively eliminate CXCR4⁺ cells in HNSCC. Remarkably, to our knowledge, this is the first study testing targeted protein-only nanoparticles in this cancer type, which may represent a novel treatment approach for HNSCC patients.

© 2022 Chinese Pharmaceutical Association and Institute of Materia Medica, Chinese Academy of Medical Sciences. Production and hosting by Elsevier B.V. This is an open access article under the CC BY-NC-ND license (<http://creativecommons.org/licenses/by-nc-nd/4.0/>).

1. Introduction

Head and neck squamous cell carcinoma (HNSCC) is the sixth most common cancer worldwide, accounting for more than 650,000 cases and 330,000 deaths annually^{1,2}. Current treatment allows loco-regional control of the disease^{3,4}, however, up to 60% of patients develop loco-regional recurrences and up to 30% distant metastases after treatment, with a median overall survival of less than one year⁵. Importantly, loco-regional recurrences and distant metastases represent the main cause of patient mortality⁶. Despite the improvement in the treatment, including novel surgical procedures, radiotherapy, new cytostatic compounds, targeted monoclonal antibodies, and immunotherapy; up to 30%–40% of HNSCC patients still die as a consequence of the disease⁵. Thus, new therapeutic strategies are urgently needed in order to improve patient survival.

In the last years, targeted-drug delivery to cancer cells has emerged as a promising alternative to existing treatments, as it potentially improves drug accumulation within tumor tissues, thus enhancing response rates while reducing side effects^{7,8}. In this regard, the chemokine receptor 4 (CXCR4) has been proposed as a promising molecular target. CXCR4 is overexpressed in a wide range of cancers, including HNSCC and has been related to enhanced invasion, migration, and angiogenesis, as well as with a stem cell phenotype, chemotherapy resistance and metastasis development^{9,10}. Importantly, our group and others have reported that CXCR4 overexpression in HNSCC primary tumors associates with a higher risk of developing loco-regional recurrences and distant metastases as well as with worse patient prognosis^{11,12}.

In this context, our group has developed the self-assembling protein nanocarrier T22-GFP-H6. This nanocarrier incorporates T22, a cationic peptide that acts as a CXCR4 antagonist, designed to inhibit HIV infection¹³. In our case, T22 was used instead as a peptidic ligand to specifically target the CXCR4 receptor, fused to the green fluorescent protein (GFP), allowing its follow up both *in vitro* and *in vivo*^{14,15}; and a polyhistidine tag (H6) necessary for T22-GFP-H6 purification and conformation^{16,17}. T22-GFP-H6 nanocarrier has already proved to be effective in targeting CXCR4⁺ cells in colorectal cancer (CRC) and diffuse large B-cell lymphoma (DLBCL) animal models^{15,18}. Remarkably, so far, no protein-based nanocarrier has been reported to selectively target HNSCC cancer cells, highlighting the relevance of this study. Moreover, T22-GFP-H6 displays great versatility as a vehicle allowing the conjugation of different chemical drugs or the incorporation of toxin domains, enabling the selective targeting and depletion of CXCR4⁺ cancer cells¹⁹. Considering the implication of CXCR4 in loco-regional recurrence and distant metastases, this approach could potentially improve current HNSCC treatment.

In this study, we report that T22-GFP-H6 nanocarrier internalizes selectively in CXCR4⁺ HNSCC cell lines. Moreover,

when administered *in vivo* in a subcutaneous CXCR4-overexpressing HNSCC model, T22-GFP-H6 mostly accumulates in the tumor compared to other non-tumor bearing organs. Finally, we show the ability of the nanocarrier to selectively deliver cytotoxic agents to CXCR4⁺ tumors. For this purpose, we intravenously administered T22-DITOX-H6 and T22-PE24-H6, two nanoparticles presenting the same multidomain-based design as T22-GFP-H6 nanocarrier but carrying the diphtheria toxin catalytic domain and the *Pseudomonas aeruginosa* exotoxin A domain, respectively. Both nanotoxins were able to induce cancer cell death and achieve a potent antitumor effect in CXCR4-overexpressing tumors in HNSCC mouse models, proving their suitability as targeted nanoparticles for anticancer therapy. This work highlights the potential use of T22-GFP-H6 derived nanoparticles to selectively target CXCR4⁺ cells in HNSCC patients with worse prognosis.

2. Materials and methods

2.1. Nanoparticles production, purification, and characterization

T22-GFP-H6, T22-PE24-H6 and T22-DITOX-H6 production and purification were described in previous work^{14,15,19}. Coding sequences introduced in the plasmid pET22b (Novagen 69744-3) for the three nanoparticles are included in Supporting Information Fig. S1.

2.2. Cell lines and cell culture

HNSCC cell lines UM-SCC-74B (74B) and UM-SCC-22A (22A)²⁰ were kindly provided by Dr. R.H. Brakenhoff and Dr. Gregory Oakley, respectively. 293T cell lines were purchased from ATCC. HNSCC cell lines were authenticated using the Cell ID Kit (Promega, Madison, WI, USA). The short tandem repeat (STR) profiles were compared with the profiles previously described²¹. All cell lines were cultured in Dulbecco's modified Eagle's medium (DMEM) containing 10% Fetal Bovine Serum (FBS), 100 U/mL penicillin/streptomycin and 2 mmol/L glutamine (Life Technologies) and incubated at 37 °C and 5% CO₂ in a humidified atmosphere.

2.3. Lentiviral CXCR4-Luciferase and Luciferase transduction

Lentiviral plasmid CXCR4-Luciferase (pLenti-III-UbC-CXCR4-2A-luc) and Luciferase (pLenti-III-UbC-luc) were purchased from Abm (Abm, Vancouver, Canada). Lentiviral particles were obtained by co-transfection of the plasmids described above with pMD.G_VSV G-poly-A vector and p8 91-Gag-Pol vector into 293T cells using lipofectamine 2000 (Life Technologies). After 48 h, cell supernatant was harvested, filtered through a 45 μm filter and used to transduce UM-SCC-74B (74B) and UM-SCC-

22A (22A) cell lines. Infected cell lines were selected in medium containing puromycin (0.8 µg/mL for 74B and 0.4 µg/mL for 22A) for 3–4 weeks until stable clones were obtained. Cell lines transduced with the CXCR4-Luciferase plasmid (74B-CXCR4⁺ and 22A-CXCR4⁺) were sorted by FACS Aria cell sorter (BD Biosciences) using PE-Cy5 mouse antihuman CXCR4 monoclonal antibody (BD Biosciences) to isolate membrane CXCR4-overexpressing cells.

2.4. Flow cytometry

CXCR4 membrane expression in the cell lines was determined by FACSCalibur (BD Biosciences) using PE-Cy5 mouse anti-human CXCR4 monoclonal antibody (BD Biosciences). The negative population was defined using the PE-Cy5 Mouse IgG2a isotype (BD Biosciences) as a control.

T22-GFP-H6 internalization was quantified by GFP fluorescence signal using FACSCalibur (BD Biosciences). Cells seeded in 6-well plates (250,000 cell/well for 74B and 500,000 cells/well for 22A) were treated with different T22-GFP-H6 concentrations (0–500 nmol/L) for different times (1, 6, and 24 h), then washed with PBS, detached from the plate, and trypsinized (1 mg/mL trypsin, Life Technologies) for 15 min at 37 °C in order to remove nonspecific binding of the nanocarrier. For the CXCR4 blocking assays, cells were preincubated with AMD3100 (1 µmol/L, Sigma) for 1 h before adding the nanocarrier. T22-GFP-H6 internalization data was analyzed using the Cell Quest Pro software and represented as mean fluorescence intensity (MFI). Buffer-treated cells were considered as the negative population. All experiments were performed in triplicate.

2.5. Western blotting

T22-GFP-H6 internalization was further studied by Western blotting (WB). For that, 74B-CXCR4⁺ cells were incubated with different T22-GFP-H6 concentrations (1, 5, 10, and 20 nmol/L) for 1 h. Then, cells were washed with PBS and proteins were extracted using RIPA buffer (Sigma). Protein samples were then sonicated, centrifuged at top speed for 10 min at 4 °C, and supernatants were stored at –20 °C to perform Western blotting assays. Protein concentration was assessed using the Pierce™ Rapid Gold BCA Protein Assay Kit (Thermo Scientific) according to the manufacturer's instructions. 50 µg of protein extracts were loaded in a 15% SDS-PAGE gel and transferred to a nitrocellulose blotting membrane (GE Healthcare life sciences). Membranes were blocked with 5% skim milk in TBS-T for 1 h at room temperature and incubated overnight at 4 °C with the primary antibodies GFP rabbit polyclonal (1:500, Santa Cruz Biotechnology) or α/β-tubulin (1:1,000, Cell Signaling). After washing with TBS-T to remove nonspecific antibody binding, membranes were incubated with the corresponding secondary antibodies (1:10,000, Jackson Immune Research) for 1 h at room temperature. Finally, membranes were further washed with TBS-T and visualized with the SuperSignal™ West Pico Chemiluminescent Substrate (Thermo Scientific) and the ChemiDoc XRS⁺ imaging system (Biorad).

2.6. Cell viability assays

The Cell Proliferation Kit II (XTT) (Roche) was used to determine the cytotoxicity of T22-DITOX-H6 and T22-PE24-H6 nanotoxins, according to the manufacturer's instructions. Cells seeded in 96-

well plates (2500 cell/well) were treated with buffer or 50 nmol/L of either T22-DITOX-H6 or T22-PE24-H6 for different times (6, 24, and 48 h). To test the ability of the nanotoxins to exert any off-target cytotoxicity upon cellular content release, 74B-CXCR4⁺ cells were seeded in 96-well plates and treated as previously explained. After 48 h, when cells were dead, supernatants were transferred to 74B mock 96-well plate cultures and further incubated for 48 h. After the different treatments, the XTT reagent was added to the plate and incubated at 37 °C for 4 h. After this incubation period, the absorbance, which directly correlates to the number of viable cells, was measured using a multi-well spectrophotometer (FLUOstar Optima, BMG Labtech). All experiments were performed in triplicate.

2.7. In vivo experiments

Four-week-old female Swiss nude mice [NU(Ico)-Foxn1tm] weighing 18–25 g were purchased from Charles River (France). Animals were housed in a specific pathogen-free (SPF) environment with sterile food and water *ad libitum*. All animal experiments were approved by the Hospital de la Santa Creu i Sant Pau Animal Ethics Committee.

Subcutaneous tumor models were obtained injecting 10 million cells either 74B mock or 74B-CXCR4⁺ in both flanks of the animal. Tumor size was measured three times per week with a caliper according to Eq. (1):

$$\text{Tumor volume} = \text{Width}^2 \times \text{Length}/2 \quad (1)$$

To assess T22-GFP-H6 biodistribution, animals bearing tumors of approximately 200 mm³ were randomized into two groups ($n = 3$ per group). One group was injected intravenously with a single dose of 200 µg T22-GFP-H6, the other one with buffer (166 mmol/L NaCO₃H pH 8). Animals were euthanized at different times post-injection (2, 6, and 24 h) and an *ex vivo* measurement of fluorescence intensity (FLI) of tumors and different organs was performed using IVIS® Spectrum 200 (PerkinElmer). For the CXCR4 blocking experiments, AMD3100 was subcutaneously injected into mice at a dose of 10 mg/kg three times (1 h before T22-GFP-H6 administration and 1 and 2 h after). After euthanizing the animals, tumors and organs were collected, fixed in 4% formaldehyde solution and paraffin-embedded. Plasma was also obtained by centrifugation of total blood, extracted from the animals by intracardiac puncture. Fluorescence intensity (FLI) data is expressed as average radiant efficiency and it has been calculated subtracting the FLI signal of buffer-treated mice to the FLI signal of T22-GFP-H6-treated animals. The FLI ratio was obtained by dividing the FLI signal of each organ by the FLI signal of the kidneys (organ with the most stable FLI signal throughout the experiment); thus being expressed as fold-change respect to kidneys.

T22-PE24-H6 and T22-DITOX-H6 cytotoxic effect was studied using the CXCR4 over-expressing subcutaneous mouse model described above ($n = 2$ per group). When tumors reached an approximate volume of 200 mm³, 30 µg of T22-DITOX-H6 or 100 µg T22-PE24-H6 were intravenously administered to the animals. After either 24 or 48 h, animals were euthanized, and tumors and normal organs were collected and fixed for further analysis. For the antitumoral effect experiment, 2 million cells either 74B mock or 74B-CXCR4⁺ were orthotopically injected in the tongue of the animals. After the detection of luminescence emitted by viable tumor cells, using IVIS® Spectrum 200,

animals were randomized into three groups ($n = 5$ per group). Nanoparticle-treated animals were intravenously administered 10 μg of T22-DITOX-H6 or T22-PE24-H6 daily up to 5 doses. On alternate days, body weight was registered and tumor growth was measured by the luminescent signal emitted by tumor cells using IVIS® Spectrum 200 system. Mice were euthanized 24 h after the fifth dose. At the end point of the experiment, tumor volume was measured with a caliper according to Eq. (2):

$$\text{Tumor volume} = \text{Width} \times \text{Length} \times \text{Depth} \quad (2)$$

and tumors and organs were collected for histological analysis.

2.8. Confocal laser scanning microscopy

Colocalization of GFP and CXCR4 within tumor tissues, liver, and kidneys was performed by immunofluorescence. Paraffin-embedded tumors and organs were cut into 4 μm sections, heated for 1 h at 60 °C, dewaxed and rehydrated. Antigen retrieval was performed using Tris–EDTA Buffer, pH 9.0 (Invitrogen) in a Decloaking Chamber™ NxGen (Biocare medical) at 110 °C for 20 min. Then, samples were washed with TBS and blocked with TBS +0.5% TritonX-100 + 3% donkey serum for 1 h at room temperature. Tissue sections were then incubated with the primary antibodies GFP chicken IgY (1:250, AVES) and CXCR4 rabbit IgG (1:250, Abcam) overnight at 4 °C. Samples were washed and incubated with the secondary antibodies anti-chicken IgY-Cy2 (1:50, Jackson Immune Research) and anti-rabbit IgG-Alexa Fluor® 568 (1:200, abcam) for 2 h at room temperature. Finally, the tumor sections were washed, stained with DAPI 0.5 $\mu\text{g}/\text{mL}$ for 10 min at RT, and mounted. Samples were visualized in a Confocal multispectral Leica SP5 AOBS microscope (Leica) and analyzed using Fiji, ImageJ software.

2.9. Histopathology, DAPI staining, and immunohistochemical analysis

In order to perform a histopathological analysis to assess any possible toxic effect, 4 μm paraffin-embedded tumor and organ sections were stained with H&E and analyzed by two independent observers (one section of the whole organ/tumor). Cell death in tumor tissues and normal organs was assessed by DAPI staining and cleaved caspase-3 immunohistochemical (IHC) staining (1:300, BD. Retrieval pH low, Dako). For DAPI staining, paraffin-embedded sections were dewaxed, rehydrated, and permeabilized with 0.5% Triton X-100. Then, slides were stained with DAPI mounting medium (ProLong™ Gold Antifade Mountant, Thermo Scientific) and visualized by fluorescence microscopy. Representative pictures were taken using an Olympus DP73 digital camera and the number of dead cells was quantified by counting the number of condensed nuclei per 10 high-power fields (magnification 400 \times). CXCR4 (1:200, Abcam, Retrieval pH high, Dako) expression was studied by immunohistochemistry (IHC) in cell pellets of the different HNSCC cell lines and tissue sections (tumor and non-tumor bearing organs). IHC staining was performed in a DAKO Autostainer Link48 following the manufacturer's instructions. Representative images were taken using an Olympus DP73 digital camera and processed with the Olympus CellD Imaging 3.3 software. CXCR4 expression levels in tumors and normal organs were quantified as mean gray values as well as cleaved caspase-3 positive cells using Fiji, ImageJ software.

2.10. Statistical analysis

Data are expressed as mean \pm Standard Error. Statistical analyses were performed using the GraphPad Prism 5 software (GraphPad Software, San Diego, California USA). Results were analyzed by Student's *t*-test. Differences were considered statistically significant when *P* value < 0.05. All experiments were performed at least in triplicates.

3. Results

3.1. T22-GFP-H6 selectively internalizes in CXCR4-overexpressing HNSCC cells

CXCR4 cell membrane expression was assessed by flow cytometry and IHC (Supporting Information Fig. S2A–S2C) for 2 different HNSCC cell lines (74B mock and 74B-CXCR4⁺, and 22A mock and 22A-CXCR4⁺). 74B mock and 22A mock cell lines did not express CXCR4, whereas the CXCR4-overexpressing cell lines (74B-CXCR4⁺ and 22A-CXCR4⁺) presented CXCR4 located in the cell membrane. 22A-CXCR4⁺ cell line showed the highest amounts of CXCR4 in the cell membrane as represented by its mean fluorescence intensity (MFI, Supporting Information Fig. S2B).

T22-GFP-H6 nanocarrier (Supporting Information Fig. S3) internalization inside the cells was measured by flow cytometry and represented as mean fluorescence intensity (MFI), which correlates with GFP presence inside the cells. Interestingly, T22-GFP-H6 only internalizes in the CXCR4-overexpressing cell lines, while MFI values for the mock cell lines remained similar to those observed in the buffer-treated cells (no statistically significant differences, Fig. 1A). Nanocarrier internalization was found to be concentration-dependant in both CXCR4-overexpressing cell lines (Fig. 1A). Moreover, T22-GFP-H6 internalization correlated with CXCR4 membrane expression, as MFI values were higher in the 22A-CXCR4⁺ cell line compared to 74B-CXCR4⁺ (Fig. 1A and Supporting Information Fig. S2B). T22-GFP-H6 internalization inside the cells was also assessed by WB confirming its entry to CXCR4⁺ cells (Fig. 1B). No statistically significant differences were found in internalization at 1, 6 and 24 h (Fig. 1C and D). T22-GFP-H6 internalization appears to be fast and sustained in time in both CXCR4⁺ cell lines.

Nanocarrier CXCR4 selective internalization was further corroborated by CXCR4 blockage using AMD3100 (CXCR4 antagonist). CXCR4-overexpressing cells pretreated with AMD3100 did not internalize the nanocarrier compared to the ones without AMD3100 (Fig. 1E and F). Thus, we have demonstrated that the T22-GFP-H6 nanocarrier internalizes within HNSCC cells via the CXCR4 receptor.

3.2. T22-GFP-H6 achieves a high tumor accumulation in subcutaneous HNSCC tumors compared to normal organs

T22-GFP-H6 tumor accumulation was measured after the administration of a 200 μg single-dose intravenous injection of the nanocarrier in CXCR4-overexpressing tumor-bearing mice. Animals were euthanized at different times (2, 6, and 24 h) and nanoparticle accumulation in tumors and normal organs was determined by GFP emitted fluorescence intensity using IVIS® Spectrum 200 system. T22-GFP-H6 was detectable in tumor tissue at the three studied time points, presenting a maximum at 6 h among the three studied time points (Fig. 2A). Importantly,

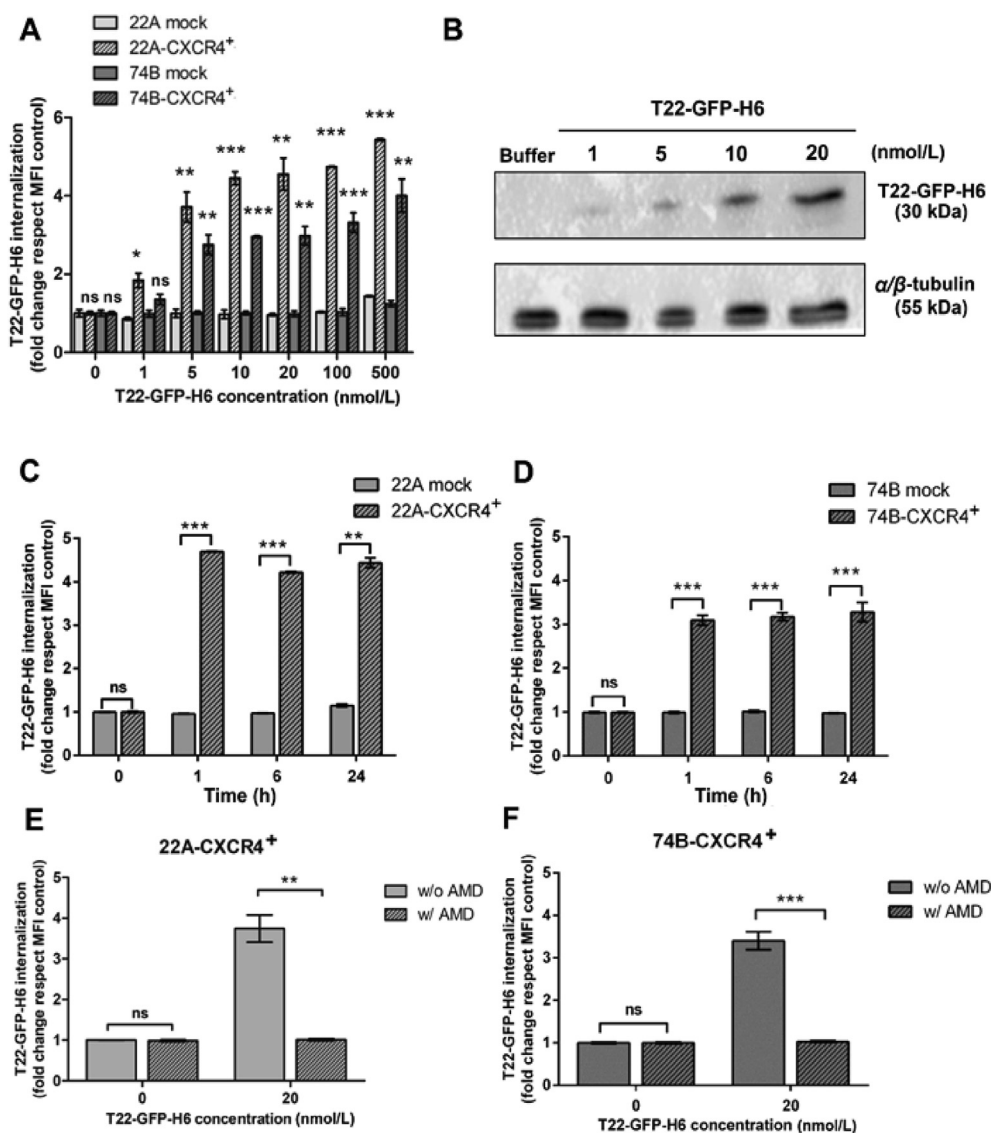


Figure 1 T22-GFP-H6 internalization in CXCR4⁺ HNSCC cell lines *in vitro*. (A) T22-GFP-H6 intracellular levels in 22A mock, 22A-CXCR4⁺, 74B mock, and 74B-CXCR4⁺ cell lines quantified by flow cytometry after a 6h exposure at different concentrations (0–500 nmol/L) of the nanocarrier. (B) Western blotting assay showing the increasing accumulation of T22-GFP-H6 inside 74B-CXCR4⁺ cells treated with different concentrations of the nanocarrier (1–20 nmol/L) for 1 h. (C) and (D) Nanocarrier internalization in 22A mock and 22A-CXCR4⁺ (C) and 74B mock and 74B-CXCR4⁺ (D) cells at three different incubation times (1, 6, and 24 h) in the presence of 20 nmol/L T22-GFP-H6. (E) and (F) AMD3100 blocking assay in 22A-CXCR4⁺ (E) and 74B-CXCR4⁺ (F) treated with a 20 nmol/L T22-GFP-H6 concentration. Data represented as mean \pm Standard error. All experiments were performed in triplicate. * $P < 0.05$; ** $P < 0.01$; *** $P < 0.001$; ns, non-significant. Statistical analysis performed by Student's *t*-test. MFI, mean fluorescence intensity.

nanocarrier accumulation was observed mainly in tumor tissues with almost no signal in non-tumor bearing organs (fold-change respect to kidneys below 1, indicated by the dashed line in Fig. 2B) (Fig. 2B and C). Remarkably, fluorescence intensity at 6 h was approximately 10-fold higher in tumor, when compared with the rest of the analyzed organs (Fig. 2B).

The area under the curve (AUC) was calculated for the time-course of the experiment in order to quantify the T22-GFP-H6 accumulation for the tumors and different healthy organs. Tumors accumulated $78.3 \pm 11.8\%$ of the total FLI measured in all organs (tumors and normal tissues, Fig. 2D and E). The rest of the organs reached distribution values lower than 10% (Fig. 2D

and E). Importantly, the liver, an organ involved in the metabolism of drugs circulating in blood, presented a value lower than 1%.

T22-GFP-H6 biodistribution was found to be consistent with CXCR4 levels in each tissue, as measured by IHC (Fig. 3A and B). Tumor tissues displayed the highest expression of the receptor compared to non-tumor bearing organs, such as liver or kidneys (67- and 26-fold, respectively). Importantly, the spleen showed lower CXCR4 levels than tumors (4-fold), presenting a light pattern consistent with CXCR4 expression by immune cells such as lymphocytes. These results imply that the accumulation of the nanocarrier mainly in tumor tissues is driven by their high CXCR4

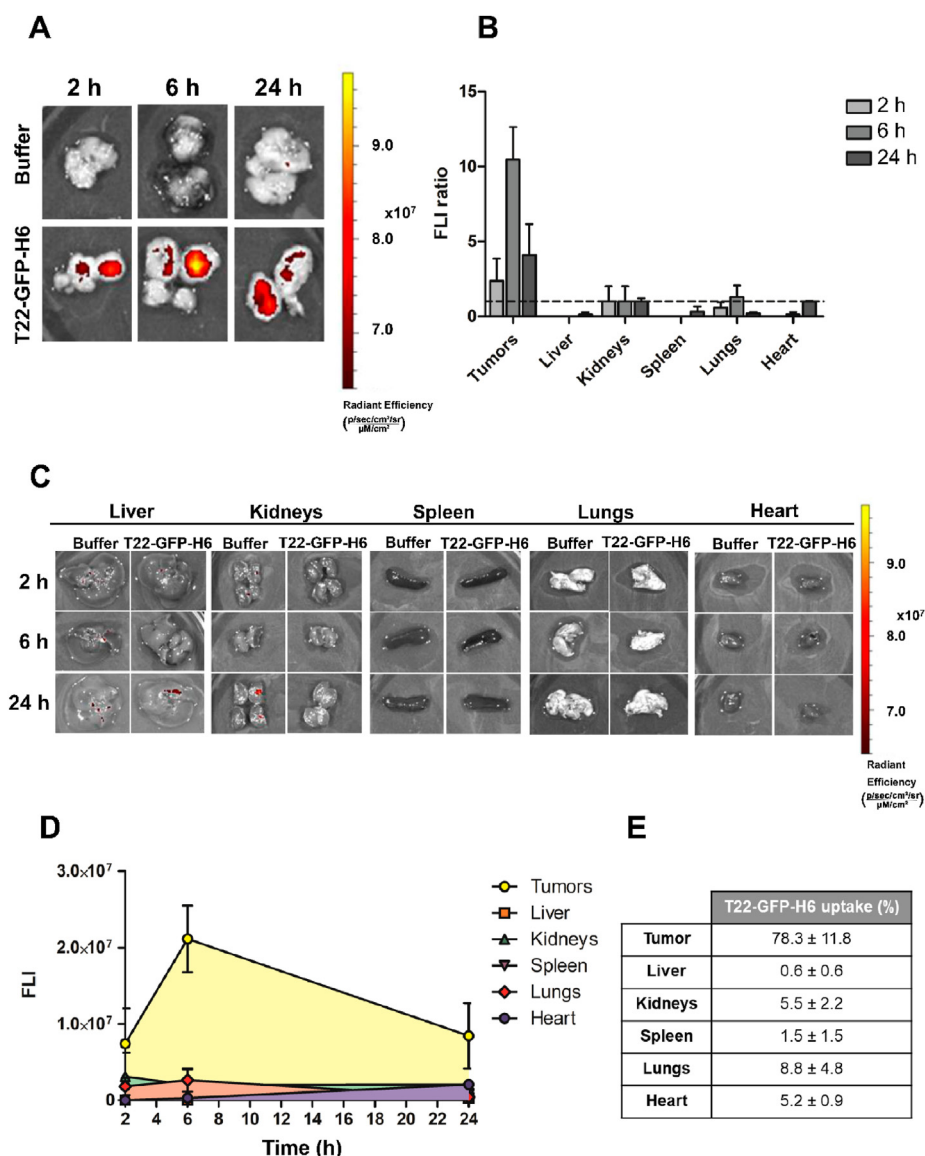


Figure 2 Biodistribution of the T22-GFP-H6 nanocarrier in a CXCR4-overexpressing subcutaneous HNSCC mouse model. (A) Representative images of emitted FLI signal in the 74B-CXCR4⁺ subcutaneous tumors 2, 6 or 24 h after the IV administration of either 200 μ g of T22-GFP-H6 or buffer. (B) FLI ratio of the registered subcutaneous tumors and normal organs (liver, kidneys, spleen, lungs, and heart) at the three time points of the experiment (2, 6, and 24 h). FLI ratio was calculated by subtracting the FLI values of the buffer-treated mice (autofluorescence) and dividing the result by the FLI signal of the kidneys (organ chosen as reference). The dashed line indicates no change in FLI ratio (fold change = 1) (C) Representative images of the FLI registered in non-tumor tissues (liver, kidneys, spleen, lungs, and heart) 2, 6 or 24 h after the nanocarrier or buffer administration, (D) Area under the curve (AUC) of registered FLI through the time course of the experiment (2, 6, and 24 h) in the subcutaneous tumors and normal organs for the T22-GFP-H6 treated animals. (E) T22-GFP-H6 accumulation (%) by the subcutaneous tumors and non-tumoral tissues throughout the experiment. Percentages were calculated by dividing the emitted FLI of each organ (calculated by the AUC) between the total emitted FLI (sum of AUC of tumors and normal organs) and are represented as mean \pm Standard error; $n = 3$ per group (total animal number 16). Statistical analysis performed by Student's *t*-test. FLI, fluorescence intensity.

expression levels. Moreover, no histological alterations were detected in the liver or kidneys (Fig. 3C), suggesting a lack of toxicity for the nanocarrier.

To further study T22-GFP-H6 *in vivo* kinetic behavior, the presence of circulating nanocarrier in plasma at different time points was studied after a single T22-GFP-H6 intravenous administration. FLI signal showed a first phase characterized by a fast biodistribution half-life ($t_{1/2} = \sim 20$ min) in plasma, followed by a second slow elimination phase, becoming practically

undetectable after 2 h (Fig. 4). These results are consistent with previous findings in other tumor models^{18,19}.

3.3. T22-GFP-H6 exhibits a selective CXCR4 tumor distribution in subcutaneous HNSCC tumors

In order to further study T22-GFP-H6 CXCR4-dependant biodistribution, 74B mock and 74B-CXCR4⁺ tumor-bearing mice were administered an intravenous 200 μ g dose of T22-GFP-H6.

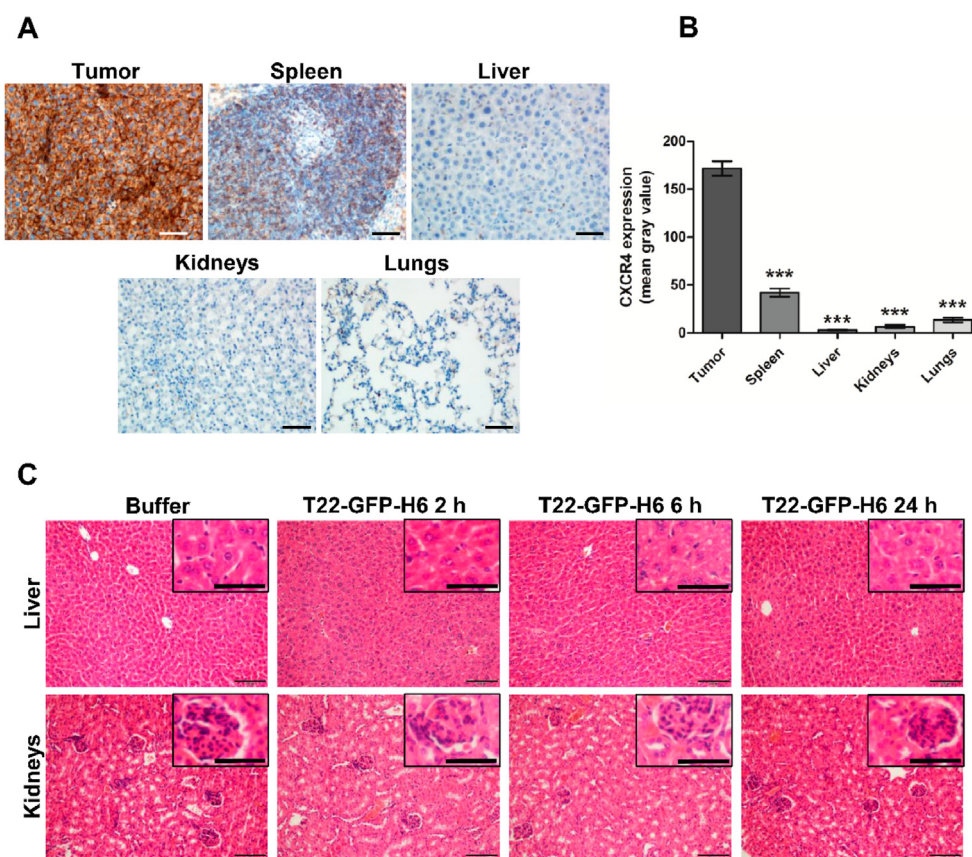


Figure 3 Immunohistochemical and histological analysis of tumors and non-tumor bearing organs from the T22-GFP-H6 biodistribution experiment. (A) Representative IHC images of the CXCR4 expression in tumor, spleen, liver, kidneys, and lungs. Scale bars = 50 μ m (B) Quantification of the CXCR4 levels in tumors and normal organs (spleen, liver, kidneys, and lungs). CXCR4 expression was quantified as mean gray value and represented as mean \pm Standard error, $n = 3$; *** $P < 0.001$. Statistical analysis performed by Student's t -test. (C) Histological analysis of liver and kidney sections stained with H&E from animals treated with either buffer or 200 μ g T22-GFP-H6 for 2, 6, and 24 h. Scale bars = 100 or 50 μ m (H&E zoom in).

Six hours post-treatment, time at which the FLI nanocarrier maximum accumulation was observed, animals were euthanized, and the fluorescence emitted by tumors and organs was registered. Results show that 74B-CXCR4⁺ tumors accumulate significantly higher amounts of T22-GFP-H6 compared to 74B mock (Fig. 5A and B).

In addition, CXCR4-dependant biodistribution was confirmed by performing an AMD3100 blocking experiment. CXCR4⁺ tumor-bearing mice were treated with three consecutive 10 mg/kg subcutaneous doses of AMD3100, one before T22-GFP-H6 intravenous injection, and two after. Animals were euthanized 6 h after T22-GFP-H6 administration, registering the emitted fluorescence as previously explained. AMD3100 administration during the T22-GFP-H6 treatment induced a statistically significant reduction in nanocarrier accumulation in tumors compared to those from animals that did not receive a prior treatment with the CXCR4 antagonist. Moreover, tumors of animals treated with both T22-GFP-H6 and AMD3100 presented a fluorescence intensity similar to those from buffer-treated mice, supporting a selective and CXCR4-dependant nanocarrier accumulation (Fig. 5A and B).

Consistently, 74B-CXCR4⁺ tumors displayed a high CXCR4 membrane expression, as detected by IHC, whereas 74B mock tumors were negative for the receptor (Fig. 5C). These results confirm the selective CXCR4 tumor distribution of the nanocarrier.

T22-GFP-H6 CXCR4 selective tumor accumulation was further confirmed by GFP and CXCR4 co-immunofluorescence (Fig. 6). At the FLI maximum time point (6 h), T22-GFP-H6 (GFP staining) was detected within tumor tissue in the nanocarrier-treated animals, whereas their buffer-treated counterparts did not present any GFP signal. CXCR4 could be observed in all tumor cells from both groups, as 100% of 74B-CXCR4⁺ cells expressed the receptor. Remarkably, nanocarrier-treated tumors presented a co-localization of T22-GFP-H6 and CXCR4 (yellow staining in merged images). This finding suggests that T22-GFP-H6 is able to interact with the CXCR4 receptor in the cell membrane leading to its internalization within CXCR4⁺ HNSCC tumor cells. Importantly, no GFP signal was detected in liver or kidneys, further corroborating a selective T22-GFP-H6 accumulation in tumor tissue (Fig. 6). These results obtained by immunohistofluorescence are in agreement with our previous IVIS findings.

3.4. The incorporation of cytotoxic domains to the nanocarrier confers cytotoxic activity in CXCR4⁺ subcutaneous HNSCC tumors without induction of systemic toxicity

To evaluate the ability of this T22-empowered nanocarrier platform to deliver cytotoxic agents into CXCR4-overexpressing HNSCC tumors, we took advantage of two nanotoxins, T22-

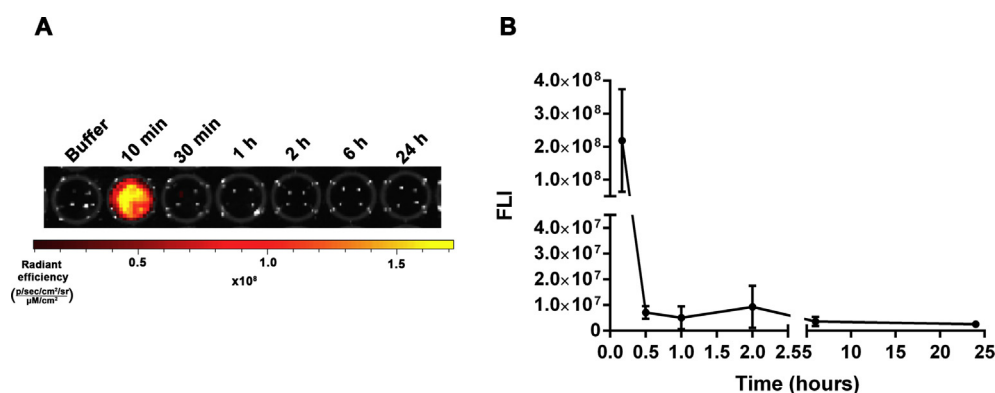


Figure 4 T22-GFP-H6 pharmacokinetics in plasma. (A) Representative images of the fluorescence signal (FLI) registered in plasma samples obtained at different times (buffer, 10 min, 30 min, 1, 2, 6, and 24 h) after T22-GFP-H6 administration. (B) Quantification of the fluorescence intensity (FLI) obtained from plasma samples through the time course of the experiment. Data represented as mean \pm Standard error. $n = 3$ per time-point (total animal number 21).

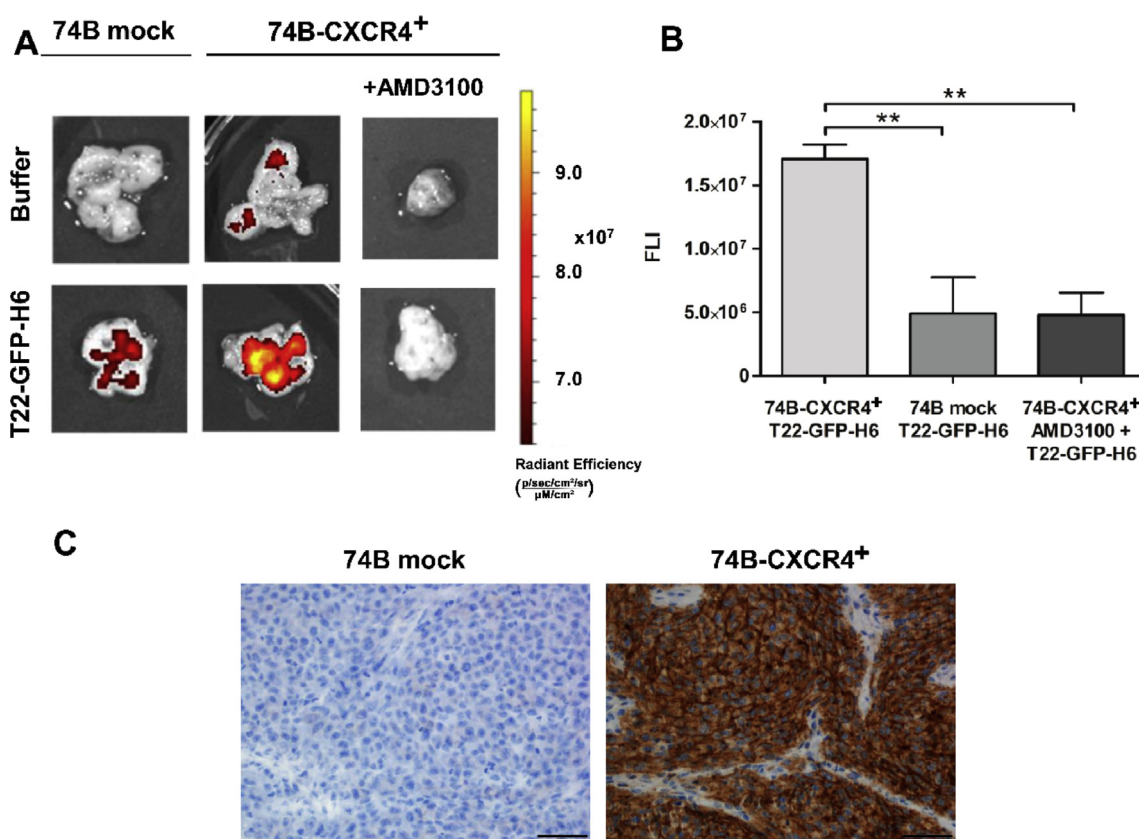


Figure 5 CXCR4-dependant T22-GFP-H6 tumor uptake by HNSCC subcutaneous tumors. (A) Representative FLI images of subcutaneous tumors generated by either the 74B mock or the 74B-CXCR4⁺ cell line 6 h after the IV administration of 200 μ g of T22-GFP-H6, AMD3100⁺ T22-GFP-H6 or buffer. (B) FLI registered signal from the 74B mock or 74B-CXCR4⁺ subcutaneous tumors treated either with T22-GFP-H6 or the combination of the CXCR4 antagonist AMD3100 and T22-GFP-H6. (C) Immunohistochemical analysis of the CXCR4 expression in 74B mock and 74B-CXCR4⁺ subcutaneous tumors. Scale bar = 50 μ m. Data represented as mean \pm Standard error. $n = 3$ per group [total animal number 6 (biodistribution in 74B mock tumors) and 9 (biodistribution in 74B-CXCR4⁺ tumors pre-treated with AMD3100)]. $**P < 0.01$. Statistical analysis performed by Student's *t*-test.

DITOX-H6, a protein nanoparticle including the diphtheria toxin catalytic domain, and T22-PE24-H6, which carries the *Pseudomonas aureoginosa* exotoxin A, both presenting a similar structure to T22-GFP-H6. Both toxins perform ADP-ribosylation of the ribosomal elongation factor 2 (EEF-2), leading to protein

synthesis inhibition and cell death (Supporting Information Fig. S4). Firstly, we evaluated their cytotoxic effect in 74B mock and 74B-CXCR4⁺ HNSCC cell lines at three different time points (6, 24, and 48 h, Supporting Information Fig. S5A–S5C). Both nanotoxins were capable of inducing cell death at 24 h, reaching

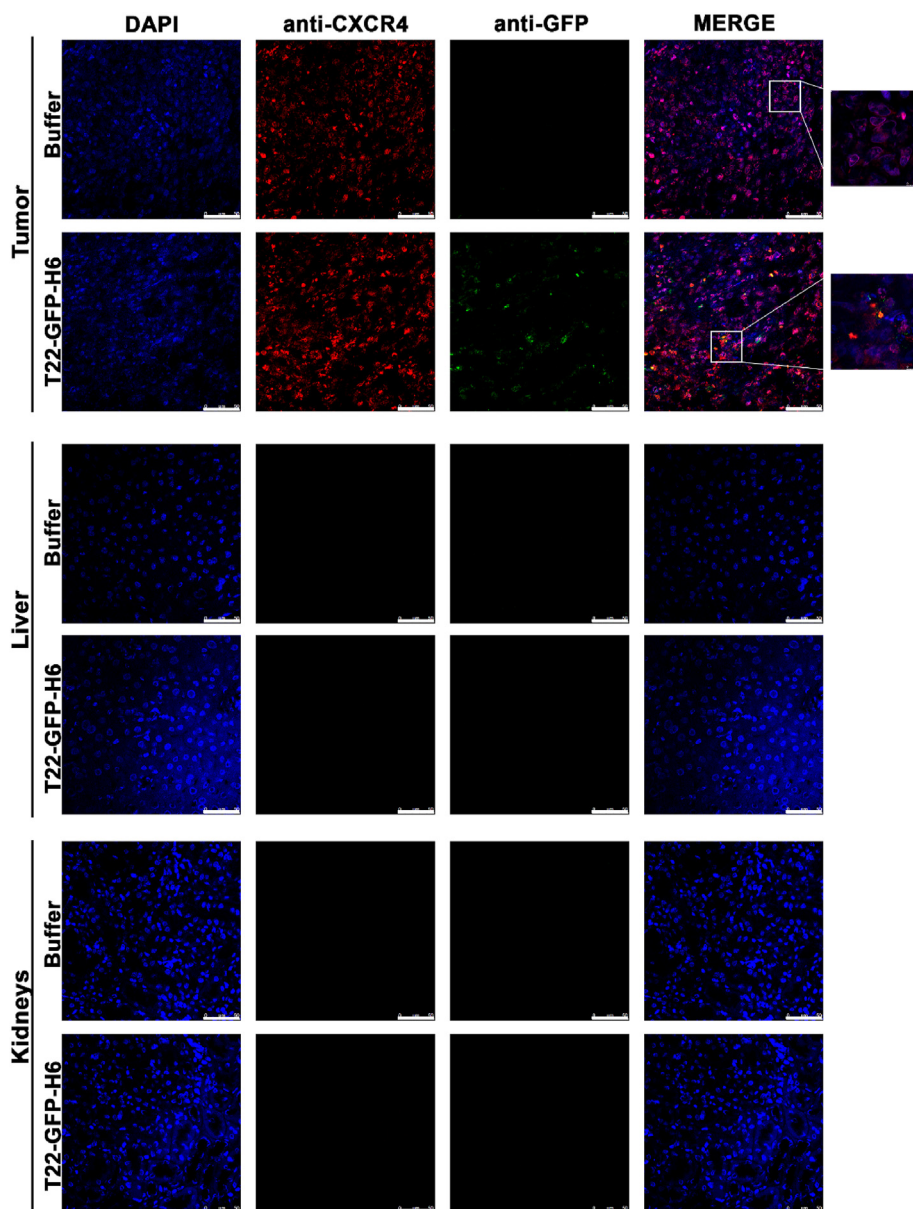


Figure 6 T22-GFP-H6 colocalizes with CXCR4⁺ tumor cells after *in vivo* nanocarrier administration, while no GFP signal is detected in liver or kidneys. Representative immunofluorescence pictures of 74B-CXCR4⁺ subcutaneous tumors, liver, and kidneys 6 h after the administration of either 200 μg of T22-GFP-H6 or buffer. T22-GFP-H6, detected by GFP staining, can be observed within the tumor tissue and colocalizing (yellow signal) with the CXCR4 receptor. On the other hand, no GFP staining was detected in liver or kidney tissue. DAPI staining (blue), anti-GFP (green), anti-CXCR4 (red), and merged images from the three channels. Scale bar = 50 or 10 μm (zoom in).

their full cytotoxicity after 48 h of exposure. Remarkably, both nanotoxins displayed a CXCR4-dependant cytotoxic effect, as 74B mock cells remained viable upon nanoparticle treatment. Moreover, to fully test the CXCR4-dependance of the cytotoxicity induced by both nanotoxins, supernatants from 74B-CXCR4⁺ cells exposed to either T22-DITOX-H6 or T22-PE24-H6 for 48 h, were transferred to 74B mock cells. After 48 h of incubation, 74B mock cells remained viable, suggesting a lack of off-target cytotoxicity once the dead cells released their cellular content (Supporting Information Fig. S5D). These results indicate that no free toxin was present in the media, suggesting that the nanotoxins are degraded in the targeted cells after exerting their cytotoxic effect.

In order to further study T22-DITOX-H6 or T22-PE24-H6 cytotoxicity, 74B-CXCR4⁺ subcutaneous tumor bearing mice were

intravenously administered with a single dose of either 30 μg of T22-DITOX-H6 or 100 μg of T22-PE24-H6. After 24 or 48 h, time points at which we had observed cytotoxic effect *in vitro*, animals were euthanized, and tumors and normal organs were collected for their histological analysis. Both nanoparticles were able to induce cell death, as detected by DNA staining with DAPI, in tumor cells both at 24 and 48 h after treatment (Fig. 7A and B). Moreover, a tendency in the increase of dead cells at 48 h compared to 24 h could be observed in the tumors treated with both nanotoxins. These results were further confirmed by cleaved caspase-3 immunohistochemical staining, showing an increase of cleaved caspase-3 positive cells 48 h after nanotoxin administration (Fig. 7C and D).

In addition, no histopathological alterations were detected in liver or kidneys, as analyzed by H&E staining (Supporting

Information Fig. S6A). Moreover, no statistically significant differences in cell death (DNA staining) were observed in either of these organs in T22-DITOX-H6 and T22-PE24-H6-treated mice (Supporting Information Figs. S6B and S6C). These results suggest the suitability of the T22-GFP-H6 based nanocarrier platform to incorporate cytotoxic polypeptides of choice for their selective delivery to CXCR4⁺ HNSCC cancer cells, reaching a potent cytotoxic effect in the absence of systemic toxicity.

3.5. T22-PE24-H6 and T22-DITOX-H6 nanotoxins induce a potent CXCR4-dependant antitumor effect in a CXCR4⁺ orthotopic HNSCC mouse model in the absence of systemic toxicity

Finally, taking into account their great cytotoxic effect, we wanted to assess the antitumor effect of both T22-DITOX-H6 and T22-PE24-H6 nanotoxins. For this purpose, animals bearing either 74B mock or 74B-CXCR4⁺ primary tumors (tongue), were daily administered with consecutive 10 µg intravenous doses of T22-DITOX-H6 or T22-PE24-H6 up to 5 doses. On alternate days, animals were weighed and tumor growth was determined by measuring the luminescent signal emitted by tumor cells using IVIS® Spectrum 200 system. Twenty-four hours after the last dose, animals were euthanized and tumors and organs were collected for further analysis.

Animals bearing 74B-CXCR4⁺ primary tumors presented differences in tumor growth between groups (Fig. 8A). Nanotoxin-treated animals showed a decrease in tumor growth compared to their nanotoxin-treated counterparts (Fig. 8A). Primary tumor growth translated in a rapid body weight loss, which was more pronounced in animals from the buffer group compared to nanotoxin-treated animals (Fig. 8B). Ultimately, this weight loss determined the end of the experiment. Moreover, tumor volumes at the end point of the experiment were statistically significantly smaller in the nanotoxin-treated animals compared to the control group (Fig. 8C). Importantly, no antitumor effect was observed in the animals bearing 74B mock primary tumors, as no differences in tumor volume or body weight were detected between buffer and nanotoxin-treated animals (Supporting Information Fig. S7).

Lastly, no toxicity was observed by H&E staining in different organs, such as liver, kidneys, intestine, or bone marrow (Supporting Information Fig. S8A), suggesting a lack of toxicity for the treatment. This result is also consistent with the lower CXCR4 expression found in these organs compared to the primary tumor (Supporting Information Fig. S8B). Altogether these results support a potent CXCR4-dependant antitumor effect without leading to any histopathological alterations in non-tumor organs.

4. Discussions

Current HNSCC treatment still includes chemotherapeutic drugs, that affect all cells of the body since they are required to be administered at high doses in order to achieve significant antitumor effect. As a consequence, patients develop important systemic toxicities derived from the treatment²². In this context, nanoparticles have emerged in the last decades as promising vehicles for cancer management^{23,24}. Nanoparticle size allows tumor accumulation through the fenestrations of tumor vasculature (EPR effect)^{25,26}. Moreover, their bigger size compared to conventional small molecular tumor drugs, allows nanoparticles to avoid renal

clearance increasing blood circulation time^{25,27}. In theory, these facts enable nanoparticles to achieve a high tumor uptake lowering the drug dose, thus diminishing systemic toxicity. However, in reality, only 0.7% of the administered dose of the nanoparticles reported in the literature is able to reach the solid tumor, mainly accumulating (>95%) in other organs such as the liver, spleen, lungs, and kidneys resulting in hepatic and renal damage and systemic toxicity^{25,28,29}. Remarkably, our results suggest otherwise, as the tumor accumulation was found to be higher than 75% of the administered dose, with less than 30% accumulation in other organs. These results were corroborated by GFP fluorescence detection and immunostaining. Moreover, normal histopathology of these organs suggests a lack of systemic toxicity, as T22-GFP-H6 mainly accumulates in tumors, avoiding adverse effects. These results are consistent with our previous findings in CRC and DLBCL cancer models^{15,18}, further confirming the suitability of T22-GFP-H6 as a promising nanocarrier in HNSCC.

The great performance of our nanocarrier might be at least partially explained by its organic composition. Many nanoparticles under research are made of inorganic materials which are poorly biocompatible and do not degrade easily, accumulating in organs such as liver and kidneys³⁰. Moreover, these inorganic nanoparticles are coated with a protein corona when present in the body fluids, hindering their interaction with target cells^{28,30–34}. Apart from its protein-only composition, T22-GFP-H6 nanocarrier presents other advantages such as its small size (around 13 nm), which is bigger than the renal filtration cut off (5–7 nm) but not big enough to be cleared out by macrophages, two big problems of current nanoparticles^{25,27}. Importantly, the multivalency of the T22-GFP-H6 nanocarrier, that incorporates around twelve T22 ligands in each self-assembled nanoparticle, yields superselectivity³⁵ that translates into selective internalization in HNSCC cells that overexpress the CXCR4 receptor, having negligible internalization in normal cells that lack or express low CXCR4 levels. These findings are consistent with the high receptor overexpression in tumors as compared to normal organs. Altogether, these facts might explain that less than 10% of the administered T22-GFP-H6 dose accumulates in liver and kidneys, without producing any histopathological damage.

Moreover, T22-GFP-H6 nanocarrier exploits the actively targeted strategy as a promising alternative to improve drug accumulation within tumor tissues^{36,37}. Interestingly, the only clinical studies for HNSCC treatment involving fully protein nanoparticles are the EphB4-HSA fusion protein, an Ephrin-B2 ligand-receptor bound to albumin, and albumin-bound rapamycin (mTOR inhibitor)³⁸. Antibody–drug conjugates (ADCs) represent another strategy for targeted drug delivery. However, it is estimated that <1% of the administered ADC dose is able to reach the tumor site, forcing the use of high doses which lead to important side effects and life-threatening toxicities. Due to these severe side effects and a limited improvement in efficacy compared to the free drug, 20 ADCs have been discontinued in the last decades. Moreover, ADCs also display a poor payload capacity, limited tumor uptake, and high toxicity^{39,40}. Nevertheless, there are still more than 70 ADCs in clinical trials, that have been improved for instance using site-specific conjugation^{41–43} or bi-specific targeting^{44,45}, for the treatment of several cancer types, including HNSCC²⁵. Altogether, these facts highlight the current interest for nano-sized and targeted drug formulations, emphasizing the relevance of our protein-based nanoparticles targeting CXCR4.

Remarkably, our results showed a T22-GFP-H6 CXCR4-dependant internalization *in vitro*, as the nanocarrier did not

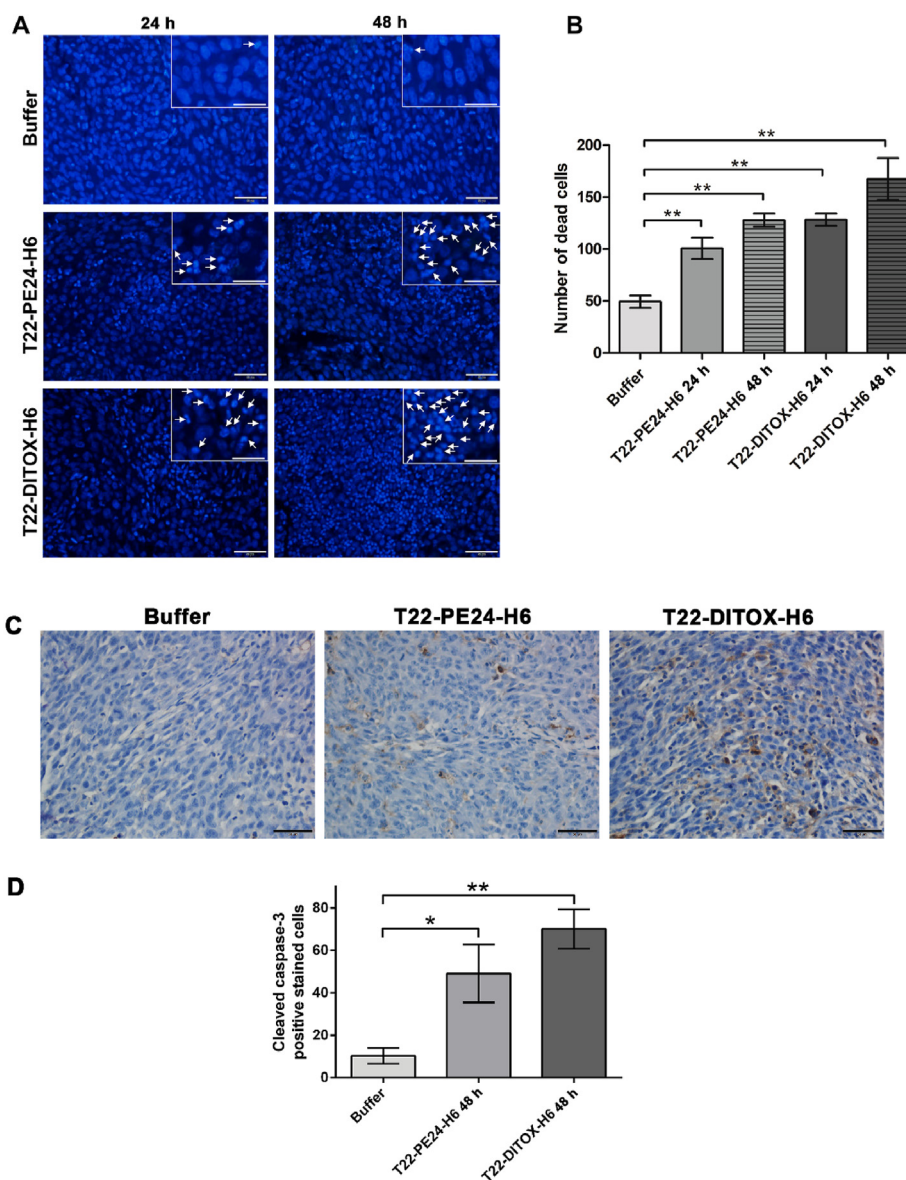


Figure 7 T22-PE24-H6 and T22-DITOX-H6 cytotoxic effect in a CXCR4⁺ subcutaneous HNSCC animal model. (A) Detection of dead cells by condensate DNA staining (DAPI) in the 74B-CXCR4⁺ subcutaneous tumors analyzed 24 or 48 h after the administration of a single dose of either T22-PE24-H6 or T22-DITOX-H6 nanotoxins. Scale bars = 50 or 25 μ m (zoom in). (B) Quantification of the number of dead cells in the nanotoxin and buffer-treated tumors 24 and 48 h after treatment. (C) Immunohistochemical detection of cleaved caspase-3 in 74B-CXCR4⁺ subcutaneous tumors 48 h after the administration of T22-PE24-H6 or T22-DITOX-H6. Scale bar = 50 μ m. (D) Quantification of the number of cleaved caspase-3 positive stained cells in tumor tissue 48 h after treatment. Dead cells were detected by condensate DNA staining using DAPI and cleaved caspase-3 IHC. Data represented as mean \pm Standard error. $n = 20$ per group (total number analyzed tissue sections per group). * $P < 0.05$; ** $P < 0.01$. Statistical analysis performed by Student's t -test.

internalize in either CXCR4⁻ cell lines or AMD3100 pre-treated CXCR4⁺ HNSCC cell lines. Moreover, nanoparticle tumor distribution was enhanced by CXCR4 targeting as it was shown by two independent experiments. Firstly, the AMD3100 blocking experiment demonstrated a lower nanocarrier tumor accumulation in AMD3100-treated animals, compared to their non-treated counterparts. Correspondingly, CXCR4-non overexpressing tumor-bearing mice also presented significantly lower T22-GFP-H6 tumor accumulation than the ones overexpressing the receptor. Furthermore, immunofluorescence results showed a co-localization of CXCR4 and T22-GFP-H6, further confirming the interaction between the nanocarrier and the receptor.

Targeting CXCR4 has emerged as a promising strategy for cancer treatment, as it is associated with metastasis and worse prognosis in several solid tumors, including HNSCC. Moreover, CXCR4 has been described as a marker for metastatic cancer stem cells (CSC), a subset of cancer cells with capacity of self-renewal and differentiation that are responsible for the formation of tumor metastases^{46–48}. Importantly, targeting the CXCR4 receptor to achieve targeted drug delivery is highly appealing since CXCR4 levels are much higher in tumor tissue compared to the normal organ in HNSCC, as well as other neoplasias^{11,12}. Altogether, these results validate T22-GFP-H6 as a promising nanoparticle for HNSCC treatment, as previously described for other cancer

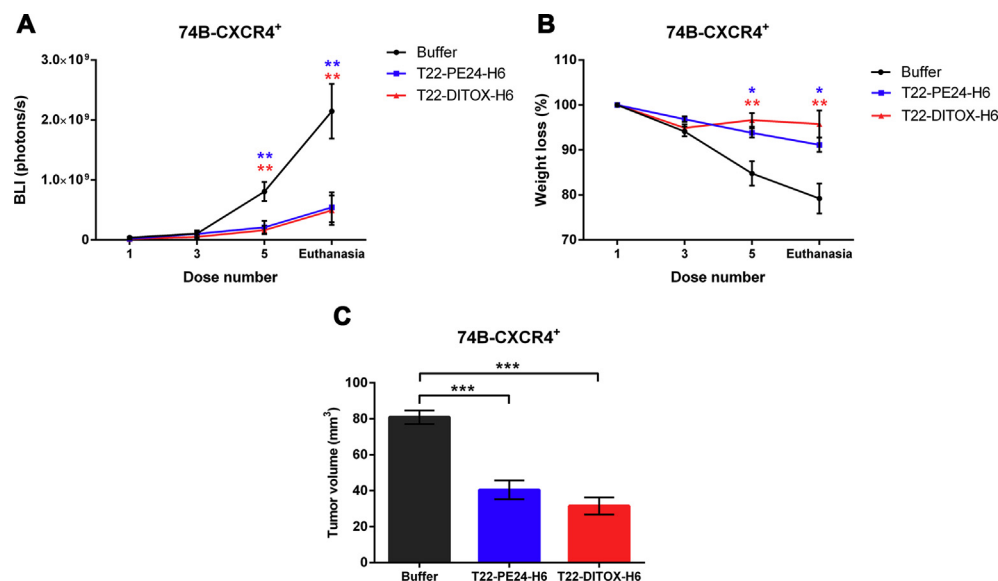


Figure 8 T22-PE24-H6 and T22-DITOX-H6 antitumor effect in a CXCR4⁺ orthotopic HNSCC animal model. (A) Evolution of tumor growth in the three experimental groups (buffer, T22-PE24-H6, and T22-DITOX-H6) measured as luminescent signal emitted by tumor cells (BLI). (B) Variation of the body weight of buffer, T22-PE24-H6, and T22-DITOX-H6 treated animals represented as percentage of body weight loss. (C) Tumor volume registered at the end point of the experiment for the three experimental groups. Data represented as mean \pm Standard error. $n = 5$ per group (total animal number 15). * $P < 0.05$; ** $P < 0.01$; *** $P < 0.001$. Statistical analysis performed by Student's *t*-test. BLI, bioluminescence intensity (photons/s).

models^{15,18}. Remarkably, to our knowledge, no protein-based nanocarrier for drug delivery has been described for the treatment of HNSCC, highlighting the relevance of this study.

Last but not least, the T22-GFP-H6 nanocarrier developed by our group has proved to be a versatile platform amenable to deliver drugs or cytotoxic polypeptides, such as bacterial toxins, to selectively eliminate CXCR4⁺ tumor cells^{49–51}. Most CXCR4 therapies are based on small receptor inhibitors (*e.g.*, AMD3100), which have presented poor efficacy, especially in solid tumors⁵². Thus, current research is focused on the combination of blocking the CXCR4 pathway with other therapies, including chemotherapy, presenting promising results^{10,52–54}. Nevertheless, these strategies still mainly rely on conventional chemotherapeutic drugs, which involve important systemic toxicities and undesired side effects for patients. Our approach goes a step further, creating protein-only nanoparticles with intrinsic cytotoxic activity by incorporating toxin domains. Following this strategy, we have developed the nanotoxins T22-PE24-H6 which incorporates an active fragment of *P. aeruginosa* exotoxin A, and T22-DITOX-H6 that includes an active fragment of the diphtheria toxin. Importantly, both nanotoxins were able to significantly induce cell death in tumor cells compared to buffer-treated mice in our CXCR4-overexpressing subcutaneous HNSCC model. In addition, T22-PE24-H6 and T22-DITOX-H6 achieved a potent CXCR4-dependant antitumor effect in a HNSCC orthotopic mouse model. Remarkably, treated mice did not present any histopathological alteration suggesting a lack of systemic toxicity for the treatment.

5. Conclusions

In conclusion, this study showed the selective internalization of the T22-GFP-H6 nanocarrier exclusively to CXCR4-overexpressing HNSCC cell lines. Moreover, upon intravenous administration in a HNSCC CXCR4-overexpressing subcutaneous mouse model, the nanocarrier mainly accumulates in tumor tissues (>75% of the administered dose) compared to non-tumor bearing

organs. This result contrasts with previously reported nanoparticles by other groups, that presented a low tumor uptake. In addition, nanocarrier tumor accumulation is mediated by the CXCR4 receptor. This finding is consistent with the high CXCR4 expression reported in tumors, compared to normal tissues, including organs of the immune system, such as the spleen. Last but not least, this T22-empowered nanocarrier platform displays a great versatility to selectively deliver cytotoxic domains to CXCR4⁺ HNSCC tumors, without inducing systemic toxicity. Altogether, these results validate the T22-GFP-H6 as a versatile platform to generate novel therapeutic nanoparticles, incorporating the small drug or the cytotoxic polypeptide of choice, to achieve the selective targeting and elimination of CXCR4⁺ cells, involved in HNSCC metastatic dissemination, which represents one of the main causes of patient mortality. Thus, selective elimination of CXCR4⁺ cells might represent a huge improvement in HNSCC therapy.

Acknowledgments

This work was supported by Instituto de Salud Carlos III (ISCIII, Spain; Co-funding from FEDER, European Union) [PI18/00650, PIE15/00028, PI15/00378 and EU COST Action CA 17140 to Ramon Mangués, PI19/01661 to Xavier León, and PI17/00584 to Miquel Quer]; Agencia Estatal de Investigación (AEI, Spain) and Fondo Europeo de Desarrollo Regional (FEDER, European Union) [grant BIO2016-76063-R, AEI/FEDER, UE to Antonio Villaverde and grant PID2019-105416RB-I00/AEI/10.13039/501100011033 to Esther Vázquez]; CIBER-BBN (Spain) [CB06/01/1031 and 4NanoMets to Ramon Mangués, VENOM4CANCER to Antonio Villaverde, NANOREMOTE to Esther Vázquez, and NANOSCAPE to Ugutz Unzueta]; AGAUR (Spain) 2017-SGR-865 to Ramon Mangués, and 2017SGR-229 to Antonio Villaverde; Josep Carreras Leukemia Research Institute (Spain) [P/AG to Ramon Mangués]. Elisa Rioja-Blanco and Laura Sánchez-

García were supported by a predoctoral fellowship from AGAUR (Spain) (2020FI_B2_00168 and 2018FI_B2_00051) co-funded by European Social Fund (ESF investing in your future, European Union). Lorena Alba-Castellón was supported by a postdoctoral fellowship from AECC (Spanish Association of Cancer Research, Spain). Antonio Villaverde received an Icrea Academia Award (Spain). Ugutz Unzueta was also supported by Grant PERIS SLT006/17/00093 from la Generalitat de Catalunya (Spain) and Miguel Servet fellowship (CP19/00028) from Instituto de Salud Carlos III (Spain) co-funded by European Social Fund (ESF investing in your future, European Union). The bioluminescent follow-up of cancer cells and toxicity studies has been performed in the ICTS-141007 Nanobiosis Platform, using its CIBER-BBN Nanotoxicology Unit (<http://www.nanbiosis.es/portfolio/u18-nanotoxicology-unit/>). Protein production has been partially performed by the ICTS “NANBIOSIS”, more specifically by the Protein Production Platform of CIBER-BBN/IBB (<http://www.nanbiosis.es/unit/u1-protein-production-platform-ppp/>).

Author contributions

We declare that all authors made fundamental contributions to the manuscript. Elisa Rioja-Blanco, Esther Vázquez, Ramon Mangues, Lorena Alba-Castellón, and Xavier León designed the study. Elisa Rioja-Blanco, Irene Arroyo-Solera, Ugutz Unzueta, and Isolda Casanova contributed in the development of the methodology. Elisa Rioja-Blanco, Irene Arroyo-Solera, Patricia Álamo, Naroa Serna, and Laura Sánchez-García acquired the data and carried out the experiments. Elisa Rioja-Blanco and Alberto Gallardo carried out the histopathological analysis. The analysis and interpretation of data was performed by Elisa Rioja-Blanco, Miquel Quer, Xavier León, Antonio Villaverde, Esther Vázquez, Ramon Mangues, and Lorena Alba-Castellón. Elisa Rioja-Blanco prepared the manuscript. Ugutz Unzueta, Isolda Casanova, Antonio Villaverde, Esther Vázquez, Ramon Mangues, and Lorena Alba-Castellón performed the manuscript reviews and revisions. The study was supervised by Esther Vázquez, Ramon Mangues, Lorena Alba-Castellón, and Xavier León. All authors revised the manuscript and approved the final version.

Conflicts of interest

Antonio Villaverde, Esther Vázquez, Ugutz Unzueta, Ramon Mangues, and Isolda Casanova are cited as inventors in PCT/EP2012/050513 covering Targeted delivery of therapeutic molecules to CXCR4 cells, and in PCT/EP2018/061732, covering Therapeutic Nanostructured Proteins. All other authors report no conflicts of interest in this work.

Appendix A. Supporting information

Supporting data to this article can be found online at <https://doi.org/10.1016/j.apsb.2021.09.030>.

References

1. Rothenberg SM, Ellisen LW. The molecular pathogenesis of head and neck squamous cell carcinoma. *J Clin Invest* 2012;**122**:1951–7.
2. Bray F, Ferlay J, Soerjomataram I, Siegel RL, Torre LA, Jemal A. Global cancer statistics 2018: GLOBOCAN estimates of incidence and mortality worldwide for 36 cancers in 185 countries. *CA - Cancer J Clin* 2018;**68**:394–424.
3. León X, Quer M, Orús C, Del Prado Venegas M, López M. Distant metastases in head and neck cancer patients who achieved loco-regional control. *Head Neck* 2000;**22**:680–6.
4. Vokes EE, Agrawal N, Seiwert TY. HPV-associated head and neck cancer. *J Natl Cancer Inst* 2015;**107**:djv344.
5. Sacco AG, Cohen EE. Current treatment options for recurrent or metastatic head and neck squamous cell carcinoma. *J Clin Oncol* 2015;**33**:3305–15.
6. de Bree R, Senft A, Coca-Pelaz A, Kowalski L, Lopez F, Mendenhall W, et al. Detection of distant metastases in head and neck cancer: changing landscape. *Adv Ther* 2018;**35**:161–72.
7. Shi J, Kantoff PW, Wooster R, Farokhzad OC. Cancer nanomedicine: progress, challenges and opportunities. *Nat Rev Cancer* 2017;**17**:20–37.
8. Mangues R, Vázquez E, Villaverde A. Targeting in cancer therapies. *Med Sci* 2016;**4**:6.
9. Albert S, Riveiro ME, Halimi C, Hourseau M, Couvelard A, Serova M, et al. Focus on the role of the CXCL12/CXCR4 chemokine axis in head and neck squamous cell carcinoma. *Head Neck* 2013;**35**:1819–28.
10. Domanska UM, Kruijzinga RC, Nagengast WB, Timmer-Bosscha H, Huls G, De Vries EGE, et al. A review on CXCR4/CXCL12 axis in oncology: no place to hide. *Eur J Cancer* 2013;**49**:219–30.
11. Knopf A, Bahadori L, Fritsche K, Piontek G, Becker C-C, Knolle P, et al. Primary tumor-associated expression of CXCR4 predicts formation of local and systemic recurrency in head and neck squamous cell carcinoma. *Oncotarget* 2017;**8**:112739–47.
12. León X, Diez S, García J, Lop J, Sumarroca A, Quer M, et al. Expression of the CXCL12/CXCR4 chemokine axis predicts regional control in head and neck squamous cell carcinoma. *Arch Oto-Rhino-Laryngol* 2016;**273**:4525–33.
13. Murakami T, Zhang T-Y, Koyanagi Y, Tanaka Y, Kim J, Suzuki Y, et al. Inhibitory mechanism of the CXCR4 antagonist T22 against human immunodeficiency virus type 1 infection. *J Virol* 2002;**76**:933–933.
14. Céspedes MV, Unzueta U, Tatkiwicz W, Sánchez-Chardi A, Conchillo-Solé O, Álamo P, et al. *In vivo* architectonic stability of fully *de novo* designed protein-only nanoparticles. *ACS Nano* 2014;**8**:4166–76.
15. Unzueta U, Céspedes MV, Ferrer-Miralles N, Casanova I, Cedano J, Corchero JL, et al. Intracellular CXCR4⁺ cell targeting with T22-empowered protein-only nanoparticles. *Int J Nanomed* 2012;**7**:4533–44.
16. Unzueta U, Ferrer-Miralles N, Cedano J, Zikung X, Pesarrodona M, Saccardo P, et al. Non-amyloidogenic peptide tags for the regulatable self-assembling of protein-only nanoparticles. *Biomaterials* 2012;**33**:8714–22.
17. López-Laguna H, Unzueta U, Conchillo-Solé O, Sánchez-Chardi A, Pesarrodona M, Cano-Garrido O, et al. Assembly of histidine-rich protein materials controlled through divalent cations. *Acta Biomater* 2019;**83**:257–64.
18. Falgàs A, Pallarès V, Unzueta U, Céspedes MV, Arroyo-Solera I, Moreno MJ, et al. A CXCR4-targeted nanocarrier achieves highly selective tumor uptake in diffuse large B-cell lymphoma mouse models. *Haematologica* 2020;**105**:741–53.
19. Sánchez-García L, Serna N, Álamo P, Sala R, Céspedes MV, Roldan M, et al. Self-assembling toxin-based nanoparticles as self-delivered antitumoral drugs. *J Control Release* 2018;**274**:81–92.
20. Brenner JC, Graham MP, Kumar B, Saunders LM, Kupfer R, Lyons RH, et al. Genotyping of 73 UM-SCC head and neck squamous cell carcinoma cell lines. *Head Neck* 2010;**32**:417–26.
21. Zhao M, Sano D, Pickering CR, Jasser SA, Henderson YC, Clayman GL, et al. Assembly and initial characterization of a panel of 85 genomically validated cell lines from diverse head and neck tumor sites. *Clin Cancer Res* 2011;**17**:7248–64.
22. Pérez-Herrero E, Fernández-Medarde A. Advanced targeted therapies in cancer: drug nanocarriers, the future of chemotherapy. *Eur J Pharm Biopharm* 2015;**93**:52–79.

23. Petros RA, Desimone JM. Strategies in the design of nanoparticles for therapeutic applications. *Nat Rev Drug Discov* 2010;**9**:615–27.
24. Wagner V, Dullaart A, Bock AK, Zweck A. The emerging nanomedicine landscape. *Nat Biotechnol* 2006;**24**:1211–7.
25. Serna N, Sánchez-García L, Unzueta U, Díaz R, Vázquez E, Mangues R, et al. Protein-based therapeutic killing for cancer therapies. *Trends Biotechnol* 2018;**36**:318–35.
26. Haley B, Frenkel E. Nanoparticles for drug delivery in cancer treatment. *Urol Oncol Semin Orig Investig* 2008;**26**:57–64.
27. Zhou Q, Dong C, Fan W, Jiang H, Xiang J, Qiu N, et al. Tumor extravasation and infiltration as barriers of nanomedicine for high efficacy: the current status and transcytosis strategy. *Biomaterials* 2020;**240**:119902.
28. Wilhelm S, Tavares AJ, Dai Q, Ohta S, Audet J, Dvorak HF, et al. Analysis of nanoparticle delivery to tumours. *Nat Rev Mater* 2016;**1**:16014.
29. Bae YH, Park K. Targeted drug delivery to tumors: myths, reality and possibility. *J Control Release* 2011;**153**:198–205.
30. Naahidi S, Jafari M, Edalat F, Raymond K, Khademhosseini A, Chen P. Biocompatibility of engineered nanoparticles for drug delivery. *J Control Release* 2013;**166**:182–94.
31. Xiao W, Gao H. The impact of protein corona on the behavior and targeting capability of nanoparticle-based delivery system. *Int J Pharm* 2018;**552**:328–39.
32. Ke PC, Lin S, Parak WJ, Davis TP, Caruso F. A decade of the protein corona. *ACS Nano* 2017;**11**:11773–6.
33. Miceli E, Kar M, Calderón M. Interactions of organic nanoparticles with proteins in physiological conditions. *J Mater Chem B* 2017;**5**:4393–405.
34. Salvati A, Pitek AS, Monopoli MP, Prapainop K, Bombelli FB, Hristov DR, et al. Transferrin-functionalized nanoparticles lose their targeting capabilities when a biomolecule corona adsorbs on the surface. *Nat Nanotechnol* 2013;**8**:137–43.
35. Liu M, Apriceno A, Sipin M, Scarpa E, Rodriguez-Arco L, Poma A, et al. Combinatorial entropy behaviour leads to range selective binding in ligand-receptor interactions. *Nat Commun* 2020;**11**:4836.
36. Lammers T, Kiessling F, Ashford M, Hennink W, Crommelin D, Strom G. Cancer nanomedicine: is targeting our target?. *Nat Rev Mater* 2016;**1**:1–2.
37. Danhier F, Feron O, Pr at V. To exploit the tumor microenvironment: passive and active tumor targeting of nanocarriers for anti-cancer drug delivery. *J Control Release* 2010;**148**:135–46.
38. Clinicaltrials.gov. Search for clinical trials in head and neck squamous cell carcinoma. Available from: <https://clinicaltrials.gov>. [Accessed 9 March 2021].
39. Masters JC, Nickens DJ, Xuan D, Shazer RL, Amantea M. Clinical toxicity of antibody drug conjugates: a meta-analysis of payloads. *Invest N Drugs* 2018;**36**:121–35.
40. Donaghy H. Effects of antibody, drug and linker on the preclinical and clinical toxicities of antibody-drug conjugates. *mAbs* 2016;**8**:659–71.
41. Junutula JR, Raab H, Clark S, Bhakta S, Leipold DD, Weir S, et al. Site-specific conjugation of a cytotoxic drug to an antibody improves the therapeutic index. *Nat Biotechnol* 2008;**26**:925–32.
42. Yamada K, Ito Y. Recent chemical approaches for site-specific conjugation of native antibodies: technologies toward next-generation antibody–drug conjugates. *ChemBiochem* 2019;**20**:2729–37.
43. Schumacher D, Hackenberger CPR, Leonhardt H, Helma J. Current status: site-specific antibody drug conjugates. *J Clin Immunol* 2016;**36**:100–7.
44. Maruani A. Bispecifics and antibody–drug conjugates: a positive synergy. *Drug Discov Today Technol* 2018;**30**:55–61.
45. Shim H. Bispecific antibodies and antibody–drug conjugates for cancer therapy: technological considerations. *Biomolecules* 2020;**10**.
46. Dalerba P, Clarke MF. Cancer stem cells and tumor metastasis: first steps into uncharted territory. *Cell Stem Cell* 2007;**1**:241–2.
47. Miki J, Furusato B, Li H, Gu Y, Takahashi H, Egawa S, et al. Identification of putative stem cell markers, CD133 and CXCR4, in hTERT-immortalized primary nonmalignant and malignant tumor-derived human prostate epithelial cell lines and in prostate cancer specimens. *Cancer Res* 2007;**67**:3153–61.
48. Faber A, Goessler UR, Hoermann K, Schultz JD, Umbreit C, Stern-Straeter J. SDF-1–CXCR4 axis: cell trafficking in the cancer stem cell niche of head and neck squamous cell carcinoma. *Oncol Rep* 2013;**29**:2325–31.
49. C spedes MV, Unzueta U, Avi n o A, Gallardo A,  lamo P, Sala R, et al. Selective depletion of metastatic stem cells as therapy for human colorectal cancer. *EMBO Mol Med* 2018;**10**:e8772.
50. Falg s A, Pallar s V, Serna N, S nchez-Garc a L, Sierra J, Gallardo A, et al. Selective delivery of T22-PE24-H6 to CXCR4⁺ diffuse large B-cell lymphoma cells leads to wide therapeutic index in a disseminated mouse model. *Theranostics* 2020;**10**:5169–80.
51. Pallar s V, Unzueta U, Falg s A, S nchez-Garc a L, Serna N, Gallardo A, et al. An Auristatin nanoconjugate targeting CXCR4⁺ leukemic cells blocks acute myeloid leukemia dissemination. *J Hematol Oncol* 2020;**13**:36.
52. Guo F, Wang Y, Liu J, Mok SC, Xue F, Zhang W. CXCL12/CXCR4: a symbiotic bridge linking cancer cells and their stromal neighbors in oncogenic communication networks. *Oncogene* 2016:816–26.
53. Chen K, Huang YH, Chen JL. Understanding and targeting cancer stem cells: therapeutic implications and challenges. *Acta Pharmacol Sin* 2013;**34**:732–40.
54. Hermann PC, Huber SL, Heeschen C. Metastatic cancer stem cells: a new target for anti-cancer therapy?. *Cell Cycle* 2008;**7**:188–93.

CHAPTER 2

CXCR4-targeted nanotoxins induce GSDME-dependent pyroptosis in head and neck squamous cell carcinoma

Elisa Rioja-Blanco, Irene Arroyo-Solera, Patricia Álamo, Isolda Casanova, Alberto Gallardo, Ugutz Unzueta, Naroa Serna, Laura Sánchez-García, Miquel Quer, Antonio Villaverde, Esther Vázquez*, Xavier León, Lorena Alba-Castellón*, Ramon Manges*

*co-corresponding authors

Journal of Experimental & Clinical Cancer Research

2022

RESEARCH

Open Access



CXCR4-targeted nanotoxins induce GSDME-dependent pyroptosis in head and neck squamous cell carcinoma

Elisa Rioja-Blanco^{1,2}, Irene Arroyo-Solera^{1,2,3}, Patricia Álamo^{1,2,3}, Isolda Casanova^{1,2,3}, Alberto Gallardo^{1,4}, Ugutz Unzueta^{1,2,3}, Naroa Serna^{3,5,6}, Laura Sánchez-García^{3,5,6}, Miquel Quer^{3,7,8}, Antonio Villaverde^{3,5,6}, Esther Vázquez^{3,5,6,9*}, Xavier León^{3,7,8}, Lorena Alba-Castellón^{1,2,11*} and Ramon Mangués^{1,2,3,10*}

Abstract

Background: Therapy resistance, which leads to the development of loco-regional relapses and distant metastases after treatment, constitutes one of the major problems that head and neck squamous cell carcinoma (HNSCC) patients currently face. Thus, novel therapeutic strategies are urgently needed. Targeted drug delivery to the chemokine receptor 4 (CXCR4) represents a promising approach for HNSCC management. In this context, we have developed the self-assembling protein nanotoxins T22-PE24-H6 and T22-DITOX-H6, which incorporate the de-immunized catalytic domain of *Pseudomonas aeruginosa* (PE24) exotoxin A and the diphtheria exotoxin (DITOX) domain, respectively. Both nanotoxins contain the T22 peptide ligand to specifically target CXCR4-overexpressing HNSCC cells. In this study, we evaluate the potential use of T22-PE24-H6 and T22-DITOX-H6 nanotoxins for the treatment of HNSCC.

Methods: T22-PE24-H6 and T22-DITOX-H6 CXCR4-dependent cytotoxic effect was evaluated in vitro in two different HNSCC cell lines. Both nanotoxins cell death mechanisms were assessed in HNSCC cell lines by phase-contrast microscopy, AnnexinV/ propidium iodide (PI) staining, lactate dehydrogenase (LDH) release assays, and western blotting. Nanotoxins antitumor effect in vivo was studied in a CXCR4⁺ HNSCC subcutaneous mouse model. Immunohistochemistry, histopathology, and toxicity analyses were used to evaluate both nanotoxins antitumor effect and possible treatment toxicity. GSMDE and CXCR4 expression in HNSCC patient tumor samples was also assessed by immunohistochemical staining.

Results: First, we found that both nanotoxins exhibit a potent CXCR4-dependent cytotoxic effect in vitro. Importantly, nanotoxin treatment triggered caspase-3/Gasdermin E (GSDME)-mediated pyroptosis. The activation of this alternative cell death pathway that differs from traditional apoptosis, becomes a promising strategy to bypass therapy resistance. In addition, T22-PE24-H6 and T22-DITOX-H6 displayed a potent antitumor effect in the absence of systemic

*Correspondence: esther.vazquez@uab.cat; lalba@santpau.cat; rmangués@santpau.cat

⁹ Institut de Biotecnologia i de Biomedicina and Departament de Genètica i de Microbiologia, Universitat Autònoma de Barcelona and CIBER, Bellaterra, Barcelona, Spain

¹⁰ Institut d'Investigacions Biomèdiques Sant Pau, Hospital de Sant Pau, CIBER and Josep Carreras Research Institute, 08041 Barcelona, Spain

¹¹ Institut d'Investigacions Biomèdiques Sant Pau, Hospital de Sant Pau and Josep Carreras Research Institute, 08041 Barcelona, Spain
Full list of author information is available at the end of the article



toxicity in a CXCR4⁺ subcutaneous HNSCC mouse model. Lastly, GSDME was found to be overexpressed in tumor tissue from HNSCC patients, highlighting the relevance of this strategy.

Conclusions: Altogether, our results show that T22-PE24-H6 and T22-DITOX-H6 represent a promising therapy for HNSCC patients. Remarkably, this is the first study showing that both nanotoxins are capable of activating caspase-3/GSDME-dependent pyroptosis, opening a novel avenue for HNSCC treatment.

Keywords: Targeted drug delivery, CXCR4, HNSCC, Pyroptosis, GSDME

Background

One of the main problems of head and neck squamous cell carcinoma (HNSCC) therapy is that up to 60% of patients develop loco-regional relapses and up to 30% distant metastases after treatment, dramatically affecting their survival. Currently, these HNSCC patients are no longer candidates for a curative therapy and the main goals are palliation and prolongation of patient survival [1, 2]. Thus, the development of drug resistance, which leads to treatment failure and relapses, constitutes a major issue in current HNSCC treatment, highlighting the urge for novel therapeutic strategies [3–6].

In this context, targeting the chemokine receptor 4 (CXCR4) has emerged as a promising approach in cancer treatment. CXCR4 overexpression in HNSCC primary tumors associates with a higher risk of developing loco-regional recurrences and distant metastases after treatment and worse overall survival [7, 8]. Moreover, preclinical and clinical data suggest that this chemokine pathway contributes to a resistant phenotype [8]. Thus, targeted drug delivery to CXCR4-overexpressing cells represents a promising antitumor strategy in HNSCC treatment.

In the last years, different protein toxins have gained relevance as moieties of antitumor drugs because of their interesting properties that can be exploited in clinical oncology [9–11]. Toxins display a great cytotoxicity in a wide range of cancer cells, presenting mechanisms of action capable of killing not only proliferating, but also quiescent cells [10]. In addition, toxins can be recombinantly produced enabling large scale production and purification. All these facts make them ideal candidates to replace current chemotherapeutic drugs. However, to prevent undesired off-target toxicities, targeted drug delivery specifically to tumor cells is key for the translation of toxin-based drugs to the clinic. In this context, different antibody-drug conjugates (ADCs) and immunotoxins have exploited this strategy. An example is the immunotoxin denileukin diftotox, that incorporates the interleukin-2 (IL-2) fused to the diphtheria exotoxin domain to target T cell lymphoma cells that overexpress the IL-2 receptor. However, it was withdrawn from the market in 2014 due to life-threatening toxicity in patients [12, 13]. In fact, immunotoxin translation to the clinic

has been jeopardized by severe off-target toxicities, especially because of their high immunogenicity and reduced targeting capacity, which limits their long-term use in patients [12, 13]. On the other hand, different ADCs have also been tested for the treatment of HNSCC, such as ABBV-321, an EGFR-targeting antibody conjugated to a pyrrolbenzodiazepine (PBD) dimer cytotoxic molecule [14]. Nevertheless, ADCs present important drug leakage during circulation, also limiting their clinical use [15–17]. Altogether, ADCs and immunotoxins present severe off-target toxicities, which dramatically narrow down their therapeutic window.

In this context, we have developed self-assembling protein nanoparticles which incorporate the de-immunized catalytic domain of *Pseudomonas aeruginosa* (PE24) exotoxin A or the diphtheria exotoxin (DITOX) domain from *Corynebacterium diphtheriae*, that specifically target CXCR4-overexpressing (CXCR4⁺) cancer cells through the T22 peptide ligand. These nanotoxins, named T22-PE24-H6 and T22-DITOX-H6 respectively, are recombinantly produced in *Escherichia coli*, where they self-assemble into multimeric nanoparticles. This fact enables a greater payload capacity while increasing the number of ligands per nanoparticle, which endows superselectivity [18]. Moreover, both nanotoxins are produced in a single step process, avoiding chemical conjugation steps, which allows a straightforward production and purification while preventing drug leakage [19].

Here, we describe the cytotoxic and antitumor effect of these two novel nanotoxins, T22-PE24-H6 and T22-DITOX-H6 that specifically target CXCR4⁺ cells, for the treatment of HNSCC. First, we evaluate the CXCR4-dependent cytotoxic effect of both nanotoxins in two different HNSCC cell lines. Moreover, we analyze the mechanisms of cell death induced by both T22-PE24-H6 and T22-DITOX-H6, finding that they are capable of activating caspase-3/Gasdermin E (GSDME) mediated pyroptosis. Since the activation of anti-apoptotic pathways is a main mechanism of resistance to both chemotherapy and radiotherapy in HNSCC [3, 5, 6, 20], the development of drugs capable of triggering cell death pathways alternative to apoptosis is an important avenue of research that could increase cure rate in HNSCC patients. Importantly, T22-PE24-H6 and T22-DITOX-H6

also present a potent antitumor effect in the absence of systemic toxicity in a CXCR4⁺ subcutaneous HNSCC mouse model. Lastly, we incorporate clinical data showing that GSDME (also named DFNA5) is overexpressed in tumor tissue of HNSCC patients, highlighting the relevance of this strategy. Thus, activating caspase-3/GSDME-dependent pyroptosis specifically in CXCR4⁺ HNSCC tumor cells may represent a novel and enticing approach for the treatment of HNSCC patients. Remarkably, this is the first study showing that T22-PE24-H6 and T22-DITOX-H6 activate caspase-3/GSDME mediated pyroptosis in oncotherapy.

Methods

Nanoparticles production, purification, and characterization

T22-PE24-H6 and T22-DITOX-H6 production, purification, and characterization have been previously described [19]. T22-PE24-H6 nanoparticles self-assemble into ~60 nm nanoparticles, whereas T22-DITOX-H6 form 38 and 90 nm nanoparticles.

Cell lines and cell culture

UM-SCC-22A (22A) and UM-SCC-74B (74B) human papillomavirus negative (HPV⁻) HNSCC cell lines [21] were kindly provided by Dr. R. H. Brakenhoff and Dr. Gregory Oakley respectively. 22A mock, 74B mock, 22A-CXCR4⁺, and 74B-CXCR4⁺ were obtained by lentiviral transduction with the plasmids pLenti-III-UbC-luc and pLenti-III-UbC-CXCR4-2A-luc (abm, Vancouver, Canada) respectively, as already described in previous work [22]. HNSCC cell lines were cultured in Dulbecco's Modified Eagle's Medium (DMEM) (Gibco, Life Technologies) supplemented with 10% Fetal Bovine Serum (FBS), 100 U/mL penicillin/ streptomycin, and 2 mM glutamine (Life Technologies) and incubated at 37°C and 5% CO₂ in a humidified atmosphere. CXCR4 expression in 22A mock, 74B mock, 22A-CXCR4⁺, and 74B-CXCR4⁺ has been already evaluated in previous work [22].

575 and 909 patient-derived cell cultures were obtained from two HNSCC patient tumor samples with high CXCR4 tumor expression. Tumor samples were disaggregated by incubation in Trypsin-EDTA 0.25% (Gibco, Life Technologies) for 2 h at 4°C, followed by further incubation with collagenase type II (200 mg/mL, Life Technologies) and DNase (20 mg/mL, Sigma-Aldrich) for 2 h at 37°C. After some mechanical disruption, samples were filtered through a 40 μm mesh, and cultured. Epithelial cell enrichment was performed by differential trypsinization and maintaining the cells in Defined Keratinocyte-SFM medium (Gibco, Life Technologies). 575 and 909 cell cultures were maintained Dulbecco's Modified Eagle Medium: Nutrient Mixture F-12 (DMEM/F-12) (Gibco,

Life Technologies) supplemented with 10% Fetal Bovine Serum (FBS), 100 U/mL penicillin/ streptomycin, 2 mM glutamine, and 400 ng/ml hydrocortisone (Life Technologies) at 37°C and 5% CO₂ in a humidified atmosphere.

Patient samples

HNSCC patient samples were obtained by the Otorhinolaryngology Department of the Hospital de la Santa Creu i Sant Pau (Barcelona, Spain) in accordance with the Institutional Review Board of the institution. Written informed consent was acquired from all the patients involved in this study.

Cell viability assays

Cell viability upon T22-PE24-H6 and T22-DITOX-H6 exposure was assessed with the Cell Proliferation Kit II (XTT) (Roche) according to the manufacturer's instructions. Cells were seeded in 96-well plates (5000 cells/well for 22A and 2500 cells/well for 74B) and treated with either buffer (166 mM NaCO₃H pH8) or different concentrations of T22-PE24-H6 or T22-DITOX-H6 (0–50 nM) for 48 h. For AMD3100 blocking experiments, 1 μM AMD3100 was added 1 h prior to the addition of the nanotoxins. For the zVAD pre-treatment, 100 μM zVAD (Calbiochem) was added to the plates and incubated at 37°C for 2 h before nanotoxin treatment. After 48 h, XTT reagent was added to the plate and further incubated at 37°C for 4 h, then absorbance, which directly correlates to the number of viable cells, was measured using a multi-well spectrophotometer (FLUOstar Optima, BMG Labtech). All experiments were performed in triplicate.

Flow cytometry

Cell death induced by T22-PE24-H6 and T22-DITOX-H6 was further assessed using the Annexin V-FITC / propidium iodide (PI) detection kit (Merck Millipore) following manufacturer's instructions. 74B-CXCR4⁺ cells were cultured in 6-well plates (25,000 cells/well) and exposed to 50 nM of either of the two nanotoxins for different times (15 h, 24 h, and 48 h). Cells were analyzed by MACS-Quant analyzer flow cytometry with the MACS Quantify version 2.3 software (Miltenyi Biotech). The experiment was performed in triplicate.

LDH release assay

LDH release from 22A-CXCR4⁺ and 74B-CXCR4⁺ cells upon nanotoxin exposure was studied using the CytoTox 96 Non-Radioactive Cytotoxicity Assay (Promega). Cells were seeded in 96-well plates (5000 cells/well for 22A and 2500 cells/well for 74B) and exposed to the nanotoxins (5 nM for T22-PE24-H6 in 22A-CXCR4⁺ cell line, 50 nM in the rest of conditions). zVAD (Calbiochem) pre-treatment was performed at a 100 μM concentration

and incubated at 37°C for 2 h prior to nanotoxin addition. After 48 h of treatment, cytotoxicity assay reagents were added according to the manufacturer's instructions, and the absorbance at 492 nm was measured using a multi-well spectrophotometer (FLUOstar Optima, BMG Labtech). All experiments were performed in triplicate.

Western blotting

T22-PE24-H6 and T22-DITOX-H6 cell death mechanisms were further studied by western blotting (WB). For that, 22A-CXCR4⁺ and 74B-CXCR4⁺ cells were treated with either of the nanotoxins (5 nM for T22-PE24-H6 in 22A-CXCR4⁺ cell line, 50 nM in the rest of conditions) for different times (15 h, 24 h, and 48 h). In the zVAD conditions, the pan-caspase inhibitor (Calbiochem) was added at 100 μM and incubated for 2 h before nanotoxin treatment. WB was also used to evaluate the GSDME expression in two patient-derived cultures (575 and 909). Cells were lysed in RIPA buffer (Sigma) containing proteinase inhibitors (Roche) and phosphatase inhibitors (Roche). The protein extracts (50 μg) were subjected to SDS-PAGE and transferred to a nitrocellulose blotting membrane (GE Healthcare life sciences). After blockage with 5% skim milk in TBS-T for 1 h at room temperature, membranes were incubated overnight at 4°C with the primary antibodies: anti-human caspase-3 (1:1000, BD Biosciences), cleaved caspase-3 (1:1000, Cell Signaling), PARP (1:2000, BD Biosciences), GSDME (1:1000, abm), and α/β-tubulin (1:1000, Cell Signaling). After washing with TBS-T to remove nonspecific antibody binding, membranes were incubated with the corresponding secondary antibodies (1:10,000, Jackson Immune Research) for 1 h at room temperature. Finally, membranes were further washed with TBS-T and visualized with the SuperSignal™ West Pico Chemiluminescent Substrate and SuperSignal™ West Femto Maximum Sensitivity Substrate (Thermo Scientific) using the ChemiDoc XRS+ imaging system (Biorad). Pro-caspase-3, cleaved caspase-3, cleaved PARP, and cleaved GSDME levels were quantified using Fiji, ImageJ software. The densitometric analysis was performed by dividing the value of each nanotoxin-treated sample by the buffer-treated sample and normalized by the loading control (α/β-tubulin). All experiments were performed at least in triplicate.

In vivo experiments

Four-week-old female Swiss nude mice (NU (Ico)-*Foxn1*tm) weighing 18–25 g were purchased from Charles River (France). Animals were housed in a specific pathogen-free (SPF) environment with sterile food and water ad libitum. All animal experiments were approved by the Hospital de la Santa Creu i Sant Pau Animal Ethics Committee.

The subcutaneous tumor model was generated by subcutaneous injection of 10 million 74B-CXCR4⁺ cells in both flanks of the animal. To assess T22-PE24-H6 and T22-DITOX-H6 antitumor effect, animals bearing tumors around 60–100 mm³ were randomized into three groups (*n* = 10 per group). Animals were intravenously administered buffer (166 mM NaCO₃H pH8), or 10 μg of either T22-PE24-H6 or T22-DITOX-H6 every day up to 8 doses. Animal body weight and tumor size were measured with a caliper (tumor volume = width² x length/2) through the time course of the treatment. Animals were euthanized 48 h after the last dose, when tumors were weighted and collected together with different organs for later analysis. Plasma was also obtained by centrifugation of total blood, extracted from the animals by intracardiac puncture.

To evaluate the possible long-term toxicity of the nanotoxins treatment, four-week-old female non-tumor bearing Swiss nude mice (NU (Ico)-*Foxn1*tm) were intravenously administered buffer or 10 μg of either T22-PE24-H6 or T22-DITOX-H6 daily up to 8 doses, similarly to the antitumor effect experiment. Animals were weighted twice a week during the study. After the last dose, blood samples were collected from the tail every week to assess cell blood count (CBC). Animals were euthanized 4 weeks after the end of the treatment and different organs were collected for histopathological analysis.

Histopathology, DAPI staining, and immunohistochemical analysis

4 μm paraffin-embedded sections obtained from tumor patient samples collected at the Hospital de la Santa Creu i Sant Pau, as well as tumors and organs extracted from the animals were used to performed different histopathological analysis. Organ sections were stained with H&E and analyzed by two independent observers (one section of the whole organ/tumor). Cell death in tumor tissues was assessed by DAPI staining, paraffin-embedded sections were dewaxed, rehydrated, and permeabilized with 0.5% Triton X-100. Then, slides were stained with DAPI mounting medium (ProLong™ Gold Antifade Mountant, Thermo Scientific) and visualized by fluorescence microscopy. Representative pictures were taken using an Olympus DP73 digital camera and the number of dead cells was quantified by counting the number of condensed nuclei per 10 high-power fields (magnification 400x). Immunohistochemical (IHC) staining of animal tumors was performed to study the cytotoxic effect of the nanotoxin treatment. CXCR4 (1:200, Abcam. Retrieval pH high, Dako) and F4/80 (ready to use, Dako) IHC were performed in a DAKO Autostainer Link48 following the manufacturer's instructions. Similarly, GSDME IHC staining (1:300, Abcam. Retrieval pH high,

Dako) was assessed in patient tumor samples. Representative images were captured using an Olympus DP73 digital camera and processed with the Olympus CellD Imaging 3.3 software. CXCR4 and F4/80 expression levels in tumors were quantified as mean gray values using Fiji, ImageJ software.

Toxicity analyses in plasma and total blood samples

To further evaluate the toxicity of T22-PE24-H6 and T22-DITOX-H6 treatment in mice, plasma glutamic oxaloacetic transaminase (GOT) and glutamic pyruvic transaminase (GPT) enzyme activities, as well as creatinine and uric acid levels were assessed in plasma samples using commercial kits (Roche) in a COBAS 6000 autoanalyzer (Roche).

Cell blood count (CBC) from buffer and nanotoxin-treated animals was analyzed using the Mindray BC-5000 Vet hematology analyzer.

Statistical analysis

Data was represented as mean \pm Standard error (SEM). Statistical analyses were performed using the GraphPad Prism 5 software (GraphPad Software, San Diego, California USA). Results were analyzed by Student t-test. Differences were considered statistically significant when p -values < 0.05 .

Results

T22-PE24-H6 and T22-DITOX-H6 exhibit a potent CXCR4-dependent cytotoxicity in HNSCC cell lines

T22-PE24-H6 and T22-DITOX-H6 cytotoxic effect was evaluated in vitro in two HNSCC cell lines, 22A mock and 22A-CXCR4⁺; and 74B mock and 74B-CXCR4⁺. Both 22A mock and 74B mock cell lines were negative for the receptor, whereas 22A-CXCR4⁺ and 74B-CXCR4⁺ displayed a strong CXCR4 membrane expression, as it has been already studied by flow cytometry and immunocytochemistry in previous work [22]. Cells were exposed to different concentrations of either of the two nanotoxins (0–50 nM) for 48 h before assessing their viability. Both T22-PE24-H6 and T22-DITOX-H6 were able to induce cell death in 22A-CXCR4⁺ and 74B-CXCR4⁺ cells, which express high levels of CXCR4 in their membranes (Fig. 1A–D). Remarkably, nanotoxins present a potent cytotoxic effect, as they were capable of inducing cell death at low concentrations (nM range) (Fig. 1A–D). IC₅₀ values were calculated for

both nanotoxins, ranging between 1 and 5 nM, further supporting T22-PE24-H6 and T22-DITOX-H6 potent cytotoxicity (Fig. 1A–D). On the other hand, neither 22A mock nor 74B mock (CXCR4 negative cells) cell viability was altered upon nanoparticle exposure, suggesting a CXCR4-dependent cytotoxic effect (Fig. 1A–D).

T22-PE24-H6 and T22-DITOX-H6 CXCR4-dependent cytotoxicity was further corroborated by pre-incubating both 22A-CXCR4⁺ and 74B-CXCR4⁺ cells with the CXCR4 antagonist AMD3100, 1 h prior to the addition of the nanotoxins. Treatment with AMD3100 blocked nanotoxin binding to CXCR4, leading to a practically complete remission of their cytotoxic effect in both CXCR4⁺ cell lines (Fig. 1E and F).

Thus, both T22-PE24-H6 and T22-DITOX-H6 display a potent CXCR4-dependent cytotoxic effect in vitro in both HNSCC cell lines.

T22-PE24-H6 and T22-DITOX-H6 nanotoxins induce pyroptosis in HNSCC cell lines

The aforementioned potent CXCR4-dependent cytotoxic effect prompted us to investigate the mechanism of cell death induced by both T22-PE24-H6 and T22-DITOX-H6 nanotoxins. Interestingly, upon nanoparticle exposure, we observed a balloon-like morphology of the cells, which clearly differ from classic apoptotic blebbing (Fig. 2A). These swelling cells were especially noticeable in the 22A-CXCR4⁺ cultures treated with either of the two nanotoxins, although they could also be observed in the 74B-CXCR4⁺ cell line (Fig. 2A). Remarkably, this balloon-like shape is a characteristic of pyroptotic cell morphology.

In addition to these observations, we performed an Annexin V/ Propidium iodide (PI) assay by flow cytometry to further study the type of cell death induced by T22-PE24-H6 and T22-DITOX-H6. In classic apoptosis, cells first undergo an early apoptosis phase (Annexin V⁺/PI⁻), followed by a late apoptosis phase (Annexin V⁺/PI⁺), characterized by plasma membrane rupture and leakage. However, in this case we did not observe these phases, revealing a lytic type of cell death, as Annexin V/PI double-positive stained cells increased upon treatment with both nanotoxins (Fig. 2B).

To further elucidate the mechanism of cell death induced by both nanotoxins, we evaluated the LDH released from cells 48 h after nanoparticle treatment,

(See figure on next page.)

Fig. 1 T22-PE24-H6 and T22-DITOX-H6 CXCR4-dependent cytotoxic effect in HNSCC cell lines. **A** and **B**) T22-PE24-H6 (**A**) and T22-DITOX-H6 (**B**) cytotoxic effect (0–50 nM) after 48 h of exposure in 22A mock and 22A-CXCR4⁺ cell lines represented as percentage of cell viability and IC₅₀ values. **C** and **D**) T22-PE24-H6 (**C**) and T22-DITOX-H6 (**D**) cytotoxic effect (0–50 nM) after 48 h of exposure in 74B mock and 74B-CXCR4⁺ cell lines represented as percentage of cell viability and IC₅₀ values. **E** and **F**) AMD3100 blocking assay (1 μ M) in 22A-CXCR4⁺ and 74B-CXCR4⁺ cell lines treated with T22-PE24-H6 (**E**) (5 nM for 22A-CXCR4⁺ and 50 nM for 74B-CXCR4⁺) and T22-DITOX-H6 (**F**) (50 nM) for 48 h. ** $p < 0.01$; *** $p < 0.001$. Each column represents the mean value of three biological replicates. Statistical analysis performed by Student t-test. Error bars indicate SEM

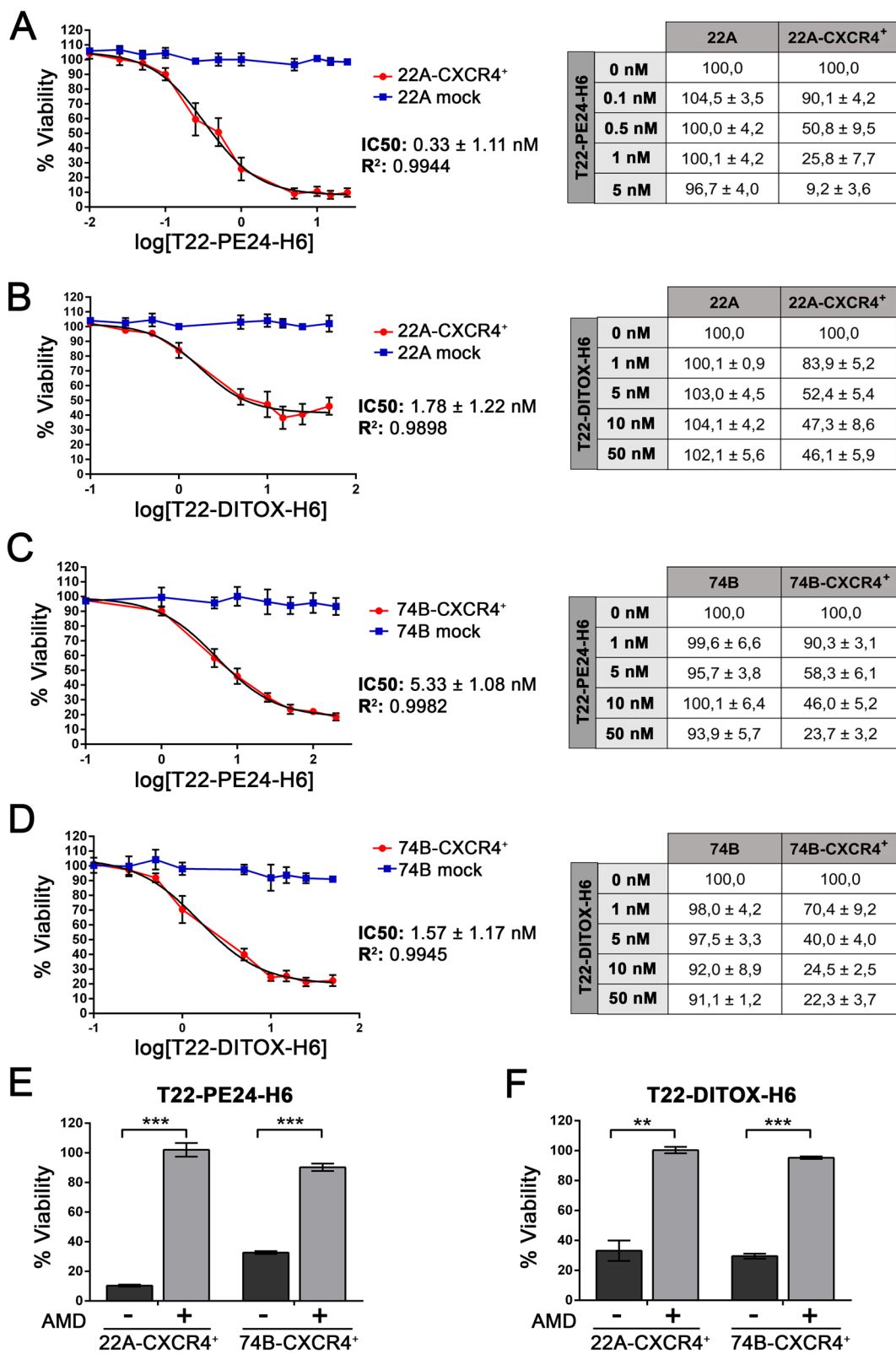


Fig. 1 (See legend on previous page.)

which correlates with cell membrane disruption and leakage. In agreement with the previous findings, nanotoxin treated cells showed an increase in LDH release, further corroborating a lytic form of cell death (Fig. 2C).

Finally, we studied different cell death markers by western blotting to determine the exact mechanisms of cell death activated by T22-PE24-H6 and T22-DITOX-H6. We found an activation of caspase-3, PARP, and GSDME in both HNSCC cell lines treated with either of the two nanotoxins (Fig. 2D). 22A-CXCR4⁺, which has shown a greater sensitivity to both nanotoxins, presented cleaved caspase-3 at 15 h and 24 h, leading to the activation of PARP and GSDME also at 15 h and 24 h. On the other hand, activation of caspase-3, PARP, and GSDME in the 74B-CXCR4⁺ cell line was only observed at 48 h (Fig. 2D, Supplementary Fig. 1). In the last years, different studies have determined that pyroptosis, a lytic form of cell death, can be triggered by GSDME N-terminal domain which is activated by cleaved caspase-3, also responsible for the proteolytic activation of PARP during apoptosis [23, 24]. Interestingly, we observed the simultaneous activation of both PARP and GSDME upon nanotoxin treatment, which has also been described in other molecular therapies [25–28].

T22-PE24-H6 and T22-DITOX-H6 activate caspase-3/GSDME-mediated pyroptosis in HNSCC cell lines

In order to validate the previous findings which suggested that the caspase-3/GSDME pathway would be responsible for nanotoxin cytotoxic effect, we exposed the cells to the pan-caspase inhibitor zVAD prior to the nanotoxin treatment. Pre-treatment with zVAD clearly abrogated balloon-like morphology of the nanotoxin treated cells, showing a decrease in cell swelling (Fig. 3A). Consequently, cell viability was also protected by pre-treating the cell with the pan-caspase inhibitor, further indicating a caspase-dependent cell death mechanism (Fig. 3B). In agreement, zVAD pre-treatment led to a reduction of LDH release in nanotoxin treated cells (Fig. 3C). Moreover, western blotting analysis revealed that as expected, caspase-3 proteolytic activation was inhibited by zVAD pre-treatment. Hence, PARP and GSDME activation were also abolished in the zVAD pre-treated cells (Fig. 3D, Supplementary Fig. 2). Thus, pre-treatment of the cells with zVAD prior to nanotoxin exposure led

to an inhibition of cell death, further corroborating the involvement of caspase-3/GSDME pathway in nanotoxin cytotoxicity. Remarkably, this is the first time that we describe the activation of this pathway by T22-PE24-H6 and T22-DITOX-H6, which opens a novel avenue for HNSCC treatment.

Nanotoxins repeated dosage potently inhibits tumor growth in a CXCR4⁺ subcutaneous HNSCC mouse model in the absence of systemic toxicity

The potent cytotoxic effect induced by both T22-PE24-H6 and T22-DITOX-H6 nanotoxins in the HNSCC cell lines encouraged us to evaluate their antineoplastic effect in vivo. For that, we generated a CXCR4-overexpressing subcutaneous mouse model. One week after the implantation, animals were intravenously administered buffer or 10 µg of either T22-PE24-H6 or T22-DITOX-H6 daily up to 8 doses. Tumor volume and body weight were measured on alternate days. Animals were euthanized 48 h after the last dose, and tumors were weighed and collected for later analysis, as well as different organs (Fig. 4A).

Treatment with T22-PE24-H6 and T22-DITOX-H6 nanotoxins clearly impaired tumor growth in the CXCR4-overexpressing subcutaneous tumors, as tumors from the buffer-treated animals reached bigger volumes compared to their nanotoxin-treated counterparts (Fig. 4B). Remarkably, treatment with T22-DITOX-H6 practically inhibited tumor growth, as tumor volumes did not significantly vary throughout the treatment. Consequently, tumor weight at the endpoint of the experiment was significantly higher in the tumors derived from buffer-treated mice compared to the nanotoxin-treated animals, especially the ones treated with T22-DITOX-H6 (Fig. 4C). In addition, nanotoxin treatment did not affect animal body weight in the time course of the experiment, suggesting a lack of systemic toxicity for the treatment (Fig. 4D).

Tumor histology was also studied to further evaluate nanotoxin antineoplastic effect. Tumors after nanotoxin repeated treatment maintained their undifferentiated phenotype (Supplementary Fig. 3A). CXCR4 expression in tumor tissue was also maintained upon nanotoxin treatment, as no differences in percentage of positive cells were observed between groups (Supplementary

(See figure on next page.)

Fig. 2 T22-PE24-H6 and T22-DITOX-H6 nanotoxins induce tumor cell pyroptosis. **A** Phase-contrast imaging of 22A-CXCR4⁺ and 74B-CXCR4⁺ cells treated with T22-PE24-H6 or T22-DITOX-H6 for 48 h exhibiting pyroptotic cell morphology (magnification 200x). **B** Flow cytometry analysis of 74B-CXCR4⁺ after 15 h, 24 h, and 48 h of exposure to T22-PE24-H6 or T22-DITOX-H6 stained with Annexin V-FITC and propidium iodide (PI). Percentage of stained cells is represented in the column graph. **C** LDH release from 22A-CXCR4⁺ and 74B-CXCR4⁺ exposed to either T22-PE24-H6 or T22-DITOX-H6 for 48 h. **D** Representative images of pro-caspase-3, cleaved caspase-3, PARP, GSDME, and tubulin immunoblotting in protein extracts from 22A-CXCR4⁺ and 74B-CXCR4⁺ cell lines treated with T22-PE24-H6 and T22-DITOX-H6 for 15 h, 24 h, and 48 h. * $p < 0.05$. Each column represents the mean value of three biological replicates. Statistical analysis performed by Student t-test. Error bars indicate SEM

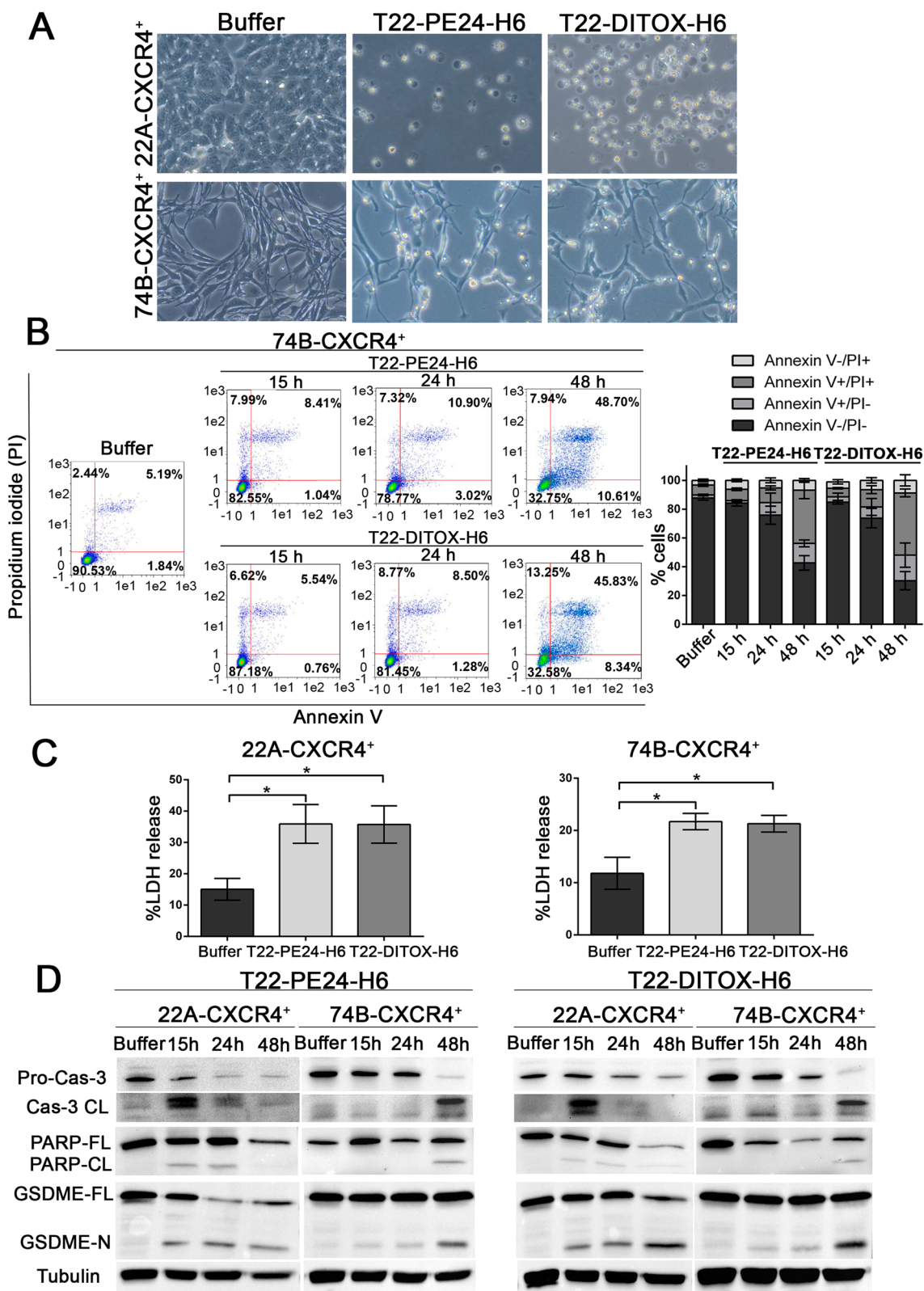


Fig. 2 (See legend on previous page.)

Fig. 3B). Besides, nanotoxin treatment induced cell death in the tumor cells as detected by condensate DNA (DAPI staining) (Fig. 5A). The number of DAPI stained cells was found to be higher in tumor treated with either of the two nanotoxins as compared to the control group, supporting nanotoxin antitumor effect (Fig. 5A). Last but not least, we wanted to assess immune cell recruitment to the tumor site, as it is described that tumor leakage from pyroptotic cells enhances the number and activity of tumor-associated macrophages (TAMs) that phagocytose tumor cells [23]. For that, we performed a F4/80 immunohistochemistry, a well-known macrophage cell marker, finding an increase in the percentage of tumor-infiltrating macrophages in nanotoxin-treated tumors as compared to the buffer-treated ones (Fig. 5B). Altogether, these results corroborate nanotoxin potent antitumor effect, suggesting that the activation of pyroptosis in tumor cells also enhances immune cell recruitment to the tumor site, further contributing to the antitumor effect.

Importantly, no off-target toxicity was observed upon nanotoxin treatment, neither in the T22-PE24-H6 nor in the T22-DITOX-H6 group. We assessed nanotoxin toxicity by histopathology (H&E staining) in liver and kidneys tissue, organs involved in the metabolism and elimination of drugs. As it could be observed by two independent observers, no histological alterations were detected in either of the two organs, which presented their normal architecture and morphology (Fig. 6A). Moreover, to further corroborate treatment's lack of toxicity, hepatic and renal function were studied by hepatic transaminases activity, as well as creatinine and uric acid levels in plasma. Results showed no statistically significant differences in transaminases activity, nor in creatinine or uric acid concentrations in plasma between control and nanotoxin treated animals (Fig. 6B-E). In addition, these values were between the normal range of a healthy animal [29]. Thus, T22-PE24-H6 and T22-DITOX-H6 nanotoxin treatment at the chosen administration conditions, does not induce off-target toxicity in the CXCR4⁺ HNSCC subcutaneous mouse model.

Moreover, to evaluate the long-term toxicity induced by nanotoxin treatment, animals received the same dosage as in the antitumor effect experiment, but were further maintained for 4 weeks after the end of the treatment

(Supplementary Fig. 4A). Importantly, non-tumor bearing mice were utilized, as the lack of tumor and consequently the absence of nanotoxin uptake by tumor tissue, will potentially increase nanotoxin concentration in the bloodstream, thus providing a better evaluation of their potential off-target toxicity. Remarkably, none of the nanotoxins, neither T22-PE24-H6 nor T22-DITOX-H6, shortly after their administration at repeated doses or 4 weeks after the end of the treatment, induced any changes in animal body weight (Supplementary Fig. 4B). In addition, cell blood count (CBC) analyses were performed weekly to assess treatment derived toxicity. No differences between buffer and nanotoxin-treated animals were observed in terms of white blood cells (white blood cell count (WBC), neutrophils, lymphocytes, monocytes, eosinophils, and basophils), red blood cells (red blood cell count (RCB), hemoglobin (HGB), hematocrit (HCT), mean cell volume (MCV), mean corpuscular hemoglobin (MCH), mean corpuscular hemoglobin concentration (MCHC), and red blood cell distribution width (RDW)), or platelets (platelet count, mean platelet volume (MPV), platelet distribution width (PDW), and plateletcrit (PCT)) (Supplementary Fig. 5). Moreover, these values were between the normal range for a healthy Swiss nude mouse. Lastly, no histopathological alterations were observed in liver, kidneys, spleen, or bone marrow, implying that nanotoxin treatment did not induce any long-term toxic effects in the animals (Supplementary Fig. 4C). Thus, the lack of change in mouse body weight, together with unaltered CBCs, and the absence of histological alterations in non-tumor tissues, indicate a lack of long-term toxicity by the nanotoxins when administered at a dosage that achieves a highly significant antitumor effect.

GSDME and CXCR4 expression in HNSCC and clinical implications

Taking into consideration these findings, we wanted to evaluate the clinical relevance of GSDME activation in HNSCC patients. Given that GSDME presents a tumor suppressive role, it has been reported that GSDME inactivation is a strategy developed by cancer cells to avoid cell death. However, both HPV⁻ HNSCC cells lines used in this study expressed GSDME, and this protein was able

(See figure on next page.)

Fig. 3 zVAD pre-treatment of 22A-CXCR4⁺ and 74B-CXCR4⁺ cells shows T22-PE24-H6 and T22-DITOX-H6 activation of caspase-3/GSDME-mediated pyroptosis. **A** Phase-contrast imaging of 22A-CXCR4⁺ and 74B-CXCR4⁺ cell lines with and without zVAD pre-treatment (100 μM) 1 h prior to the addition of T22-PE24-H6 or T22-DITOX-H6 (magnification 200x). zVAD clearly inhibits pyroptotic cell morphology in both cell lines. **B** Cell viability of 22A-CXCR4⁺ and 74B-CXCR4⁺ cells either pre-treated or not with zVAD before the addition of T22-PE24-H6 and T22-DITOX-H6 nanotoxins. **C** LDH release from 22A-CXCR4⁺ and 74B-CXCR4⁺ treated with T22-PE24-H6 or T22-DITOX-H6 for 48 h, with and without zVAD pre-treatment. **D** Representative images of pro-caspase-3, cleaved caspase-3, PARP, GSDME, and tubulin western blots of samples from 22A-CXCR4⁺ and 74B-CXCR4⁺ cell lines exposed to the inhibitor zVAD before nanotoxin treatment for 48 h. * $p < 0.05$; ** $p < 0.01$. Each column represents the mean value of three biological replicates. Statistical analysis performed by Student t-test. Error bars indicate SEM

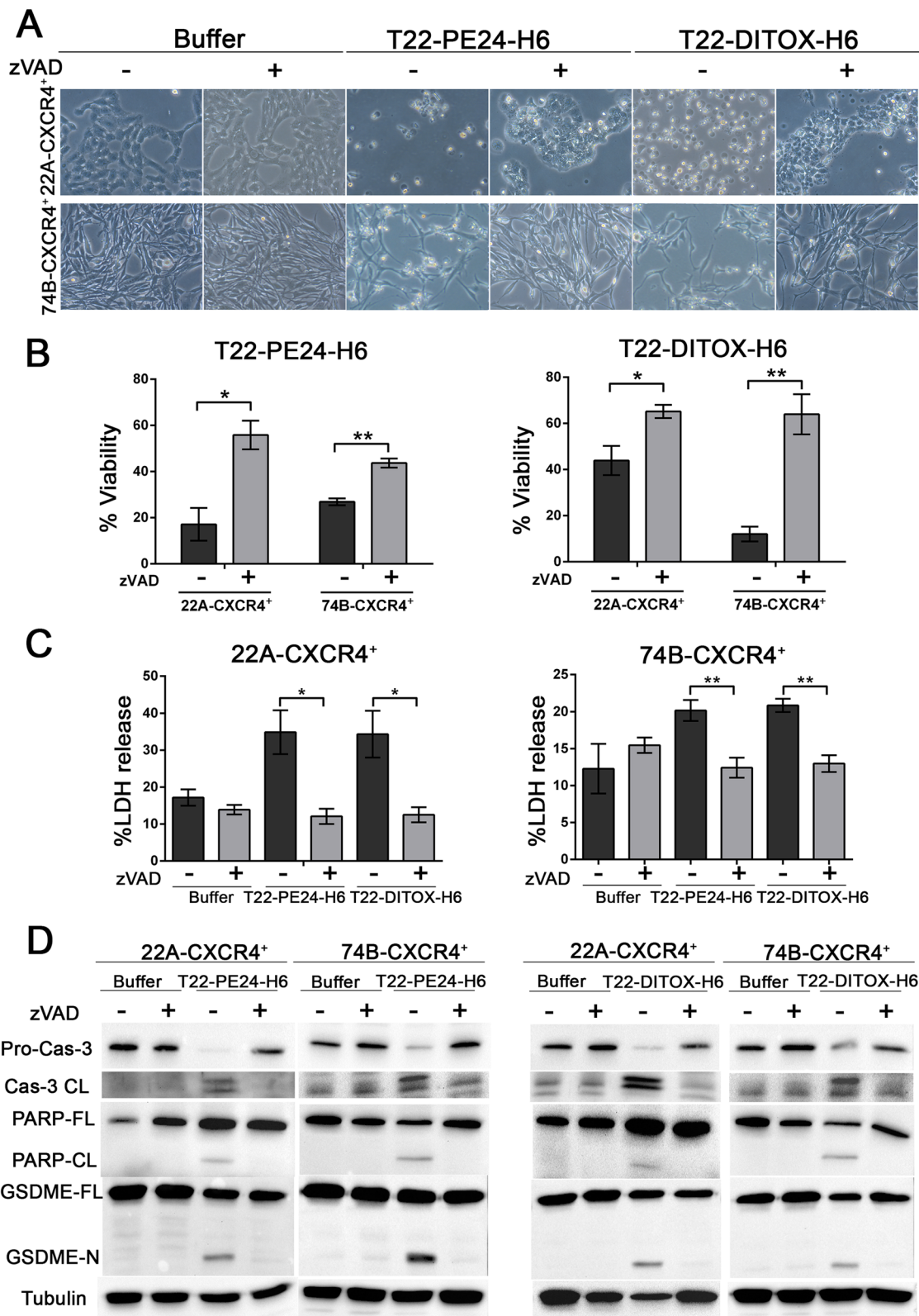


Fig. 3 (See legend on previous page.)

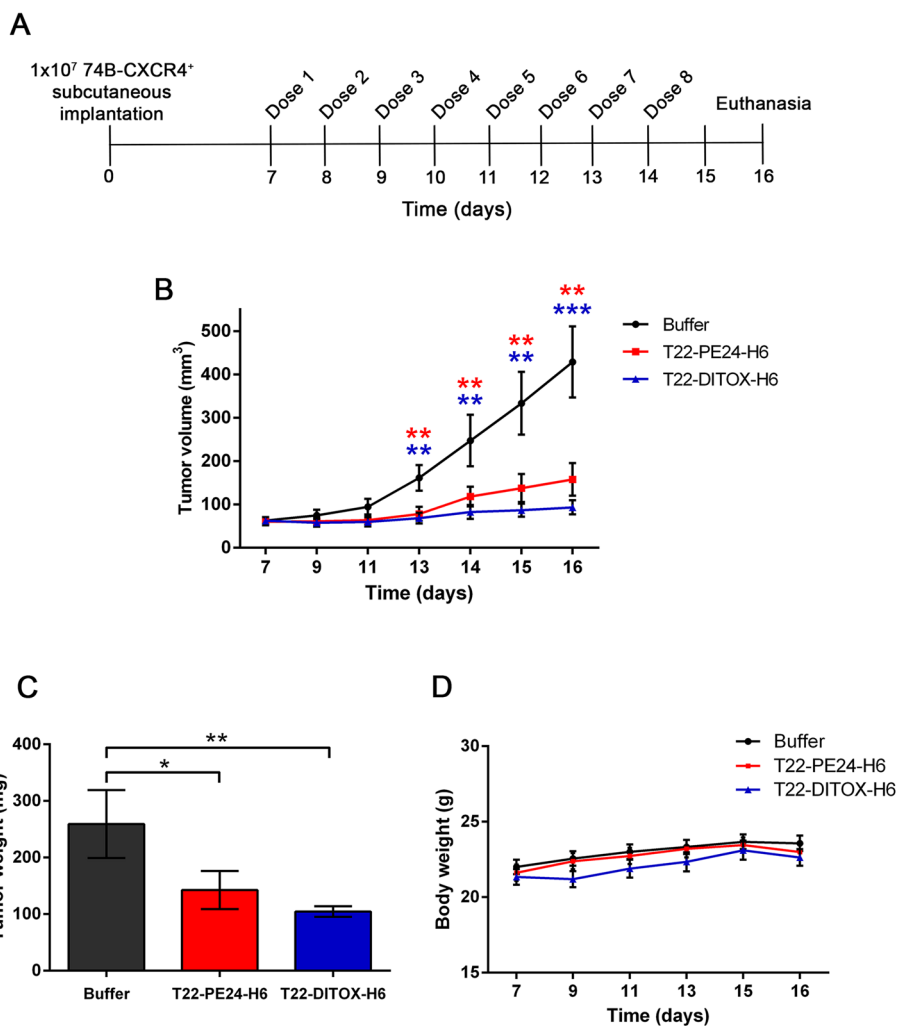
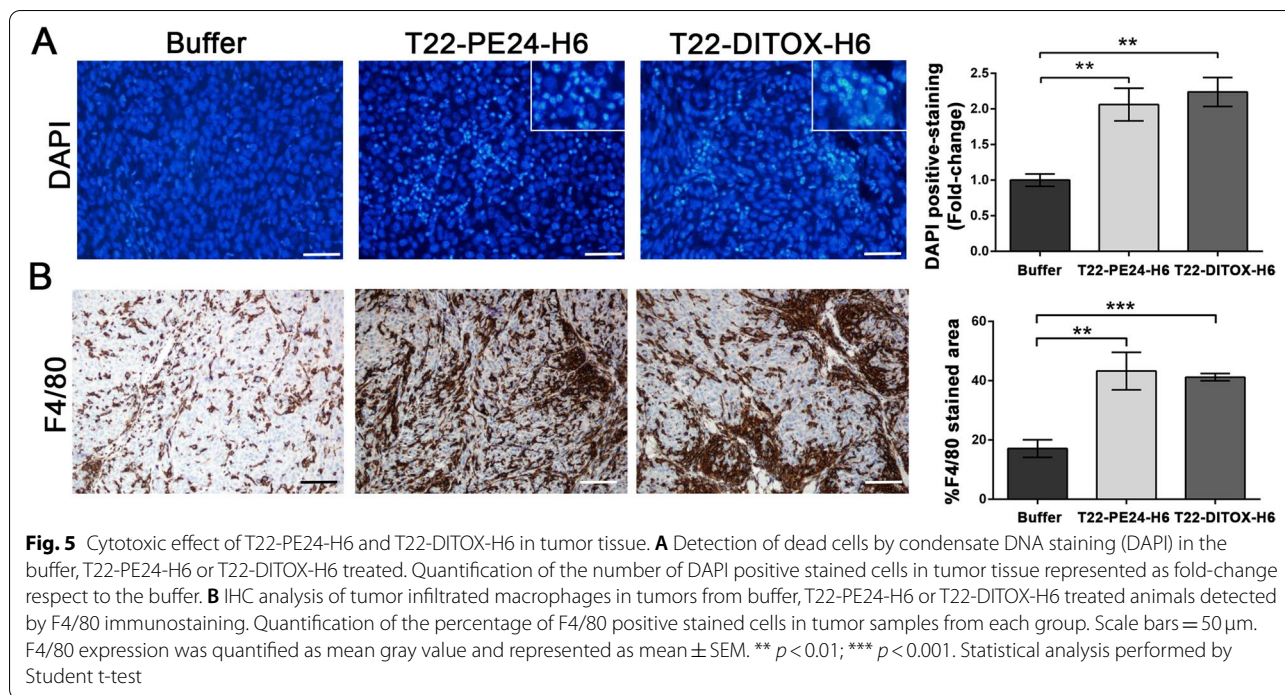


Fig. 4 T22-PE24-H6 and T22-DITOX-H6 antitumor effect in a CXCR4⁺ HNSCC subcutaneous mouse model. **A**) Schematic representation of the experimental design followed in this study. **B**) Variation of the tumor volume in each group (buffer, T22-PE24-H6, and T22-DITOX-H6) in the time course of the experiment. **C**) Tumor weight registered at the end point of the experiment for the three experimental groups. **D**) Body weight of buffer, T22-PE24-H6, and T22-DITOX-H6 treated animals along the study. * $p < 0.05$; ** $p < 0.01$; *** $p < 0.001$; $n = 10$ per group (total animal number 30). Statistical analysis performed by Student t-test. Error bars indicate SEM

to exert its activity upon nanotoxin treatment. Moreover, two patient-derived samples obtained from CXCR4⁺ tumors maintained in vitro also expressed the protein (Fig. 7A). Thus, to further investigate GSDME expression in HNSCC, we conducted an analysis using data from The Cancer Genome Atlas (TCGA) with the UALCAN analysis software [30]. First, we found that CXCR4 is overexpressed in tumoral tissue compared to healthy tissue (Supplementary Fig. 6). Similarly, DFNA5 (gene encoding GSDME) was also overexpressed in tumors compared to non-tumor tissue (Supplementary Fig. 7A). Moreover, DFNA5 was more expressed in HPV⁻ tumors compared to the HPV⁺ ones (Supplementary Fig. 7B).

Interestingly, high DFNA5 expression in tumor tissue correlated with worse overall survival (OS) (Supplementary Fig. 7C). These results prompted us to perform a IHC analysis of GSDME expression in a cohort of 17 HNSCC patients (Fig. 7B). First, we assessed the CXCR4 expression in the HNSCC samples finding that 88.2% were positive for the receptor (Fig. 7C). Moreover, 94.1% of these patient samples presented positive GSDME staining, independently of their prognosis (Fig. 7C). Importantly, 87.5% of the patient samples expressing GSDME were also positive for CXCR4 immunostaining (Fig. 7C). This subset of patients could potentially benefit from a CXCR4-targeted treatment capable of activating



GSDME, such as the nanotoxins T22-PE24-H6 and T22-DITOX-H6. Thus, we found that GSDME is widely expressed in HNSCC patients highlighting the relevance of GSDME-dependent pyroptosis in disease course and opening a novel avenue for future treatments.

Discussion

In this study (which rationale is summarized in Supplementary Fig. 8), we report for the first time that targeted toxin delivery to CXCR4-overexpressing (CXCR4⁺) human HNSCC cells, achieved by the T22-PE24-H6 and T22-DITOX-H6 nanotoxins, activates caspase-3/GSDME-dependent pyroptosis in CXCR4⁺ cancer cells. Consequently, nanotoxin treatment leads to a potent blockade of tumor growth in a HNSCC model, without inducing systemic toxicity. Importantly, activation of this cell death mechanism alternative to apoptosis is expected to overcome the low response rate to chemotherapy and radiotherapy in HNSCC patients [5, 31].

We meticulously demonstrate that both nanotoxins activate caspase-3/GSDME-dependent pyroptosis in CXCR4⁺ human HNSCC cell lines. First, we have reported that, upon nanotoxin treatment, HNSCC cell lines displayed distinctive pyroptotic features, including balloon-like morphology, increase in LDH release, and lytic cell death. These observations associated with caspase-3 activation followed by GSDME cleavage to generate the pyroptotic effector pore inducer GSDME N-terminus, as detected by immunoblotting.

Importantly, pre-treatment with the pan-caspase inhibitor zVAD blocked all the above described pyroptotic features. Thus, the selective bacterial exotoxin release in CXCR4⁺ HNSCC cells activate caspase-3/GSDME switch from apoptosis to pyroptosis, as described for different untargeted and targeted drugs in other cancer types [24, 25, 32–34].

In addition, and according to the potent cytotoxicity (low nanomolar IC₅₀) observed in vitro, repeated intravenous administration of each nanotoxin in a subcutaneous CXCR4⁺ HNSCC mouse model, induced a potent blockade of tumor growth, flattening the growth curves, especially for the T22-DITOX-H6 nanotoxin, in the absence of systemic toxicity or adverse effects. This high therapeutic window is most likely due to the strict CXCR4-dependent killing achieved by the nanostructured toxins. T22-PE24-H6 and T22-DITOX-H6 internalize exclusively in CXCR4⁺ cells, releasing their toxin domains by furin cleavage upon cell internalization, leading to EF-2 inactivation and protein synthesis inhibition that results in cell death [19]. This effect was demonstrated in vitro in two different HNSCC cell lines, showing that only CXCR4⁺ cells are killed by the nanotoxins and also by the demonstration of a complete cell death blockade by AMD3100 (CXCR4 antagonist) exposure prior to nanotoxins treatment.

Consistently, our previous work supports the selective biodistribution of the nanotoxins to the high

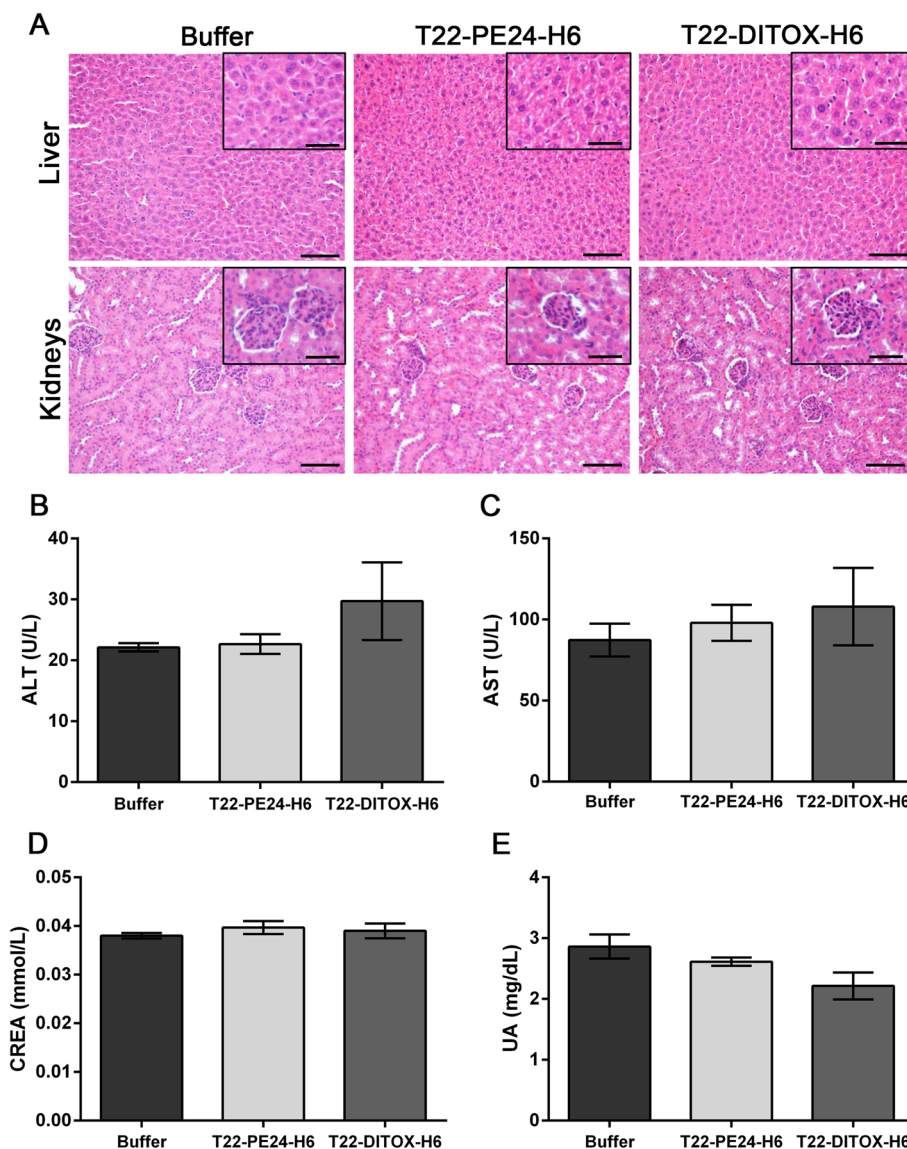
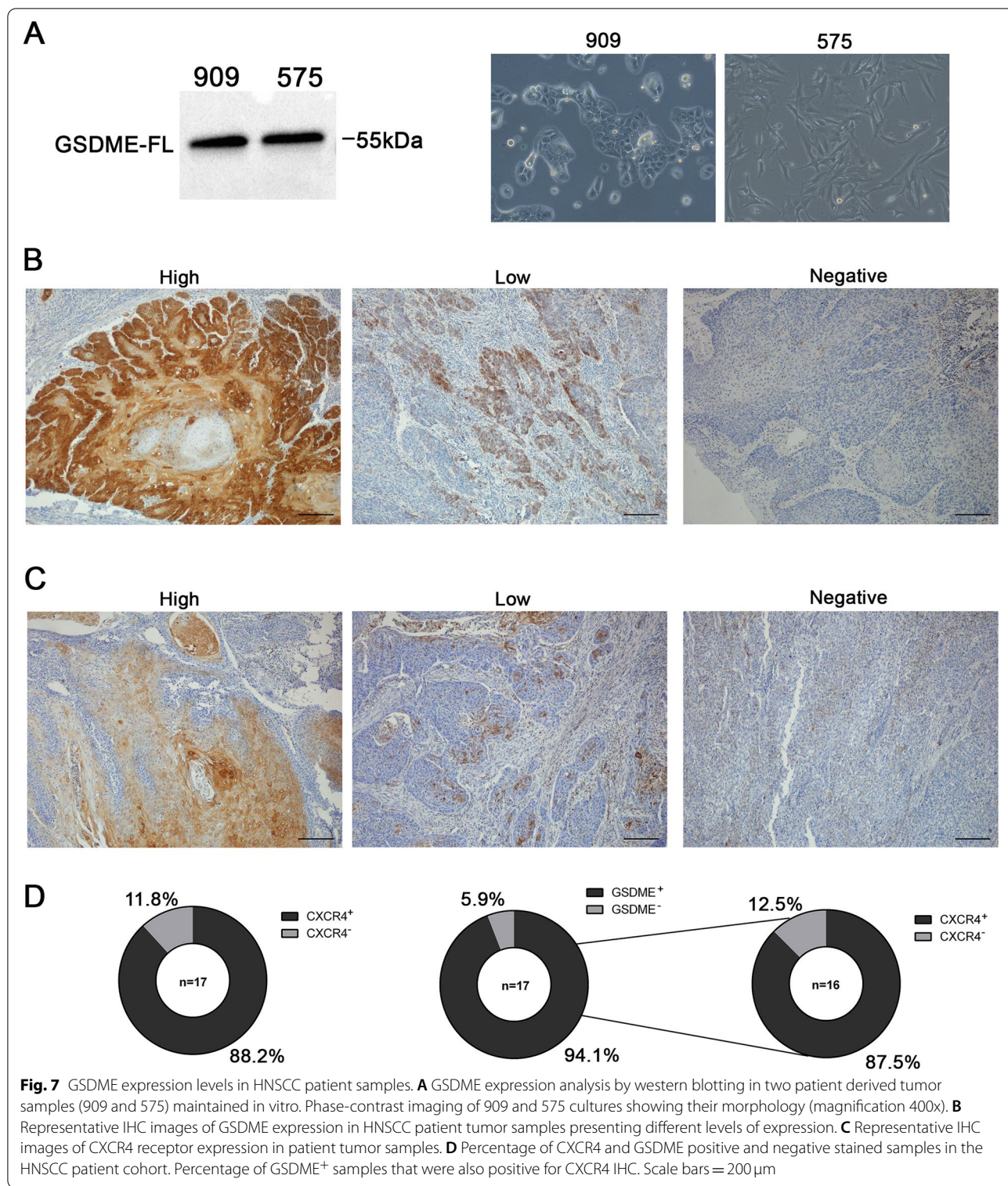


Fig. 6 T22-PE24-H6 and T22-DITOX-H6 toxicity assessment. **A** Histopathological analysis by H&E staining in liver and kidneys samples from buffer, T22-PE24-H6 or T22-DITOX-H6 treated animals. **B, C, D,** and **E** Oxaloacetic transaminase (GOT) (**B**), and glutamic pyruvic transaminase (GPT) (**C**) enzyme activities, as well as creatinine (**D**) and uric acid (**E**) levels in plasma samples from buffer, T22-PE24-H6 or T22-DITOX-H6 treated animals. Scale bars = 100 μm and 50 μm (zoom in). Statistical analysis performed by Student t-test. Error bars indicate SEM

CXCR4-overexpressing tumor tissue, avoiding the accumulation and off-target toxicity in normal organs with low or negligible CXCR4 expression. In this context, we have recently reported this high tumor selectivity using a CXCR4-targeted fluorescent nanocarrier, that displays the exact self-assembling nanoparticle structure of the nanotoxins, in HNSCC, colorectal cancer [35], and lymphoma [36] models. Their size above the 7 nm renal filtration cut-off allows a high recirculation in the bloodstream, while the multivalency derived from the display of multiple T22 peptide domains enables superselectivity

[18] regarding CXCR4⁺ target cell internalization, which exploits the CXCR4 overexpression in tumor compared to normal tissue.

Moreover, innate antitumor immunity may have contributed to the anticancer activity based on the dramatic increase in tumor-infiltrating macrophages (TAM) found in nanotoxin-treated animals. It has been reported that GSDME activation enhances antitumor effect by stimulating TAM phagocytosis, as well as NKs and CD8⁺ T lymphocytes activation [6, 23, 37]. Although preliminary, these findings may suggest an activation of the pyroptotic



pathway in vivo upon treatment, leading to an enhanced immune cell recruitment to the tumor site.

Importantly, different studies have described that conventional chemotherapy threatening off-target

toxicities are induced by the activation of GSDME mediated pyroptosis in non-tumor cells, as these agents lack tumor targeting capacity [24, 38, 39]. In contrast, our CXCR4-targeted nanotoxins,

administered at a repeated dosage schedule, did not induce acute systemic toxicity (at the end of treatment) nor long-term toxicity (4 weeks after treatment), in the HNSCC mouse model, displaying undetectable markers of toxicity in plasma, unaltered cell blood count and lack of histological alterations in non-tumor organs, at a dosage that achieves a potent antitumor effect. Thus, a strict targeted drug delivery to cancer cells is crucial to prevent GSDME activation in healthy tissues.

Regarding the clinical relevance of our results, it is important to highlight that apoptosis avoidance is the main mechanism of resistance to radiotherapy, cisplatin, 5-fluorouracil or docetaxel/paclitaxel, leading to treatment failure and patient death [3, 5, 6, 20]. Moreover, CXCR4 overexpression, in HNSCC and other neoplasias, also associates with resistance, relapse and metastatic potential [7, 8, 40]. Thus, our nanotoxin approach aims to overcome tumor resistance and increase cure rates in HNSCC, by switching cell death induction from apoptosis to caspase-3/GSDME-dependent pyroptosis, as pursued in other cancer types [34, 37, 41].

Interestingly, a large percent of HNSCC patients could be candidates to targeted nanotoxin therapy since in our 17-patient cohort, 88.2% were positive for the CXCR4 receptor, 94% of them expressed GSDME in tumor tissue, whereas 87% of GSDME⁺ tumors also co-expressed CXCR4. Moreover, we have also studied CXCR4 expression in two different cell cultures derived from HNSCC patient tumor samples, named as 575 and 909. Interestingly, although both patient samples presented a strong CXCR4 expression, when cultured in vitro, 575 and 909 cell cultures lost their CXCR4 expression with successive culture passages. Remarkably, when re-inoculated in vivo in immunodeficient mice, the generated tumors expressed again CXCR4 (Supplementary Fig. 9). These results demonstrate that CXCR4 expression is downregulated in vitro, suggesting that CXCR4 regulation plays an important role in tumor progression in vivo. In addition, our TGCA analysis of HNSCC samples showed that GSDME overexpression in tumor compared to normal tissue, correlates with worse OS, which may be explained by the reported lack of tumor infiltrated lymphocytes in GSDME⁺ HNSCC tumors by other authors [42]. Consistently with our results, GSDME overexpression in tumor tissue has also been reported in different cancer types [25, 32, 43, 44], which contrasts with the assumption that GSDME is silenced in tumors given its tumor suppressor role [23, 24, 45–49]. In any case, it is clear that CXCR4 and GSDME markers could be used to select HNSCC patients that might benefit from our nanotoxin therapy.

So far, most of the targeted drugs to treat resistant HNSCC have failed at early stages. Immunotoxins based on *Pseudomonas* exotoxin that target mesothelin in HNSCC stopped development in early clinical trials [50]. Similarly, ADCs targeting different surface markers (EGFR, c-MET, HER2, etc.) conjugated to the PBD toxin or the microtubule inhibitor Auristatin, did not progress due to toxicity concerns [14]. Only the EGFR inhibitor cetuximab and the PD-1/PD-L1 immune checkpoint inhibitors pembrolizumab, nivolumab, and durvalumab, improve survival in recurrent or metastatic HNSCC [51]. We believe that T22-PE24-H6 and T22-DITOX-H6 nanotoxins present important features that will exceed the performance of current immunotoxins and ADCs. These nanotoxins are formed by self-assembly of multiple monomers, displaying numerous targeting ligands that confer superselectivity, and the ability to incorporate multiple cytotoxic domains into a single nanotoxin (Supplementary Fig. 8). These facts contrast with immunotoxins or ADCs, that display only one ligand per molecule, a lower cytotoxic payload, and show drug leakage during circulation inducing off-target effects [12, 13, 15–17].

Conclusions

In summary, the activation of caspase-3/GSDME-dependent pyroptosis by nanostructured toxins targeting CXCR4 opens a novel and virtually unexplored therapeutic approach for HNSCC or other cancer types. Thus, T22-PE24-H6 and T22-DITOX-H6 nanotoxin treatments may turn sensitive the recurrent or metastatic HNSCC because of their ability to trigger a cell death mechanism alternative to apoptosis, since apoptosis blockade is the main mechanism of resistance to currently used chemotherapy and radiotherapy in HNSCC patients [5, 6]. Additionally, the nanotoxin switch from non-inflammatory apoptosis to the inflammatory pyroptosis may also engage immune cells that could enhance anti-tumor immunity.

Abbreviations

HNSCC: Head and neck squamous cell carcinoma; CXCR4: Chemokine receptor 4; GSDME: Gasdermin E; LDH: Lactate dehydrogenase; ADC: Antibody-drug conjugate; IL-2: Interleukin-2; PBD: Pyrrolobenzodiazepine; HPV: Human papilloma virus; DMEM: Dulbecco's Modified Eagle's Medium; FBS: Fetal Bovine Serum; PI: Propidium iodide; WB: Western Blotting; SPF: Specific pathogen-free; IHC: Immunohistochemistry; GOT: Glutamic oxaloacetic transaminase; GPT: Glutamic pyruvic transaminase; SD: Standard deviation; SEM: Standard error; TAM: Tumor-associated macrophage; H&E: Hematoxylin-eosin; WBC: White blood cell count; RCB: Red blood cell count; HGB: Hemoglobin; HCT: Hematocrit; MCV: Mean cell volume; MCH: Mean corpuscular hemoglobin; MCHC: Mean corpuscular hemoglobin concentration; RDW: Red blood cell distribution width; MPV: Mean platelet volume; PDW: Platelet distribution width; PCT: Plateletcrit.

Supplementary Information

The online version contains supplementary material available at <https://doi.org/10.1186/s13046-022-02267-8>.

Additional file 1.

Acknowledgements

The authors would like to thank Clara Seira (IIB-Sant Pau, Barcelona) for her technical support, and Dr. Gemma Vilahur (IIB-Sant Pau, Barcelona) for letting us use the Mindray BC-5000 Vet hematology analyzer.

Authors' contributions

We declare that all authors made fundamental contributions to the manuscript. ERB, EV, RM, LAC, and XL designed the study. ERB, IAS, UU, and IC contributed to the development of the methodology. ERB, IAS, PA, NS, and LSG acquired the data and carried out the experiments. ERB and AG carried out the histopathological analysis. The analysis and interpretation of data was performed by ERB, MQ, XL, AV, EV, RM, and LAC. ERB prepared the manuscript. UU, IC, AV, EV, RM, and LAC performed the manuscript reviews and revisions. The study was supervised by EV, RM, and LAC. All authors revised the manuscript and approved the final version.

Funding

This work was supported by grants PI21/00150, PI18/00650, PIE15/00028, PI15/00378 and EU COST Action CA 17140 to Ramon Mangues, PI19/01661 to Xavier León, and PI17/00584 to Miquel Quer, founded by Instituto de Salud Carlos III (ISCIII, Co-funding from FEDER, Spain). Grants BIO2016-76063-R, AEI/FEDER, UE to Antonio Villaverde and PID2019-105416RB-I00/AEI/<https://doi.org/10.13039/501100011033> to Esther Vázquez, founded by Agencia Estatal de Investigación (AEI) and Fondo Europeo de Desarrollo Regional (FEDER) (Spain). CIBER-BBN (Spain) grants CB06/01/1031 and 4NanoMets to Ramon Mangues, VENOM4CANCER to Antonio Villaverde, NANOREMOTE to Esther Vázquez, and NANOSCAPE to Ugutz Unzueta. AGAUR 2017- SGR-865 (Spain) to Ramon Mangues, and 2017SGR-229 (Spain) to Antonio Villaverde. Josep Carreras Leukemia Research Institute (Spain) P/AG to Ramon Mangues. Elisa Rioja-Blanco and Laura Sánchez-García were supported by a predoctoral fellowship from AGAUR (2020FI_B2 00168 and 2018FI_B2_00051 (Spain)) co-funded by European Social Fund (ESF investing in your future). Lorena Alba-Castellón was supported by a postdoctoral fellowship from AECC (Spanish Association of Cancer Research, Spain). Antonio Villaverde was granted an Icrea Academia Award (Spain). Ugutz Unzueta was also supported by Grant PERIS SLT006/17/00093 from la Generalitat de Catalunya (Spain) and Miguel Servet fellowship (CP19/00028) from Instituto de Salud Carlos III (Spain) co-funded by European Social Fund (ESF investing in your future). The toxicity studies have been performed in the ICTS-141007 Nanobiosis Platform, using its CIBER-BBN Nanotoxicology Unit (<http://www.nanobiosis.es/portfoli/u18-nanotoxicology-unit/>). Protein production has been partially performed by the ICTS "NANBIO-SIS", more specifically by the Protein Production Platform of CIBER-BBN/ IIB (<http://www.nanobiosis.es/unit/u1-protein-production-platform-ppp/>).

Availability of data and materials

The datasets used and/or analysed during the current study are available from the corresponding author on reasonable request.

Declarations

Ethics approval and consent to participate

HNSCC patient samples were obtained in accordance with the Hospital de la Santa Creu i Sant Pau Institutional Review Board. Written informed consent was acquired from all the patients involved in this study. All animal experiments were approved by the Hospital de la Santa Creu i Sant Pau Animal Ethics Committee.

Consent for publication

Not applicable.

Competing interests

Antonio Villaverde, Esther Vázquez, Ugutz Unzueta, Ramon Mangues, and Isolda Casanova are cited as inventors in PCT/EP2012/050513 covering

Targeted delivery of therapeutic molecules to CXCR4 cells, and in PCT/EP2018/061732, covering Therapeutic Nanostructured Proteins. All other authors report no conflicts of interest in this work.

Author details

¹Institut d'Investigació Biomèdica Sant Pau (IIB-Sant Pau), Sant Quintí, 77, 08041 Barcelona, Spain. ²Institut de Recerca contra la Leucèmia Josep Carreras, 08025 Barcelona, Spain. ³CIBER de Bioingeniería, Biomateriales y Nanomedicina (CIBER-BBN), Monforte de Lemos 3-5, 28029 Madrid, Spain. ⁴Department of Pathology, Hospital de la Santa Creu i Sant Pau, Sant Quintí, 89, 08041 Barcelona, Spain. ⁵Institut de Biotecnologia i de Biomedicina, Universitat Autònoma de Barcelona, 08193 Bellaterra, Spain. ⁶Departament de Genètica i de Microbiologia, Universitat Autònoma de Barcelona, 08193 Bellaterra, Spain. ⁷Department of Otorhinolaryngology, Hospital de la Santa Creu i Sant Pau, Universitat Autònoma de Barcelona, Sant Quintí, 89, 08041 Barcelona, Spain. ⁸Department of Surgery, Hospital de la Santa Creu i Sant Pau, Universitat Autònoma de Barcelona, Sant Quintí, 89, 08041 Barcelona, Spain. ⁹Institut de Biotecnologia i de Biomedicina and Departament de Genètica i de Microbiologia, Universitat Autònoma de Barcelona and CIBER, Bellaterra, Barcelona, Spain. ¹⁰Institut d'Investigacions Biomèdiques Sant Pau, Hospital de Sant Pau, CIBER and Josep Carreras Research Institute, 08041 Barcelona, Spain. ¹¹Institut d'Investigacions Biomèdiques Sant Pau, Hospital de Sant Pau and Josep Carreras Research Institute, 08041 Barcelona, Spain.

Received: 23 September 2021 Accepted: 19 January 2022

Published online: 04 February 2022

References

- Sacco AG, Cohen EE. Current treatment options for recurrent or metastatic head and neck squamous cell carcinoma. *J Clin Oncol*. 2015;33:3305–15.
- Johnson DE, Burtneß B, Leemans CR, Lui WY, Bauman JE, Grandis JR. Head and neck squamous cell carcinoma. *Nat Rev Dis Prim*. 2020;6:92.
- Picon H, Guddati AK. Mechanisms of resistance in head and neck cancer. *Am J Cancer Res*. 2020;10:2742–51.
- López-Verdín S, Lavalle-Carrasco J, Carreón-Burciaga RG, Serafin-Higuera N, Molina-Frecheró N, González-González R, et al. Molecular markers of anticancer drug resistance in head and neck squamous cell carcinoma: a literature review. *Cancers (Basel)*. 2018;10(10):376.
- Kanno Y, Chen C-Y, Lee H-L, Chiou J-F, Chen Y-J. Molecular mechanisms of chemotherapy resistance in head and neck cancers. *Front Oncol*. 2021;11:640392.
- Raudenská M, Balvan J, Masařík M. Cell death in head and neck cancer pathogenesis and treatment. *Cell Death Dis*. 2021;12:192.
- León X, Díez S, García J, Lop J, Sumarroca A, Quer M, et al. Expression of the CXCL12/CXCR4 chemokine axis predicts regional control in head and neck squamous cell carcinoma. *Eur Arch Otorhinolaryngol*. 2016;273:4525–33.
- De-Colle C, Menegakis A, Mönnich D, Welz S, Boeke S, Sipos B, et al. SDF-1/CXCR4 expression is an independent negative prognostic biomarker in patients with head and neck cancer after primary radiochemotherapy. *Radiother Oncol*. 2018;126:125–31.
- Pastan I, Hassan R, Fitzgerald DJ, Kreitman RJ. Immunotoxin therapy of cancer. *Nat Rev Cancer England*. 2006;6:559–65.
- Alewine C, Hassan R, Pastan I. Advances in anticancer immunotoxin therapy. *Oncologist*. 2015;20:176–85.
- Wu T, Zhu J. Recent development and optimization of *pseudomonas aeruginosa* exotoxin immunotoxins in cancer therapeutic applications. *Int Immunopharmacol*. 2021;96:107759.
- Vallera DA, Kreitman RJ. Immunotoxins targeting B cell malignancy—Progress and problems with immunogenicity. *Biomedicines*. 2018;7(1):1.
- Kim J-S, Jun S-Y, Kim Y-S. Critical issues in the development of immunotoxins for anticancer therapy. *J Pharm Sci*. 2020;109:104–15.
- Perrotti V, Caponio VCA, Mascitti M, Lo Muzio L, Piatelli A, Rubini C, et al. Therapeutic potential of antibody-drug conjugate-based therapy in head and neck cancer: a systematic review. *Cancers (Basel)*. 2021;13(13):3126.
- Beck A, Goetsch L, Dumontet C, Corvaia N. Strategies and challenges for the next generation of antibody-drug conjugates. *Nat Rev Drug Discov*. 2017;16:315–37.

16. Wolska-Washer A, Robak T. Safety and tolerability of antibody-drug conjugates in Cancer. *Drug Saf*. 2019;42:295–314.
17. Masters JC, Nickens DJ, Xuan D, Shazer RL, Amantea M. Clinical toxicity of antibody drug conjugates: a meta-analysis of payloads. *Invest New Drugs*. 2018;36:121–35.
18. Liu M, Apriceno A, Sipin M, Scarpa E, Rodriguez-Arco L, Poma A, et al. Combinatorial entropy behaviour leads to range selective binding in ligand-receptor interactions. *Nat Commun*. 2020;11:4836.
19. Sánchez-García L, Serna N, Álamo P, Sala R, Céspedes MV, Roldan M, et al. Self-assembling toxin-based nanoparticles as self-delivered antitumoral drugs. *J Control Release*. 2018;274:81–92.
20. Holohan C, Van Schaeybroeck S, Longley DB, Johnston PG. Cancer drug resistance: an evolving paradigm. *Nat Rev Cancer*. 2013;13:714–26.
21. Brenner JC, Graham MP, Kumar B, Saunders LM, Kupfer R, Lyons RH, et al. Genotyping of 73 UM-SCC head and neck squamous cell carcinoma cell lines. *Head Neck*. 2010;32:417–26.
22. Rioja-Blanco E, Arroyo-Solera I, Álamo P, Casanova I, Gallardo A, Unzueta U, et al. Self-assembling protein nanocarrier for selective delivery of cytotoxic polypeptides to CXCR4+ head and neck squamous cell carcinoma tumors. *Acta Pharm Sin B*. 2021; Available from: <https://www.sciencedirect.com/science/article/pii/S2211383521003919>.
23. Zhang Z, Zhang Y, Xia S, Kong Q, Li S, Liu X, et al. Gasdermin E suppresses tumour growth by activating anti-tumour immunity. *Nature*. 2020;579:415–20.
24. Wang Y, Gao W, Shi X, Ding J, Liu W, He H, et al. Chemotherapy drugs induce pyroptosis through caspase-3 cleavage of a gasdermin. *Nature*. 2017;547:99–103.
25. Lu H, Zhang S, Wu J, Chen M, Cai MC, Fu Y, et al. Molecular targeted therapies elicit concurrent apoptotic and GSDME-dependent pyroptotic tumor cell death. *Clin Cancer Res*. 2018;24:6066–77.
26. Zhang X, Zhang P, An L, Sun N, Peng L, Tang W, et al. Miltirone induces cell death in hepatocellular carcinoma cell through GSDME-dependent pyroptosis. *Acta Pharm Sin B*. 2020;10:1397–413.
27. Zhang Y, Yang J, Wen Z, Chen X, Yu J, Yuan D, et al. A novel 3',5'-diprenylated chalcone induces concurrent apoptosis and GSDME-dependent pyroptosis through activating PKC δ /JNK signal in prostate cancer. *Aging (Albany NY)*. 2020;12:9103–24.
28. Kong Y, Feng Z, Chen A, Qi Q, Han M, Wang S, et al. The natural flavonoid Galangin elicits apoptosis, Pyroptosis, and autophagy in glioblastoma. *Front Oncol*. 2019;9:942.
29. Cañes L, Martí-Pàmies I, Ballester-Servera C, Alonso J, Serrano E, Briones AM, et al. High NOR-1 (neuron-derived orphan receptor 1) expression strengthens the Vascular Wall response to angiotensin II leading to aneurysm formation in mice. *Hypertens (Dallas, Tex 1979)*. 2021;77:557–70.
30. Chandrashekar DS, Bashel B, Balasubramanya SAH, Creighton CJ, Ponce-Rodriguez I, Chakravarthi BVSK, et al. UALCAN: a portal for facilitating tumor subgroup gene expression and survival analyses. *Neoplasia*. 2017;19:649–58.
31. Wang L, Qin X, Liang J, Ge P. Induction of Pyroptosis: a promising strategy for Cancer treatment. *Front Oncol*. 2021;11:635774.
32. Zhang C-C, Li C-G, Wang Y-F, Xu L-H, He X-H, Zeng Q-Z, et al. Chemotherapeutic paclitaxel and cisplatin differentially induce pyroptosis in A549 lung cancer cells via caspase-3/GSDME activation. *Apoptosis*. 2019;24:312–25.
33. Tsuchiya K. Switching from apoptosis to Pyroptosis: Gasdermin-elicited inflammation and antitumor immunity. *Int J Mol Sci*. 2021;22(1):426.
34. Jiang M, Qi L, Li L, Li Y. The caspase-3/GSDME signal pathway as a switch between apoptosis and pyroptosis in cancer. *Cell Death Discov*. 2020;6:112.
35. Céspedes MV, Unzueta U, Tatkiwicz W, Sánchez-Chardi A, Conchillo-Solé O, Álamo P, et al. In vivo architectonic stability of fully de novo designed protein-only nanoparticles. *ACS Nano*. 2014;8:4166–76.
36. Falgàs A, Pallarès V, Unzueta U, Céspedes MV, Arroyo-Solera I, Moreno MJ, et al. A CXCR4-targeted nanocarrier achieves highly selective tumor uptake in diffuse large B-cell lymphoma mouse models. *Haematologica*. 2020;105:741–53.
37. Yu P, Zhang X, Liu N, Tang L, Peng C, Chen X. Pyroptosis: mechanisms and diseases. *Signal Transduct Target Ther*. 2021;6:128.
38. Wang Y-Y, Liu X-L, Zhao R. Induction of Pyroptosis and its implications in Cancer management. *Front Oncol*. 2019;9:971.
39. Huang Z, Zhang Q, Wang Y, Chen R, Wang Y, Huang Z, et al. Inhibition of caspase-3-mediated GSDME-derived pyroptosis aids in noncancerous tissue protection of squamous cell carcinoma patients during cisplatin-based chemotherapy. *Am J Cancer Res*. 2020;10:4287–307.
40. Chatterjee S, Behnam Azad B, Nimmagadda S. The intricate role of CXCR4 in cancer. *Adv Cancer Res*. 2014;124:31–82.
41. Wu D, Wang S, Yu G, Chen X. Cell death mediated by the Pyroptosis pathway with the aid of nanotechnology: prospects for Cancer therapy. *Angew Chem Int Ed Engl*. 2021;60:8018–34.
42. Liu Z, Liu H, Dong Q, Li H, Zhang B, Liu Y, et al. Prognostic role of DFNA5 in head and neck squamous cell carcinoma revealed by systematic expression analysis: Research Square; 2020. <https://doi.org/10.21203/rs.3.rs-114898/v1>.
43. Wu M, Wang Y, Yang D, Gong Y, Rao F, Liu R, et al. A PLK1 kinase inhibitor enhances the chemosensitivity of cisplatin by inducing pyroptosis in oesophageal squamous cell carcinoma. *EBioMedicine*. 2019;41:244–55.
44. Zhou B, Zhang J-Y, Liu X-S, Chen H-Z, Ai Y-L, Cheng K, et al. Tom20 senses iron-activated ROS signaling to promote melanoma cell pyroptosis. *Cell Res*. 2018;28:1171–85.
45. Xia X, Wang X, Cheng Z, Qin W, Lei L, Jiang J, et al. The role of pyroptosis in cancer: pro-cancer or pro-“host”? *Cell Death Dis*. 2019;10. <https://doi.org/10.1038/s41419-019-1883-8>.
46. Lage H, Helmbach H, Grottko C, Dietel M, Schadendorf D. DFNA5 (ICERE-1) contributes to acquired etoposide resistance in melanoma cells. *FEBS Lett*. 2001;494:54–9.
47. Kim MS, Chang X, Yamashita K, Nagpal JK, Baek JH, Wu G, et al. Aberrant promoter methylation and tumor suppressive activity of the DFNA5 gene in colorectal carcinoma. *Oncogene*. 2008;27:3624–34.
48. Akino K, Toyota M, Suzuki H, Imai T, Maruyama R, Kusano M, et al. Identification of DFNA5 as a target of epigenetic inactivation in gastric cancer. *Cancer Sci*. 2007;98:88–95.
49. Kim MS, Lebron C, Nagpal JK, Chae YK, Chang X, Huang Y, et al. Methylation of the DFNA5 increases risk of lymph node metastasis in human breast cancer. *Biochem Biophys Res Commun*. 2008;370:38–43.
50. Hassan R, Ho M. Mesothelin targeted cancer immunotherapy. *Eur J Cancer*. 2008;44:46–53.
51. Cramer JD, Burtness B, Le QT, Ferris RL. The changing therapeutic landscape of head and neck cancer. *Nat Rev Clin Oncol*. 2019;16:669–83.

Publisher's Note

Springer Nature remains neutral with regard to jurisdictional claims in published maps and institutional affiliations.

Ready to submit your research? Choose BMC and benefit from:

- fast, convenient online submission
- thorough peer review by experienced researchers in your field
- rapid publication on acceptance
- support for research data, including large and complex data types
- gold Open Access which fosters wider collaboration and increased citations
- maximum visibility for your research: over 100M website views per year

At BMC, research is always in progress.

Learn more biomedcentral.com/submissions



CHAPTER 3

A Novel CXCR4-Targeted Diphtheria Toxin Nanoparticle Inhibits Invasion and Metastatic Dissemination in a Head and Neck Squamous Cell Carcinoma Mouse Model

Elisa Rioja-Blanco, Alberto Gallardo, Irene Arroyo-Solera, Patricia Álamo, Isolda Casanova, Ugutz Unzueta, Naroa Serna, Laura Sánchez-García, Miquel Quer, Antonio Villaverde, Esther Vázquez*, Xavier León, Lorena Alba-Castellón*, Ramon Manges*



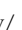



*co-corresponding authors

Pharmaceutics

2022

Article

A Novel CXCR4-Targeted Diphtheria Toxin Nanoparticle Inhibits Invasion and Metastatic Dissemination in a Head and Neck Squamous Cell Carcinoma Mouse Model

Elisa Rioja-Blanco ^{1,2}, Alberto Gallardo ^{1,3}, Irene Arroyo-Solera ^{1,2,4}, Patricia Álamo ^{1,2,4}, Isolda Casanova ^{1,2,4}, Ugutz Unzueta ^{1,2,4,5}, Naroa Serna ^{4,5,6}, Laura Sánchez-García ^{4,5,6}, Miquel Quer ^{4,7}, Antonio Villaverde ^{4,5,6}, Esther Vázquez ^{4,5,6,*}, Xavier León ^{4,7}, Lorena Alba-Castellón ^{1,2,*} and Ramon Mangues ^{1,2,4,*}

- ¹ Institut d'Investigació Biomèdica Sant Pau (IIB-Sant Pau), Sant Quintí, 77, 08041 Barcelona, Spain; erioja@santpau.cat (E.R.-B.); agallardo@santpau.cat (A.G.); iarroyo@santpau.cat (I.A.-S.); palamo@santpau.cat (P.Á.); icasanova@santpau.cat (I.C.); uunzueta@santpau.cat (U.U.)
- ² Institut de Recerca contra la Leucèmia Josep Carreras, 08025 Barcelona, Spain
- ³ Department of Pathology, Hospital de la Santa Creu i Sant Pau, Sant Quintí, 89, 08041 Barcelona, Spain
- ⁴ CIBER de Bioingeniería, Biomateriales y Nanomedicina (CIBER-BBN), Monforte de Lemos 3-5, 28029 Madrid, Spain; narooas@nanoligent.com (N.S.); laurasanchezgarcia92@gmail.com (L.S.-G.); mquer@santpau.cat (M.Q.); antoni.villaverde@uab.cat (A.V.); xleon@santpau.cat (X.L.)
- ⁵ Departament de Genètica i de Microbiologia, Universitat Autònoma de Barcelona, 08193 Bellaterra, Spain
- ⁶ Institut de Biotecnologia i de Biomedicina, Universitat Autònoma de Barcelona, 08193 Bellaterra, Spain
- ⁷ Department of Otorhinolaryngology, Hospital de la Santa Creu i Sant Pau, Universitat Autònoma de Barcelona, Sant Quintí, 89, 08041 Barcelona, Spain
- * Correspondence: esther.vazquez@uab.cat (E.V.); lalba@santpau.cat (L.A.-C.); rmangues@santpau.cat (R.M.); Tel.: +34-935-537-921 (L.A.-C.); +34-935-537-919 (R.M.)



Citation: Rioja-Blanco, E.; Gallardo, A.; Arroyo-Solera, I.; Álamo, P.; Casanova, I.; Unzueta, U.; Serna, N.; Sánchez-García, L.; Quer, M.; Villaverde, A.; et al. A Novel CXCR4-Targeted Diphtheria Toxin Nanoparticle Inhibits Invasion and Metastatic Dissemination in a Head and Neck Squamous Cell Carcinoma Mouse Model. *Pharmaceutics* **2022**, *14*, 887. <https://doi.org/10.3390/pharmaceutics14040887>

Academic Editors: Magdalena Markowicz-Piasecka and Kristiina Huttunen

Received: 15 March 2022

Accepted: 15 April 2022

Published: 18 April 2022

Publisher's Note: MDPI stays neutral with regard to jurisdictional claims in published maps and institutional affiliations.



Copyright: © 2022 by the authors. Licensee MDPI, Basel, Switzerland. This article is an open access article distributed under the terms and conditions of the Creative Commons Attribution (CC BY) license (<https://creativecommons.org/licenses/by/4.0/>).

Abstract: Loco-regional recurrences and metastasis represent the leading causes of death in head and neck squamous cell carcinoma (HNSCC) patients, highlighting the need for novel therapies. Chemokine receptor 4 (CXCR4) has been related to loco-regional and distant recurrence and worse patient prognosis. In this regard, we developed a novel protein nanoparticle, T22-DITOX-H6, aiming to selectively deliver the diphtheria toxin cytotoxic domain to CXCR4⁺ HNSCC cells. The antimetastatic effect of T22-DITOX-H6 was evaluated in vivo in an orthotopic mouse model. IVIS imaging system was utilized to assess the metastatic dissemination in the mouse model. Immunohistochemistry and histopathological analyses were used to study the CXCR4 expression in the cancer cells, to evaluate the effect of the nanotoxin treatment, and its potential off-target toxicity. In this study, we report that CXCR4⁺ cancer cells were present in the invasive tumor front in an orthotopic mouse model. Upon repeated T22-DITOX-H6 administration, the number of CXCR4⁺ cancer cells was significantly reduced. Similarly, nanotoxin treatment effectively blocked regional and distant metastatic dissemination in the absence of systemic toxicity in the metastatic HNSCC mouse model. The repeated administration of T22-DITOX-H6 clearly abrogates tumor invasiveness and metastatic dissemination without inducing any off-target toxicity. Thus, T22-DITOX-H6 holds great promise for the treatment of CXCR4⁺ HNSCC patients presenting worse prognosis.

Keywords: CXCR4; head and neck cancer; targeted drug delivery; protein nanoparticles; diphtheria toxin; metastasis

1. Introduction

Head and neck squamous cell carcinoma represents a major cause of mortality, with more than 850,000 new cases and 400,000 deaths worldwide in 2020 [1]. Current treatment, consisting of a combination of surgery, chemotherapy, and radiotherapy, achieves loco-regional control of the disease in a variable proportion of patients. Treatment regimens for recurrent and metastatic HNSCC patients present low response rates and limited survival

benefits. Remarkably, around 60% of HNSCC patients develop loco-regional recurrence and up to 30% develop distant metastases after treatment, representing the leading cause of patient mortality [2].

Different molecular pathways have been related to metastatic dissemination in HNSCC, including the transforming growth factor β (TGF- β), the fibroblast growth factor receptor (FGFR), and the chemokine receptor 4 (CXCR4), among others [3–7]. CXCR4 and its ligand, CXCL12, play a key role in the carcinogenic process. CXCR4 is also overexpressed in more than 20 cancer types compared to the normal organs, including HNSCC [8]. Importantly, our group and others have previously reported that CXCR4 overexpression in HNSCC primary tumors correlates with loco-regional and distant recurrence and has an impact on patient prognosis [9,10]. Moreover, CXCR4 overexpression has also been related to higher tumor grade, lymph node metastasis, and poor overall survival [11]. Thus, in recent decades, CXCR4 has been exploited as a molecular target for cancer treatment. Research has focused on the development of CXCR4 antagonists, mainly small molecules, peptides, and antibodies, that can act directly on tumor cells or by regulating the tumor microenvironment [8,12]. Currently, plerixafor (AMD3100) remains the only CXCR4 antagonist on the market. Many other inhibitors have been designed with enhanced properties. Among them, polymeric plerixafor (PAMD) represents a promising strategy, presenting an improved toxicity profile and an enhanced anti-metastatic effect [13,14]. However, most of these inhibitors still present low tolerability and short half-life in circulation. Furthermore, current clinical trials involving CXCR4 antagonists are used in combination with conventional chemotherapeutic drugs.

Targeted drug delivery to CXCR4 represents a promising alternative to molecularly targeted therapy via CXCR4 inhibitors. While the latter only focuses on inhibiting CXCR4 signaling, our approach is to deliver cytotoxic compounds directly to CXCR4-overexpressing cells, aiming to selectively deplete these cancer cells, which display stem-cell-like properties and enhanced metastatic potential [11,15,16]. In addition, targeted drug delivery theoretically enables the use of higher doses while reducing off-target effects and toxicity, which are major problems of current chemotherapy [17,18]. In this framework, our group designed the T22-DITOX-H6 nanotoxin, which incorporates the T22 peptide, a CXCR4 ligand, to selectively target CXCR4-overexpressing cells, fused to the catalytic domain of the diphtheria toxin. This platform aims to deliver the cytotoxic compound selectively to CXCR4-overexpressing cancer cells without off-target toxicity in non-tumor bearing organs. This study investigates the potential use of T22-DITOX-H6 nanotoxin to prevent regional and distant metastasis in a HNSCC mouse model in the absence of systemic toxicity. To our knowledge, this is the first study involving CXCR4-targeted protein nanoparticles for the treatment of HNSCC metastatic development, which holds great promise as a future therapy for HNSCC patients.

2. Materials and Methods

2.1. Production, Purification, and Characterization of Nanoparticles

T22-DITOX-H6 protein nanoparticles were recombinantly produced in *Escherichia coli*, purified, and characterized as previously described [19]. T22-DITOX-H6 nanotoxin monomers self-assemble into 38- and 90-nanometer nanoparticles [19].

2.2. Cell Lines and Culture

UM-SCC-74B (74B) human-papillomavirus-negative (HPV⁻) HNSCC cell line [20] was kindly provided by Dr. Gregory Oakley. The 74B-Luci cell line was obtained by lentiviral transduction with the plasmid pLenti-III-UbC-luc (abm, Vancouver, BC, Canada) as already described in previous work [21]. The 74B-Luci cell line was cultured in Dulbecco's Modified Eagle's Medium (DMEM) (Gibco, Thermo Fisher Scientific, Waltham, MA, USA) supplemented with 10% fetal bovine serum (FBS), 100 U/mL penicillin/streptomycin, and 2 mM glutamine (Gibco, Thermo Fisher Scientific, Waltham, MA, USA) and incubated at

37 °C and 5% CO₂ in a humidified atmosphere. CXCR4 expression in 74B-Luci has already been evaluated in previous work [21].

2.3. *In Vivo* Experiments

For all experiments, four-week-old female mice weighing 18–25 g were purchased from Charles River (Saint Germain-Nuelles, France). Animals were housed in a specific pathogen-free (SPF) environment with sterile food and water ad libitum. All animal experiments were approved by the Hospital de la Santa Creu i Sant Pau Animal Ethics Committee (Ethical approval code 9721, 20 February 2018). Animal body weight was evaluated throughout the course of the experiments to ensure animal welfare. A 10% weight loss was considered the humane endpoint for the experiments. For the study of the CXCR4 expression in the invasive fronts of the tumors, 3×10^5 74B-Luci cells were orthotopically inoculated (tongue) in NSG mice (NOD-scid IL2Rgamma^{null}) ($n = 3$). Primary tumors were collected for later analyses 7 days after the cell inoculation, when animals started losing weight as a consequence of primary tumor growth.

To evaluate the effect of T22-DITOX-H6 repeated administration in the invasive fronts of the primary tumors, Swiss nude mice (NU(Ico)-Foxn1^{nu}) ($n = 8$) were orthotopically inoculated with 1 million 74B-Luci cells. One day after the implantation, animals were randomized into two groups ($n = 4$) and intravenously administered up to five doses of either buffer (166 mM NaCO₃H, pH 8) or 10 µg of T22-DITOX-H6 every day. Seven days after the tumor implantation, animals were euthanized, and organs were collected for histopathological analyses.

The antimetastatic effect of T22-DITOX-H6 was assessed in a disseminated mouse model that replicates the metastatic pattern of the disease. To this end, NSG mice (NOD-scid IL2Rgamma^{null}) ($n = 14$) were inoculated with 5×10^4 74B-Luci cells in the tongue. Forty-eight hours after tumor implantation, animals were randomized into control and treated groups ($n = 7$). Control animals were intravenously administered buffer (166 mM NaCO₃H, pH 8) and treated animals 10 µg of T22-DITOX-H6 every other day for up to 14 doses. Metastatic dissemination to the cervical lymph nodes was semi-quantitatively evaluated every week (days 2, 8, 16, 22, and 30 post-tumor implantation) by measuring tumor cells' bioluminescent signal (BLI, total radiance photons in the region of interest (ROI)) using the IVIS[®] Spectrum 200 (PerkinElmer, Waltham, MA, USA). For that, mice were intraperitoneally injected with firefly D-luciferin (2.25 mg/mouse, PerkinElmer) 5 min before IVIS evaluation and anesthetized with 3% isoflurane. Thirty days after the beginning of the experiment, when cervical lymph node infiltration started to cause distress in the mice, animals were euthanized and primary tumor, cervical lymph nodes, lungs, and liver BLI were semi-quantified *ex vivo* in the whole area of the tumor/organ. Next, primary tumors and other relevant organs were collected in 4% formaldehyde for further analysis. All BLI measurements were performed in the luminescence/photograph mode with the auto exposure setting. BLI images were analyzed with Living Image[®] Analysis Software (PerkinElmer). Results were expressed as total flux of BLI (photons/second; radiance photons) ± SEM.

2.4. Histopathology, Immunofluorescence, and Immunohistochemical Analysis

Four-micrometer paraffin-embedded sections obtained from tumors and organs extracted from the animals were utilized for all histopathological and immunostaining analyses.

Colocalization of CXCR4 and Human Vimentin in the invasive front of tumor tissues was performed by immunofluorescence. Paraffin-embedded tumor sections were heated for 1 h at 60 °C, dewaxed and rehydrated. Samples were subjected to antigen retrieval using Tris-EDTA buffer, pH 9.0 (Invitrogen, Thermo Fisher Scientific, Waltham, MA, USA) in a Decloaking Chamber[™] NxGen (Biocare medical, Concord, CA, USA) at 110 °C for 20 min. Blockage was performed by incubating the samples in TBS + 0.5% TritonX-100 + 3% donkey serum for 1 h at room temperature. Next, samples were incubated with the primary antibodies human vimentin mouse IgG (ready to use, Dako, Glostrup, Denmark) and

CXCR4 rabbit IgG (1:250, Abcam, Cambridge, UK) overnight at 4 °C. Tissue sections were then incubated with the secondary antibodies anti-mouse IgG-Alexa Fluor[®] 546 (1:200, Abcam) and anti-rabbit IgG-Alexa Fluor[®] 488 (1:200, Abcam) for 2 h at room temperature. Before mounting, the tumor sections were stained with 0.5 µg/mL DAPI (Sigma-Aldrich, Saint Louis, MO, USA) for 10 min at room temperature. Samples were visualized by fluorescence microscopy and representative pictures were taken with an Olympus DP73 digital camera (Olympus Corporation, Tokyo, Japan) and analyzed using Fiji, ImageJ software (National Institutes of Health, Bethesda, MD, USA).

For histopathological analyses, organ sections were stained with hematoxylin eosin (H&E) and analyzed by two independent observers. CXCR4 (1:200, Abcam, Retrieval pH high, Dako, Glostrup, Denmark) and Human Vimentin (ready to use, Dako, Glostrup, Denmark) immunohistochemical (IHC) staining were performed in a Dako Autostainer Link48 (Glostrup, Denmark), following the manufacturer's instructions. Representative images were captured using an Olympus DP73 digital camera and processed with Olympus CellD Imaging 3.3 software (Olympus Corporation, Tokyo, Japan).

2.5. Statistical Analysis

Data were represented as mean ± standard error (SEM). Statistical analyses were performed using the GraphPad Prism 5 software (GraphPad, San Diego, CA, USA). Results were analyzed by Scheirer–Ray–Hare test, Fisher's test, and Mann–Whitney test. Differences were considered statistically significant when *p*-values < 0.05.

3. Results

3.1. CXCR4⁺ Tumor Cells Are Enriched in the Tumor Budding in a HNSCC Mouse Model

Since CXCR4 overexpression in tumor tissue has been related to enhanced migration, metastatic potential, and a higher risk of recurrence in HNSCC, we wanted to evaluate its suitability as a receptor for targeted drug delivery. Considering the relevance of the CXCR4 receptor in HNSCC prognosis, we wanted to further study CXCR4 expression in a HNSCC orthotopic mouse model. For that, human HNSCC 74B-Luci cells were inoculated orthotopically in the tongues of the mice to generate primary tumors. Both CXCR4 and human vimentin IHC staining were performed in consecutive primary tumor slides. Human vimentin IHC staining was used as a marker for the selective detection of tumor cells, since the 74B cell line constitutively expresses vimentin. Moreover, the anti-human-vimentin antibody utilized does not cross-react with mouse vimentin; thus, it is able to detect cancer cells even as single cells in mouse tissues. Remarkably, although the vast majority of the cancer cells within the primary tumor were CXCR4⁻ (Figure S1), when observing the tumor margin, several single cells and cell clusters that expressed CXCR4 invading the stromal tissue of the tumor edge were detected (Figure 1A). Moreover, some of these CXCR4⁺ cells were also positive for human-vimentin expression, implying that they were cancer cells (Figure 1A). In order to confirm these observations, CXCR4 and human vimentin co-immunofluorescent staining was performed on the tumor samples. The CXCR4⁺ vimentin⁺ cells were observed in the tumor budding in the primary tumor margin, demonstrating that the CXCR4⁺ cells previously identified by IHC were indeed human cancer cells (vimentin⁺) (Figure 1B). These results clearly suggest that CXCR4 plays an important role in the invasion and dissemination of cancer cells from primary tumor sites, which has already been demonstrated for other cancer types [11,15,16].

3.2. T22-DITOX-H6 Nanotoxin Treatment Abrogates Tumor-Cell Invasion In Vivo

The detection of these CXCR4⁺ tumor cells in the invasive front of the primary tumors exhorted us to investigate the potential anti-invasive effect of the T22-DITOX-H6 nanotoxin. T22-DITOX-H6 includes the CXCR4 ligand T22, fused to the cytotoxic domain of the diphtheria toxin, which is able to selectively internalize and eliminate CXCR4⁺ HNSCC cancer cells [21,22]. In this context, we generated an orthotopic HNSCC mouse model through the inoculation of the 74B-Luci cells in the mouse tongues. The animals

were administered up to five doses of either buffer (166 mM NaCO₃H, pH 8) or 10 µg of T22-DITOX-H6 on a daily basis and euthanized 48 h after the end of the treatment (day 7 after tumor cell inoculation), at which point the tumors and other relevant organs were collected for later analyses (Figure S2A). Human vimentin IHC staining revealed that nanotoxin repeated administration clearly diminished the number of cancer cells (vimentin⁺) in the tumor invasive front (Figure 2A,B). In agreement with this finding, the CXCR4⁺ cells in the tumor budding were also reduced upon nanotoxin treatment (Figure 2C,D). As expected, no variation in primary tumor volume was observed between the control and nanotoxin-treated animals, as the CXCR4 expression within the tumor tissue was negligible (Figure S3). Altogether, these findings clearly suggest that successive T22-DITOX-H6 administration effectively eliminates CXCR4⁺ invasive cancer cells endowed with metastatic potential.

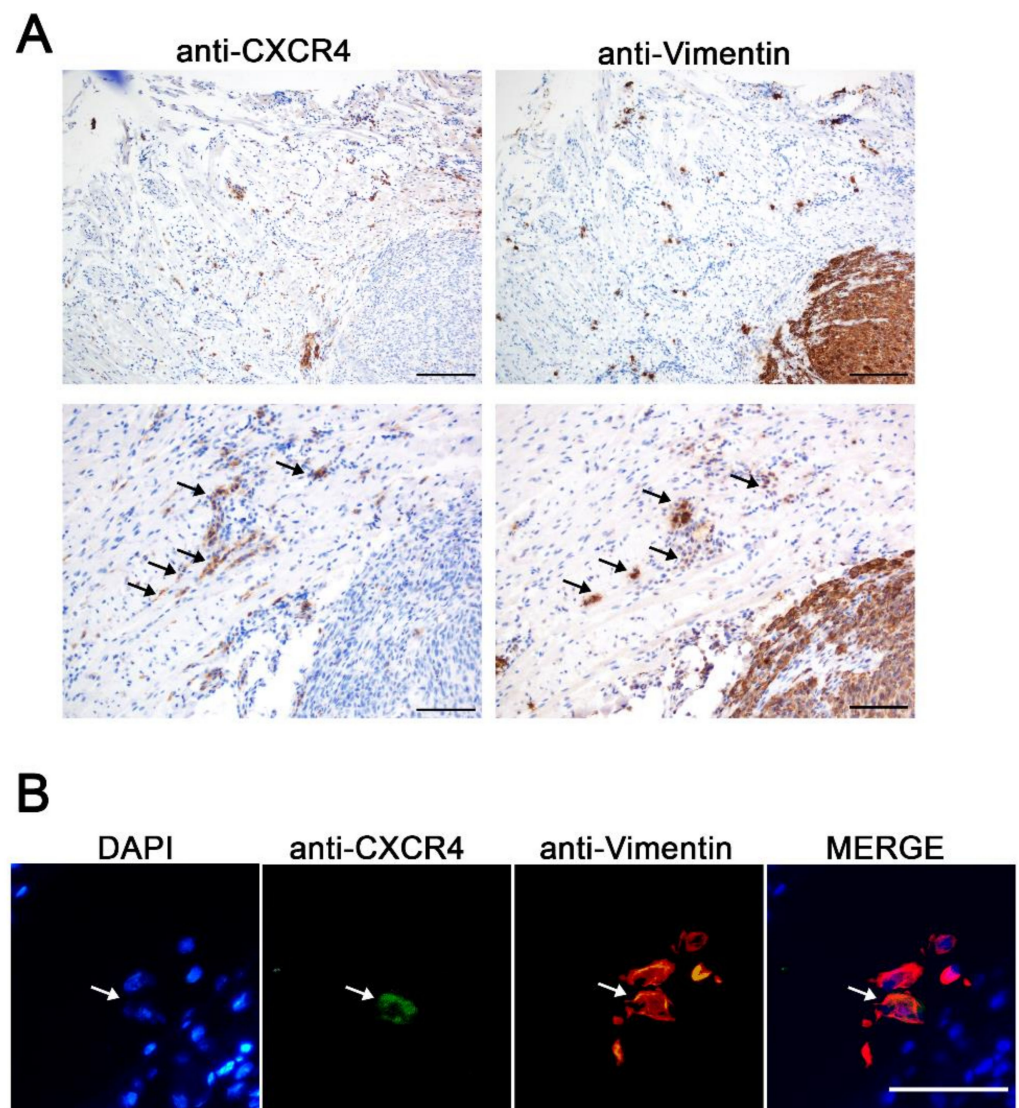


Figure 1. CXCR4 expression in the tumor invasive front generated in the HNSCC orthotopic mouse model. (A) Representative CXCR4 and human-vimentin IHC images of the tumor budding showing the presence of CXCR4⁺ cancer cells invading the surrounding tissue. Scale bars = 200 µm and 100 µm. (B) CXCR4 and human-vimentin immunofluorescence staining in the invasive front of the orthotopic tumor samples. Scale bars = 50 µm.

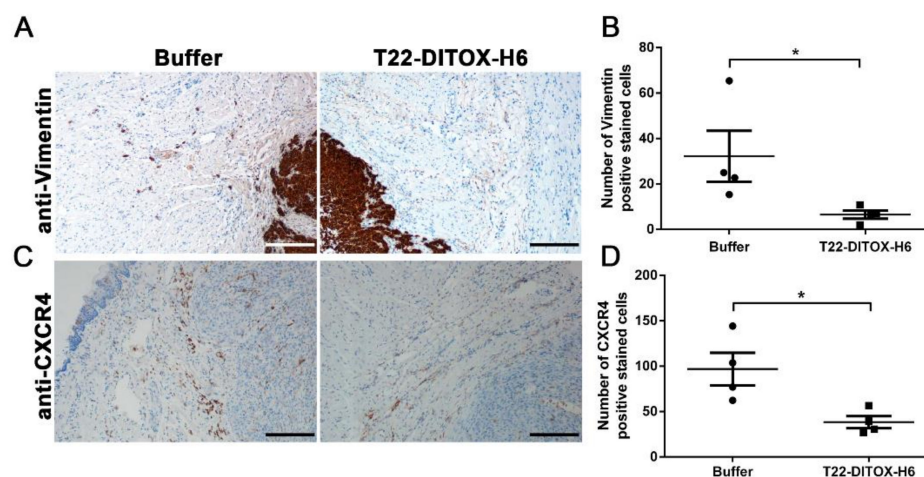


Figure 2. Anti-invasive T22-DITOX-H6 effect in the tumor front in a HNSCC orthotopic mouse model. (A) Representative human-vimentin IHC images of tumors collected from buffer- and T22-DITOX-H6-treated animals, showing a reduction in the number of human-vimentin-positive stained cells in the invasive front of the tumors after the nanotoxin treatment. Scale bar = 200 μ m. (B) Quantification of the number of human-vimentin-positive stained cells in the tumor budding in the control and nanotoxin-treated tumors. (C) CXCR4 IHC analysis of the invasive front of tumors derived from control and nanotoxin-treated mice, displaying a reduction in the number of CXCR4⁺ cells upon T22-DITOX-H6 treatment. Scale bar = 200 μ m. (D) Quantification of the number of CXCR4-positive stained cells in the aforementioned CXCR4 IHC images. * $p < 0.05$; $n = 4$ per group (total animal number 8). Statistical analysis was performed by Mann–Whitney test. Error bars indicate SEM.

3.3. T22-DITOX-H6 Repeated Dosage Inhibits Metastatic Dissemination in a HNSCC Orthotopic Mouse Model in the Absence of Systemic Toxicity

The aforementioned potent inhibition of tumor-cell invasion prompted us to further investigate the potential antimetastatic activity of T22-DITOX-H6 in an orthotopic mouse model that replicates the metastatic pattern observed in HNSCC patients. Animals were administered up to 14 doses of either buffer (166 mM NaCO₃H, pH 8) or 10 μ g of T22-DITOX-H6 on alternate days. Tumor-cell dissemination was assessed weekly *in vivo* by measuring the bioluminescent signal emitted by tumor cells (BLIs). Forty-eight hours after the last dose (day 30 after tumor-cell inoculation), the animals were euthanized. BLI of the primary tumors and different relevant organs was evaluated *ex vivo*. Then, primary tumors and organs were collected for immunohistochemical studies (Figure S2B).

Regional metastatic dissemination to the cervical lymph nodes was evaluated during the course of the experiment by a semi-quantitative measurement of the bioluminescent signal emitted by the tumor cells (Figure 3A–C). Remarkably, the buffer-treated animals presented greater cervical-lymph-node cancer-cell infiltration compared to the nanotoxin-treated mice (Figure 3A). Semi-quantification of the emitted bioluminescent signal by cervical lymph nodes during the experiment clearly showed that the T22-DITOX-H6 treatment abrogated cervical lymph node tumor infiltration (Figure 3B). In agreement, the area under the curve (AUC) for the lymph nodes' bioluminescent signal was also significantly smaller in the nanotoxin-treated group (Figure 3C). The follow-up of the bioluminescent signal *in vivo* was further validated *ex vivo* at euthanasia, confirming the reduction in cervical-lymph-node tumor infiltration resulting from the nanotoxin treatment (Figure S4A,B). Accordingly, the T22-DITOX-H6 treatment affected the percentage of animals with cervical-lymph-node dissemination, with a 57% reduction (71% of the control animals, versus 14% of the treated animals) (Figure 3D). Importantly, six animals from the nanotoxin-treated group were metastasis-free, whereas only two control animals presented no lymph-node tumor infiltration at the end of the experiment. The metastatic cells were also detected by human-vimentin IHC staining, revealing that the lymph nodes collected from the buffer-treated animals were vimentin⁺, further corroborating their

infiltration by the tumor cells (Figure 3E). Remarkably, cervical lymph node infiltration was macroscopically detected in the control animals, while their nanotoxin-treated counterparts presented a normal appearance, with an absence of visible cancer masses (Figure 3F). In agreement, tumor-cell infiltration also affected the cervical-lymph-node area, with the cervical lymph nodes derived from the nanotoxin-treated animals being significantly smaller compared to their buffer-treated counterparts (Figure 3G). Thus, T22-DITOX-H6 repeated administration in the disseminated mouse model clearly inhibited regional cervical lymph node metastasis.

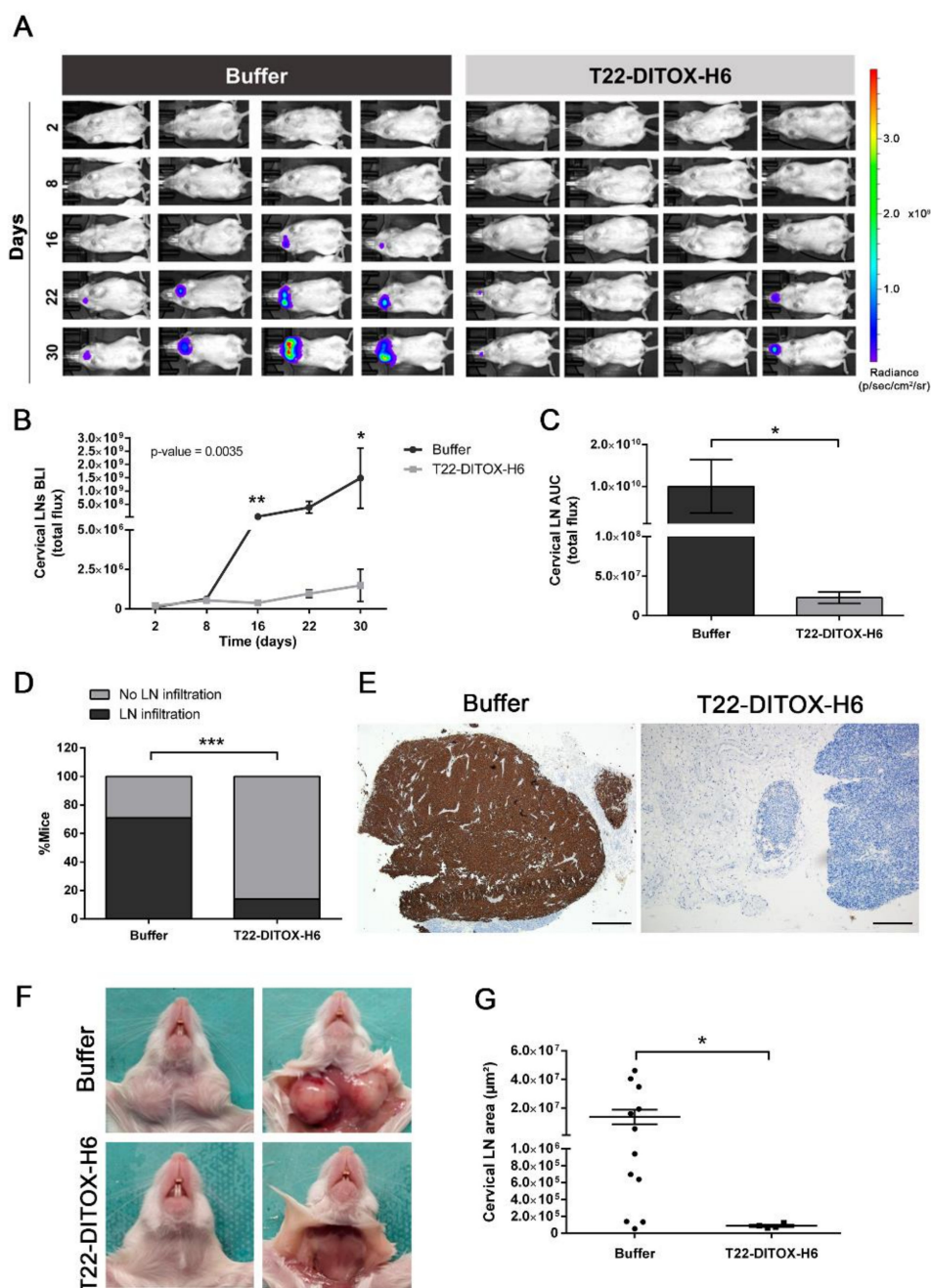


Figure 3. T22-DITOX-H6 repeated administration reduces the occurrence of regional dissemination to the cervical lymph nodes in a HNSCC-disseminated mouse model. (A) Bioluminescence intensity (BLI) emitted by 74B-Luci cancer cells during the experiment in the buffer- and T22-DITOX-H6-treated animals. (B) Semi-quantification of the emitted BLI in the cervical lymph nodes (LNs) throughout the

experiment in the control and treated groups. (C) Area under the curve (AUC) of the registered BLI emitted by cervical lymph nodes (LN) in the time course of the experiment for both control and nanotoxin-treated animals. (D) Percentage of the animals presenting cervical-lymph-node (LN) infiltration at the endpoint of the experiment in the buffer- and T22-DITOX-H6-treated groups. (E) Human vimentin IHC analysis of cervical lymph node samples from control and treated animals at the endpoint of the experiment (day 30 post-tumor-cell inoculation). Scale bars = 500 μ m and 200 μ m. (F) Representative images of the cervical lymph nodes (LN) from a buffer-treated animal (up) and a nanotoxin-treated animal (down) at euthanasia. Animals from the buffer-treated group presented macroscopic infiltrated lymph nodes. (G) Quantification of the area of the cervical lymph nodes observed in the human-vimentin IHC samples collected from buffer- and T22-DITOX-H6 groups. * $p < 0.05$; ** $p < 0.01$; *** $p < 0.001$; $n = 7$ per group (total animal number 14). Statistical analysis was performed by Scheirer–Ray–Hare test, Mann–Whitney test, and Fisher’s test. Error bars indicate SEM.

Furthermore, distant metastatic dissemination to the lungs and liver, two commonly observed metastatic sites in advanced-HNSCC patients, was also assessed at the end of the experiment (Figure 4). Ex vivo evaluation of the bioluminescent signal emitted by the lung (Figure S4C,D) and liver (Figure S4E,F) samples at the endpoint of the experiment showed a reduction in the tumor-cell dissemination upon T22-DITOX-H6 repeated administration. Lung metastatic foci were detected by human-vimentin IHC, as no macroscopic metastases were visible at first sight, neither in the buffer-treated animals, nor in the nanotoxin-treated animals. Human-vimentin immunostaining allowed the precise detection of the lung metastatic foci, which were not only formed by cancer cell clusters, but also by single cells (Figure 4A). Importantly, the repeated dosage of nanotoxin dramatically impaired lung metastatic dissemination, as five animals from the treated group presented no metastatic infiltration while no buffer-treated animals were metastasis-free after the treatment, representing a 70% reduction in the occurrence of lung metastases (100% in the buffer-treated animals, compared to 30% in the nanotoxin-treated group) (Figure 4B). Furthermore, the number of lung metastatic foci, both single-cell and cluster, observed in the animals from the control group was significantly higher than the number detected in the nanotoxin-treated group, further corroborating the antimetastatic effect of the T22-DITOX-H6 treatment (Figure 4C).

Similarly, human-vimentin IHC was also utilized to study the metastatic dissemination to the liver, since no macroscopic metastatic foci could be observed directly (Figure 4D). Remarkably, the T22-DITOX-H6 treatment clearly abrogated liver metastases. First, the percentage of animals displaying liver metastatic foci decreased as a consequence of the nanotoxin treatment, with a 43% reduction in the liver metastasis occurrence (100% metastatic animals in the buffer-treated group, versus 57% in the T22-DITOX-H6-treated group). Thus, three out of seven nanotoxin-treated animals were completely free of liver metastases (Figure 4E). In agreement with this finding, the number of both single and cluster metastatic foci was reduced in the T22-DITOX-H6 group compared to the buffer-treated animals, also implying that the nanotoxin treatment reduced the development of liver metastasis in this model (Figure 4F).

Finally, no systemic toxicity derived from the repeated administration of T22-DITOX-H6 was observed in the animals. The H&E staining of the livers and kidneys (the organs involved in drug metabolism and elimination) after treatment showed no histopathological alterations (Figure 5A). Spleen samples were also studied; since some leukocytes express CXCR4, the spleen constitutes a potential site for on-target toxicity. Importantly, the spleen H&E analysis also showed that the normal architecture of the organ was preserved after nanotoxin treatment (Figure 5A). In addition, no differences in body weight were detected between the control and T22-DITOX-H6-treated animals throughout the experiment, further confirming the lack of off-target toxicity of the treatment (Figure 5B).

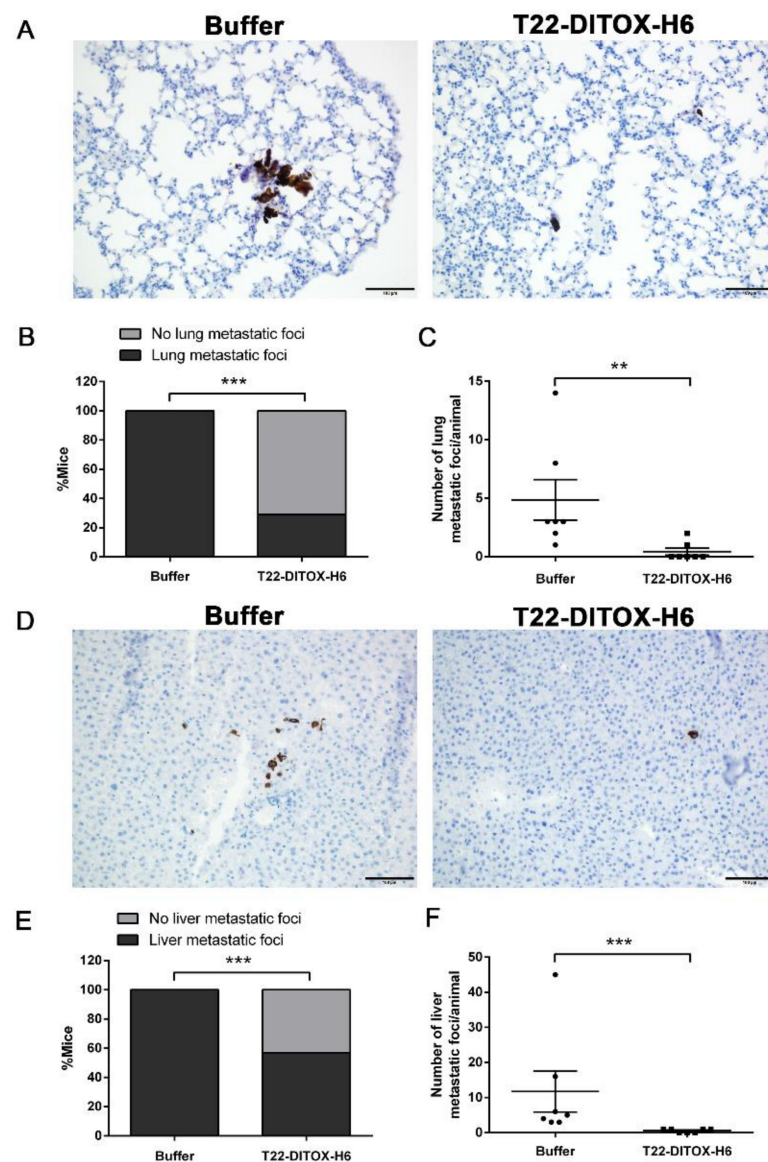


Figure 4. T22-DITOX-H6 repeated administration inhibits distant metastatic dissemination to lungs and liver in a HNSCC-disseminated mouse model. (A) Representative human-vimentin IHC images of lung metastatic foci in samples obtained from buffer- and nanotoxin-treated mice. Scale bars = 100 μ m. (B) Percentage of the animals from control and treated groups displaying lung metastases detected by human-vimentin IHC. (C) Quantification of the number of lung metastatic foci in each animal from the buffer- and T22-DITOX-H6-treated groups. (D) Human-vimentin IHC images showing the metastatic foci in the liver samples collected from control and treated mice. Scale bars = 100 μ m. (E) Percentage of the animals from buffer- and T22-DITOX-H6 groups presenting liver metastases detected by human-vimentin IHC. (F) Quantification of the number of liver metastatic foci in each animal from the buffer- and nanotoxin-treated groups. ** $p < 0.01$; *** $p < 0.001$; $n = 7$ per group (total animal number 14). Statistical analysis was performed by Mann–Whitney test and Fisher’s test. Error bars indicate SEM.

Thus, intravenous T22-DITOX-H6 repeated administration dramatically blocked both regional and distant dissemination of the HNSCC cells in this orthotopic mouse model able to replicate the metastatic pattern observed in HNSCC patients. It is important to mention that no primary tumor shrinkage was observed after the treatment (Figure S5), as has been already mentioned for a previous experiment (Figure S3).

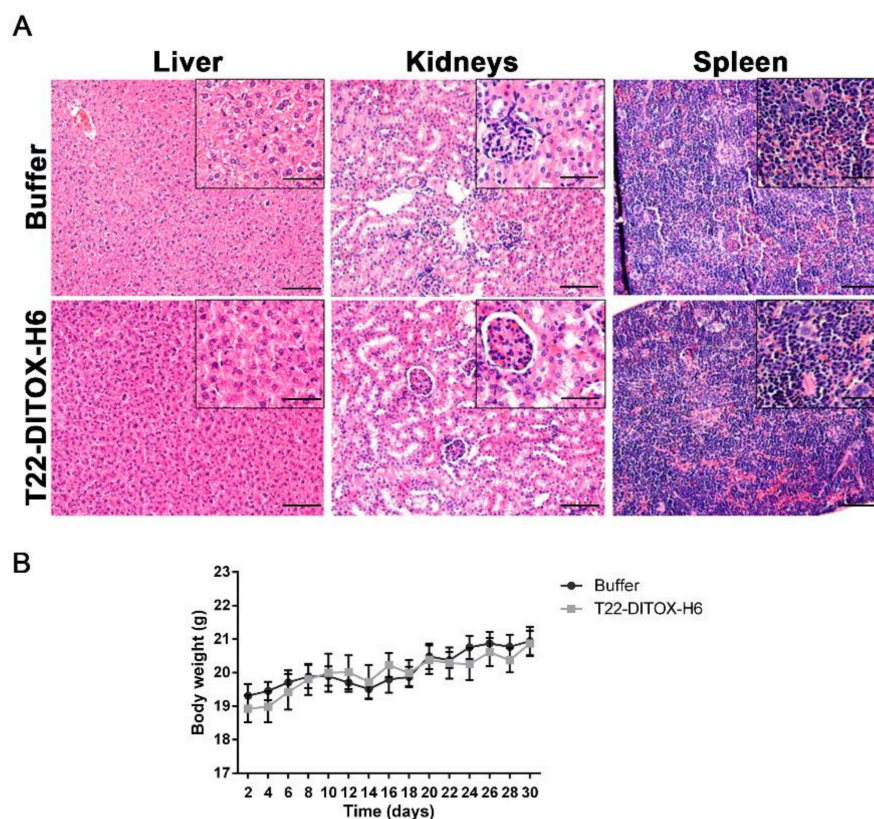


Figure 5. Evaluation of the systemic toxicity derived from T22-DITOX-H6 administration in the HNSCC-disseminated mouse model. (A) Histopathological analysis by H&E staining in liver, kidneys, and spleen samples collected from buffer- and T22-DITOX-H6-treated groups. Scale bars = 100 μ m and 50 μ m (zoom in) (B) Body weights of buffer- and nanotoxin-treated animals over the course of the experiment. Error bars indicate SEM.

4. Discussion

In this work, we showed for the first time that targeted delivery of the diphtheria cytotoxic domain to CXCR4-overexpressing human HNSCC via the T22-DITOX-H6 nanotoxin effectively eliminates the cancer cells present in the invasive front of primary tumors, thus demonstrating a potent anti-invasive effect. In addition, the repeated administration of T22-DITOX-H6 in a HNSCC-disseminated mouse model that replicates the metastatic pattern found in patients achieved a potent antimetastatic effect, which included a dramatic blockage of regional lymph node dissemination and a potent inhibition of distant metastasis to the lungs and liver, without inducing systemic toxicity in the animals. Remarkably, the nanotoxin treatment presented no effect on the primary tumor, suggesting that T22-DITOX-H6 is capable of selectively eliminating the CXCR4-overexpressing cells responsible for the metastatic process. Importantly, metastatic dissemination still represents the main cause of HNSCC patient mortality [23–25], highlighting the necessity for novel therapeutic strategies, such as our targeted drug delivery approach.

Notably, we detected CXCR4⁺ human HNSCC cells in the edges of primary tumors in an orthotopic mouse model. These CXCR4⁺ cancer cells, located in the tumor front, are empowered with a greater invasive and metastatic potential, and have also been described in other cancer types, in which they have been identified as cancer stem cells (CSCs) [26–28]. In this framework, repeated T22-DITOX-H6 administration effectively eliminated the CXCR4⁺ HNSCC cancer cells in the invasive front of the primary tumors. Thus, the selective elimination of these highly metastatic CXCR4⁺ cancer cells would potentially block metastatic dissemination.

Consequently, T22-DITOX-H6 nanotoxin repeated intravenous administration in a HNSCC mouse model induced a potent blockage of tumor metastasis, both regional and distant, in the absence of systemic toxicity. In vivo BLI was utilized to semi-quantitatively evaluate the regional tumor dissemination to the cervical lymph nodes. Although it is an extremely useful technique for preclinical cancer studies, in vivo BLI is limited by spatial resolution and poor signal tissue penetration, which prevented us from detecting in vivo tumor cell infiltration in the organs located deeper in the mouse body, such as lungs and liver [29]. To overcome these limitations, a semi-quantitative ex vivo BLI assessment of the relevant explanted organs was performed at euthanasia, revealing an effect of the nanotoxin treatment in blocking the metastatic dissemination. Moreover, the BLI semi-quantitative measures were further corroborated by the IHC analyses, which showed that, in fact, the nanotoxin-treated animals presented a reduction in both regional and distant tumor metastasis. Importantly, the nanotoxin treatment induced a 57% reduction in the regional dissemination to the cervical lymph nodes, a major metastatic site in HNSCC patients. Over 40% of HNSCC patients present cervical lymph node dissemination at diagnosis, and up to 30% of early-stage patients are still at risk of developing regional metastases during the disease, dramatically affecting their prognosis and survival [30,31]. In addition, nanotoxin treatment also reduced the distant metastatic dissemination to both the lungs and liver, with reductions of 70% and 43%, respectively. Although distant dissemination is not especially frequent at presentation, up to 30% of HNSCC patients develop metastases in the time course of their disease, presenting a very poor prognosis with a median overall survival of less than one year [2,32]. Moreover, the vast majority of recurrent and metastatic HNSCC patients are only candidates for palliative treatment, emphasizing the urgent need for novel curative therapies [32,33]. However, it is important to comment that a percentage of the nanotoxin-treated animals still presented metastases after treatment, suggesting that targeting the CXCL12/CXCR4 axis might not be sufficient to completely ablate metastatic dissemination. These results pave the way for further exploration of the combination of T22-DITOX-H6 treatment with other therapies, such as targeted drugs against TGF- β or FGFR that are also involved in the HNSCC metastatic spread [3–7].

Current HNSCC treatment still mainly relies on conventional chemotherapeutic drugs, as well as molecularly targeted drugs (cetuximab) and immune checkpoint inhibitors (pembrolizumab) [32,33]. Although the incorporation of novel targeted therapies has improved patient survival, the response rates to both cetuximab and pembrolizumab are quite low [34,35]. Chemotherapeutic drugs lack selectivity, thus inducing important off-target toxicities in non-tumor-bearing organs, compromising patients life quality [36,37]. Moreover, therapy resistance, both to chemotherapy and to molecular therapies, is an important drawback of current treatments, preventing complete remission and leading to recurrence [38,39]. In this framework, the T22-DITOX-H6 nanotoxin represents a promising approach for HNSCC treatment, as it aims to deliver cytotoxic compounds exclusively to CXCR4⁺ cancer cells. Our previous work demonstrated the selective accumulation of nanoparticles in CXCR4-overexpressing tumor tissues [21], together with a CXCR4-dependent cytotoxic effect and a potent antitumor effect in vivo [22]. Here, we demonstrate, for the first time, that the T22-DITOX-H6 nanotoxin induces potent anti-invasive and antimetastatic effects in vivo. Other targeted drug delivery strategies have also been explored for HNSCC treatment. Different immunotoxins, such as VB4-845 and SS1P, both including the *Pseudomonas aeruginosa* exotoxin fused to anti-EpCAM or mesothelin targeting moieties, have undergone clinical trials for the treatment of HNSCC. However, none of them has yet reached the market, due to immunogenicity, off-target toxicity concerns, and a lack of antitumor effect due to poor tumor uptake [40,41]. By contrast, our T22-based nanotoxin presents interesting features, including efficient single-step production and purification in recombinant bacteria, easy production scale-up, biocompatibility, and a lack of off-target toxicity [19]. Moreover, while immunotoxins display only one targeting moiety per molecule and a low cytotoxic payload [42,43], this T22-based nanotoxin is produced by the self-assembly of multiple monomers, conferring superselectivity derived from the

display of multiple T22 ligands [44]. However, it is relevant to take into consideration that the antineoplastic effect of T22-DITOX-H6 has only been evaluated in immunodeficient mice displaying a compromised immune system. Since immunogenicity represents a major drawback of immunotoxins, a thorough evaluation of T22-DITOX-H6's effect on the immune system is key to its further clinical translation. In addition, different immune cells, such as lymphocytes, constitutively express CXCR4; they thus represent potential targets for nanotoxin treatment. To assess these questions, our group is currently developing syngeneic mouse models for different cancer types, including HNSCC, to study the effect of nanotoxin treatment on immunocompetent animals. Nonetheless, the potent anti-invasive and anti-metastatic effect demonstrated in the present article clearly supports the relevance of T22-DITOX-H6 as a promising treatment for HNSCC patients. Altogether, T22-DITOX-H6 holds great promise for future clinical translation.

5. Conclusions

In conclusion, CXCR4 expression in the invasive front of HNSCC primary tumors supports the previously reported implication of the receptor in the invasive and metastatic processes. Moreover, CXCR4 overexpression in HNSCC cancer cells compared to healthy tissue makes it an ideal entryway for targeted drug delivery. Thus, T22-DITOX-H6's ability to eliminate CXCR4⁺ cancer cells presenting a more invasive and metastatic phenotype blocks HNSCC's invasiveness and its metastatic dissemination to the cervical lymph nodes, lungs, and liver, in the absence of histopathological alterations. Altogether, the T22-DITOX-H6 nanotoxin represents a promising alternative treatment for HNSCC patients that are still at risk of developing metastatic disease and recurrence, which significantly compromise their clinical outcome and survival.

Supplementary Materials: The following supporting information can be downloaded at: <https://www.mdpi.com/article/10.3390/pharmaceutics14040887/s1>. Figure S1: CXCR4 expression in 74B-Luci primary-tumor samples in the orthotopic mouse model; Figure S2: Schematic representation of the experimental design followed in the studies; Figure S3: Tumor-size assessment in the experiment that evaluated T22-DITOX-H6's anti-invasive effect; Figure S4: Ex vivo bioluminescence evaluation in the metastatic organs; Figure S5: Evaluation of the primary tumor size in buffer- and nanotoxin-treated animals in the experiment that evaluated T22-DITOX-H6's antimetastatic effect.

Author Contributions: Conceptualization, E.V., R.M., L.A.-C. and X.L.; methodology, E.R.-B., I.A.-S., P.Á., U.U., N.S. and L.S.-G.; validation, E.R.-B., I.A.-S., P.Á., U.U., N.S. and L.S.-G.; formal analysis, E.R.-B. and A.G.; investigation, E.R.-B. and A.G.; data curation, E.R.-B. and A.G.; writing—original draft preparation, E.R.-B.; writing—review and editing, I.C., U.U., M.Q., A.V., E.V., X.L., L.A.-C. and R.M.; supervision, E.V., L.A.-C. and R.M.; project administration, L.A.-C. and R.M.; funding acquisition, U.U., M.Q., A.V., E.V., X.L. and R.M. All authors have read and agreed to the published version of the manuscript.

Funding: This research was funded by Instituto de Salud Carlos III (ISCIII, co-funding from FEDER, Spain) (grant numbers PI21/00150, PI21/00232, PI20/00400, PI18/00650, PIE15/00028, PI15/00378, EU COST Action CA 17140, PI19/01661, PI17/00584, and CP19/00028); Agencia Estatal de Investigación (AEI) and Fondo Europeo de Desarrollo Regional (FEDER) (Spain) (grant numbers BIO2016-76063-R and PID2019-105416RB-I00/AEI/10.13039/501100011033); CIBER-BBN (Spain) [grant numbers CB06/01/1031, 4NanoMets, VENOM4CANCER, NANOREMOTE, and NANOSCAPE]; AGAUR co-funded by European Social Fund (ESF: Investing in Your Future) (grant numbers 2017-SGR-865, 2017-SGR-229, 2020FI_B2 00168, and 2018FI_B2_00051); Josep Carreras Leukemia Research Institute (Spain); AECC (Spanish Association of Cancer Research, Spain); Generalitat de Catalunya (Spain) (grant number PERIS SLT006/17/00093). Toxicity was assessed in the ICTS-141007 Nanbiosis Platform, part of the CIBER-BBN Nanotoxicology Unit. Available online: <http://www.nanbiosis.es/portfolio/u18-nanotoxicology-unit/> (accessed on 14 April 2022). Protein production was partially performed by the ICTS "NANBIOSIS", more specifically on the Protein Production Platform of CIBER-BBN/IBB. Available online: <http://www.nanbiosis.es/unit/u1-protein-production-platform-ppp/> (accessed on 14 April 2022).

Institutional Review Board Statement: The animal study protocol was approved by the Ethics Committee of Institut de Recerca Hospital de la Santa Creu i Sant Pau, Barcelona (protocol code 9721, date of approval 20 February 2018).

Informed Consent Statement: Not applicable.

Data Availability Statement: Data is available from the corresponding author upon justified demand.

Conflicts of Interest: Antonio Villaverde, Esther Vázquez, Ugutz Unzueta, Ramon Mangues, and Isolda Casanova are included as authors in the patent PCT/EP2012/050513 related to the targeted delivery of therapeutic molecules to CXCR4 cells, and Antonio Villaverde, Esther Vázquez, Ugutz Unzueta, Ramon Mangues, Isolda Casanova, Naroa Serna, and Laura Sánchez-García are included in PCT/EP2018/061732, covering therapeutic nanostructured proteins. All other authors declare no conflict of interest.

References

1. Sung, H.; Ferlay, J.; Siegel, R.L.; Laversanne, M.; Soerjomataram, I.; Jemal, A.; Bray, F. Global Cancer Statistics 2020: GLOBOCAN Estimates of Incidence and Mortality Worldwide for 36 Cancers in 185 Countries. *CA Cancer J. Clin.* **2021**, *71*, 209–249. [[CrossRef](#)] [[PubMed](#)]
2. Sacco, A.G.; Cohen, E.E. Current Treatment Options for Recurrent or Metastatic Head and Neck Squamous Cell Carcinoma. *J. Clin. Oncol. Off. J. Am. Soc. Clin. Oncol.* **2015**, *33*, 3305–3313. [[CrossRef](#)]
3. Wang, Y.; Wu, C.; Zhang, C.; Li, Z.; Zhu, T.; Chen, J.; Ren, Y.; Wang, X.; Zhang, L.; Zhou, X. TGF- β -Induced STAT3 Overexpression Promotes Human Head and Neck Squamous Cell Carcinoma Invasion and Metastasis through Malat1/MiR-30a Interactions. *Cancer Lett.* **2018**, *436*, 52–62. [[CrossRef](#)] [[PubMed](#)]
4. Pang, X.; Tang, Y.L.; Liang, X.H. Transforming Growth Factor- β Signaling in Head and Neck Squamous Cell Carcinoma: Insights into Cellular Responses. *Oncol. Lett.* **2018**, *16*, 4799–4806. [[CrossRef](#)] [[PubMed](#)]
5. Huang, T.; Huang, W.; Lu, H.; Zhang, B.; Ma, J.; Zhao, D.; Wang, Y.; Yu, D.; He, X. Identification and Validation a TGF- β -Associated Long Non-Coding RNA of Head and Neck Squamous Cell Carcinoma by Bioinformatics Method. *J. Transl. Med.* **2018**, *16*, 46. [[CrossRef](#)] [[PubMed](#)]
6. Ileana Dumbrava, E.; Alfattal, R.; Miller, V.A.; Tsimberidou, A.M. Complete Response to a Fibroblast Growth Factor Receptor Inhibitor in a Patient With Head and Neck Squamous Cell Carcinoma Harboring FGFR Amplifications. *JCO Precis. Oncol.* **2018**, *2*, 1–7. [[CrossRef](#)]
7. Chen, Q.; Chu, L.; Li, X.; Li, H.; Zhang, Y.; Cao, Q.; Zhuang, Q. Investigation of an FGFR-Signaling-Related Prognostic Model and Immune Landscape in Head and Neck Squamous Cell Carcinoma. *Front. Cell Dev. Biol.* **2022**, *9*, 801715. [[CrossRef](#)]
8. Pernas, S.; Martin, M.; Kaufman, P.A.; Gil-Martin, M.; Gomez Pardo, P.; Lopez-Tarruella, S.; Manso, L.; Ciruelos, E.; Perez-Fidalgo, J.A.; Hernando, C.; et al. Balixafortide plus Eribulin in HER2-Negative Metastatic Breast Cancer: A Phase 1, Single-Arm, Dose-Escalation Trial. *Lancet Oncol.* **2018**, *19*, 812–824. [[CrossRef](#)]
9. León, X.; Diez, S.; García, J.; Lop, J.; Sumarroca, A.; Quer, M.; Camacho, M. Expression of the CXCL12/CXCR4 Chemokine Axis Predicts Regional Control in Head and Neck Squamous Cell Carcinoma. *Eur. Arch. Oto-Rhino-Laryngol.* **2016**, *273*, 4525–4533. [[CrossRef](#)]
10. De-Colle, C.; Menegakis, A.; Mönnich, D.; Welz, S.; Boeke, S.; Sipos, B.; Fend, F.; Mauz, P.-S.; Tinhofer, I.; Budach, V.; et al. SDF-1/CXCR4 Expression Is an Independent Negative Prognostic Biomarker in Patients with Head and Neck Cancer after Primary Radiochemotherapy. *Radiother. Oncol. J. Eur. Soc. Ther. Radiol. Oncol.* **2018**, *126*, 125–131. [[CrossRef](#)]
11. Albert, S.; Hourseau, M.; Halimi, C.; Serova, M.; Descatoire, V.; Barry, B.; Couvelard, A.; Riveiro, M.E.; Tijeras-Raballand, A.; De Gramont, A.; et al. Prognostic Value of the Chemokine Receptor CXCR4 and Epithelial-to-Mesenchymal Transition in Patients with Squamous Cell Carcinoma of the Mobile Tongue. *Oral Oncol.* **2012**, *48*, 1263–1271. [[CrossRef](#)] [[PubMed](#)]
12. Luker, G.D.; Yang, J.; Richmond, A.; Scala, S.; Festuccia, C.; Schottelius, M.; Wester, H.J.; Zimmermann, J. At the Bench: Pre-Clinical Evidence for Multiple Functions of CXCR4 in Cancer. *J. Leukoc. Biol.* **2021**, *109*, 969–989. [[CrossRef](#)] [[PubMed](#)]
13. Li, J.; Oupický, D. Effect of Biodegradability on CXCR4 Antagonism, Transfection Efficacy and Antimetastatic Activity of Polymeric Plerixafor. *Biomaterials* **2014**, *35*, 5572–5579. [[CrossRef](#)] [[PubMed](#)]
14. Li, J.; Zhu, Y.; Hazeldine, S.T.; Li, C.; Oupický, D. Dual-Function CXCR4 Antagonist Polyplexes to Deliver Gene Therapy and Inhibit Cancer Cell Invasion. *Angew. Chemie-Int. Ed.* **2012**, *51*, 8740–8743. [[CrossRef](#)]
15. Albert, S.; Riveiro, M.E.; Halimi, C.; Hourseau, M.; Couvelard, A.; Serova, M.; Barry, B.; Raymond, E.; Faivre, S. Focus on the Role of the CXCL12/CXCR4 Chemokine Axis in Head and Neck Squamous Cell Carcinoma. *Head Neck* **2013**, *35*, 1819–1828. [[CrossRef](#)]
16. Domanska, U.M.; Kruizinga, R.C.; Nagengast, W.B.; Timmer-Boscha, H.; Huls, G.; De Vries, E.G.E.; Walenkamp, A.M.E. A Review on CXCR4/CXCL12 Axis in Oncology: No Place to Hide. *Eur. J. Cancer* **2013**, *49*, 219–230. [[CrossRef](#)] [[PubMed](#)]
17. Shi, J.; Kantoff, P.W.; Wooster, R.; Farokhzad, O.C. Cancer Nanomedicine: Progress, Challenges and Opportunities. *Nat. Rev. Cancer* **2017**, *17*, 20–37. [[CrossRef](#)]

18. Mangués, R.; Vázquez, E.; Villaverde, A. Targeting in Cancer Therapies. *Med. Sci.* **2016**, *4*, 6. [[CrossRef](#)]
19. Sánchez-García, L.; Serna, N.; Álamo, P.; Sala, R.; Céspedes, M.V.; Roldan, M.; Sánchez-Chardi, A.; Unzueta, U.; Casanova, I.; Mangués, R.; et al. Self-Assembling Toxin-Based Nanoparticles as Self-Delivered Antitumoral Drugs. *J. Control. Release* **2018**, *274*, 81–92. [[CrossRef](#)]
20. Brenner, J.C.; Graham, M.P.; Kumar, B.; Saunders, L.M.; Kupfer, R.; Lyons, R.H.; Bradford, C.R.; Carey, T.E. Genotyping of 73 UM-SCC Head and Neck Squamous Cell Carcinoma Cell Lines. *Head Neck* **2010**, *32*, 417–426. [[CrossRef](#)]
21. Rioja-Blanco, E.; Arroyo-Solera, I.; Álamo, P.; Casanova, I.; Gallardo, A.; Unzueta, U.; Serna, N.; Sánchez-García, L.; Quer, M.; Villaverde, A.; et al. Self-Assembling Protein Nanocarrier for Selective Delivery of Cytotoxic Polypeptides to CXCR4⁺ Head and Neck Squamous Cell Carcinoma Tumors. *Acta Pharm. Sin. B* **2021**, *12*, 2595–2608. [[CrossRef](#)]
22. Rioja-Blanco, E.; Arroyo-Solera, I.; Álamo, P.; Casanova, I.; Gallardo, A.; Unzueta, U.; Serna, N.; Sánchez-García, L.; Quer, M.; Villaverde, A.; et al. CXCR4-Targeted Nanotoxins Induce GSDME-Dependent Pyroptosis in Head and Neck Squamous Cell Carcinoma. *J. Exp. Clin. Cancer Res.* **2022**, *41*, 49. [[CrossRef](#)] [[PubMed](#)]
23. Pontes, F.; Garcia, A.R.; Domingues, I.; João Sousa, M.; Felix, R.; Amorim, C.; Salgueiro, F.; Mariano, M.; Teixeira, M. Survival Predictors and Outcomes of Patients with Recurrent and/or Metastatic Head and Neck Cancer Treated with Chemotherapy plus Cetuximab as First-Line Therapy: A Real-World Retrospective Study. *Cancer Treat. Res. Commun.* **2021**, *27*, 100375. [[CrossRef](#)] [[PubMed](#)]
24. Beckham, T.H.; Leeman, J.E.; Xie, P.; Li, X.; Goldman, D.A.; Zhang, Z.; Sherman, E.; McBride, S.; Riaz, N.; Lee, N.; et al. Long-Term Survival in Patients with Metastatic Head and Neck Squamous Cell Carcinoma Treated with Metastasis-Directed Therapy. *Br. J. Cancer* **2019**, *121*, 897–903. [[CrossRef](#)] [[PubMed](#)]
25. Bhave, S.L.; Teknos, T.N.; Pan, Q. Molecular Parameters of Head and Neck Cancer Metastasis. *Crit. Rev. Eukaryot. Gene Expr.* **2011**, *21*, 143–153. [[CrossRef](#)] [[PubMed](#)]
26. Hermann, P.C.; Huber, S.L.; Herrler, T.; Aicher, A.; Ellwart, J.W.; Guba, M.; Bruns, C.J.; Heeschen, C. Distinct Populations of Cancer Stem Cells Determine Tumor Growth and Metastatic Activity in Human Pancreatic Cancer. *Cell Stem Cell* **2007**, *1*, 313–323. [[CrossRef](#)] [[PubMed](#)]
27. Cioffi, M.; D’Alterio, C.; Camerlingo, R.; Tirino, V.; Consales, C.; Riccio, A.; Ieranò, C.; Cecere, S.C.; Losito, N.S.; Greggi, S.; et al. Identification of a Distinct Population of CD133⁺CXCR4⁺ Cancer Stem Cells in Ovarian Cancer. *Sci. Rep.* **2015**, *5*, 10357. [[CrossRef](#)]
28. Li, X.; Bu, W.; Meng, L.; Liu, X.; Wang, S.; Jiang, L.; Ren, M.; Fan, Y.; Sun, H. CXCL12/CXCR4 Pathway Orchestrates CSC-like Properties by CAF Recruited Tumor Associated Macrophage in OSCC. *Exp. Cell Res.* **2019**, *378*, 131–138. [[CrossRef](#)]
29. Vandergaast, R.; Khongwichit, S.; Jiang, H.; DeGrado, T.R.; Peng, K.-W.; Smith, D.R.; Russell, S.J.; Suksanpaisan, L. Enhanced Noninvasive Imaging of Oncology Models Using the NIS Reporter Gene and Bioluminescence Imaging. *Cancer Gene Ther.* **2020**, *27*, 179–188. [[CrossRef](#)]
30. Marcu, S.D.E.-L.G. Local Metastasis in Head and Neck Cancer-an Overview. In *Contemporary Issues in Head and Neck Cancer Management*; IntechOpen: London, UK, 2015; p. 6.
31. Sproll, C.; Freund, A.K.; Hassel, A.; Hölbling, M.; Aust, V.; Storb, S.H.; Handschel, J.; Teichmann, C.; Depprich, R.; Behrens, B.; et al. Immunohistochemical Detection of Lymph Node-DTCs in Patients with Node-Negative HNSCC. *Int. J. Cancer* **2017**, *140*, 2112–2124. [[CrossRef](#)]
32. Borcoman, E.; Marret, G.; Le Tourneau, C. Paradigm Change in First-Line Treatment of Recurrent and/or Metastatic Head and Neck Squamous Cell Carcinoma. *Cancers* **2021**, *13*, 2573. [[CrossRef](#)] [[PubMed](#)]
33. Lau, A.; Yang, W.; Li, K.-Y.; Su, Y. Systemic Therapy in Recurrent or Metastatic Head and Neck Squamous Cell Carcinoma-A Systematic Review and Meta-Analysis. *Crit. Rev. Oncol. Hematol.* **2020**, *153*, 102984. [[CrossRef](#)] [[PubMed](#)]
34. Tejani, M.A.; Cohen, R.B.; Mehra, R. The Contribution of Cetuximab in the Treatment of Recurrent and/or Metastatic Head and Neck Cancer. *Biologics* **2010**, *4*, 173–185. [[CrossRef](#)] [[PubMed](#)]
35. Mehra, R.; Seiwert, T.Y.; Gupta, S.; Weiss, J.; Gluck, I.; Eder, J.P.; Burtness, B.; Tahara, M.; Keam, B.; Kang, H.; et al. Efficacy and Safety of Pembrolizumab in Recurrent/Metastatic Head and Neck Squamous Cell Carcinoma: Pooled Analyses after Long-Term Follow-up in KEYNOTE-012. *Br. J. Cancer* **2018**, *119*, 153–159. [[CrossRef](#)]
36. Lin, A.; Giuliano, C.J.; Palladino, A.; John, K.M.; Abramowicz, C.; Yuan, M.L.; Sausville, E.L.; Lukow, D.A.; Liu, L.; Chait, A.R.; et al. Off-Target Toxicity Is a Common Mechanism of Action of Cancer Drugs Undergoing Clinical Trials. *Sci. Transl. Med.* **2019**, *11*, eaaw8412. [[CrossRef](#)]
37. Livshits, Z.; Rao, R.B.; Smith, S.W. An Approach to Chemotherapy-Associated Toxicity. *Emerg. Med. Clin. N. Am.* **2014**, *32*, 167–203. [[CrossRef](#)]
38. Picon, H.; Guddati, A.K. Mechanisms of Resistance in Head and Neck Cancer. *Am. J. Cancer Res.* **2020**, *10*, 2742–2751.
39. López-Verdín, S.; Lavalle-Carrasco, J.; Carreón-Burciaga, R.G.; Serafín-Higuera, N.; Molina-Frechero, N.; González-González, R.; Bologna-Molina, R. Molecular Markers of Anticancer Drug Resistance in Head and Neck Squamous Cell Carcinoma: A Literature Review. *Cancers* **2018**, *10*, 376. [[CrossRef](#)]
40. Wu, T.; Zhu, J. Recent Development and Optimization of Pseudomonas Aeruginosa Exotoxin Immunotoxins in Cancer Therapeutic Applications. *Int. Immunopharmacol.* **2021**, *96*, 107759. [[CrossRef](#)]

41. Havaei, S.M.; Aucoin, M.G.; Jahanian-Najafabadi, A. Pseudomonas Exotoxin-Based Immunotoxins: Over Three Decades of Efforts on Targeting Cancer Cells with the Toxin. *Front. Oncol.* **2021**, *11*, 1–17. [[CrossRef](#)]
42. Vallera, D.A.; Kreitman, R.J. Immunotoxins Targeting B Cell Malignancy-Progress and Problems with Immunogenicity. *Biomedicines* **2018**, *7*, 1. [[CrossRef](#)] [[PubMed](#)]
43. Kim, J.-S.; Jun, S.-Y.; Kim, Y.-S. Critical Issues in the Development of Immunotoxins for Anticancer Therapy. *J. Pharm. Sci.* **2020**, *109*, 104–115. [[CrossRef](#)] [[PubMed](#)]
44. Liu, M.; Apriceno, A.; Sipin, M.; Scarpa, E.; Rodriguez-Arco, L.; Poma, A.; Marchello, G.; Battaglia, G.; Angioletti-Uberti, S. Combinatorial Entropy Behaviour Leads to Range Selective Binding in Ligand-Receptor Interactions. *Nat. Commun.* **2020**, *11*, 4836. [[CrossRef](#)] [[PubMed](#)]

DISCUSSION

1. T22-GFP-H6 nanocarrier achieves a high uptake in CXCR4⁺ HNSCC tumors

Current cancer therapy still comprises conventional small chemotherapeutic drugs that lack selectivity, thus affecting both cancer cells and healthy tissues. Moreover, their low tumor accumulation forces the administration of higher doses leading to important systemic toxicities in non-tumor bearing organs (Taylor et al., 2021; Mittal and Sharma, 2022). Targeted drug delivery selectively to cancer cells represents a major challenge in the development of novel anticancer treatments. In this framework, nanoparticles and nanocarriers aim to enhance tumor drug accumulation while preventing off-target toxic effects. These vehicles increase drug size and stability in circulation, preventing renal clearance and enhancing drug circulation time (Shi et al., 2017; Wei et al., 2021). Besides, thanks to the enhanced permeability and retention (EPR) effect, nanoparticles potentially accumulate in tumor tissues, avoiding non-tumor bearing organs that present a normal endothelial architecture (Matsumura and Maeda, 1986). However, preclinical and clinical data show that in reality less than 0.7% of the administrated nanoparticle dose reaches the tumor (Jain and Stylianopoulos, 2010; Wilhelm et al., 2016). In fact, current nanoparticle approaches present small improvements in terms of tumor accumulation, rendering clinical benefits mainly by diminishing off-target toxicities and enabling the administration of higher doses (Gonzalez-Valdivieso et al., 2021; Tewabe et al., 2021). This lack of tumor uptake might be at least partially explained by the fact that clinical data suggests that the EPR effect is highly heterogeneous in cancer patients (Park, 2013; Danhier, 2016; Sindhvani et al., 2020). Thus, increasing drug tumor accumulation remains a challenge. Active targeting aims at enhancing tumor uptake by directing the drugs to receptors and surface molecules that are overexpressed in tumor tissues. Despite the huge potential of this strategy, no actively-targeted nanoparticle has been commercialized so far, mostly being at preclinical stages (Pearce and O'Reilly, 2019; Manzari et al., 2021). An example of actively-targeted nanoparticle is BIND-014, a polymeric nanoparticle targeting the prostate-specific membrane antigen (PSMA) to deliver docetaxel to tumor cells. BIND-014 entered clinical trials for the treatment of metastatic prostate cancer and advanced head and neck carcinoma among other solid tumors, but it was discontinued after a phase II study due to low efficacy (He et al., 2019).

In this context, the T22-based nanoparticles studied in this project exploit the actively-targeted strategy towards CXCR4-overexpressing cancer cells. The extensive study of the T22-GFP-H6 nanocarrier included in the first chapter showed a CXCR4-dependent internalization *in vitro* in the HNSCC cell lines, demonstrated by two independent techniques (flow cytometry and western blotting). Selective targeted drug delivery is key to prevent any undesired off-target cytotoxic effects in CXCR4 negative cells.

Importantly, we also reported a >75% nanocarrier tumor accumulation, with negligible biodistribution to other non-tumor bearing organs in a CXCR4-overexpressing HNSCC subcutaneous mouse model. This result represents a major improvement compared to the previously reported nanoparticles in the literature (Jain and Stylianopoulos, 2010; Wilhelm et al., 2016). Moreover, tumor accumulation was also CXCR4-dependent, further demonstrating the active targeting towards the receptor. This tumor accumulation was also demonstrated by two independent techniques (fluorescence imaging and immunodetection). Consequently, nanocarrier accumulation in other organs was negligible, resulting in no toxicities in relevant organs such as liver, kidneys, lungs, and spleen, that present lower or none CXCR4 expression compared to the tumors. Importantly, most nanoparticles synthesized so far, especially inorganic ones, accumulate mainly in the liver reducing tumor uptake and leading to life-threatening toxicities (Li et al., 2012; De Matteis, 2017; Sukhanova et al., 2018; Najahi-Missaoui et al., 2021). Thus, T22-GFP-H6 represents a remarkable improvement in terms of selectivity and tumor accumulation, important features for anticancer therapies. Further research will be needed to uncover the mechanisms that govern the exit of the CXCR4-targeted nanoparticles from the blood compartment towards the interstitial tumor space.

2. Advantages of the T22-based protein nanoparticles compared to other nanoparticle approaches

The protein composition of the T22-based nanoparticles, that further determines their physicochemical properties, constitutes an important advantage compared to other nanoparticle strategies. Protein nanoparticles are recombinantly produced in cell factories (bacteria, mammalian cells, etc.) in an economic, environmentally-friendly, and scalable process (Ferrer-Miralles and Villaverde, 2013; Sanchez-Garcia et al., 2016). Besides, their protein composition ensures a good biocompatibility in patients (Lohcharoenkal et al., 2014; Hong et al., 2020), overcoming one of the major problems of many nanoparticles, especially inorganic ones, that are not biodegradable. Moreover, protein nanoparticles still allow surface modifications, such as covalent binding and conjugation of different chemotherapeutic compounds or targeting ligands (Hong et al., 2020). Another important drawback of most nanoparticles, including inorganic nanoparticles and liposomes, is that they present a protein corona in circulation, affecting their biodistribution and targeting capabilities. This protein corona allows the recognition of the nanoparticles by Kupffer cells of the mononuclear phagocytic system (MPS) in the liver sinusoids, leading to their clearance via phagocytosis (Wilhelm et al., 2016; Rampado et al., 2020; Singh et al., 2021). A major advantage of protein nanoparticles is the lack of protein corona in circulation, thus increasing their circulation time by avoiding

liver metabolization while preserving their targeting capacity (De Pinho Favaro et al., 2018). Taking into consideration their advantageous properties, different strategies have been exploited to develop protein nanoparticles. However, the only protein-based nanoparticle available in the market is Abraxane (albumin-bound paclitaxel), devoid of any specific targeting and whose mechanism of drug delivery to the tumors has not been fully elucidated (Yardley, 2013; Chen et al., 2015).

Apart from their protein composition, the T22-based nanoparticles display other interesting features. This targeted drug delivery platform is produced recombinantly in *E. coli*, where the interaction of the polyhistidine tags of different monomers mediated by divalent cations leads to their self-assembly into nanoparticles (López-Laguna et al., 2019, 2020, 2022). In addition, the T22 cationic peptides also contribute to nanoparticle formation (Céspedes et al., 2014). These non-covalent interactions enable the formation of 14 nM nanoparticles in the case of T22-GFP-H6, 60 nm for T22-PE24-H6, and 38 and 90 nm for T22-DITOX-H6 (Céspedes et al., 2014; Sánchez-García et al., 2018a). In all cases, sizes are ideal for targeted drug delivery, being bigger than 7 nm to avoid renal filtration and smaller than 100 nm to prevent macrophage clearance (Pérez-Herrero and Fernández-Medarde, 2015; Serna et al., 2018). Indeed, a previous work has demonstrated that upon intravenous injection in a subcutaneous mouse model, monomers biodistributed mainly to the kidneys, indicating their renal clearance, whereas the self-assembled nanoparticle version did not show renal accumulation (Céspedes et al., 2014). These results highlight the relevance of the self-assembly to increase drug circulation time and avoid renal elimination. In agreement, we have reported an important nanoparticle tumor uptake, with negligible liver and kidney accumulation in a subcutaneous HNSCC mouse model, further supporting the importance of the protein self-assembly into well-organized nanoparticles for an optimal drug delivery. While the H6 tags interact to promote the assembly process, the T22 cationic domains remain free to interact with CXCR4, as we have clearly demonstrated both *in vitro* and *in vivo* in the HNSCC models. In addition, as a consequence of the self-assembly, the T22-based nanoparticles display multiple T22 ligands per nanoparticle, enabling a superselective targeting to CXCR4-overexpressing cancer cells (Martinez-Veracoechea and Frenkel, 2011; Liu et al., 2020).

3. The T22-based nanotoxins display a potent antitumor and antimetastatic effect

The versatility of the T22-based nanoparticles also allows the incorporation of cytotoxic domains to the structure to develop therapeutic nanoparticles. Following this strategy, we have previously developed T22-PE24-H6 and T22-DITOX-H6 nanotoxins, that

incorporate the de-immunized catalytic domain of *Pseudomonas aeruginosa* exotoxin A (PE) and the diphtheria toxin catalytic domain (DITOX), respectively (Sánchez-García et al., 2018a).

Bacterial toxins present a great potential as anticancer agents, displaying a potent cytotoxic effect even at low concentrations (Baindara and Mandal, 2020). However, due to their potent cytotoxic effect, nanotoxins must be coupled to a targeting moiety to reduce their cytotoxicity in healthy tissues. In the last decades, different targeting moieties, mainly monoclonal antibodies (mAbs), have been linked to toxin domains (mainly PE and DITOX) to create immunotoxins (Pastan et al., 2006; Akbari et al., 2017; Li et al., 2017). In 1999, the FDA approved the first immunotoxin for the treatment of cutaneous T-cell lymphoma, Denileukin diftitox (Ontak) (Kadin and Vonderheid, 2010). However, it was withdrawn from the market due to its severe toxic effects. Indeed, off-target toxicities, together with immunogenic reactions, constitute major drawbacks of immunotoxins, importantly compromising their clinical use (Mazor and Pastan, 2020). Early release of the payload in circulation due to unstable linkage of the toxin domain represents one of the reasons behind immunotoxins high toxicity. In contrast, the T22-based nanotoxins incorporate the toxin domains in their protein structure, avoiding conjugation steps and preventing unspecific drug leakage. In addition, immunotoxins utilize truncated bacterial toxin domains with reduced immunogenicity by eliminating their native receptor binding domain and the B and T-cell epitopes to prevent their recognition by the immune system (Kreitman, 2009; Mazor et al., 2018; Mazor and Pastan, 2020). This strategy was also followed when designing the T22-nanotoxins, that only incorporate the catalytic domain of PE. Importantly, PE24 instead of the commonly used PE38 was introduced in the T22-nanotoxin, including different mutations to eliminate several B and T-cell epitopes, and reducing its immunogenicity compared to previous versions (Kaplan et al., 2016). In addition, T22-PE24-H6 nanotoxin incorporates furin cleavage sites between the T22 ligand and the toxin domain to ensure its release exclusively upon internalization in the target cells (Sánchez-García et al., 2018a).

Apart from immunotoxins, antibody drug conjugates (ADCs) constitute one of the most widely used platforms for targeted drug delivery (Khongorzul et al., 2020; Tong et al., 2021). Different ADCs are currently in preclinical and clinical trials for the treatment of HNSCC (Perrotti et al., 2021). However, to date no ADC has been approved for the treatment of HNSCC. Nevertheless, nine ADCs are currently approved as anticancer treatments, and many others are in clinical and preclinical development, highlighting the current interest in targeted drug delivery approaches (Drago et al., 2021). In a similar way to immunotoxins, the drug is chemically coupled to the targeting moiety, thus also

presenting issues regarding premature payload release which leads to off-target toxic effects. Moreover, both systems present a limited effect in solid tumors, mainly because of the poor capacity to penetrate tumor tissues (Tolcher, 2016; Nejadmoghaddam et al., 2019). In fact, it is estimated that <1% of the ADC administered dose reaches the tumor (Beck et al., 2017; Nagayama et al., 2017; Joubert et al., 2020). Interestingly, almost all the ADCs currently in the market are for the treatment of hematological malignancies, which might be explained by their poor tumor accumulation in solid tumors. In addition, both ADCs and immunotoxins present only two binding epitopes for targeting and also a limited payload capacity. In contrast, T22-based nanoparticles are produced by self-assembly of multiple monomers, thus displaying multiple binding and cytotoxic domains per nanoparticle. This fact might contribute to the high CXCR4-dependent tumor accumulation found in our HNSCC subcutaneous mouse model. Likewise, T22-PE24-H6 and T22-DITOX-H6 also present a CXCR4-dependent cytotoxic effect, ensuring a selective elimination of the CXCR4-overexpressing tumor cells. Most importantly, similarly to T22-GFP-H6, this selectivity is also translated *in vivo*, with an important antitumor effect exclusively in CXCR4⁺ HNSCC primary tumors. Moreover, no cytotoxic effect in CXCR4 negative cells was detected once the nanotoxins exerted their cytotoxic effect, ensuring no off-target cytotoxicity. In addition, both nanotoxins also displayed a potent antitumor effect upon repeated administration in a subcutaneous CXCR4-overexpressing HNSCC mouse model, in the absence of systemic toxicity.

Nanotoxins lack of systemic toxicity was further evaluated in the CXCR4⁺ subcutaneous mouse model. In addition to the observation of a normal architecture in liver and kidneys after treatment, we also performed a biochemical analysis in plasma samples. Normal transaminases activity and creatinine and uric acid levels were detected, further corroborating the lack of liver and renal toxicity after nanotoxin treatment. Moreover, nanotoxin treatment did not induce any long term systemic toxic effects in healthy animals, neither in terms of liver and renal toxicity nor in the different cell blood populations. Indeed, the number of leukocytes (eosinophils, basophils, monocyte, and lymphocytes) right after the 8th dose treatment and 4 weeks after was between the normal range for a healthy animal. Importantly, some leukocytes constitutively express CXCR4, thus representing a potential target for the T22-based nanotoxins. In addition, other CXCR4-expressing tissues such as the spleen and bone marrow also preserved their normal architecture, further corroborating the lack of on-target toxicity of T22-PE24-H6 and T22-DITOX-H6.

Last but not least, T22-DITOX-H6 repeated administration effectively eliminated the invading CXCR4⁺ cancer cells present in the primary tumor front. Consequently,

nanotoxin repeated administration was capable of blocking regional metastatic dissemination to cervical lymph nodes, as well as distant dissemination to both lungs and liver, in the absence of systemic toxicity in an orthotopic mouse model that replicates the metastatic pattern found in HNSCC patients. These results suggest that, at least in this HNSCC mouse model, the CXCR4/CXCL12 axis represents the main signaling pathway involved in the metastatic dissemination.

4. T22-nanotoxins induce a novel mechanism of cell death alternative to apoptosis

In terms of mechanism of action, both T22-PE24-H6 and T22-DITOX-H6 nanotoxins internalize in the target cells by endocytosis and ultimately inactivate the ribosomal EF-2, leading to protein synthesis inhibition and cell death (Alewine et al., 2015; Sánchez-García et al., 2018b). This mechanism of action confers them the capability of eliminating both proliferative and quiescent cells, representing an important advantage compared to conventional chemotherapeutic drugs (Alewine et al., 2015). Remarkably, we have described for the first time that both nanotoxins induce cell death via caspase-3/GSDME dependent pyroptosis. This activation has been thoroughly demonstrated in chapter 2 in two different CXCR4⁺ HNCSS cell lines. First, upon nanotoxin exposure, CXCR4⁺ HNCSS cells presented a pyroptotic-like morphology, displaying cell swelling. In addition, a lytic form of cell death was confirmed by two independent techniques, Annexin V-PI flow cytometry assay and LDH release assay. Lastly, we confirmed the activation of the caspase-3/GSDME pyroptotic pathway by western blotting. All these results were corroborated by zVAD pretreatment, that effectively blocked pyroptotic activation further demonstrating that the mechanism of cell death triggered by both nanotoxins was caspase-dependent, most likely through activation of the caspase-3/GSDME pathway. Recent studies have shown that pyroptosis activation presents an antitumor effect (Wang et al., 2019; Xia et al., 2019). Since the evasion of apoptosis constitutes one of the mechanisms by which cancer cells develop therapy resistance, the induction of alternative types of cell death represents a promising avenue of research in therapy development (Igney and Krammer, 2002; Wu et al., 2021). Moreover, as a pro-inflammatory type of cell death, the activation of pyroptosis induces immune cell recruitment to the tumor site, potentially enhancing the therapeutic effect (Zhang et al., 2020; Raudenská et al., 2021; Yu et al., 2021). In this regard, a recent study has shown that GSDME presents a tumor suppressive role by recruiting tumor-associated macrophages (TAMs) to the tumor site (Zhang et al., 2020). Similarly, upon nanotoxin repeated administration in a CXCR4⁺ subcutaneous HNSCC mouse model, we detected an increase in the number of TAMs infiltrating the nanotoxin-treated tumors. This observation further supports the activation of pyroptosis upon nanotoxin treatment,

presenting a potent antitumor effect, especially for T22-DITOX-H6 that practically inhibited tumor growth. Consequently, TAMs infiltration might have contributed to T22-PE24-H6 and T22-DITOX-H6 antitumor effect.

However, the activation of GSDME in healthy tissues, such as the gastrointestinal tract, has been associated with severe chemotherapy off-target toxicities (Wang et al., 2017). Thus, targeted drug delivery is pivotal to avoid the activation of GSDME-dependent pyroptosis in non-tumor bearing organs. In this context, the T22-based nanotoxins ensure the activation of pyroptosis exclusively in the CXCR4⁺ cancer cells, avoiding systemic toxicities. In addition, to evaluate the clinical relevance of GSDME activation in HNSCC tumor, we performed an analysis of the GSDME expression in a HNSCC TCGA dataset, showing that GSDME was overexpressed in tumor samples compared to the healthy tissue. More in depth, we also studied GSDME expression by IHC in a small HNSCC patient cohort. In agreement, the vast majority of the CXCR4⁺ tumor samples expressed GSDME, supporting the potential therapeutic benefit of activating this cell death pathway in HNSCC. Remarkably, our results contradict the current hypothesis that GSDME is silenced in cancer cells as a mechanism to evade cell death (Wang et al., 2017). Thus, the activation of GSDME-dependent pyroptosis in HNSCC tumors represents a promising avenue of research for future treatments.

5. Targeting the CXCR4/CXL12 axis in HNSCC

Altogether, these results indicate that CXCR4 represents an ideal target for HNSCC therapies. CXCR4 is overexpressed in tumors compared to the healthy tissue in many different cancer types, including HNSCC (Zhao et al., 2015). In this regard, we performed an analysis using a TCGA dataset to compare CXCR4 in normal versus HNSCC cancer tissues, showing an overexpression of the receptor in tumors. This fact highlights the relevance of CXCR4 as a good entryway for targeted drug delivery. In addition, in previous work we have described a correlation between CXCR4 tumor expression in HNSCC patients and a higher risk of developing loco-regional recurrence (León et al., 2016). Moreover, many studies have also shown a correlation between CXCR4 overexpression and lymph node dissemination, metastasis, and poor survival in HNSCC (Albert et al., 2013; De-Colle et al., 2018). CXCR4 overexpression has also been related to enhance invasion, migration, stemness, and metastatic potential, not only in HNSCC, but also in other cancer types (Kucia et al., 2005; Costea et al., 2006; Gelmini et al., 2008; Faber et al., 2013b). Despite the relevance of CXCR4, only the small CXCR4 antagonist plerixafor (AMD3100) is currently in the market for hematopoietic stem cell (HSC) mobilization. However, plerixafor is not used in the clinic for the treatment of solid

tumors and presents side effects regarding the normal hematopoietic balance after its long-term administration (Liu et al., 2016).

Besides the small inhibitor plerixafor, other CXCR4-targeted therapies are undergoing preclinical and clinical studies, mainly in combination with conventional chemotherapy (Pernas et al., 2018; Luker et al., 2021). Remarkably, the T22-nanotoxins go a step further, aiming to selectively deplete the CXCR4⁺ cancer cells with enhanced metastatic potential. Interestingly, we report that two HNSCC tumor derived xenografts that presented a strong CXCR4 expression, lost the expression of the receptor upon epithelial cell isolation and *in vitro* culture. However, when re-inoculated in immunocompromised mice, the generated tumors expressed again CXCR4. This result suggests a complex regulation of the receptor that has not been fully elucidated and might explain that the HNSCC cell lines cultured *in vitro* were all CXCR4 negative. Although the CXCR4 negative cell lines used in this work do not re-express CXCR4 in the tumor bulk when injected either subcutaneously or orthotopically, we have identified CXCR4⁺ cancer cells in the primary tumor invasive front in an orthotopic HNSCC mouse model, suggesting that CXCR4 is involved in the enhanced migration and metastatic potential of these cancer cells. Importantly, recurrence and metastasis represent the leading causes of mortality in HNSCC patients (Sacco and Cohen, 2015). Despite the therapeutic improvement, including molecularly targeted drugs (cetuximab) and immune-checkpoint inhibitors (pembrolizumab), recurrent and/or metastatic patients are mainly candidates for palliative treatment, with a median OS of less than one year (Sacco and Cohen, 2015; Borcoman et al., 2021). These facts highlight the relevance of novel therapeutic alternatives capable of preventing metastatic dissemination, such as T22-DITOX-H6.

6. Clinical translation of the T22-nanotoxins and future perspectives

In the present thesis, we carried out a preclinical study of the T22-GFP-H6 nanocarrier and the T22-PE24-H6 and T22-DITOX-H6 nanotoxins both *in vitro* and *in vivo* in different HNSCC mouse models. The studied T22-based nanoparticles hold a plethora of promising characteristics for their future clinical use as anticancer agents. Nonetheless, it is important to consider that only immunocompromised mice were utilized in this study. Thus, a more in-depth analysis of the response of the immune system upon nanoparticle administration in immunocompetent models is crucial for their translation towards the clinic. In this regard, ongoing projects in the lab aim to develop syngenic mouse models, mainly for colorectal cancer but also for HNSCC, to test the T22-based nanoparticles and investigate their potential immunogenicity. So far, preliminary results showed that both nanotoxins can be safely inoculated in both BALB/c and C57BL/6. Further studies

are needed to study the immune reaction and the maximum tolerated dose that could be administered to these animals. In addition, syngenic mouse models will also help to further study the activation of pyroptosis *in vivo* and the immune cell recruitment to the tumor site.

Regarding nanoparticle production and characterization, different versions of the T22-based nanoparticles including human scaffold proteins have been produced to prevent immunogenic reactions and ensure a better clinical translation of the nanoparticles. In addition, several nanoconjugates have been also developed including different chemotherapeutic drugs, such as floxuridine (FdU) and monomethyl auristatin E (MMAE), bound to the T22-nanoparticle, presenting improved linkers to ensure a stable conjugation and prevent unspecific drug leakage. Moreover, a better understanding of the T22-nanoparticles structure and the self-assembly process is key to design more tailored nanoparticles following the H6-divalent cations oligomerization approach. In this regard, Prof. Villaverde's group is currently working on elucidating the structure of the T22-GFP-H6 nanoparticle by cryo-electron microscopy (cryo-EM), that will help to unravel the interaction between polyhistidine tails to form the nanoparticles.

Lastly, a more in-depth study of the role of CXCR4 in the metastatic development in HNSCC would be beneficial for the development of improved therapies. In this context, obtaining a 74B CXCR4 knock-out (KO) cell line and generating an orthotopic mouse model will help to understand the involvement of the receptor in invasion and metastasis. In addition, the development of patient-derived tumor xenografts (PDXs) from the CXCR4⁺ HNSCC patient samples in humanized mouse models will also help to further elucidate the role of the receptor in the tumorigenic and metastatic process. Moreover, these models will also be helpful to test the T22-based nanoparticles directly in patient samples, rendering a more clinical translation approach.

CONCLUSIONS

Chapter 1: Self-assembling protein nanocarrier for the selective delivery of cytotoxic polypeptides to CXCR4⁺ head and neck squamous cell carcinoma tumors

- T22-GFP-H6 displays a CXCR4-dependent internalization *in vitro* in CXCR4⁺ HNSCC cell lines.
- T22-GFP-H6 mainly accumulates in tumor tissues in a CXCR4-overexpressing HNSCC subcutaneous mouse model, with negligible biodistribution to non-tumor bearing organs. Importantly, the nanocarrier tumor accumulation is also mediated by CXCR4.
- The incorporation of cytotoxic domains to the nanoparticle to generate immunotoxins (T22-PE24-H6 and T22-DITOX-H6) confers them cytotoxicity towards the CXCR4⁺ HNSCC cell lines *in vitro*.
- T22-PE24-H6 and T22-DITOX-H6 administration in an orthotopic HNSCC mouse model shows a potent CXCR4-dependent antitumor effect in the absence of systemic toxicity.

Chapter 2: CXCR4-targeted nanotoxins induce GSDME-dependent pyroptosis in head and neck squamous cell carcinoma

- T22-PE24-H6 and T22-DITOX-H6 present a potent CXCR4-dependent cytotoxic effect in the CXCR4⁺ HNSCC cell lines.
- Both nanotoxins activate caspase-3/GSDME-dependent pyroptosis in the CXCR4⁺ HNSCC cell lines.
- T22-PE24-H6 and T22-DITOX-H6 nanotoxins display a potent antitumor effect in a CXCR4-overexpressing HNSCC subcutaneous mouse model in the absence of toxic effects in non-tumor bearing organs.
- Nanotoxin treatment enhances macrophage recruitment to the tumor site further supporting the activation of pyroptosis *in vivo*.
- GSDME is largely expressed in CXCR4⁺ HNSCC patient tumor samples indicating the relevance of the GSDME-mediated pyroptosis activation in therapeutic development.

Chapter 3: A novel CXCR4-targeted diphtheria toxin nanoparticle inhibits invasion and metastatic dissemination in a head and neck squamous cell carcinoma mouse model

- CXCR4⁺ tumor cells are enriched in the tumor invasive front in an orthotopic HNSCC mouse model.

CONCLUSIONS

- T22-DITOX-H6 repeated administration effectively eliminates the CXCR4-overexpressing cells present in the tumor budding.
- Successive T22-DITOX-H6 administration in an orthotopic HNSCC mouse model that replicates the metastatic pattern found in patients induces a potent blockage of both regional dissemination to the cervical lymph nodes and distant metastasis in the lungs and liver, without inducing toxic effects in healthy tissues.

LIST OF PUBLICATIONS

The following published research articles were included in the present thesis:

- 1- **Rioja-Blanco E**, Arroyo-Solera I, Álamo P, Casanova I, Gallardo A, Unzueta U, Serna N, Sánchez-García L, Quer M, Villaverde A, Vázquez E*, Mangues R*, Alba-Castellón L*, León X. Self-assembling protein nanocarrier for selective delivery of cytotoxic polypeptides to CXCR4+ head and neck squamous cell carcinoma tumors. *Acta Pharmaceutica Sinica B*. 2021. DOI: 10.1016/j.apsb.2021.09.030.
- 2- **Rioja-Blanco E**, Arroyo-Solera I, Álamo P, Casanova I, Gallardo A, Unzueta U, Serna N, Sánchez-García L, Quer M, Villaverde A, Vázquez E*, León X, Alba-Castellón L*, Mangues R*. CXCR4-targeted nanotoxins induce GSDME-dependent pyroptosis in head and neck squamous cell carcinoma. *J Exp Clin Cancer Res*. 2022 Feb 4;41(1):49. DOI: 10.1186/s13046-022-02267-8.
- 3- **Rioja-Blanco E**, Gallardo A, Arroyo-Solera I, Álamo P, Casanova I, Unzueta U, Serna N, Sánchez-García L, Quer M, Villaverde A, Vázquez E*, León X, Alba-Castellón L*, Mangues R*. A Novel CXCR4-Targeted Diphtheria Toxin Nanoparticle Inhibits Invasion and Metastatic Dissemination in a Head and Neck Squamous Cell Carcinoma Mouse Model. *Pharmaceutics*. 2022 Apr 18;14(4):887. DOI: 10.3390/pharmaceutics14040887.

Other co-authored articles not included in this thesis:

- 4- Sala R, **Rioja-Blanco E**, Serna N, Sánchez-García L, Álamo P, Alba-Castellón L, Casanova I, López-Pousa A, Unzueta U, Céspedes MV, Vázquez E*, Villaverde A, Mangues R*. GSDMD-dependent pyroptotic induction by a multivalent CXCR4-targeted nanotoxin blocks colorectal cancer metastases. *Drug Delivery*. 2022. DOI: 10.1080/10717544.2022.2069302.

ANNEX: SUPPLEMENTARY INFORMATION

CHAPTER 1

Self-assembling protein nanocarrier for selective delivery of cytotoxic polypeptides to CXCR4⁺ head and neck squamous cell carcinoma tumors

Elisa Rioja-Blanco, Irene Arroyo-Solera, Patricia Álamo, Isolda Casanova, Alberto Gallardo, Ugutz Unzueta, Naroa Serna, Laura Sánchez-García, Miquel Quer, Antonio Villaverde, Esther Vázquez*, Ramon Mangués*, Lorena Alba-Castellón*, Xavier León

*co-corresponding authors

Acta Pharmaceutica Sinica B

2021

Supporting Information for

ORIGINAL ARTICLE

Self-assembling protein nanocarrier for selective delivery of cytotoxic polypeptides to CXCR4⁺ head and neck squamous cell carcinoma tumors

Elisa Rioja-Blanco^{a,b}, Irene Arroyo-Solera^{a,b,c}, Patricia Álamo^{a,b,c}, Isolda Casanova^{a,b,c}, Alberto Gallardo^{a,d}, Ugutz Unzueta^{a,b,c}, Naroa Serna^{c,e,f}, Laura Sánchez-García^{c,e,f}, Miquel Quer^{c,g}, Antonio Villaverde^{c,e,f}, Esther Vázquez^{c,e,f,*}, Ramon Mangués^{a,b,c,*}, Lorena Alba-Castellón^{a,b,*}, Xavier León^{c,g}

^a*Institut d'Investigació Biomèdica Sant Pau (IIB-Sant Pau), Barcelona 08041, Spain*

^b*Institut de Recerca contra la Leucèmia Josep Carreras, Barcelona 08025, Spain*

^c*CIBER de Bioingeniería, Biomateriales y Nanomedicina (CIBER-BBN), Madrid 28029, Spain*

^d*Department of Pathology, Hospital de la Santa Creu i Sant Pau, Barcelona 08041, Spain*

^e*Institut de Biotecnologia i de Biomedicina, Universitat Autònoma de Barcelona, Bellaterra 08193, Spain*

^f*Departament de Genètica i de Microbiologia, Universitat Autònoma de Barcelona, Bellaterra 08193, Spain*

^g*Department of Otorhinolaryngology, Hospital de la Santa Creu i Sant Pau, Barcelona 08041, Spain*

Received 5 July 2021; received in revised form 3 September 2021; accepted 15 September 2021

*Corresponding authors. Tel.: +34 935537919 (Ramon Mangués); +34 935537921 (Lorena Alba-Castellón).

E-mail addresses: esther.vazquez@uab.cat (Esther Vázquez), rmangues@santpau.cat (Ramon Mangues), lalba@santpau.cat (Lorena Alba-Castellón).

T22-GFP-H6:

NdeI - (CATATG)CGTCTGTTGGTGTATCGTAAATGCTATAAAGGCTATTGCTATCGTAA-
ATGTCGTGGTGGTAGCAGCCGTAGCAGCAGCAAAGGTGAAGAAGTGTACCGGTGTTGTTCCGATTCTGGTTGAACTGGATGGT
GATGTTAATGGCCATAAATTTTCAGTTAGCGGTGAAGGTGAAGGTGATGCAACCTATGGTAACTGACCTGAAATTTATTGCACC
ACCGGTAACTGCCGGTCCGTTCCGTGGCCGACCCCTGGTTACCACCTGACCTATGGTGTTCAGTGTTCAGTGTTCAGCCGTTATCCGGATCACAT
GAAACGCCATGATTTTTTAAAAGCGCAATGCCGGAAGGTTATGTTTCAGGAACGTACCATTAGCTTTAAAGATGATGGCAATTACAA
AACCCGTGCCGAAGTAAATTTGAAGGTGATACCCTGGTGAATCGCATTGAACTGAAAGGCATTGATTTAAAGAAGATGGTAATAT
TCTGGCCATAAAGTGAATATACTATAATAGCCATAATGTATATCACCGCAGATAAACAGAAAAATGGCATTAAAGCCAACCTTTA
AAATTCGCCATAATATGAAGATGGCAGCGTTCAGCTGGCAGATCATTATCAGCAGAATACCCCGATTGGTGTGGTCCGGTTCG
CTGCCGATAATCATTATCTGAGCACCCAGAGCGCACTGAGCAAAGATCCGAATGAAACCGTATCACATGGTCTGCTGGAATT
GTTACCGCAGCAGGTATTACCCATGGTATGGATGAACTGTATAAACATCATCATACCATCATTAA(AAGCTT)-HindIII

MRRWCYRKCYKGYCYRKCRGGSSRSSKGEELFTGVVPIVVELDGDVNGHKFSVSGEGEG-
DATYGLKTLKFICTTKGLPVPWPTLVTTLYGVQCFSRYPDHMKRHDFFKSAMPEGYVQERTISFKDDGNYKTRAEVKFEGDNLVNRIE
LKGDIFKEDGNILGHKLEYNYNHNVYITADKQKNGIKANFKIRHNIEDGSVQLADHYQQNPTIGDGPVLLPDNHVYSTQSALSKDPNEK
RDHMVLEFVTAAGITHGMEDELYKHHHHHH

T22-PE24-H6:

NdeI - (CATATG)CGTCTGTTGGTGTATCGCAAATGCTATAAAGGTTATTGCTACCGTAA-
ATGTCGTGGTGGTAGCAGCCGTAGCAGTCATCGTACGCTCGTGGTGGGAACAGCTGGGTGGTAGCCCGACCGGTGCAG
AATTTCTGGGTGATGGTGGTGTAGCTTTAGCACCCGTGGCACCCAGAATTTGACCGTTGAACTGCTGCTGCAGGCACATGC
ACAGCTGGAAGAAGCTGGTATGTTTTGTTGGTTATCATGGCACCTTCTGGAAGCAGCACAGAGCATTGTTTTGGTGGTGGTGG
CAGCAGTAGCCAGGATCTGGCAGCAATTTGGCAGGTTTCTATATTGCCGGTATCGGGCACTGGCCTATGGTATGCACAGGA
TCAAGAACCAGGATGCAGCAGGTCGTTATCGTAAATGGTGCAGTCTGCGTGTATTATGTTCCGGCAAGCAGCCCTGCCTGGTTTTATC
GTACCAGCCTGACCCTGGCAGCACCCGGAAGCAGCCGGTGAAGTGGAAACGTCTGATTGGTTCATCCGCTGCCCTGGCAGTGGAT
GCAATTACCGTCCGGAAGAAGAGCCGGTCTGTTGAAACCAATTCGGGTTGGCCTCTGGCAGAACGTCACCGTTGTTATCCGA
GCGCAATTCGACCGATCCGCGTAAATGTGGGTGGTGTATCGGATCCGAGCAGCATTCCGGATAAAGAACAGGCAATTAGCGCACT
GCCGGATTATGCAAGCCAGCCTGTAACCCGCTCGTGAAGATCTGAAACATCATCATACCATCATAAAGACGAGCTGAA(AAG
CTT) - HindIII

MRRWCYRKCYKGYCYRKCRGGSSRSRHRQPRGWEQLGGSPTGAEFLGDGGDVSFSTRGT-
QNWTVRLLQAHAQLEERGVVFGYHGTFLAAQSVIFGVVAARSQDLAAIWAGFYIAGDPALAYGYAQDQEPDAAGRIRNGALLRVY
VPASSLPGFYRSLTAAPEAAAGEVERLIGHPLPLALDAITGPEEEGGRLTILGWPLAERTVVIPSAIPTDPRNVGGDLDPSSIPDKEQAI
SALPDYASQPGKPPREDLKHHHHHHKDEL

T22-DITOX-H6:

NdeI - (CATATG)GGTGCAGATGATGTTGTTGATAGCAGCAAAGTTCCTGATGGAACCTTCAG-
CAGCTATCATGGCACCACCCGGTATGTTGGATAGCATTACGAAAGGTATTACGAAACCGGAAAGCGGCACCCAGGGTAATTATG
ATGATGATTGAAAGGCTTCTATAGCACCGATAACAAATATGATGCAGCCGTTATAGCGTGGATAATGAAATCCGCTGAGCGGTA
AAGCCGGTGGTGTGTTGTTAAAGTTACCTATCCGGGTCTGACCAAAGTCTGGCACTGAAAGTTGATAATGCCGAAACCATCAAAAA
GAACTGGGTCTGAGCCTGACCGAACCGCTGATGGAACAGGTTGGCACCAGAAATTTATCAACGTTTTGGTGTGGTGCAGGCC
GTGTTGTGCTGAGCCTGCCGTTTGCAGAAGGTAGCAGCAGCGTTGAATATATCAATAATGGGAACAGGCAAAAGCCCTGAGCGT
TGAACGGAAATCAATTTGAAACCCGTGTTAAACGTGGTCAAGATGCAATGATGAATACATGGCACAGGCATGTGAGGTAATC
GTGTTCTGCTAGCGTTGGTAGCAGCCTGAGCTGATTAATCTGATTGGGATGTGATTCCGACAAAAACCAAAACGAAAAATCGAA
AGCCTGAAAGAACATGGTCCGATCAAAAAACAAATGAGCGAAAGCCGAAATAAACCCGTGAGCGAAGAAAAAGCAAAACAGTATC
TGGAAAGATTTACCAGACCCGACTGGAACATCCGGAACCTGAGCGAACTGAAACCCGTTACCGGCACCAATCCGGTTTTTCCCG
GTGCAAAATATGCAGCATGGCAGTTAATGTTGCACAGGTTATGATAGCGAAACCCGAGATAATCTGAAAAAACCCAGCAGCA
CTGAGCATTCTGCTGGTATTGGTAGCGTTATGGGTATTGCAGATGGTGCAGTGCATCATAATACCGAAGAAATGTTGCCAGAG
CATTGCCCTGAGCAGTCTGATGGTTCGCCAGGCAATTCGCTGGTGGTGAACCTGGTGTGATATTGGTTTTGCAGCCTATAACTTTG
TCGAGAGCATCATTAACTGTTTCAGGTTGTCATAATAGCTATAATCGTCCGGCATATAGTCCGGGTATAAAACCCATCATACCA
CCATCATTAA(AAGCTT)-HindIII

MGADDVVDSSKSFVMENFSSYHGTKPGYVDSIQKGIQPKSGTQGNVDDDWKGFYSTDNKY-
DAAGYSVDNENPLSGKAGGVVKTYPGLTKVLKVDNAETIKKELGLSLTEPLMEQVGTTEFIKRFQDASRVVLSLPAEAGSSSVEYI
NNWEQAKALSVELEINFETRGRKRGQDAMYEQMAQACAGNRVRSVSSLSCLINLDWDVIRDKTKIESLKEHGIPIKNMSEPNKTV
SEEKAKQYLEEFHQTALEHPSELKLVTVGTNPVAFAGANYAAWAVNVAQVIDSETADNLEKTTAALSILPGIGSVMGADGAVHHNTEIV
AQSIALSSLMVAQIPLVGLVDIGFAAYNFVESIINLFQVVHNSYNRPAYSPGHKTHHHHHH

Figure S1 Protein coding sequences of T22-GFP-H6, T22-PE24-H6, and T22-DITOX-H6 included in the plasmids. All three proteins were cloned in the plasmid pET22b (Novagen 69744-3) and recombinantly produced in *E. coli*.

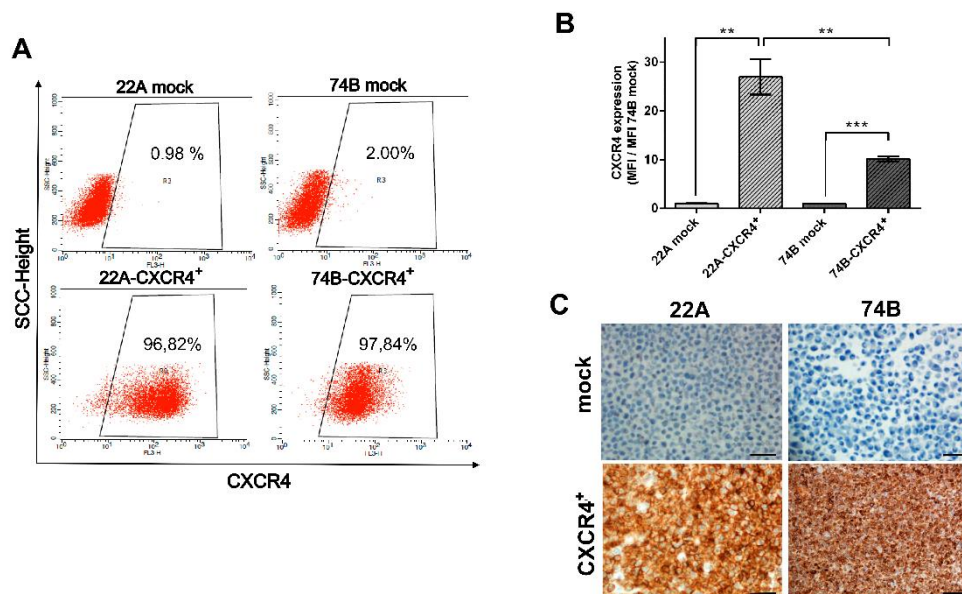


Figure S2 CXCR4 membrane expression in the different HNSCC cell lines. A) Flow cytometry populations of the 22A mock, 22A-CXCR4⁺, 74B mock, and 74B-CXCR4⁺ cell lines showing their different percentages of CXCR4 membrane expression. B) Quantification of the relative mean fluorescence intensity (MFI) values obtained by flow cytometry for the previously mentioned HNSCC cell lines. C) Immunocytochemical analysis of the levels of expression of the CXCR4 receptor in the 22A mock, 22A-CXCR4⁺, 74B mock, and 74B-CXCR4⁺ HNSCC cell lines. Scale bars = 50 or 100 μm (74B-CXCR4⁺). Data represented as mean \pm Standard error. All experiments were performed in triplicate. ** $P < 0.01$; *** $P < 0.001$. Statistical analysis performed by Student's *t*-test.

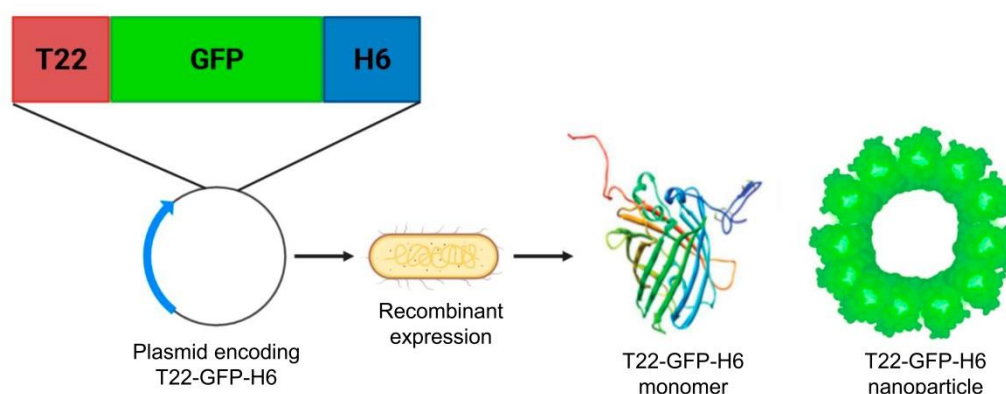


Figure S3 Schematic representation T22-GFP-H6 production and monomeric and nanoparticle structures as explained in detail in Unzueta et al. 2012¹⁵. T22-GFP-H6 is recombinantly expressed in *E. coli*, where an average of 12 monomers of the protein (predicted structure shown in the figure) self-assemble to create multivalent nanoparticles of approximately 13 nm. Created with BioRender.com.

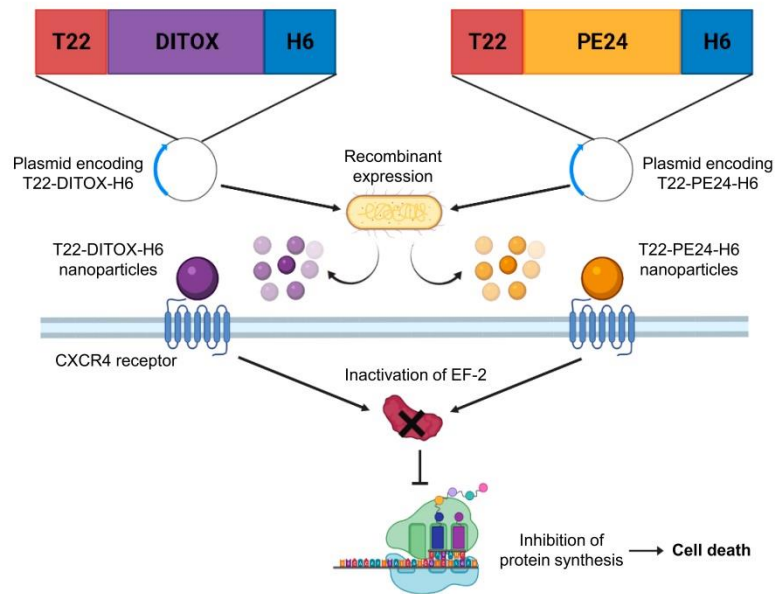


Figure S4 Diagram describing the production and predicted mechanism of action of T22-DITOX-H6 and T22-PE24-H6 nanotoxins as explained in detail in Serna, S á nchez-Garc í a *et al.* 2018¹⁹. T22-DITOX-H6 and T22-PE24-H6 are recombinantly produced in *E. coli* where they spontaneously self-assemble into nanoparticles, similarly to the T22-GFP-H6 nanocarrier. Both nanotoxins are able to interact with the CXCR4 receptor in the cell membrane and, upon binding, internalize within the cell by endocytosis. Once inside the cell, both toxins exert their cytotoxic activity by inactivating the ribosomal elongation factor 2 (EEF-2), thus inhibiting protein synthesis and leading to cell death. Created with BioRender.com.

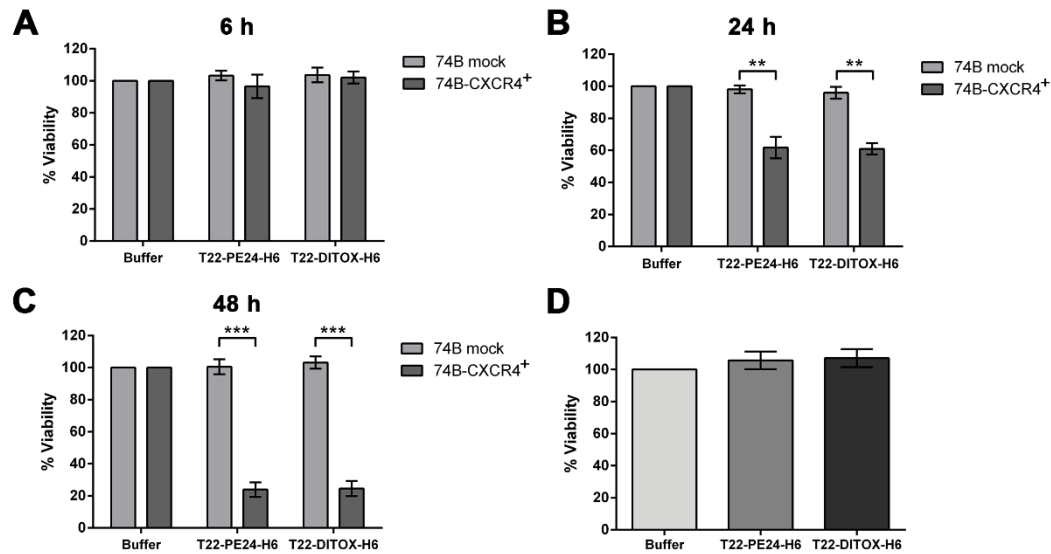


Figure S5 T22-PE24-H6 and T22-DITOX-H6 nanotoxins CXCR4-dependant cytotoxic effect in HNSCC cell lines. (A-C) T22-PE24-H6 and T22-DITOX-H6 cytotoxic effect (50 nmol/L) after 6 h (A), 24 h (B), and 48 h (C) of exposure in 74B mock and 74B-CXCR4⁺ cell lines represented as percentage of cell viability. (D) Lack of off-target cytotoxic effect of the nanotoxins in 74B mock cell cultures after 48h of exposure to supernatants from 74B-CXCR4⁺ cells treated for 48h with T22-PE24-H6 or T22-DITOX-H6. Data represented as mean \pm Standard error. All experiments were performed in triplicate. ** $P < 0.01$; *** $P < 0.001$. Statistical analysis performed by Student's *t*-test.

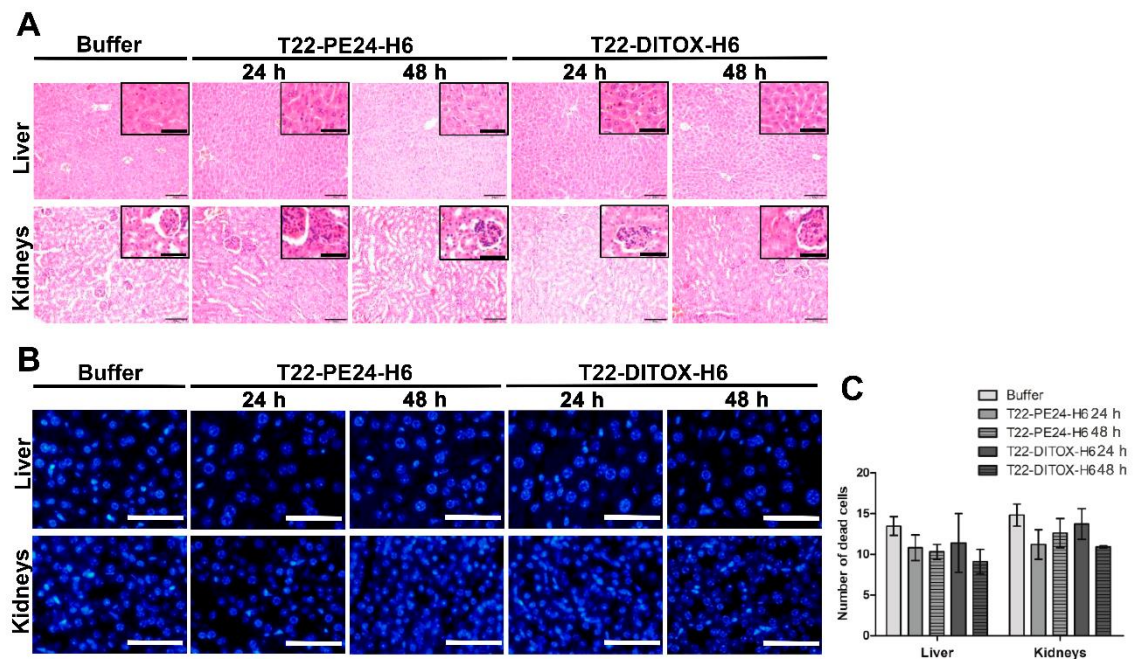


Figure S6 Lack of toxicity of T22-PE24-H6 and T22-DITOX-H6 nanotoxins in a CXCR4-overexpressing mouse model. (A) Histological analysis of liver and kidneys sections (H&E) 24 and 48 h after the treatment (buffer, T22-PE24-H6 or T22-DITOX-H6). (B) Analysis of the number of dead cells in the liver and kidneys after treatment with both nanotoxins compared to the buffer-treated animals. (C) Quantification of the number of cells presenting condensate nuclei (DAPI staining), which correlates with cell death, in the liver and kidneys 24 and 48 h after the IV administration of either buffer or the nanotoxins. Scale bars = 100 or 50 μm (zoom in) (H&E), and 50 μm (DAPI staining); $n=20$ per group (total number analyzed tissue sections per group). Statistical analysis performed by Student's *t*-test.

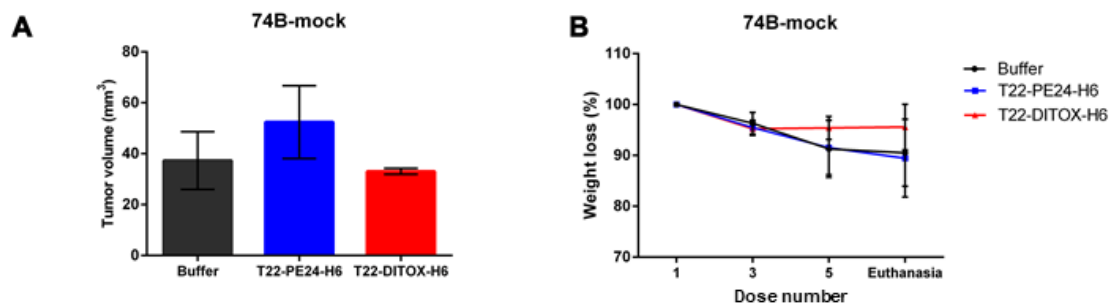


Figure S7 Lack of antitumor effect of T22-PE24-H6 and T22-DITOX-H6 nanotoxins in a 74B mock orthotopic HNSCC mouse model. (A) Tumor volumes registered at the end point of the experiment in the three experimental groups (buffer, T22-PE24-H6, and T22-DITOX-H6). (B) Body weight loss in the time course of the experiment in buffer, T22-PE24-H6, and T22-DITOX-H6 treated animals represented as percentage of body weight loss. Body weight loss is a consequence of primary tumor growth. Data represented as mean \pm Standard error. $n = 4$ per group (total animal number 12). Statistical analysis performed by Student's *t*-test.

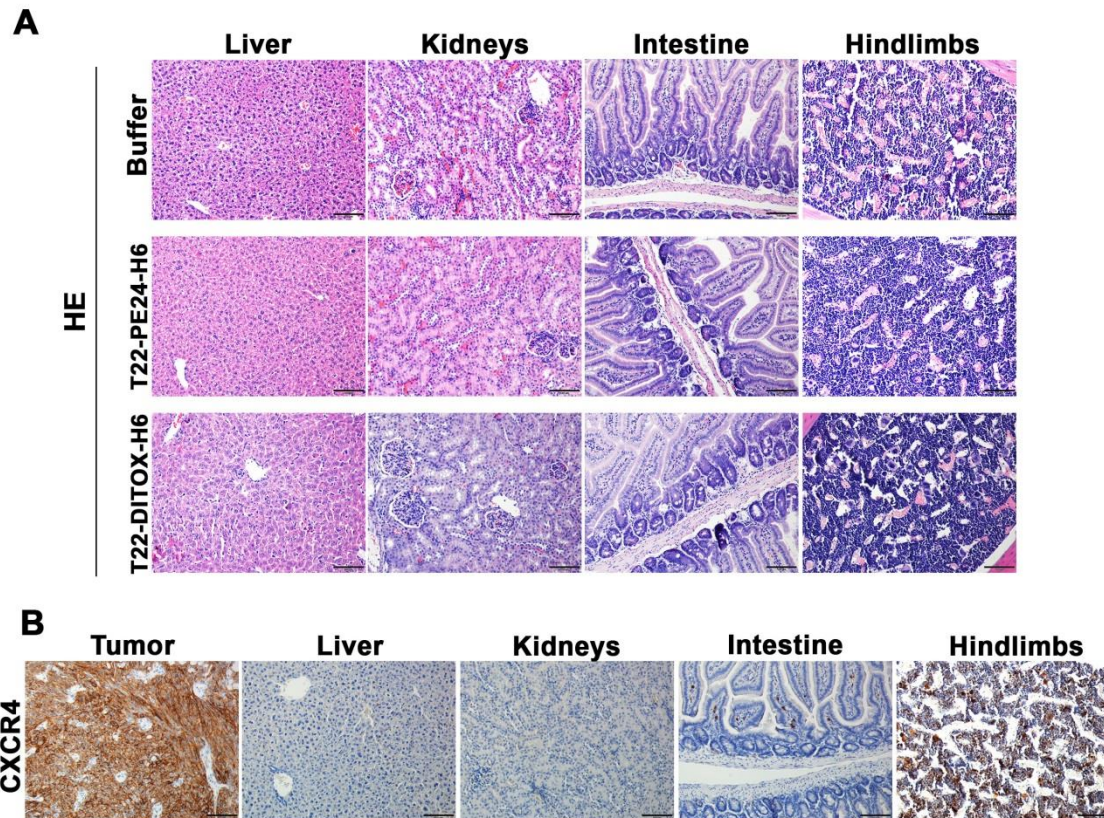


Figure S8 Lack of systemic toxicity of T22-PE24-H6 and T22-DITOX-H6 nanotoxins in a 74B-CXCR4⁺ orthotopic mouse model. (A) Histological analysis of liver, kidneys, intestine, and hindlimbs (bone marrow) sections (H&E) after the treatment with either buffer, or 10 μ g of nanotoxin (T22-PE24-H6 or T22-DITOX-H6) up to 5 consecutive doses. (B) CXCR4 IHC staining of tumor, liver, kidneys, intestine, and hindlimbs (bone marrow) sections showing the expression of the receptor in each tissue. Scale bar = 100 μ m; $n=5$ per group (total animal number 15).

ANNEX: SUPPLEMENTARY INFORMATION

CHAPTER 2

CXCR4-targeted nanotoxins induce GSDME-dependent pyroptosis in head and neck squamous cell carcinoma

Elisa Rioja-Blanco, Irene Arroyo-Solera, Patricia Álamo, Isolda Casanova, Alberto Gallardo, Ugutz Unzueta, Naroa Serna, Laura Sánchez-García, Miquel Quer, Antonio Villaverde, Esther Vázquez*, Xavier León, Lorena Alba-Castellón*, Ramon Manges*

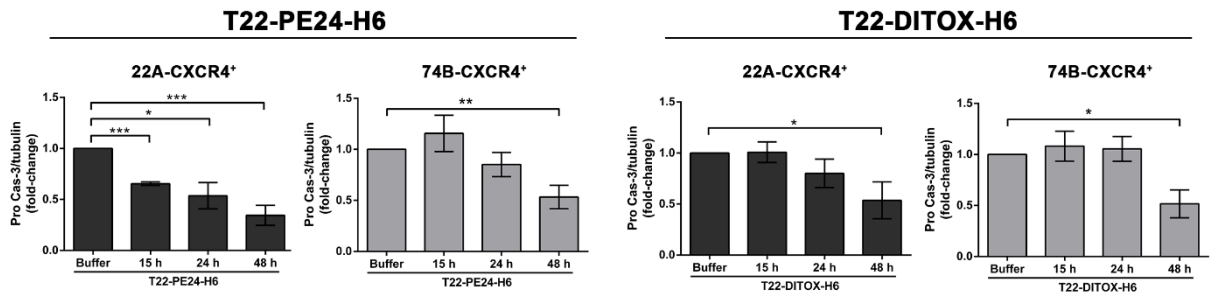
*co-corresponding authors

Journal of Experimental & Clinical Cancer Research

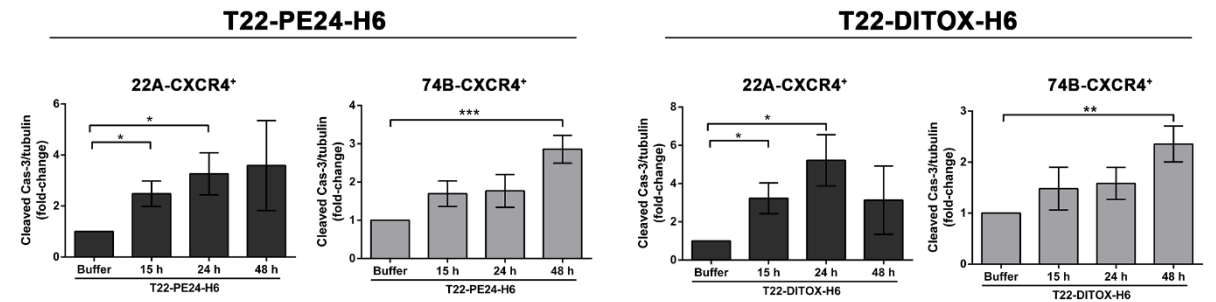
2022

Supplementary data

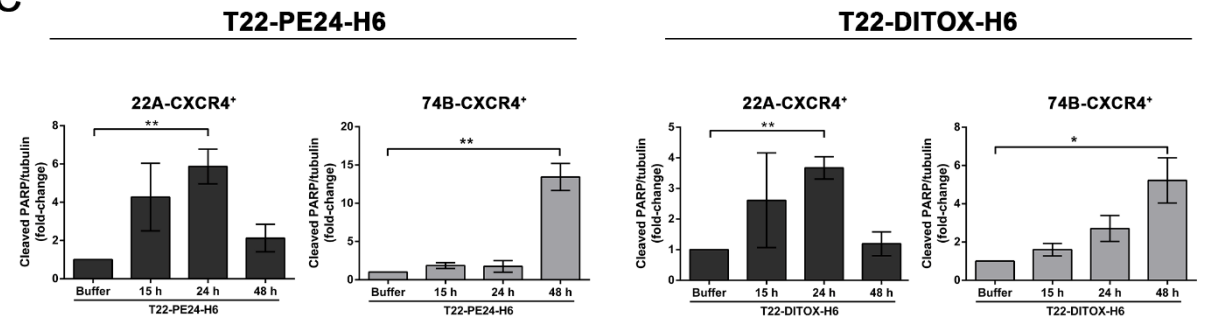
A



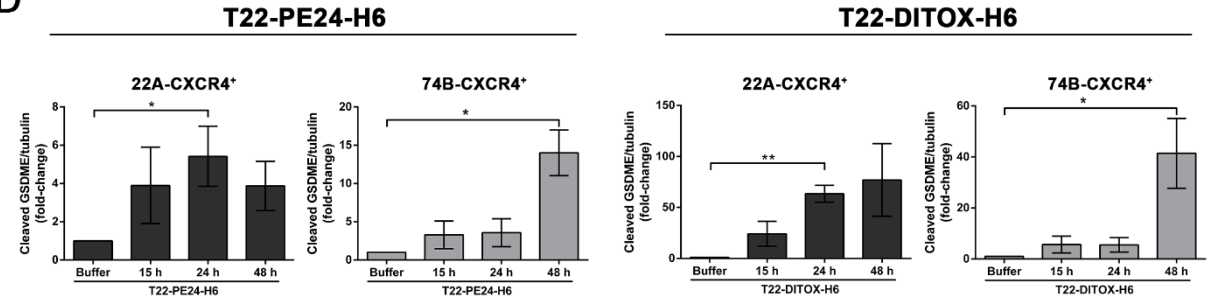
B



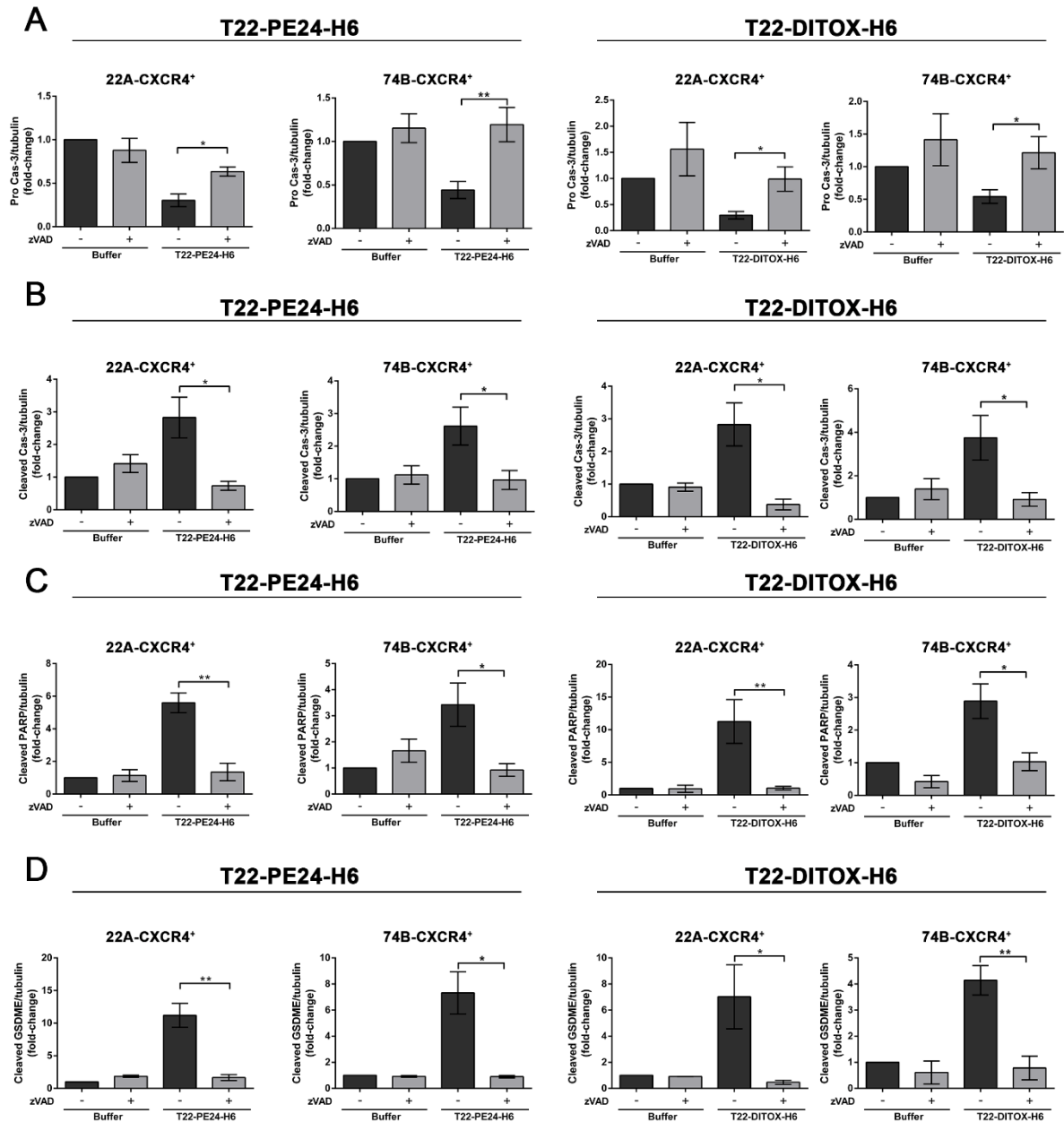
C



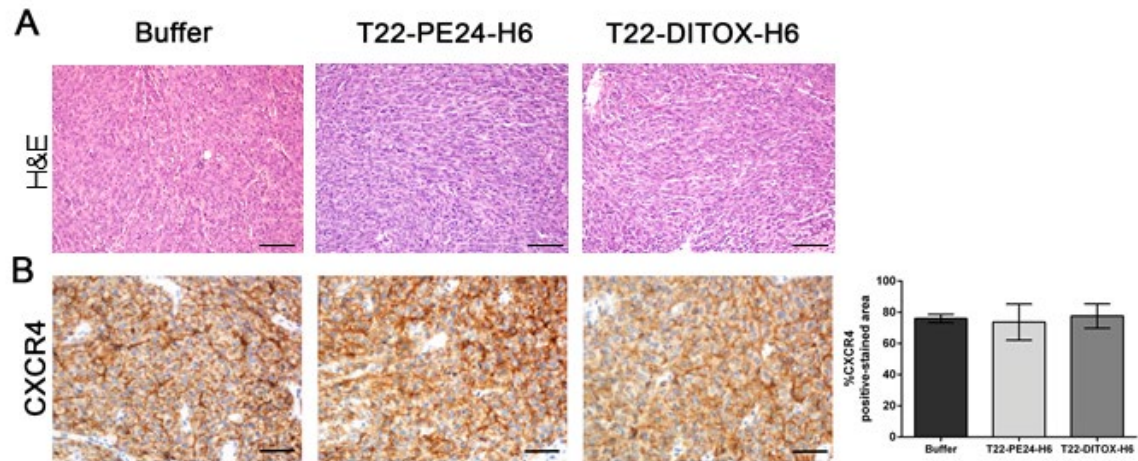
D



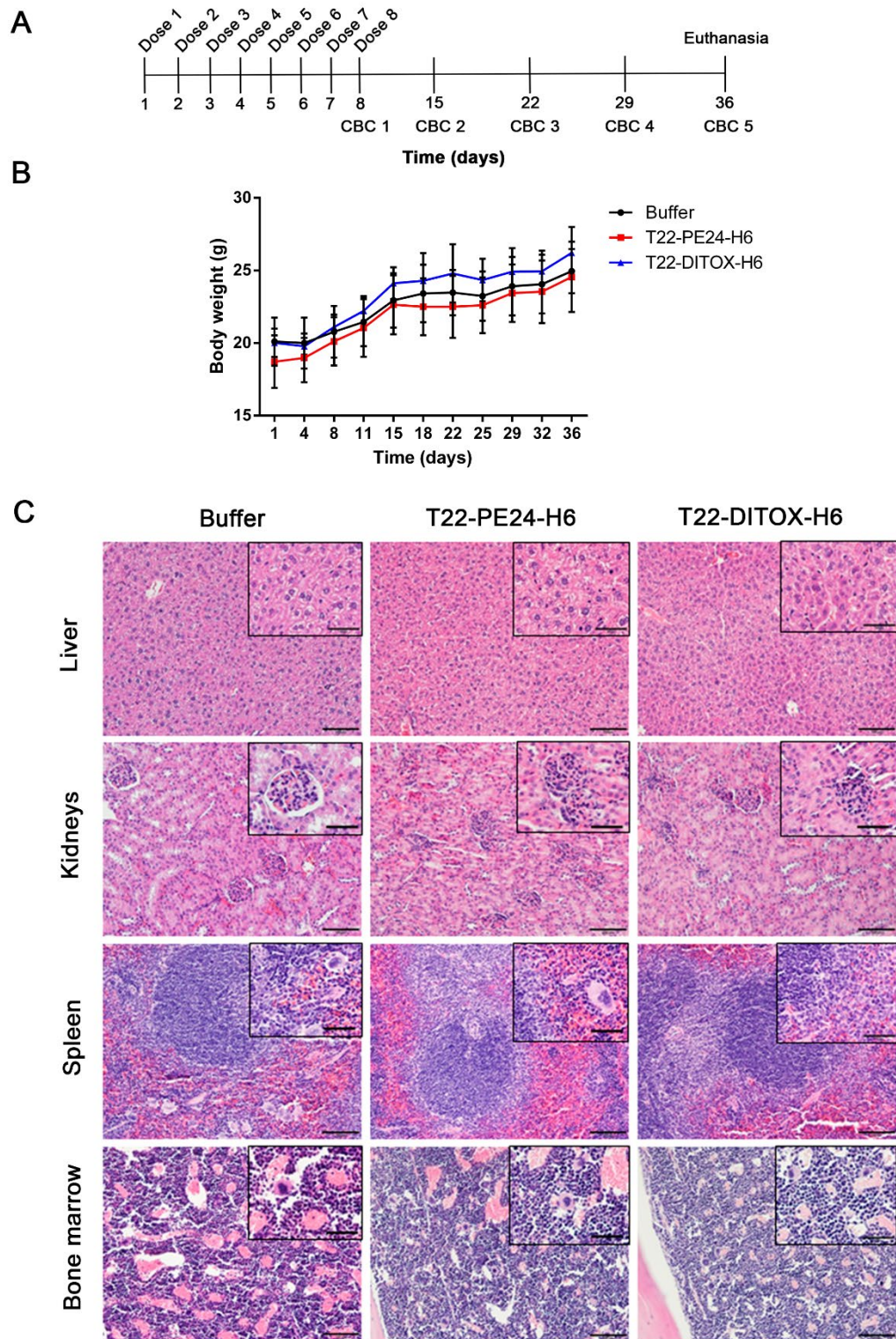
Supplementary figure 1. Quantitation of relative protein intensity for different pyroptotic markers after nanotoxin treatment. Pro-caspase-3 (A), cleaved caspase-3 (B), cleaved PARP (C), and cleaved GSDME (D) western blotting intensity quantification from protein extracts from 22A-CXCR4⁺ and 74B-CXCR4⁺ cell lines treated with T22-PE24-H6 and T22-DITOX-H6 for 15 h, 24 h, and 48 h. * $p < 0.05$; ** $p < 0.01$; *** $p < 0.001$. Each column represents the mean value of at least three biological replicates. Statistical analysis performed by Student t-test. Error bars indicate SEM.



Supplementary figure 2. Quantitation of relative protein intensity of different pyroptotic markers in HNSCC cell lines pre-treated with the pan-caspase inhibitor zVAD before nanotoxin treatment. Pro-caspase-3 (A), cleaved caspase-3 (B), cleaved PARP (C), and cleaved GSDME (D) western blotting intensity quantification from protein extracts from 22A-CXCR4⁺ and 74B-CXCR4⁺ cell lines pre-treated with zVAD prior to the nanotoxin treatment for 15 h, 24 h, and 48 h. * p<0.05; ** p<0.01. Each column represents the mean value of at least three biological replicates. Statistical analysis performed by Student t-test. Error bars indicate SEM.

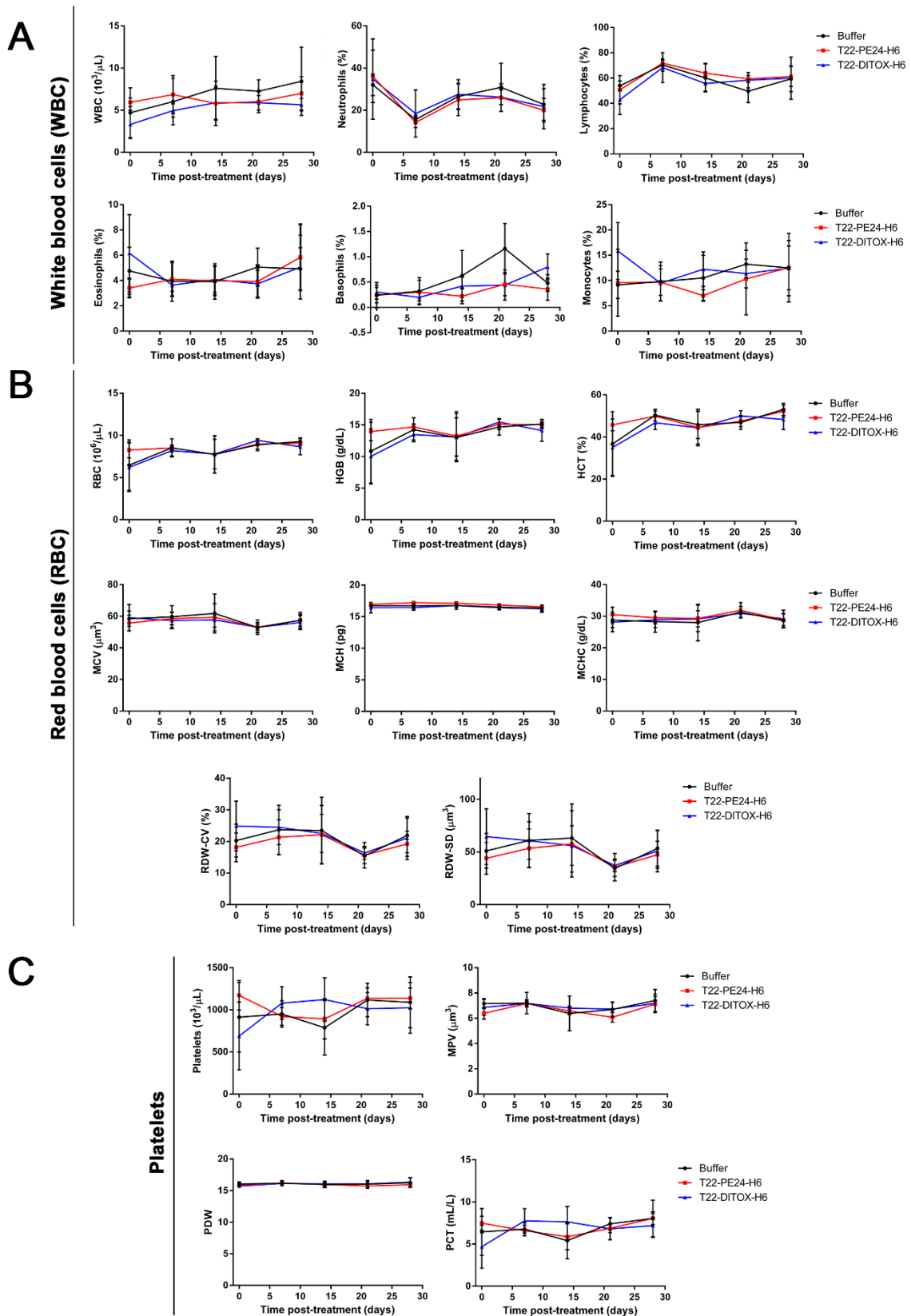


Supplementary figure 3. Histological analysis of the subcutaneous tumors obtained at the end of the repeated dose nanotoxin treatment. A) H&E images from the buffer, T22-PE24-H6, and T22-DITOX-H6 tumors. B) Representative IHC images of the CXCR4 expression in tumor samples from buffer, T22-PE24-H6, and T22-DITOX-H6 treated animals. Quantification of the percentage of CXCR4 positive stained cells in tumors from each group. Scale bars = 100 μ m and 50 μ m. CXCR4 expression was quantified as mean gray value and represented as mean \pm SEM.

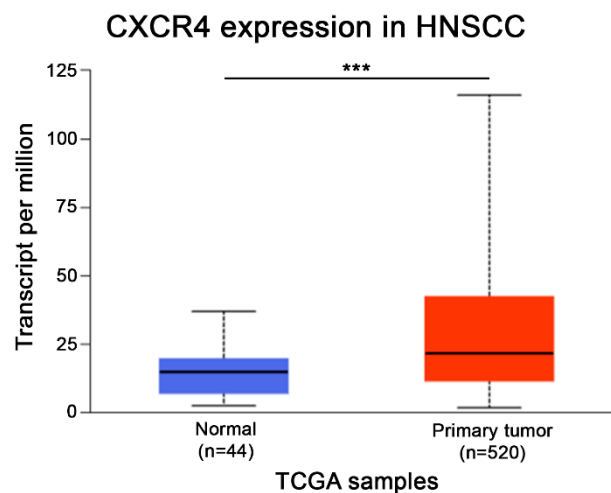


Supplementary figure 4. T22-PE24-H6 and T22-DITOX-H6 lack long-term off-target toxicity in non-tumor tissues. A) Schematic representation of the experimental procedure conducted in this study. B) Variation of the body weight in each group (buffer, T22-PE24-H6, and T22-DITOX-H6) along the time course of the experiment. C)

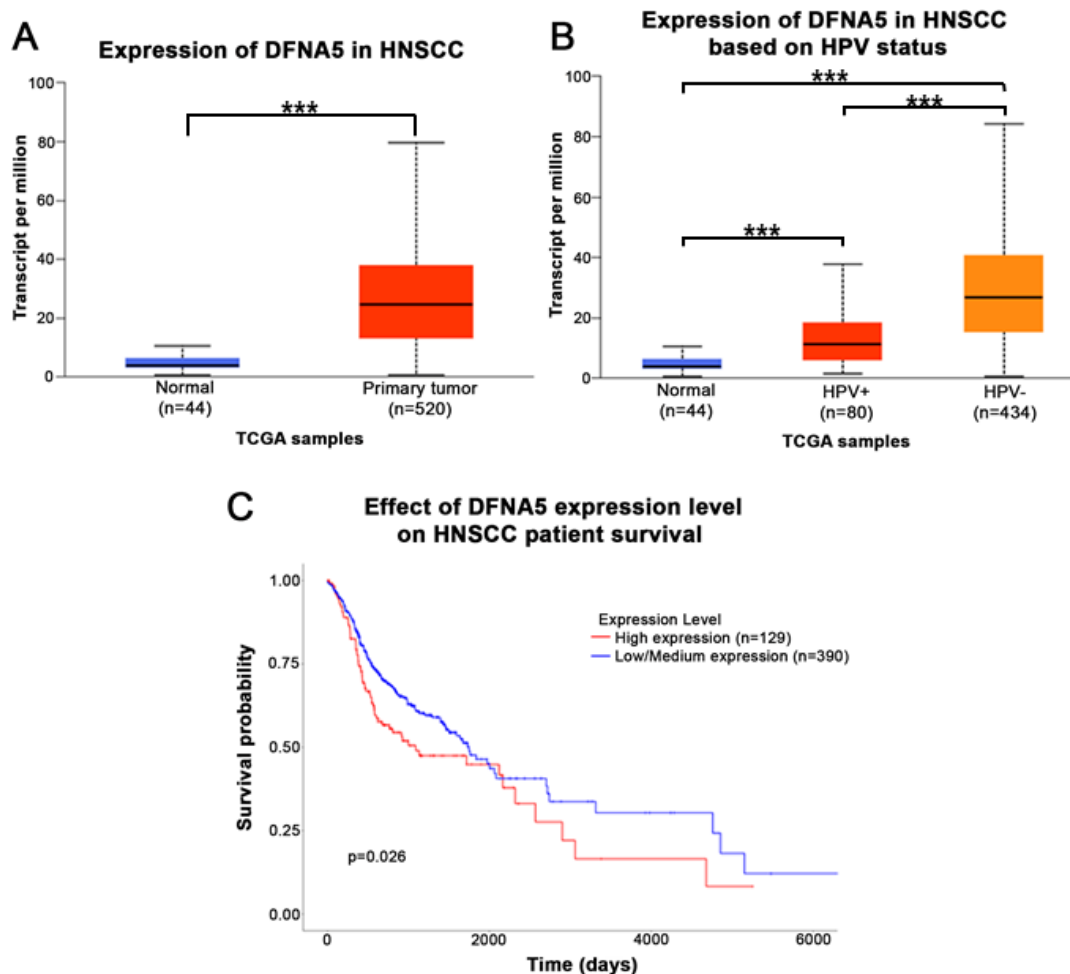
Representative H&E images of liver, kidneys, spleen, and bone marrow from buffer, T22-PE24-H6, and T22-DITOX-H6 treated animals. Scale bars = 100 μ m and 50 μ m (zoom in). Statistical analysis performed by Student t-test. Error bars indicate SEM.



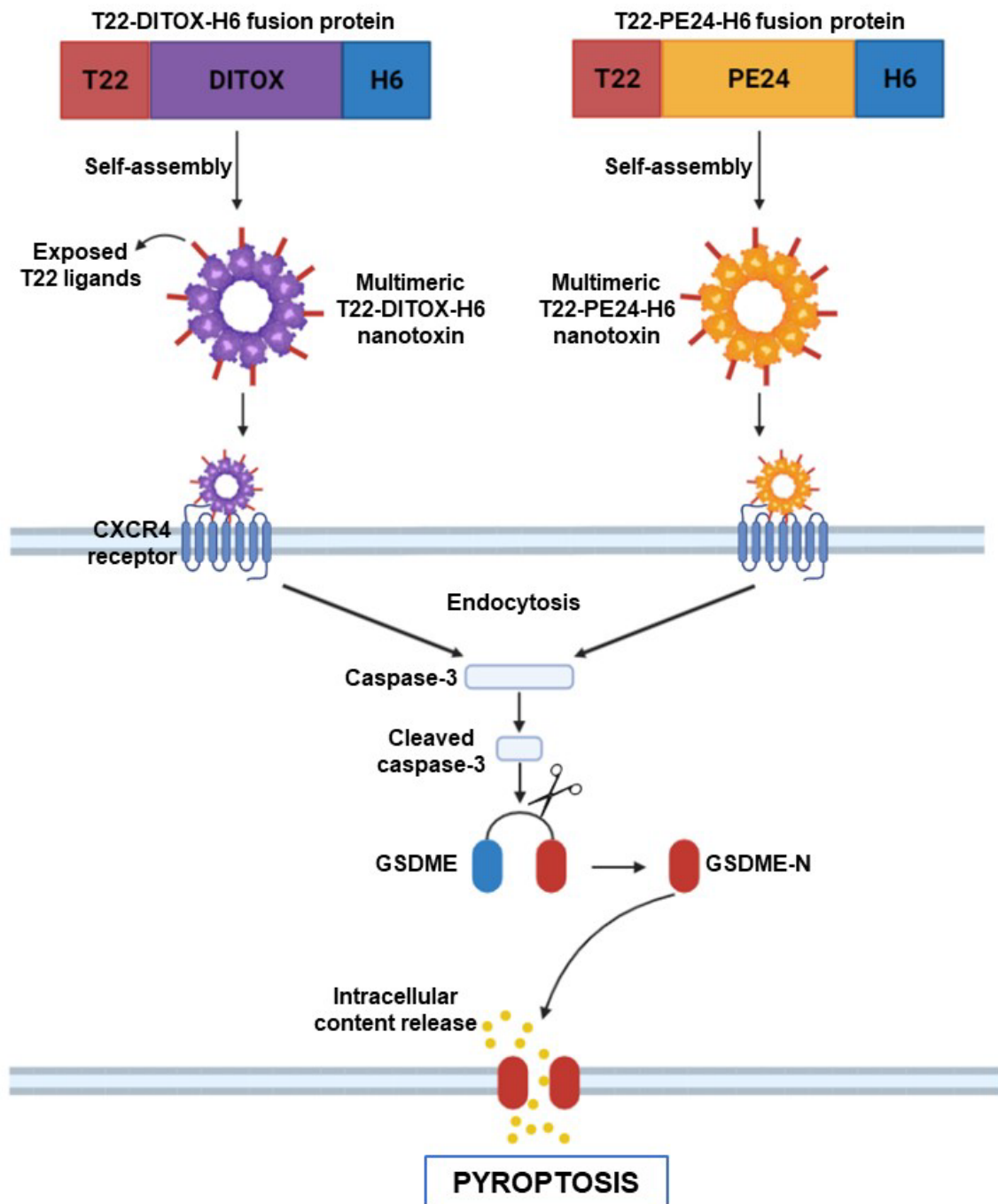
Supplementary figure 5. Cell blood count (CBC) analysis to evaluate long-term toxicity after repeated T22-PE24-H6 or T22-DITOX-H6 administration. A) Evaluation of total white blood cells (WBC), neutrophils, lymphocytes, eosinophils, basophils, and monocytes in each experimental group (buffer, T22-PE24-H6, and T22-DITOX-H6) through the time course of the experiment. B) Red blood cells (RBC) and RBC indices analyses (hemoglobin (HGB), hematocrit (HCT), mean cell volume (MCV), mean corpuscular hemoglobin (MCH), mean corpuscular hemoglobin concentration (MCHC), and red blood cells distribution width (RDW)) from buffer and nanotoxin treatment mice during the experiment. C) Platelets and platelet indices (mean platelet volume (MPV), platelet distribution width (PDW), and plateletcrit (PCT)) registered throughout the experiment in each experimental group. n=5 per group (total animal number 15). Statistical analysis performed by Student t-test. Error bars indicate SD.



Supplementary figure 6. TCGA analysis of the expression of CXCR4 in HNSCC patients. Transcriptomic analysis of the expression of CXCR4 in normal tissue compared to primary tumor samples from HNSCC patients. Analysis was performed using data from the TCGA with the UALCAN analysis software. *** p<0.001.

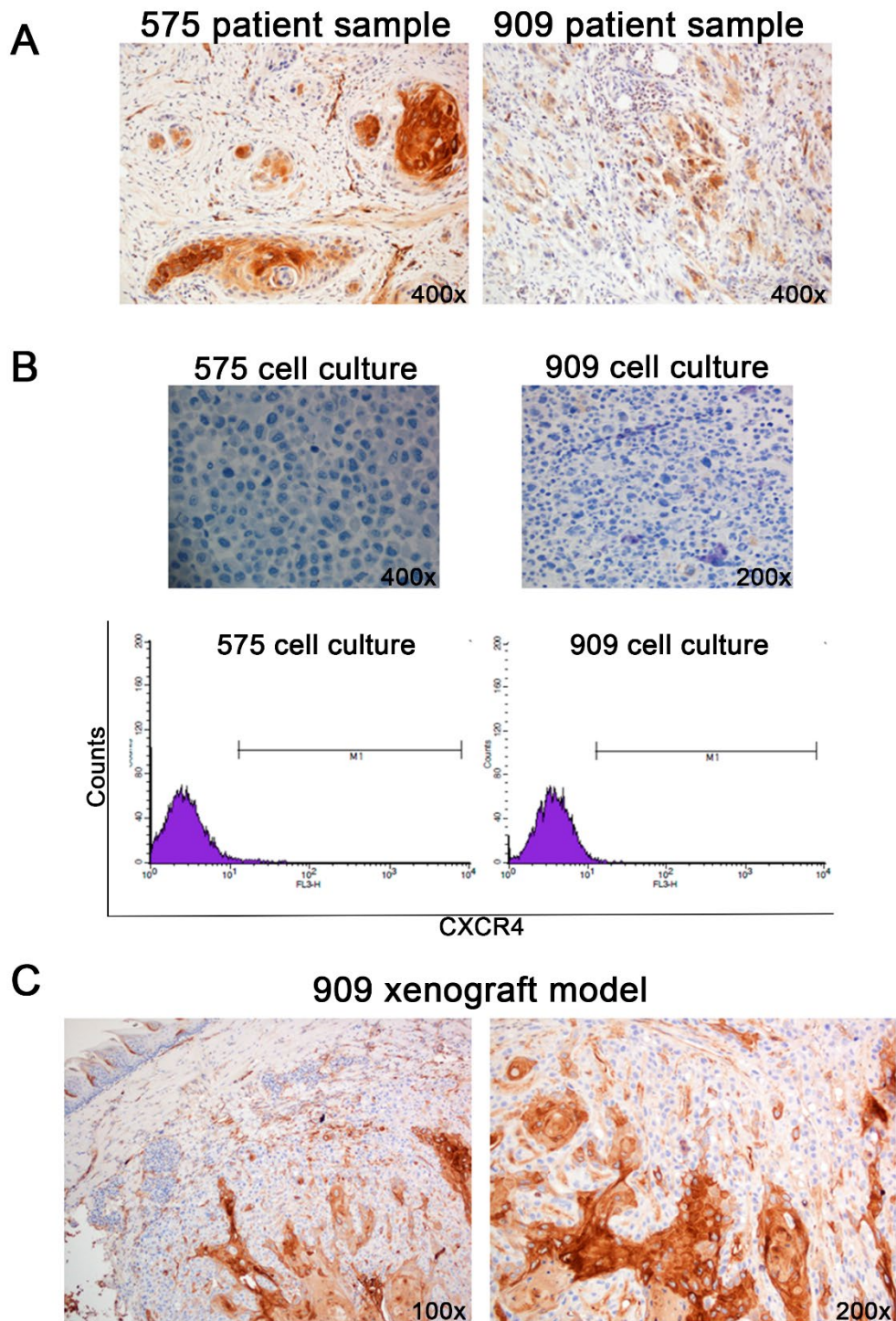


Supplementary figure 7. TCGA analysis of the expression of GSDME in HNSCC patients. A) Transcriptomic analysis of the expression of GSDME in normal tissue compared to primary tumor samples from HNSCC patients. B) Expression of GSDME in normal tissue compared to primary tumor samples from HPV⁺ and HPV⁻ HNSCC patients. B) Effect of the GSDME expression level on HNSCC patient survival. Analysis was performed using data from the TCGA with the UALCAN analysis software. *** p<0.001.



Supplementary figure 8. Schematic summary of the mechanism of action of T22-PE24-H6 and T22-DITOX-H6 nanotoxins. Representation of the T22-PE24-H6 and T22-DITOX-H6 fusion proteins and multimeric structures. Interaction of the nanotoxins with the CXCR4 receptor in the cell membrane, leading to their internalization by endocytosis. Toxin domains inside the cell trigger the caspase-3 activation, which in turn induces the cleavage of the GSDME, liberating the GSDME-N terminal domain. Several GSDME-N domains oligomerize to form pores in the cell membrane, leading to the

release of the intracellular content and the activation of pyroptosis. Created using BioRender.



Supplementary figure 9. CXCR4 expression in 575 and 909 patient-derived cell cultures. A) CXCR4 expression in the original patient samples for 575 and 909 by immunohistochemistry. B) Immunocytochemical and flow cytometry analysis of 575 and 909 patient samples cultured in vitro. C) Immunohistochemical analysis of CXCR4

expression in tumors generated from 909 cell cultures implanted orthotopically in immunodeficient mice.

ANNEX: SUPPLEMENTARY INFORMATION

CHAPTER 3

*A Novel CXCR4-Targeted Diphtheria Toxin Nanoparticle Inhibits Invasion
and Metastatic Dissemination in a Head and Neck Squamous Cell
Carcinoma Mouse Model*

Elisa Rioja-Blanco, Alberto Gallardo, Irene Arroyo-Solera, Patricia Álamo, Isolda Casanova, Ugutz Unzueta, Naroa Serna, Laura Sánchez-García, Miquel Quer, Antonio Villaverde, Esther Vázquez*, Xavier León, Lorena Alba-Castellón*, Ramon Manges*

*co-corresponding authors

Pharmaceutics

2022

Supplementary Materials: A Novel CXCR4-Targeted Diphtheria Toxin Nanoparticle Inhibits Invasion and Metastatic Dissemination in a Head-and-Neck Squamous-Cell-Carcinoma Mouse Model

Elisa Rioja-Blanco , Alberto Gallardo, Irene Arroyo-Solera, Patricia Álamo, Isolda Casanova, Ugutz Unzueta, Naroa Serna, Laura Sánchez-García, Miquel Quer, Antonio Villaverde, Esther Vázquez, Xavier León, Lorena Alba-Castellón and Ramon Mangues

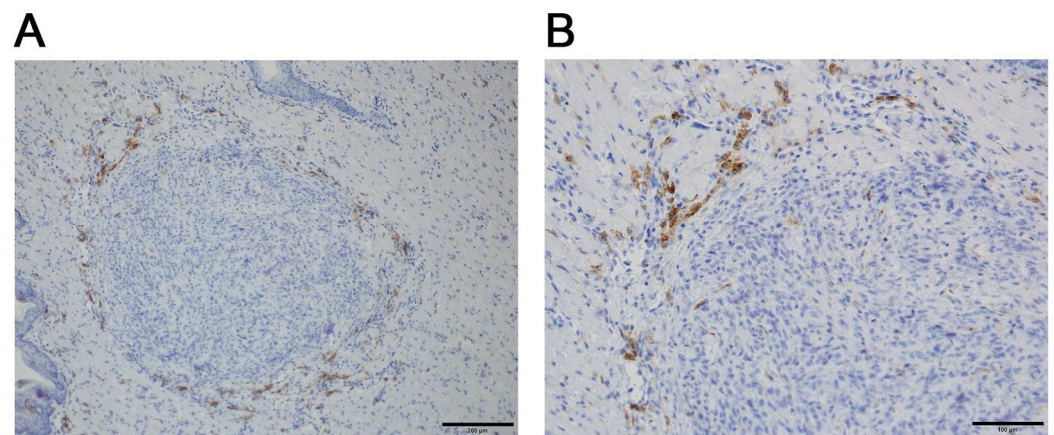


Figure S1. CXCR4 expression in 74B-Luci primary tumor samples in the orthotopic mouse model. CXCR4 IHC representative images of a 74B-Luci orthotopic tumor. **A)** Overall expression of CXCR4 within the primary tumor and in the tumor margins. **B)** Detailed image of the CXCR4 expression in the tumor invasive front, clearly showing a strong CXCR4 expression in the tumor budding, while primary tumor tissue presents a negligible expression of the receptor. Scale bars = 200 μm and 100 μm .

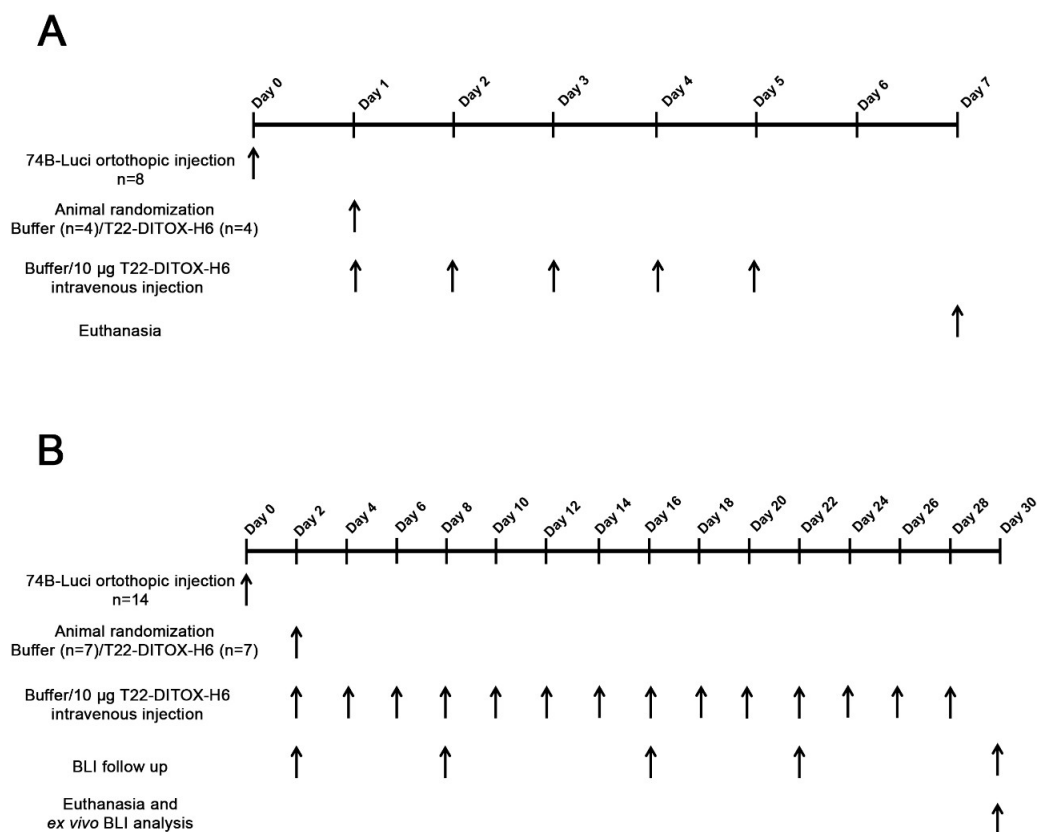


Figure S2. Schematic representation of the experimental design followed in the studies. **A)** Timeline of the experiment that evaluated the T22-DITOX-H6 anti-invasive effect, including all the relevant studies performed. **B)** Experimental design followed during the experiment that assessed the anti-metastatic effect of T22-DITOX-H6 repeated administration, including the study groups, animal number, details on the treatment administration and BLI acquisition, and euthanasia.

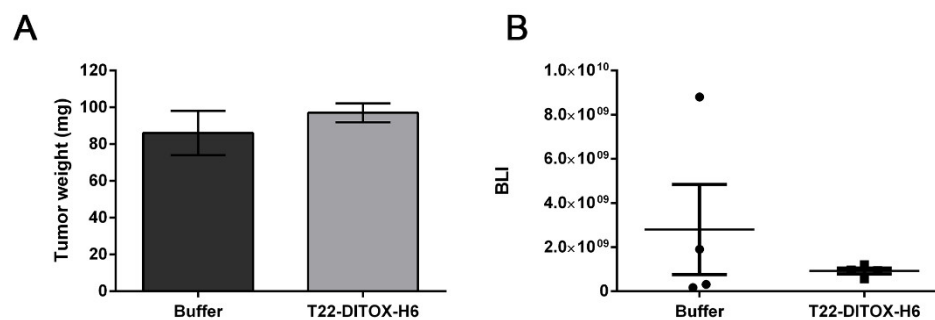


Figure S3. Tumor size assessment in the experiment that evaluated T22-DITOX-H6 anti-invasive effect. **A)** Tumor weight registered at euthanasia for buffer and nanotoxin-treated animals. **B)** BLI emitted by the primary tumors at the end point of the experiment in both buffer and T22-DITOX-H6 groups. No statistical differences were found between groups. $n = 4$ per group (total animal number 8). Statistical analysis was performed by Mann-Whitney test. Error bars indicate SEM.

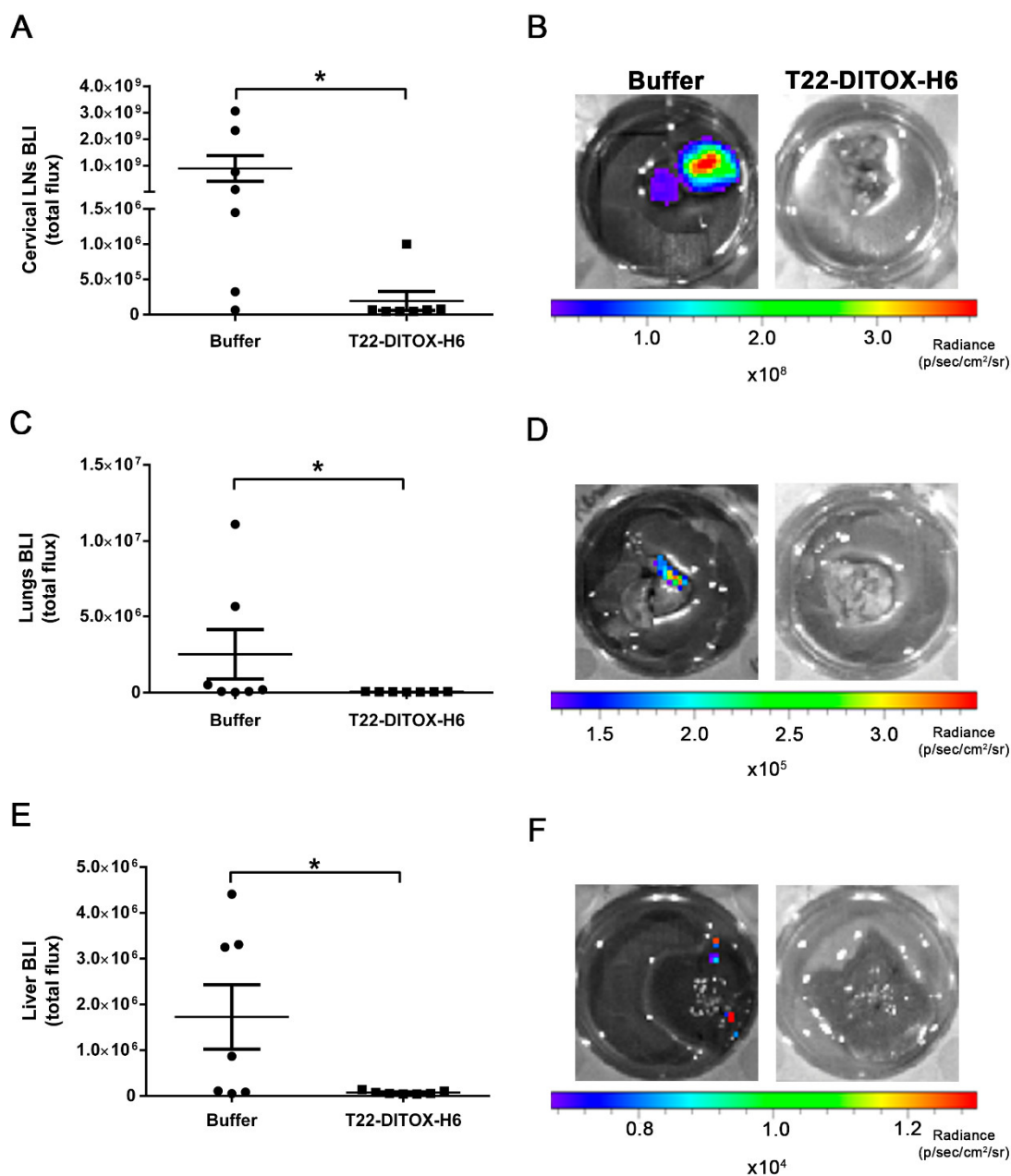


Figure S4. Ex vivo bioluminescence evaluation in the metastatic organs. BLI was semi-quantified in the explanted relevant organs at the endpoint of the experiment that evaluated T22-DITOX-H6 anti-metastatic effect. **A)** Semi-quantification of the BLI emitted by the explanted cervical lymph nodes obtained from buffer and nanotoxin-treated animals. **B)** Representative BLI images of cervical lymph nodes from control and T22-DITOX-H6 groups. **C)** Evaluation of the BLI emitted by lung samples from control and T22-DITOX-H6 treated mice. **D)** BLI images of a lung obtained from a control animal and a nanotoxin-treated one. **E)** Assessment of the BLI from livers explanted from buffer and T22-DITOX-H6 groups. **F)** Images showing the BLI emitted by liver samples derived from control and nanotoxin-treated animals. * $p < 0.05$. Statistical analysis was performed by Mann-Whitney test. Error bars indicate SEM.

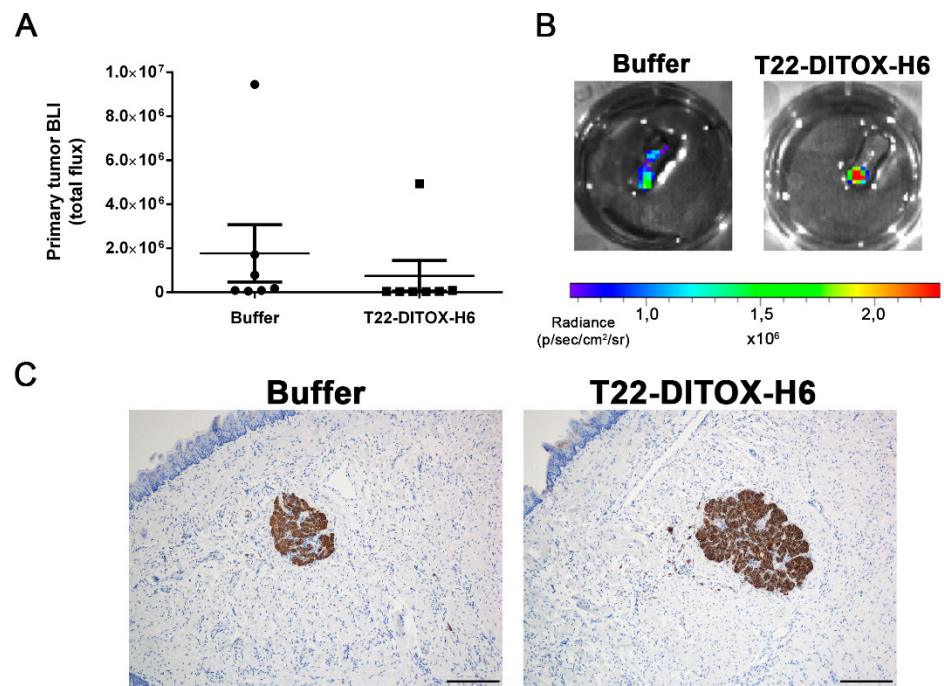


Figure S5. Evaluation of the primary tumor size in buffer and nanotoxin-treated animals in the experiment that evaluated T22-DITOX-H6 antimetastatic effect. **A)** Semi-quantification of the BLI emitted by primary tumors from buffer and nanotoxin-treated animals at the end of the experiment. No statistical differences were found between groups. **B)** Representative BLI images of two primary tumor samples from buffer and T22-DITOX-H6-treated animals. **C)** Anti-Human Vimentin IHC images from buffer and T22-DITOX-H6 primary tumor samples. Scale bar = 200 μm ; $n = 7$ per group (total animal number 14). Statistical analysis performed by Mann-Whitney test. Error bars indicate SEM.

REFERENCES

1. Aceto, N., Bardia, A., Miyamoto, D. T., Donaldson, M. C., Wittner, B. S., Spencer, J. A., et al. (2014). Circulating tumor cell clusters are oligoclonal precursors of breast cancer metastasis. *Cell* 158, 1110–1122. doi:10.1016/j.cell.2014.07.013.
2. Akbari, B., Farajnia, S., Ahdi Khosroshahi, S., Safari, F., Yousefi, M., Dariushnejad, H., et al. (2017). Immunotoxins in cancer therapy: Review and update. *Int. Rev. Immunol.* 36, 207–219. doi:10.1080/08830185.2017.1284211.
3. Akolkar, D., Patil, D., Crook, T., Limaye, S., Page, R., Datta, V., et al. (2019). Circulating ensembles of tumor-associated cells: A redoubtable new systemic hallmark of cancer. *Int. J. Cancer* 944, 1–10. doi:10.1002/ijc.32815.
4. Albert, S., Riveiro, M. E., Halimi, C., Hourseau, M., Couvelard, A., Serova, M., et al. (2013). Focus on the role of the CXCL12/CXCR4 chemokine axis in head and neck squamous cell carcinoma. *Head Neck* 35, 1819–1828. doi:10.1002/hed.23217.
5. Alewine, C., Hassan, R., and Pastan, I. (2015). Advances in anticancer immunotoxin therapy. *Oncologist* 20, 176–185. doi:10.1634/theoncologist.2014-0358.
6. American Cancer Society. Cancer Facts & Figures 2020. Atlanta: American Cancer Society; 2020.
7. Angus, L., Smid, M., Wilting, S. M., van Riet, J., Van Hoeck, A., Nguyen, L., et al. (2019). The genomic landscape of metastatic breast cancer highlights changes in mutation and signature frequencies. *Nat. Genet.* 51, 1450–1458. doi:10.1038/s41588-019-0507-7.
8. Argiris, A., Karamouzis, M. V, Raben, D., and Robert L, F. (2018). Head and neck cancer. *Med. Radiol.*, 91–126. doi:10.1007/174_2017_32.
9. Avendaño, C., Menéndez, J. C., Avendaño, C., and Menéndez, J. C. (2008). *Chapter 2 – Antimetabolites*. doi:10.1016/B978-0-444-52824-7.00002-0.
10. Ayob, A. Z., and Ramasamy, T. S. (2018). Cancer stem cells as key drivers of tumour progression. *J. Biomed. Sci.* 25, 1–18. doi:10.1186/s12929-018-0426-4.
11. Baidara, P., and Mandal, S. M. (2020). Bacteria and bacterial anticancer agents as a promising alternative for cancer therapeutics. *Biochimie* 177, 164–189. doi:https://doi.org/10.1016/j.biochi.2020.07.020.
12. Battle, E., and Clevers, H. (2017). Cancer stem cells revisited. *Nat. Med.* 23, 1124–1134. doi:10.1038/nm.4409.
13. Baudino, T. A. (2015). Send Orders for Reprints to reprints@benthamscience.ae Targeted Cancer Therapy: The Next Generation of Cancer Treatment. *Curr. Drug Discov. Technol.* 12, 3–20. doi:10.2174/1570163812666150602144310.
14. Bauml, J. M., Aggarwal, C., and Cohen, R. B. (2019). Immunotherapy for head and neck cancer: where are we now and where are we going? *Ann. Transl. Med.* 7, S75.

- doi:10.21037/atm.2019.03.58.
15. Beck, A., Goetsch, L., Dumontet, C., and Corvaia, N. (2017). Strategies and challenges for the next generation of antibody-drug conjugates. *Nat. Rev. Drug Discov.* 16, 315–337. doi:10.1038/nrd.2016.268.
 16. Borcoman, E., Marret, G., and Le Tourneau, C. (2021). Paradigm Change in First-Line Treatment of Recurrent and/or Metastatic Head and Neck Squamous Cell Carcinoma. *Cancers* 13. doi:10.3390/cancers13112573.
 17. Braig, F., Kriegs, M., Voigtlaender, M., Habel, B., Grob, T., Biskup, K., et al. (2017). Cetuximab Resistance in Head and Neck Cancer Is Mediated by EGFR-K(521) Polymorphism. *Cancer Res.* 77, 1188–1199. doi:10.1158/0008-5472.CAN-16-0754.
 18. Bray, F., Ferlay, J., Soerjomataram, I., Siegel, R. L., Torre, L. A., and Jemal, A. (2018). Global cancer statistics 2018: GLOBOCAN estimates of incidence and mortality worldwide for 36 cancers in 185 countries. *CA. Cancer J. Clin.* 68, 394–424. doi:10.3322/caac.21492.
 19. Busillo, J. M., and Benovic, J. L. (2007). Regulation of CXCR4 signaling. *Biochim. Biophys. Acta - Biomembr.* 1768, 952–963. doi:10.1016/j.bbmem.2006.11.002.
 20. Butterfield, J. T., Kim, H., Knauer, D. J., Nevala, W. K., and Markovic, S. N. (2017). Identification of a peptide-peptide binding motif in the coating of nab-paclitaxel nanoparticles with clinical antibodies: Bevacizumab, rituximab, and trastuzumab. *Sci. Rep.* 7, 1–9. doi:10.1038/s41598-017-15251-6.
 21. Byrne, J. D., Betancourt, T., and Brannon-Peppas, L. (2008). Active targeting schemes for nanoparticle systems in cancer therapeutics. *Adv. Drug Deliv. Rev.* 60, 1615–1626. doi:10.1016/j.addr.2008.08.005.
 22. Carneiro, B. A., and El-Deiry, W. S. (2020). Targeting apoptosis in cancer therapy. *Nat. Rev. Clin. Oncol.* doi:10.1038/s41571-020-0341-y.
 23. Celià-Terrassa, T., and Kang, Y. (2018). Metastatic niche functions and therapeutic opportunities. *Nat. Cell Biol.* 20, 868–877. doi:10.1038/s41556-018-0145-9.
 24. Céspedes, M. V., Unzueta, U., Aviñó, A., Gallardo, A., Álamo, P., Sala, R., et al. (2018). Selective depletion of metastatic stem cells as therapy for human colorectal cancer. *EMBO Mol. Med.* 10. doi:10.15252/emmm.201708772.
 25. Céspedes, M. V., Unzueta, U., Tatkiewicz, W., Sánchez-Chardi, A., Conchillo-Solé, O., Álamo, P., et al. (2014). In vivo architectonic stability of fully de novo designed protein-only nanoparticles. *ACS Nano* 8, 4166–4176. doi:10.1021/nn4055732.
 26. Chaffer, C. L., and Weinberg, R. A. (2011). A perspective on cancer cell metastasis. *Science (80-)*. 331, 1559–1564. doi:10.1126/science.1203543.
 27. Chen, K., Huang, Y. H., and Chen, J. L. (2013). Understanding and targeting cancer

- stem cells: Therapeutic implications and challenges. *Acta Pharmacol. Sin.* 34, 732–740. doi:10.1038/aps.2013.27.
28. Chen, L., Huang, C. F., Li, Y. C., Deng, W. W., Mao, L., Wu, L., et al. (2018). Blockage of the NLRP3 inflammasome by MCC950 improves anti-tumor immune responses in head and neck squamous cell carcinoma. *Cell. Mol. Life Sci.* 75, 2045–2058. doi:10.1007/s00018-017-2720-9.
29. Chen, N., Brachmann, C., Liu, X., Pierce, D. W., Dey, J., Kerwin, W. S., et al. (2015). Albumin-bound nanoparticle (nab) paclitaxel exhibits enhanced paclitaxel tissue distribution and tumor penetration. *Cancer Chemother. Pharmacol.* 76, 699–712. doi:10.1007/s00280-015-2833-5.
30. Corchero, J. L., Vázquez, E., García-Fruitós, E., Ferrer-Miralles, N., and Villaverde, A. (2014). Recombinant protein materials for bioengineering and nanomedicine. *Nanomedicine* 9, 2817–2828. doi:10.2217/nnm.14.153.
31. Costea, D. E., Tsinkalovsky, O., Vintermyr, O. K., Johannessen, A. C., and Mackenzie, I. C. (2006). Cancer stem cells - New and potentially important targets for the therapy of oral squamous cell carcinoma. *Oral Dis.* 12, 443–454. doi:10.1111/j.1601-0825.2006.01264.x.
32. Cramer, J. D., Burtness, B., Le, Q. T., and Ferris, R. L. (2019). The changing therapeutic landscape of head and neck cancer. *Nat. Rev. Clin. Oncol.* 16, 669–683. doi:10.1038/s41571-019-0227-z.
33. Dalerba, P., and Clarke, M. F. (2007). Cancer Stem Cells and Tumor Metastasis: First Steps into Uncharted Territory. *Cell Stem Cell* 1, 241–242. doi:10.1016/j.stem.2007.08.012.
34. Danhier, F. (2016). To exploit the tumor microenvironment: Since the EPR effect fails in the clinic, what is the future of nanomedicine? *J. Control. Release* 244, 108–121. doi:10.1016/j.jconrel.2016.11.015.
35. Danhier, F., Feron, O., and Préat, V. (2010). To exploit the tumor microenvironment: Passive and active tumor targeting of nanocarriers for anti-cancer drug delivery. *J. Control. Release* 148, 135–146. doi:10.1016/j.jconrel.2010.08.027.
36. De-Colle, C., Menegakis, A., Mönnich, D., Welz, S., Boeke, S., Sipos, B., et al. (2018). SDF-1/CXCR4 expression is an independent negative prognostic biomarker in patients with head and neck cancer after primary radiochemotherapy. *Radiother. Oncol. J. Eur. Soc. Ther. Radiol. Oncol.* 126, 125–131. doi:10.1016/j.radonc.2017.10.008.
37. de Bree, R., Senft, A., Coca-Pelaz, A., Kowalski, L., Lopez, F., Mendenhall, W., et al. (2018). Detection of Distant Metastases in Head and Neck Cancer: Changing

- Landscape. *Adv. Ther.* 35, 161–172. doi:10.1007/s12325-018-0662-8.
38. de Lázaro, I., and Mooney, D. J. (2020). A nanoparticle's pathway into tumours. *Nat. Mater.* 19, 486–487. doi:10.1038/s41563-020-0669-9.
39. De Matteis, V. (2017). Exposure to Inorganic Nanoparticles: Routes of Entry, Immune Response, Biodistribution and In Vitro/In Vivo Toxicity Evaluation. *Toxics* 5, 29. doi:10.3390/toxics5040029.
40. De Pinho Favaro, M. T., Sánchez-García, L., Sánchez-Chardi, A., Roldán, M., Unzueta, U., Serna, N., et al. (2018). Protein nanoparticles are nontoxic, tuneable cell stressors. *Nanomedicine* 13, 255–268. doi:10.2217/nnm-2017-0294.
41. Desai, N. P., and Desai, I. (2009). Nab Technology: A Drug Delivery Platform Utilising Endothelial gp 60 Receptor-based Transport and Tumour-derived SPARC for Targeting I. in.
42. Deschler, D. G., Moore, M. G., and Smith, R. V. (2014). *TNM Staging of Head and Neck Cancer and Neck Dissection Classification*. doi:RC280.N35P63 2008.
43. Dillekås, H., Rogers, M. S., and Straume, O. (2019). Are 90% of deaths from cancer caused by metastases? *Cancer Med.* 8, 5574–5576. doi:10.1002/cam4.2474.
44. Domanska, U. M., Kruizinga, R. C., Nagengast, W. B., Timmer-Bosscha, H., Huls, G., De Vries, E. G. E., et al. (2013). A review on CXCR4/CXCL12 axis in oncology: No place to hide. *Eur. J. Cancer* 49, 219–230. doi:10.1016/j.ejca.2012.05.005.
45. Donaghy, H. (2016). Effects of antibody, drug and linker on the preclinical and clinical toxicities of antibody-drug conjugates. *MAbs* 8, 659–671. doi:10.1080/19420862.2016.1156829.
46. Drago, J. Z., Modi, S., and Chandarlapaty, S. (2021). Unlocking the potential of antibody–drug conjugates for cancer therapy. *Nat. Rev. Clin. Oncol.* 18, 327–344. doi:10.1038/s41571-021-00470-8.
47. Dragu, D. L., Necula, L. G., Bleotu, C., Diaconu, C. C., and Chivu-Economescu, M. (2015). Therapies targeting cancer stem cells: Current trends and future challenges. *World J. Stem Cells* 7, 1185–201. doi:10.4252/wjsc.v7.i9.1185.
48. Dy, G. K., and Adjei, A. A. (2013). ONLINE CONTINUING EDUCATION ACTIVITY Understanding, Recognizing, and Managing Toxicities of Targeted Anticancer Therapies. *Cancer J Clin* 6363, 249–279. doi:10.1002/caac.21184.
49. Economopoulou, P., Kotsantis, I., Kyrodimos, E., Lianidou, E. S., and Psyrris, A. (2017). Liquid biopsy: An emerging prognostic and predictive tool in Head and Neck Squamous Cell Carcinoma (HNSCC). Focus on Circulating Tumor Cells (CTCs). *Oral Oncol.* 74, 83–89. doi:10.1016/j.oraloncology.2017.09.012.
50. Faber, A., Goessler, U. R., Hoermann, K., Schultz, J. D., Umbreit, C., and Stern-

- Straeter, J. (2013a). SDF-1-CXCR4 axis: Cell trafficking in the cancer stem cell niche of head and neck squamous cell carcinoma. *Oncol. Rep.* 29, 2325–2331. doi:10.3892/or.2013.2380.
51. Faber, A., Hoermann, K., Stern-Straeter, J., Schultz, D. J., and Goessler, U. R. (2013b). Functional effects of SDF-1 α on a CD44+ CXCR4+ squamous cell carcinoma cell line as a model for interactions in the cancer stem cell niche. *Oncol. Rep.* 29, 579–584. doi:10.3892/or.2012.2171.
52. Fang, Y., Tian, S., Pan, Y., Li, W., Wang, Q., Tang, Y., et al. (2020). Pyroptosis: A new frontier in cancer. *Biomed. Pharmacother.* 121. doi:10.1016/j.biopha.2019.109595.
53. Ferlito, A., Shaha, A. R., Silver, C. E., Rinaldo, A., and Mondin, V. (2001). Incidence and sites of distant metastases from head and neck cancer. *ORL. J. Otorhinolaryngol. Relat. Spec.* 63, 202–207. doi:10.1159/000055740.
54. Ferrer-Miralles, N., Corchero, J. L., Kumar, P., Cedano, J. A., Gupta, K. C., Villaverde, A., et al. (2011). Biological activities of histidine-rich peptides; merging biotechnology and nanomedicine. *Microb. Cell Fact.* 10, 101. doi:10.1186/1475-2859-10-101.
55. Ferrer-Miralles, N., Rodríguez-Carmona, E., Corchero, J. L., García-Fruitós, E., Vázquez, E., and Villaverde, A. (2015). Engineering protein self-assembling in protein-based nanomedicines for drug delivery and gene therapy. *Crit. Rev. Biotechnol.* 35, 209–221. doi:10.3109/07388551.2013.833163.
56. Ferrer-Miralles, N., and Villaverde, A. (2013). Bacterial cell factories for recombinant protein production; expanding the catalogue. *Microb. Cell Fact.* 12, 113. doi:10.1186/1475-2859-12-113.
57. Fischer, K. R., Durrans, A., Lee, S., Sheng, J., Li, F., Wong, S. T. C., et al. (2015). Epithelial-to-mesenchymal transition is not required for lung metastasis but contributes to chemoresistance. *Nature* 527, 472–476. doi:10.1038/nature15748.
58. Fojo, A. T., and Parkinson, D. R. (2010). Biologically targeted cancer therapy and marginal benefits: Are we making too much of too little or are we achieving too little by giving too much? *Clin. Cancer Res.* 16, 5972–5980. doi:10.1158/1078-0432.CCR-10-1277.
59. Gelmini, S., Mangoni, M., Serio, M., Romagnani, P., and Lazzeri, E. (2008). The critical role of SDF-1/CXCR4 axis in cancer and cancer stem cells metastasis. *J. Endocrinol. Invest.* 31, 809–819. doi:10.1007/BF03349262.
60. Gong, Y., Fan, Z., Luo, G., Yang, C., Huang, Q., Fan, K., et al. (2019). The role of necroptosis in cancer biology and therapy. *Mol. Cancer* 18, 1–17.

- doi:10.1186/s12943-019-1029-8.
61. Gonzalez-Valdivieso, J., Girotti, A., Schneider, J., and Arias, F. J. (2021). Advanced nanomedicine and cancer: Challenges and opportunities in clinical translation. *Int. J. Pharm.* 599, 120438. doi:<https://doi.org/10.1016/j.ijpharm.2021.120438>.
 62. Gout, S., Tremblay, P. L., and Huot, J. (2008). Selectins and selectin ligands in extravasation of cancer cells and organ selectivity of metastasis. *Clin. Exp. Metastasis* 25, 335–344. doi:10.1007/s10585-007-9096-4.
 63. Gradishar, W. J. (2006). Albumin-bound paclitaxel: a next-generation taxane. *Expert Opin. Pharmacother.* 7, 1041–1053. doi:10.1517/14656566.7.8.1041.
 64. Guan, X. (2015). Cancer metastases: Challenges and opportunities. *Acta Pharm. Sin. B* 5, 402–418. doi:10.1016/j.apsb.2015.07.005.
 65. Guo, F., Wang, Y., Liu, J., Mok, S. C., Xue, F., and Zhang, W. (2016). CXCL12/CXCR4: A symbiotic bridge linking cancer cells and their stromal neighbors in oncogenic communication networks. *Oncogene* 35, 816–826. doi:10.1038/onc.2015.139.
 66. Gupta, G. P., and Massagué, J. (2006). Cancer Metastasis: Building a Framework. *Cell*. doi:10.1016/j.cell.2006.11.001.
 67. He, H., Liu, L., Morin, E. E., Liu, M., and Schwendeman, A. (2019). Survey of Clinical Translation of Cancer Nanomedicines—Lessons Learned from Successes and Failures. *Acc. Chem. Res.* 52, 2445–2461. doi:10.1021/acs.accounts.9b00228.
 68. Heldin, C.-H., Rubin, K., Pietras, K., and Ostman, A. (2004). High interstitial fluid pressure - an obstacle in cancer therapy. *Nat. Rev. Cancer* 4, 806–813. doi:10.1038/nrc1456.
 69. Hermann, P. C., Huber, S. L., and Heeschen, C. (2008). Metastatic cancer stem cells: A new target for anti-cancer therapy? *Cell Cycle* 7, 188–193. doi:10.4161/cc.7.2.5326.
 70. Hermann, P. C., Huber, S. L., Herrler, T., Aicher, A., Ellwart, J. W., Guba, M., et al. (2007). Distinct Populations of Cancer Stem Cells Determine Tumor Growth and Metastatic Activity in Human Pancreatic Cancer. *Cell Stem Cell* 1, 313–323. doi:<https://doi.org/10.1016/j.stem.2007.06.002>.
 71. Holohan, C., Van Schaeybroeck, S., Longley, D. B., and Johnston, P. G. (2013). Cancer drug resistance: an evolving paradigm. *Nat. Rev. Cancer* 13, 714–726. doi:10.1038/nrc3599.
 72. Hong, S., Choi, D. W., Kim, H. N., Park, C. G., Lee, W., and Park, H. H. (2020). Protein-Based Nanoparticles as Drug Delivery Systems. *Pharmaceutics* 12, 604. doi:10.3390/pharmaceutics12070604.

73. <https://clinicaltrials.gov>. (accessed 26/04/2022)
74. Huang, C. F., Chen, L., Li, Y. C., Wu, L., Yu, G. T., Zhang, W. F., et al. (2017). NLRP3 inflammasome activation promotes inflammation-induced carcinogenesis in head and neck squamous cell carcinoma. *J. Exp. Clin. Cancer Res.* 36, 1–13. doi:10.1186/s13046-017-0589-y.
75. Igney, F. H., and Krammer, P. H. (2002). Death and anti-death: tumour resistance to apoptosis. *Nat. Rev. Cancer* 2, 277–288. doi:10.1038/nrc776.
76. Ishikawa, T., Nakashiro, K.-I., Hara, S., Klosek K., S., Li, C., Shintani, S., et al. (2006). CXCR4 expression is associated with lymph-node metastasis of oral squamous cell carcinoma. *Int J Oncol* 28, 61–66. doi:10.3892/ijo.28.1.61.
77. J., M.-V. F., and Daan, F. (2011). Designing super selectivity in multivalent nanoparticle binding. *Proc. Natl. Acad. Sci.* 108, 10963–10968. doi:10.1073/pnas.1105351108.
78. Jain, R. K., and Stylianopoulos, T. (2010). Delivering nanomedicine to solid tumors. *Nat. Rev. Clin. Oncol.* 7, 653–664. doi:10.1038/nrclinonc.2010.139.
79. Jolly, M. K., Boareto, M., Huang, B., Jia, D., Lu, M., Ben-Jacob, E., et al. (2015). Implications of the Hybrid Epithelial/Mesenchymal Phenotype in Metastasis. *Front. Oncol.* 5, 155. doi:10.3389/fonc.2015.00155.
80. Joubert, N., Beck, A., Dumontet, C., and Denevault-Sabourin, C. (2020). Antibody–Drug Conjugates: The Last Decade. *Pharm.* 13. doi:10.3390/ph13090245.
81. Junutula, J. R., Raab, H., Clark, S., Bhakta, S., Leipold, D. D., Weir, S., et al. (2008). Site-specific conjugation of a cytotoxic drug to an antibody improves the therapeutic index. *Nat. Biotechnol.* 26, 925–932. doi:10.1038/nbt.1480.
82. Kadin, M. E., and Vonderheid, E. C. (2010). Denileukin diftitox—a step towards a “magic bullet” for CTCL. *Nat. Rev. Clin. Oncol.* 7, 430–432. doi:10.1038/nrclinonc.2010.105.
83. Kanno, Y., Chen, C.-Y., Lee, H.-L., Chiou, J.-F., and Chen, Y.-J. (2021). Molecular Mechanisms of Chemotherapy Resistance in Head and Neck Cancers. *Front. Oncol.* 11, 640392. doi:10.3389/fonc.2021.640392.
84. Kaplan, G., Lee, F., Onda, M., Kolyvas, E., Bhardwaj, G., Baker, D., et al. (2016). Protection of the Furin Cleavage Site in Low-Toxicity Immunotoxins Based on Pseudomonas Exotoxin A. *Toxins (Basel)*. 8, 217. doi:10.3390/toxins8080217.
85. Ke, P. C., Lin, S., Parak, W. J., Davis, T. P., and Caruso, F. (2017). A Decade of the Protein Corona. *ACS Nano* 11, 11773–11776. doi:10.1021/acsnano.7b08008.
86. Keam, B., Lee, K., Lee, S., Kim, J., Kim, J. H., Wu, H., et al. (2019). A Phase II Study of Genexol-PM and Cisplatin as Induction Chemotherapy in Locally Advanced Head

- and Neck Squamous Cell Carcinoma. *Oncologist* 24, 751-e231. doi:10.1634/theoncologist.2019-0070.
87. Khongorzul, P., Ling, C. J., Khan, F. U., Ihsan, A. U., and Zhang, J. (2020). Antibody-drug conjugates: A comprehensive review. *Mol. Cancer Res.* 18, 3–19. doi:10.1158/1541-7786.MCR-19-0582.
88. Ko, S., and Gunasekaran, S. (2006). Preparation of sub-100-nm β -lactoglobulin (BLG) nanoparticles. *J. Microencapsul.* 23, 887–898. doi:10.1080/02652040601035143.
89. Kong, Y., Feng, Z., Chen, A., Qi, Q., Han, M., Wang, S., et al. (2019). The Natural Flavonoid Galangin Elicits Apoptosis, Pyroptosis, and Autophagy in Glioblastoma. *Front. Oncol.* 9, 942. doi:10.3389/fonc.2019.00942.
90. Kreitman, R. J. (2009). Recombinant immunotoxins containing truncated bacterial toxins for the treatment of hematologic malignancies. *BioDrugs* 23, 1–13. doi:10.2165/00063030-200923010-00001.
91. Kucia, M., Reca, R., Miekus, K., Wanzeck, J., Wojakowski, W., Janowska-Wieczorek, A., et al. (2005). Trafficking of Normal Stem Cells and Metastasis of Cancer Stem Cells Involve Similar Mechanisms: Pivotal Role of the SDF-1-CXCR4 Axis. *Stem Cells* 23, 879–894. doi:10.1634/stemcells.2004-0342.
92. Lammers, T., Kiessling, F., Ashford, M., Hennink, W., Crommelin, D., and Strom, G. (2016). Cancer nanomedicine: Is targeting our target? *Nat. Rev. Mater.* 1, 1–2. doi:10.1038/natrevmats.2016.69.
93. Lee, E. J., Lee, N. K., and Kim, I. S. (2016). Bioengineered protein-based nanocage for drug delivery. *Adv. Drug Deliv. Rev.* 106, 157–171. doi:10.1016/j.addr.2016.03.002.
94. Lee, Y. T., Tan, Y. J., and Oon, C. E. (2018). Molecular targeted therapy: Treating cancer with specificity. *Eur. J. Pharmacol.* 834, 188–196. doi:10.1016/j.ejphar.2018.07.034.
95. Leemans, C. R., Snijders, P. J. F., and Brakenhoff, R. H. (2018). The molecular landscape of head and neck cancer. *Nat. Rev. Cancer* 18, 269–282. doi:10.1038/nrc.2018.11.
96. León, X., Diez, S., García, J., Lop, J., Sumarroca, A., Quer, M., et al. (2016). Expression of the CXCL12/CXCR4 chemokine axis predicts regional control in head and neck squamous cell carcinoma. *Eur. Arch. oto-rhino-laryngology Off. J. Eur. Fed. Oto-Rhino-Laryngological Soc. Affil. with Ger. Soc. Oto-Rhino-Laryngology - Head Neck Surg.* 273, 4525–4533. doi:10.1007/s00405-016-4144-9.
97. Li, M., Liu, Z. S., Liu, X. L., Hui, Q., Lu, S. Y., Qu, L. L., et al. (2017). Clinical targeting

- recombinant immunotoxins for cancer therapy. *Onco. Targets. Ther.* 10, 3645–3665. doi:10.2147/OTT.S134584.
98. Li, X., Wang, L., Fan, Y., Feng, Q., and Cui, F. (2012). Biocompatibility and Toxicity of Nanoparticles and Nanotubes. *J. Nanomater.* 2012, 548389. doi:10.1155/2012/548389.
99. Liu, M., Apriceno, A., Sipin, M., Scarpa, E., Rodriguez-Arco, L., Poma, A., et al. (2020). Combinatorial entropy behaviour leads to range selective binding in ligand-receptor interactions. *Nat. Commun.* 11, 4836. doi:10.1038/s41467-020-18603-5.
100. Liu, T., Li, X., You, S., Bhuyan, S. S., and Dong, L. (2016). Effectiveness of AMD3100 in treatment of leukemia and solid tumors: from original discovery to use in current clinical practice. *Exp. Hematol. Oncol.* 5, 19. doi:10.1186/s40164-016-0050-5.
101. Lohcharoenkal, W., Wang, L., Chen, Y. C., and Rojanasakul, Y. (2014). Protein nanoparticles as drug delivery carriers for cancer therapy. *Biomed Res. Int.* 2014. doi:10.1155/2014/180549.
102. López-Laguna, H., Sánchez, J., Unzueta, U., Mangues, R., Vázquez, E., and Villaverde, A. (2020). Divalent Cations: A Molecular Glue for Protein Materials. *Trends Biochem. Sci.* 45, 992–1003. doi:10.1016/j.tibs.2020.08.003.
103. López-Laguna, H., Unzueta, U., Conchillo-Solé, O., Sánchez-Chardi, A., Pesarrodona, M., Cano-Garrido, O., et al. (2019). Assembly of histidine-rich protein materials controlled through divalent cations. *Acta Biomater.* 83, 257–264. doi:10.1016/j.actbio.2018.10.030.
104. López-Laguna, H., Voltà-Durán, E., Parladé, E., Villaverde, A., Vázquez, E., and Unzueta, U. (2022). Insights on the emerging biotechnology of histidine-rich peptides. *Biotechnol. Adv.* 54, 107817. doi:10.1016/j.biotechadv.2021.107817.
105. Lu, H., Zhang, S., Wu, J., Chen, M., Cai, M.-C., Fu, Y., et al. (2018). Molecular Targeted Therapies Elicit Concurrent Apoptotic and GSDME-Dependent Pyroptotic Tumor Cell Death. *Clin. cancer Res. an Off. J. Am. Assoc. Cancer Res.* 24, 6066–6077. doi:10.1158/1078-0432.CCR-18-1478.
106. Lu, W., Xiong, C., Zhang, R., Shi, L., Huang, M., Zhang, G., et al. (2012). Receptor-mediated transcytosis: A mechanism for active extravascular transport of nanoparticles in solid tumors. *J. Control. Release* 161, 959–966. doi:https://doi.org/10.1016/j.jconrel.2012.05.014.
107. Luker, G. D., Yang, J., Richmond, A., Scala, S., Festuccia, C., Schottelius, M., et al. (2021). At the Bench: Pre-clinical evidence for multiple functions of CXCR4 in cancer. *J. Leukoc. Biol.* 109, 969–989. doi:10.1002/JLB.2BT1018-715RR.

108. Luo, J., Solimini, N. L., and Elledge, S. J. (2009). Principles of cancer therapy: oncogene and non-oncogene addiction. *Cell* 136, 823–837. doi:10.1016/j.cell.2009.02.024.
109. Lydiatt, W., O’Sullivan, B., and Patel, S. (2018). Major Changes in Head and Neck Staging for 2018. *Am. Soc. Clin. Oncol. Educ. B.*, 505–514. doi:10.1200/edbk_199697.
110. Major, A. G., Pitty, L. P., and Farah, C. S. (2013). Cancer stem cell markers in head and neck squamous cell carcinoma. *Stem Cells Int.* 2013. doi:10.1155/2013/319489.
111. Mangués, R., Vázquez, E., and Villaverde, A. (2016). Targeting in Cancer Therapies. *Med. Sci.* 4, 6. doi:10.3390/medsci4010006.
112. Manzari, M. T., Shamay, Y., Kiguchi, H., Rosen, N., Scaltriti, M., and Heller, D. A. (2021). Targeted drug delivery strategies for precision medicines. *Nat. Rev. Mater.* 6, 351–370. doi:10.1038/s41578-020-00269-6.
113. Maruani, A. (2018). Bispecifics and antibody–drug conjugates: A positive synergy. *Drug Discov. Today Technol.* 30, 55–61. doi:10.1016/j.ddtec.2018.09.003.
114. Marur, S., D’Souza, G., Westra, W. H., and Forastiere, A. A. (2010). HPV-associated head and neck cancer: A virus-related cancer epidemic. *Lancet Oncol.* 11, 781–789. doi:10.1016/S1470-2045(10)70017-6.
115. Marur, S., and Forastiere, A. A. (2008). Head and neck cancer: Changing epidemiology, diagnosis, and treatment. *Mayo Clin. Proc.* 83, 489–501. doi:10.4065/83.4.489.
116. Masters, J. C., Nickens, D. J., Xuan, D., Shazer, R. L., and Amantea, M. (2018). Clinical toxicity of antibody drug conjugates: a meta-analysis of payloads. *Invest. New Drugs* 36, 121–135. doi:10.1007/s10637-017-0520-6.
117. Matsumura, Y., and Maeda, H. (1986). A new concept for macromolecular therapeutics in cancer chemotherapy: mechanism of tumor-tropic accumulation of proteins and the antitumor agent smancs. *Cancer Res.* 46, 6387–6392.
118. Mazor, R., King, E. M., and Pastan, I. (2018). Strategies to Reduce the Immunogenicity of Recombinant Immunotoxins. *Am. J. Pathol.* 188, 1736–1743. doi:https://doi.org/10.1016/j.ajpath.2018.04.016.
119. Mazor, R., and Pastan, I. (2020). Immunogenicity of Immunotoxins Containing Pseudomonas Exotoxin A: Causes, Consequences, and Mitigation. *Front. Immunol.* 11. doi:10.3389/fimmu.2020.01261.
120. McMullen, K. P., Chalmers, J. J., Lang, J. C., Kumar, P., and Jatana, K. R. (2016). Circulating tumor cells in head and neck cancer: A review. *World J.*

- Otorhinolaryngol. Neck Surg.* 2, 109–116. doi:10.1016/j.wjorl.2016.05.003.
121. Mehra, R., Seiwert, T. Y., Gupta, S., Weiss, J., Gluck, I., Eder, J. P., et al. (2018). Efficacy and safety of pembrolizumab in recurrent/metastatic head and neck squamous cell carcinoma: pooled analyses after long-term follow-up in KEYNOTE-012. *Br. J. Cancer* 119, 153–159. doi:10.1038/s41416-018-0131-9.
 122. Miao, M., De Clercq, E., and Li, G. (2020). Clinical significance of chemokine receptor antagonists. *Expert Opin. Drug Metab. Toxicol.* 16, 11–30. doi:10.1080/17425255.2020.1711884.
 123. Miceli, E., Kar, M., and Calderón, M. (2017). Interactions of organic nanoparticles with proteins in physiological conditions. *J. Mater. Chem. B* 5, 4393–4405. doi:10.1039/c7tb00146k.
 124. Miele, E., Spinelli, G. P., Miele, E., Tomao, F., and Tomao, S. (2009). Albumin-bound formulation of paclitaxel (Abraxane® ABI-007) in the treatment of breast cancer. *Int. J. Nanomedicine* 4, 99–105. doi:10.2147/ijn.s3061.
 125. Miles, F. L., Pruitt, F. L., Van Golen, K. L., and Cooper, C. R. (2008). Stepping out of the flow: Capillary extravasation in cancer metastasis. *Clin. Exp. Metastasis* 25, 305–324. doi:10.1007/s10585-007-9098-2.
 126. Mishan, M. A., Ahmadiankia, N., and Bahrami, A. R. (2016). CXCR4 and CCR7: Two eligible targets in targeted cancer therapy. *Cell Biol. Int.* 40, 955–967. doi:10.1002/cbin.10631.
 127. Mitragotri, S., and Stayton, P. (2014). Organic nanoparticles for drug delivery and imaging. *MRS Bull.* 39, 219–223. doi:10.1557/mrs.2014.11.
 128. Mittal, A., and Sharma, A. (2022). Current status of systemic therapy in head and neck cancer. *J. Chemother.* 34, 9–24. doi:10.1080/1120009X.2021.1955201.
 129. Mohajertehran, F., Sahebkar, A., Zare, R., and Mohtasham, N. (2018). The promise of stem cell markers in the diagnosis and therapy of epithelial dysplasia and oral squamous cell carcinoma. *J. Cell. Physiol.* 233, 8499–8507. doi:10.1002/jcp.26789.
 130. Mohme, M., Riethdorf, S., and Pantel, K. (2017). Circulating and disseminated tumour cells - mechanisms of immune surveillance and escape. *Nat. Rev. Clin. Oncol.* 14, 155–167. doi:10.1038/nrclinonc.2016.144.
 131. Moskovitz, J. M., and Ferris, R. L. (2018). Tumor Immunology and Immunotherapy for Head and Neck Squamous Cell Carcinoma. *J. Dent. Res.* 97, 622–626. doi:10.1177/0022034518759464.
 132. Murakami, T., Zhang, T.-Y., Koyanagi, Y., Tanaka, Y., Kim, J., Suzuki, Y., et al. (2002). Inhibitory Mechanism of the CXCR4 Antagonist T22 against Human

- Immunodeficiency Virus Type 1 Infection. *J. Virol.* 76, 933–933. doi:10.1128/jvi.76.2.933.2002.
133. Muraro, E., Fanetti, G., Lupato, V., Giacomarra, V., Steffan, A., Gobitti, C., et al. (2021). Cetuximab in locally advanced head and neck squamous cell carcinoma: Biological mechanisms involved in efficacy, toxicity and resistance. *Crit. Rev. Oncol. Hematol.* 164, 103424. doi:10.1016/j.critrevonc.2021.103424.
134. Naahidi, S., Jafari, M., Edalat, F., Raymond, K., Khademhosseini, A., and Chen, P. (2013). Biocompatibility of engineered nanoparticles for drug delivery. *J. Control. Release* 166, 182–194. doi:10.1016/j.jconrel.2012.12.013.
135. Nabors, L. B., Surboeck, B., and Grisold, W. (2016). *Complications from pharmacotherapy*. 1st ed. Elsevier B.V. doi:10.1016/B978-0-12-802997-8.00014-1.
136. Nagarajan, K., Soundarapandian, K., Thorne, R. F., Li, D., and Li, D. (2019). Activation of Pyroptotic Cell Death Pathways in Cancer: An Alternative Therapeutic Approach. *Transl. Oncol.* 12, 925–931. doi:10.1016/j.tranon.2019.04.010.
137. Nagayama, A., Ellisen, L. W., Chabner, B., and Bardia, A. (2017). Antibody-Drug Conjugates for the Treatment of Solid Tumors: Clinical Experience and Latest Developments. *Target. Oncol.* 12, 719–739. doi:10.1007/s11523-017-0535-0.
138. Najahi-Missaoui, W., Arnold, R. D., and Cummings, B. S. (2021). Safe Nanoparticles: Are We There Yet? *Int. J. Mol. Sci.* 22. doi:10.3390/ijms22010385.
139. Nejadmoghaddam, M.-R., Minai-Tehrani, A., Ghahremanzadeh, R., Mahmoudi, M., Dinarvand, R., and Zarnani, A.-H. (2019). Antibody-Drug Conjugates: Possibilities and Challenges. *Avicenna J. Med. Biotechnol.* 11, 3–23. Available at: <https://pubmed.ncbi.nlm.nih.gov/30800238>.
140. Nieto, M. A., Huang, R. Y.-J., Jackson, R. A., and Thiery, J. P. (2016). EMT: 2016. *Cell* 166, 21–45. doi:https://doi.org/10.1016/j.cell.2016.06.028.
141. Okushi, Mohammad, R. M., Muqbil, I., Lowe, L., Yedjou, C., Hsu, H.-Y., et al. (2015). Broad targeting of resistance to apoptosis in cancer. *Semin. Cancer Biol.* 35, S78–S103. doi:10.1016/j.semcancer.2015.03.001.Broad.
142. Paget, S. (1989). The distribution of secondary growths in cancer of the breast. 1889. *Cancer Metastasis Rev.* 8, 98–101.
143. Pagliarini, R., Shao, W., and Sellers, W. R. (2015). Oncogene addiction: pathways of therapeutic response, resistance, and road maps toward a cure. *EMBO Rep.* 16, 280–296. doi:10.15252/embr.201439949.
144. Pal, A., Barrett, T. F., Paolini, R., Parikh, A., and Puram, S. V (2021). Partial EMT in head and neck cancer biology: a spectrum instead of a switch. *Oncogene* 40, 5049–5065. doi:10.1038/s41388-021-01868-5.

145. Pandit, S., Dutta, D., and Nie, S. (2020). Active transcytosis and new opportunities for cancer nanomedicine. *Nat. Mater.* 19, 478–480. doi:10.1038/s41563-020-0672-1.
146. Pantel, K., and Speicher, M. R. (2016). The biology of circulating tumor cells. *Oncogene* 35, 1216–1224. doi:10.1038/onc.2015.192.
147. Park, K. (2013). Questions on the role of the EPR effect in tumor targeting. *J. Control. Release* 172, 391. doi:https://doi.org/10.1016/j.jconrel.2013.10.001.
148. Pascual, G., Avgustinova, A., Mejetta, S., Martín, M., Castellanos, A., Attolini, C. S.-O., et al. (2017). Targeting metastasis-initiating cells through the fatty acid receptor CD36. *Nature* 541, 41–45. doi:10.1038/nature20791.
149. Pastan, I., Hassan, R., Fitzgerald, D. J., and Kreitman, R. J. (2006). Immunotoxin therapy of cancer. *Nat. Rev. Cancer* 6, 559–565. doi:10.1038/nrc1891.
150. Pearce, A. K., and O'Reilly, R. K. (2019). Insights into Active Targeting of Nanoparticles in Drug Delivery: Advances in Clinical Studies and Design Considerations for Cancer Nanomedicine. *Bioconjug. Chem.* 30, 2300–2311. doi:10.1021/acs.bioconjchem.9b00456.
151. Pei, R., Shi, Y., Lv, S., Dai, T., Zhang, F., Liu, S., et al. (2021). Nivolumab vs Pembrolizumab for Treatment of US Patients With Platinum-Refractory Recurrent or Metastatic Head and Neck Squamous Cell Carcinoma: A Network Meta-analysis and Cost-effectiveness Analysis. *JAMA Netw. open* 4, e218065. doi:10.1001/jamanetworkopen.2021.8065.
152. Peitzsch, C., Nathansen, J., Schniewind, S. I., Schwarz, F., and Dubrovskaja, A. (2019). Cancer stem cells in head and neck squamous cell carcinoma: Identification, characterization and clinical implications. *Cancers (Basel)*. 11. doi:10.3390/cancers11050616.
153. Pérez-Herrero, E., and Fernández-Medarde, A. (2015). Advanced targeted therapies in cancer: Drug nanocarriers, the future of chemotherapy. *Eur. J. Pharm. Biopharm.* 93, 52–79. doi:10.1016/j.ejpb.2015.03.018.
154. Pernas, S., Martin, M., Kaufman, P. A., Gil-Martin, M., Gomez Pardo, P., Lopez-Tarruella, S., et al. (2018). Balixafortide plus eribulin in HER2-negative metastatic breast cancer: a phase 1, single-arm, dose-escalation trial. *Lancet Oncol.* 19, 812–824. doi:10.1016/S1470-2045(18)30147-5.
155. Perrotti, V., Caponio, V. C. A., Mascitti, M., Lo Muzio, L., Piattelli, A., Rubini, C., et al. (2021). Therapeutic Potential of Antibody-Drug Conjugate-Based Therapy in Head and Neck Cancer: A Systematic Review. *Cancers (Basel)*. 13. doi:10.3390/cancers13133126.

156. Petros, R. A., and Desimone, J. M. (2010). Strategies in the design of nanoparticles for therapeutic applications. *Nat. Rev. Drug Discov.* 9, 615–627. doi:10.1038/nrd2591.
157. Picon, H., and Guddati, A. K. (2020). Mechanisms of resistance in head and neck cancer. *Am. J. Cancer Res.* 10, 2742–2751.
158. Piechutta, M., and Berghoff, A. S. (2019). New emerging targets in cancer immunotherapy: The role of Cluster of Differentiation 40 (CD40/TNFR5). *ESMO Open* 4. doi:10.1136/esmooopen-2019-000510.
159. Pozzobon, T., Goldoni, G., Viola, A., and Molon, B. (2016). CXCR4 signaling in health and disease. *Immunol. Lett.* 177, 6–15. doi:10.1016/j.imlet.2016.06.006.
160. Prasetyanti, P. R., and Medema, J. P. (2017). Intra-tumor heterogeneity from a cancer stem cell perspective. *Mol. Cancer* 16, 41. doi:10.1186/s12943-017-0600-4.
161. Prat, A., Navarro, A., Paré, L., Reguart, N., Galván, P., Pascual, T., et al. (2017). Immune-related gene expression profiling after PD-1 blockade in non-small cell lung carcinoma, head and neck squamous cell carcinoma, and melanoma. *Cancer Res.* 77, 3540–3550. doi:10.1158/0008-5472.CAN-16-3556.
162. Rampado, R., Crotti, S., Caliceti, P., Pucciarelli, S., and Agostini, M. (2020). Recent Advances in Understanding the Protein Corona of Nanoparticles and in the Formulation of “Stealthy” Nanomaterials. *Front. Bioeng. Biotechnol.* 8. doi:10.3389/fbioe.2020.00166.
163. Raudenská, M., Balvan, J., and Masařík, M. (2021). Cell death in head and neck cancer pathogenesis and treatment. *Cell Death Dis.* 12, 192. doi:10.1038/s41419-021-03474-5.
164. Reya, T., Morrison, S. J., Clarke, M. F., and Weissman, I. L. (2001). Stem cells, cancer, and cancer stem cells. *Nature* 414, 105–111. doi:10.1038/35102167.
165. Richards, D. A., Maruani, A., and Chudasama, V. (2016). Antibody fragments as nanoparticle targeting ligands: a step in the right direction. *Chem. Sci.* 8, 63–77. doi:10.1039/c6sc02403c.
166. Robert I., H., and Shin, D. M. (2008). Recent advances in head and neck cancer. *N. Engl. J. Med.* 359, 1143–54. doi:10.1056/NEJMra0707975.
167. Sabath, D. E. (2018). Minimal Residual Disease ☆. *Ref. Modul. Biomed. Sci.* 9, 665–674. doi:10.1016/b978-0-12-801238-3.66097-x.
168. Sacco, A. G., and Cohen, E. E. (2015). Current Treatment Options for Recurrent or Metastatic Head and Neck Squamous Cell Carcinoma. *J. Clin. Oncol. Off. J. Am. Soc. Clin. Oncol.* 33, 3305–3313. doi:10.1200/JCO.2015.62.0963.

169. Sakashita, T., Homma, A., Hatakeyama, H., Furusawa, J., Kano, S., Mizumachi, T., et al. (2015). Comparison of acute toxicities associated with cetuximab-based bioradiotherapy and platinum-based chemoradiotherapy for head and neck squamous cell carcinomas: A single-institution retrospective study in Japan. *Acta Otolaryngol.* 135, 853–858. doi:10.3109/00016489.2015.1030772.
170. Salvati, A., Pitek, A. S., Monopoli, M. P., Prapainop, K., Bombelli, F. B., Hristov, D. R., et al. (2013). Transferrin-functionalized nanoparticles lose their targeting capabilities when a biomolecule corona adsorbs on the surface. *Nat. Nanotechnol.* 8, 137–143. doi:10.1038/nnano.2012.237.
171. Sanchez-Garcia, L., Martín, L., Mangués, R., Ferrer-Mirallés, N., Vázquez, E., and Villaverde, A. (2016). Recombinant pharmaceuticals from microbial cells: a 2015 update. *Microb. Cell Fact.* 15, 33. doi:10.1186/s12934-016-0437-3.
172. Sánchez-García, L., Serna, N., Álamo, P., Sala, R., Céspedes, M. V., Roldán, M., et al. (2018). Self-assembling toxin-based nanoparticles as self-delivered antitumoral drugs. *J. Control. Release* 274, 81–92. doi:10.1016/j.jconrel.2018.01.031.
173. Santuray, R. T., Johnson, D. E., and Grandis, J. R. (2018). New Therapies in Head and Neck Cancer. *Trends in Cancer* 4, 385–396. doi:10.1016/j.trecan.2018.03.006.
174. Schoonen, L., and Van Hest, J. C. M. (2014). Functionalization of protein-based nanocages for drug delivery applications. *Nanoscale* 6, 7124–7141. doi:10.1039/c4nr00915k.
175. Schumacher, D., Hackenberger, C. P. R., Leonhardt, H., and Helma, J. (2016). Current Status: Site-Specific Antibody Drug Conjugates. *J. Clin. Immunol.* 36, 100–107. doi:10.1007/s10875-016-0265-6.
176. Senkomago, V., Henley, S. J., Thomas, C. C., Mix, J. M., Markowitz, L. E., and Saraiya, M. (2019). Human Papillomavirus – Attributable Cancers — United States, 2012 – 2016. 68, 2012–2016.
177. Seow, Y., and Wood, M. J. (2009). Biological gene delivery vehicles: Beyond viral vectors. *Mol. Ther.* 17, 767–777. doi:10.1038/mt.2009.41.
178. Serna, N., Sánchez-García, L., Unzueta, U., Díaz, R., Vázquez, E., Mangués, R., et al. (2018). Protein-Based Therapeutic Killing for Cancer Therapies. *Trends Biotechnol.* 36, 318–335. doi:10.1016/j.tibtech.2017.11.007.
179. Shaloam, D., and Tchounwou, P. B. (2014). Cisplatin in cancer therapy: Molecular mechanisms of action. *Eur. J. Pharmacol.* 740, 364–378. doi:10.1016/j.ejphar.2014.07.025.Cisplatin.

180. Shamir, E. R., Pappalardo, E., Jorgens, D. M., Coutinho, K., Tsai, W.-T., Aziz, K., et al. (2014). Twist1-induced dissemination preserves epithelial identity and requires E-cadherin. *J. Cell Biol.* 204, 839–856. doi:10.1083/jcb.201306088.
181. Sharma, S. V, and Settleman, J. (2007). Oncogene addiction: setting the stage for molecularly targeted cancer therapy. *Genes Dev.* 21, 3214–3231. doi:10.1101/gad.1609907.
182. Shaw, R., and Beasley, N. (2016). Aetiology and risk factors for head and neck cancer: United Kingdom National Multidisciplinary Guidelines. *J. Laryngol. Otol.* 130, S9–S12. doi:10.1017/s0022215116000360.
183. Shi, J., Kantoff, P. W., Wooster, R., and Farokhzad, O. C. (2017). Cancer nanomedicine: progress, challenges and opportunities. *Nat. Rev. Cancer* 17, 20–37. doi:10.1038/nrc.2016.108.
184. Shi, J., Zhao, Y., Wang, K., Shi, X., Wang, Y., Huang, H., et al. (2015). Cleavage of GSDMD by inflammatory caspases determines pyroptotic cell death. *Nature* 526, 660–665. doi:10.1038/nature15514.
185. Shibata, H., Saito, S., and Uppaluri, R. (2021). Immunotherapy for Head and Neck Cancer: A Paradigm Shift From Induction Chemotherapy to Neoadjuvant Immunotherapy. *Front. Oncol.* 11, 1–11. doi:10.3389/fonc.2021.727433.
186. Shim, H. (2020). Bispecific antibodies and antibody–drug conjugates for cancer therapy: Technological considerations. *Biomolecules* 10. doi:10.3390/biom10030360.
187. Siegel, R. L., Miller, K. D., Fuchs, H. E., and Jemal, A. (2021). Cancer Statistics, 2021. *CA. Cancer J. Clin.* 71, 7–33. doi:10.3322/caac.21654.
188. Siegel, R. L., Miller, K. D., and Jemal, A. (2019). Cancer statistics, 2019. *CA. Cancer J. Clin.* 69, 7–34. doi:10.3322/caac.21551.
189. Sindhwani, S., Syed, A. M., Ngai, J., Kingston, B. R., Maiorino, L., Rothschild, J., et al. (2020). The entry of nanoparticles into solid tumours. *Nat. Mater.* 19, 566–575. doi:10.1038/s41563-019-0566-2.
190. Singh, N., Marets, C., Boudon, J., Millot, N., Saviot, L., and Maurizi, L. (2021). In vivo protein corona on nanoparticles: does the control of all material parameters orient the biological behavior? *Nanoscale Adv.* 3, 1209–1229. doi:10.1039/D0NA00863J.
191. Singh, R., Letai, A., and Sarosiek, K. (2019). Regulation of apoptosis in health and disease: the balancing act of BCL-2 family proteins. *Nat. Rev. Mol. Cell Biol.* 20, 175–193. doi:10.1038/s41580-018-0089-8.
192. Sproll, C., Fluegen, G., and Stoecklein, N. H. (2018). Minimal residual

- disease in head and neck cancer and esophageal cancer. *Adv. Exp. Med. Biol.* 1100, 55–82. doi:10.1007/978-3-319-97746-1_4.
193. Strilic, B., and Offermanns, S. (2017). Intravascular Survival and Extravasation of Tumor Cells. *Cancer Cell* 32, 282–293. doi:10.1016/j.ccell.2017.07.001.
194. Suárez, C., Rodrigo, J. P., Ferlito, A., Cabanillas, R., Shaha, A. R., and Rinaldo, A. (2006). Tumours of familial origin in the head and neck. *Oral Oncol.* 42, 965–978. doi:10.1016/j.oraloncology.2006.03.002.
195. Sukhanova, A., Bozrova, S., Sokolov, P., Berestovoy, M., Karaulov, A., and Nabiev, I. (2018). Dependence of Nanoparticle Toxicity on Their Physical and Chemical Properties. *Nanoscale Res. Lett.* 13, 44. doi:10.1186/s11671-018-2457-x.
196. Sung, H., Ferlay, J., Siegel, R. L., Laversanne, M., Soerjomataram, I., Jemal, A., et al. (2021). Global Cancer Statistics 2020: GLOBOCAN Estimates of Incidence and Mortality Worldwide for 36 Cancers in 185 Countries. *CA. Cancer J. Clin.* 71, 209–249. doi:10.3322/caac.21660.
197. Szczerba, B. M., Castro-Giner, F., Vetter, M., Krol, I., Gkountela, S., Landin, J., et al. (2019). Neutrophils escort circulating tumour cells to enable cell cycle progression. *Nature* 566, 553–557. doi:10.1038/s41586-019-0915-y.
198. Takes, R. P., Rinaldo, A., Silver, C. E., Haigentz, M., Woolgar, J. A., Triantafyllou, A., et al. (2012). Distant metastases from head and neck squamous cell carcinoma. Part I. Basic aspects. *Oral Oncol.* 48, 775–779. doi:10.1016/j.oraloncology.2012.03.013.
199. Tan, Y. S., Sansanaphongpricha, K., Prince, M. E. P., Sun, D., Wolf, G. T., and Lei, Y. L. (2018). Engineering Vaccines to Reprogram Immunity against Head and Neck Cancer. *J. Dent. Res.* 97, 627–634. doi:10.1177/0022034518764416.
200. Taylor, K., Krüger, M., and Singer, S. (2021). Long-term toxicity among head and neck cancer patients—A systematic review. *Onkologe* 27, 145–149. doi:10.1007/s00761-021-00914-x.
201. Teicher, B. A., and Fricker, S. P. (2010). CXCL12 (SDF-1)/CXCR4 pathway in cancer. *Clin. Cancer Res.* 16, 2927–2931. doi:10.1158/1078-0432.CCR-09-2329.
202. Tewabe, A., Abate, A., Tamrie, M., Seyfu, A., and Abdela Siraj, E. (2021). Targeted Drug Delivery - From Magic Bullet to Nanomedicine: Principles, Challenges, and Future Perspectives. *J. Multidiscip. Healthc.* 14, 1711–1724. doi:10.2147/JMDH.S313968.
203. Tolcher, A. W. (2016). Antibody drug conjugates: lessons from 20 years of clinical experience. *Ann. Oncol.* 27, 2168–2172.

- doi:<https://doi.org/10.1093/annonc/mdw424>.
204. Tong, J. T. W., Harris, P. W. R., Brimble, M. A., and Kavianinia, I. (2021). An Insight into FDA Approved Antibody-Drug Conjugates for Cancer Therapy. *Molecules* 26, 5847. doi:10.3390/molecules26195847.
205. Tsao, S. W., Tsang, C. M., and Lo, K. W. (2017). Epstein-barr virus infection and nasopharyngeal carcinoma. *Philos. Trans. R. Soc. B Biol. Sci.* 372. doi:10.1098/rstb.2016.0270.
206. Tsou, L. K., Huang, Y. H., Song, J. S., Ke, Y. Y., Huang, J. K., and Shia, K. S. (2018). Harnessing CXCR4 antagonists in stem cell mobilization, HIV infection, ischemic diseases, and oncology. *Med. Res. Rev.* 38, 1188–1234. doi:10.1002/med.21464.
207. Tuma, P. L., and Hubbard, A. L. (2003). Transcytosis: Crossing cellular barriers. *Physiol. Rev.* 83, 871–932. doi:10.1152/physrev.00001.2003.
208. Uchida, D., Kuribayashi, N., Kinouchi, M., Sawatani, Y., Shimura, M., Mori, T., et al. (2018). Effect of a novel orally bioavailable CXCR4 inhibitor, AMD070, on the metastasis of oral cancer cells. *Oncol. Rep.* 40, 303–308. doi:10.3892/or.2018.6400.
209. Uchida, D., Onoue, T., Kuribayashi, N., Tomizuka, Y., Tamatani, T., Nagai, H., et al. (2011). Blockade of CXCR4 in oral squamous cell carcinoma inhibits lymph node metastases. *Eur. J. Cancer* 47, 452–459. doi:10.1016/j.ejca.2010.09.028.
210. Unzueta, U., Céspedes, M. V., Ferrer-Miralles, N., Casanova, I., Cedano, J., Corchero, J. L., et al. (2012a). Intracellular CXCR4+ cell targeting with T22-empowered protein-only nanoparticles. *Int. J. Nanomedicine* 7, 4533–4544. doi:10.2147/IJN.S34450.
211. Unzueta, U., Ferrer-Miralles, N., Cedano, J., Zikung, X., Pesarrodonna, M., Saccardo, P., et al. (2012b). Non-amyloidogenic peptide tags for the regulatable self-assembling of protein-only nanoparticles. *Biomaterials* 33, 8714–8722. doi:10.1016/j.biomaterials.2012.08.033.
212. Vazquez, E., Mangues, R., and Villaverde, A. (2016). Functional recruitment for drug delivery through protein-based nanotechnologies. *Nanomedicine* 11, 1333–1336. doi:10.2217/nnm-2016-0090.
213. Ventola, C. L. (2017). Progress in nanomedicine: Approved and investigational nanodrugs. *P T* 42, 742–755.
214. Vokes, E. E., Agrawal, N., and Seiwert, T. Y. (2015). HPV-Associated Head and Neck Cancer. *J. Natl. Cancer Inst.* 107, djv344. doi:10.1093/jnci/djv344.
215. Wagner, V., Dullaart, A., Bock, A. K., and Zweck, A. (2006). The emerging

- nanomedicine landscape. *Nat. Biotechnol.* 24, 1211–1217. doi:10.1038/nbt1006-1211.
216. Wang, Y.-Y., Liu, X.-L., and Zhao, R. (2019). Induction of Pyroptosis and Its Implications in Cancer Management. *Front. Oncol.* 9, 971. doi:10.3389/fonc.2019.00971.
217. Wang, Y., Gao, W., Shi, X., Ding, J., Liu, W., He, H., et al. (2017). Chemotherapy drugs induce pyroptosis through caspase-3 cleavage of a gasdermin. *Nature* 547, 99–103. doi:10.1038/nature22393.
218. Wei, G., Wang, Y., Yang, G., Wang, Y., and Ju, R. (2021). Recent progress in nanomedicine for enhanced cancer chemotherapy. *Theranostics* 11, 6370–6392. doi:10.7150/thno.57828.
219. Weinstein, I. B. (2002). Cancer. Addiction to oncogenes--the Achilles heel of cancer. *Science* 297, 63–64. doi:10.1126/science.1073096.
220. Wilhelm, S., Tavares, A. J., Dai, Q., Ohta, S., Audet, J., Dvorak, H. F., et al. (2016). Analysis of nanoparticle delivery to tumours. *Nat. Rev. Mater.* 1. doi:10.1038/natrevmats.2016.14.
221. Wong, D., and Korz, W. (2008). Translating an antagonist of chemokine receptor CXCR4: From bench to bedside. *Clin. Cancer Res.* 14, 7975–7980. doi:10.1158/1078-0432.CCR-07-4846.
222. Wu, D., Wei, C., Li, Y., Yang, X., and Zhou, S. (2021). Pyroptosis, a New Breakthrough in Cancer Treatment. *Front. Oncol.* 11. doi:10.3389/fonc.2021.698811.
223. Wu, X. L., Tu, Q., Faure, G., Gallet, P., Kohler, C., and Bittencourt, M. D. C. (2016). Diagnostic and Prognostic Value of Circulating Tumor Cells in Head and Neck Squamous Cell Carcinoma: A systematic review and meta-analysis. *Sci. Rep.* 6. doi:10.1038/srep20210.
224. Xia, X., Wang, X., Cheng, Z., Qin, W., Lei, L., Jiang, J., et al. (2019). The role of pyroptosis in cancer: pro-cancer or pro-“host”? *Cell Death Dis.* 10. doi:10.1038/s41419-019-1883-8.
225. Xiao, W., and Gao, H. (2018). The impact of protein corona on the behavior and targeting capability of nanoparticle-based delivery system. *Int. J. Pharm.* 552, 328–339. doi:10.1016/j.ijpharm.2018.10.011.
226. Yamada, K., and Ito, Y. (2019). Recent Chemical Approaches for Site-Specific Conjugation of Native Antibodies: Technologies toward Next-Generation Antibody–Drug Conjugates. *ChemBioChem* 20, 2729–2737. doi:10.1002/cbic.201900178.

227. Yardley, D. A. (2013). nab-Paclitaxel mechanisms of action and delivery. *J. Control. Release* 170, 365–372. doi:10.1016/j.jconrel.2013.05.041.
228. Yu, P., Zhang, X., Liu, N., Tang, L., Peng, C., and Chen, X. (2021). Pyroptosis: mechanisms and diseases. *Signal Transduct. Target. Ther.* 6, 128. doi:10.1038/s41392-021-00507-5.
229. Zhang, C.-C., Li, C.-G., Wang, Y.-F., Xu, L.-H., He, X.-H., Zeng, Q.-Z., et al. (2019). Chemotherapeutic paclitaxel and cisplatin differentially induce pyroptosis in A549 lung cancer cells via caspase-3/GSDME activation. *Apoptosis* 24, 312–325. doi:10.1007/s10495-019-01515-1.
230. Zhang, X., Zhang, P., An, L., Sun, N., Peng, L., Tang, W., et al. (2020a). Miltirone induces cell death in hepatocellular carcinoma cell through GSDME-dependent pyroptosis. *Acta Pharm. Sin. B* 10, 1397–1413. doi:10.1016/j.apsb.2020.06.015.
231. Zhang, Y., Yang, J., Wen, Z., Chen, X., Yu, J., Yuan, D., et al. (2020b). A novel 3',5'-diprenylated chalcone induces concurrent apoptosis and GSDME-dependent pyroptosis through activating PKC δ /JNK signal in prostate cancer. *Aging (Albany, NY)* 12, 9103–9124. doi:10.18632/aging.103178.
232. Zhang, Z., Zhang, Y., Xia, S., Kong, Q., Li, S., Liu, X., et al. (2020c). Gasdermin E suppresses tumour growth by activating anti-tumour immunity. *Nature* 579, 415–420. doi:10.1038/s41586-020-2071-9.
233. Zhao, H., Guo, L., Zhao, H., Zhao, J., Weng, H., and Zhao, B. (2015). CXCR4 over-expression and survival in cancer: a system review and meta-analysis. *Oncotarget* 6, 5022–5040. doi:10.18632/oncotarget.3217.
234. Zhou, Q., Dong, C., Fan, W., Jiang, H., Xiang, J., Qiu, N., et al. (2020). Tumor extravasation and infiltration as barriers of nanomedicine for high efficacy: The current status and transcytosis strategy. *Biomaterials* 240, 119902. doi:10.1016/j.biomaterials.2020.119902.
235. Zolot, R. S., Basu, S., and Million, R. P. (2013). Antibody-drug conjugates. *Nat. Rev. Drug Discov.* 12, 259–260. doi:10.1038/nrd3980.